



**SUBSURFACE REMOBILISATION AND
INTRUSION OF SAND: CASE STUDIES
FROM THE FAROE SHETLAND BASIN
AND SE UTAH.**

Simon Shoulders

**Submitted in partial fulfilment of the requirements for the
degree of Ph.D.**

Cardiff University

January 2005

UMI Number: U584719

All rights reserved

INFORMATION TO ALL USERS

The quality of this reproduction is dependent upon the quality of the copy submitted.

In the unlikely event that the author did not send a complete manuscript and there are missing pages, these will be noted. Also, if material had to be removed, a note will indicate the deletion.



UMI U584719

Published by ProQuest LLC 2013. Copyright in the Dissertation held by the Author.
Microform Edition © ProQuest LLC.

All rights reserved. This work is protected against
unauthorized copying under Title 17, United States Code.



ProQuest LLC
789 East Eisenhower Parkway
P.O. Box 1346
Ann Arbor, MI 48106-1346

ABSTRACT

This study has explored the phenomenon of basin-wide sand intrusion. Two case studies from regions with very different tectonic and depositional histories, host rock successions and intrusion geometries have been used to examine sand intrusion in the subsurface. Striking first-order similarities between the two contrasting case studies are apparent; 1) the basin-wide nature of the sand intrusion event; 2) the strong temporal link between the intrusion of sand and major tectonic events within the basin. It therefore appears likely that sand remobilisation in the subsurface and subsequent sand intrusion was triggered by earthquake activity. The case studies are presented as four papers produced for publication, supported by a review of previous work and a discussion of the case study results.

A broad-based approach using a range of geological techniques was used to examine problems in our understanding associated with basin-wide fluid escape and sand intrusion. The first of the two case study areas consists of a region (in excess of 10,000 km²) of large-scale conical sandstone intrusions hosted within a deep-water Eocene-Oligocene succession consisting of claystone and bio-siliceous ooze in Tranche 6 of the Faroe-Shetland Basin. The emplacement of the conical sandstone intrusions occurred during the Late Miocene, coincident with a phase of basin inversion. Polygonal faults were exploited as conduits to feed the conical intrusions, however intrusion propagation occurred along new fractures rather than exploiting the pre-existing polygonal fault network. The second case study is a region of sandstone pipes hosted within the sand-dominated rocks of the Middle Jurassic Carmel Formation and Entrada Sandstone in SE Utah. Pipes formed before the deposition of the Middle Jurassic Cannonville Member of the Entrada Sandstone across the region. Pipe formation was coincident with increased tectonic shortening and the inception of eastward tilting of the basin due to uplift to the west. Fluid-flow velocity during pipe formation is constrained to around 1.6 cms⁻¹ based on calculations of settling velocity of grains present within the pipe fill.

CONTENTS

PREFACE

Contents	ii
Acknowledgements	vii
List of Figures	viii
List of Tables	xvii

CHAPTER 1 – INTRODUCTION AND LITERATURE REVIEW	1
1.1 INTRODUCTION	1
1.2 LITERATURE REVIEW	2
1.2.1 Introduction	2
1.2.2 The physical characteristics of sandstone intrusions	6
<i>1.2.21 Sandstone intrusion geometry</i>	6
<i>1.2.22 Intrusion scale</i>	10
<i>1.2.23 Burial depth of the parent body during the intrusive event</i>	12
<i>1.2.24 Spatial distribution and orientation of sandstone intrusions</i>	13
<i>1.2.25 Intrusive materials</i>	14
<i>1.2.26 Internal structures and grain-size distributions</i>	17
<i>1.2.27 Cements present within sandstone intrusions</i>	18
1.2.3 Sandstone intrusion distribution	21
<i>1.2.31 Tectonic setting</i>	21
<i>1.2.32 Depositional environment of parent body</i>	24
<i>1.2.33 Exotic and unusual settings for sand intrusion</i>	25
1.2.4 Mechanisms of sand intrusion	28
<i>1.2.41 Hydrodynamic setting</i>	28
<i>1.2.42 Triggering mechanism</i>	29
<i>1.2.43 Hydraulic fracture and fracture reactivation</i>	32
<i>1.2.44 Parent body remobilisation and sand transport</i>	35
<i>1.2.45 Physical effects of liquefaction and fluidisation</i>	39
<i>1.2.46 Fluids and diagenesis</i>	39

1.2.5 Post-emplacment modification of sandstone intrusions	41
1.2.6 Summary	43
1.3 AIMS OF STUDY	44
CHAPTER 2 – CONSTRAINING THE DEPTH AND TIMING OF LARGE-SCALE CONICAL SANDSTONE INTRUSIONS	46
2.1 ABSTRACT	46
2.2 INTRODUCTION	47
2.3 REGIONAL GEOLOGICAL SETTING	49
2.4 THREE-DIMENSIONAL SEISMIC INTERPRETATION	49
2.5 FOLDING OF THE INTRA-NEOGENE UNCONFORMITY	54
2.6 DISCUSSION	56
CHAPTER 3 – LARGE-SCALE CONICAL INTRUSIONS AND POLYGONAL FAULT SYSTEMS IN TRANCHE 6, FAROE-SHETLAND BASIN	60
3.1 ABSTRACT	60
3.2 INTRODUCTION	61
3.3 GEOLOGICAL SETTING	66
3.4 DATA AND METHODOLOGY	68
3.5 SEISMIC INTERPRETATION OF THE STUDY AREA	71
3.5.1 Characteristics of polygonal faults within the study area	73
3.5.2 Characteristics of large-scale conical amplitude anomalies within the study area	83
3.5.3 Networks of high-amplitude reflections	85
3.5.4 Distribution of conical amplitude anomalies in the study area	87
3.5.5 Geometry of conical high-amplitude anomalies	89
3.5.6 Dip of conical high-amplitude anomalies	91
3.5.7 Origin of conical high-amplitude anomalies in the Faroe-Shetland Basin	91
3.5.8 Folding of the INU and the timing of sandstone intrusion	92
3.5.9 Interactions between conical sandstone intrusions and polygonal faults	95
3.6 DISCUSSION	98
3.6.1 Key observations	98

3.6.2 Timing of polygonal faulting in Tranche 6	99
3.6.3 Post intrusion compaction	102
3.6.4 Conical sandstone intrusions in Tranche 6	106
3.6.5 Origin and implications of sandstone intrusions in Tranche 6	108
3.7 CONCLUSIONS	110

CHAPTER 4 – MIDDLE JURASSIC CYLINDRICAL SANDSTONE PIPES OF SE UTAH: PALAEOSEISMITES AND LONG-TERM CONDUITS FOR FLUID FLOW

113	
4.1 ABSTRACT	113
4.2 INTRODUCTION	115
4.3 GEOLOGICAL SETTING	117
4.3.1 Tectonic setting	117
<i>4.3.11 Jurassic shortening</i>	118
<i>4.3.12 Early-Mid Cretaceous Cordilleran uplift and shortening</i>	119
4.3.2 Stratigraphic setting	121
4.3.4 Distribution of sandstone pipes in SE Utah	126
4.4 PHYSICAL CHARACTERISTICS OF SANDSTONE PIPES	129
4.4.1 General characteristics of sandstone pipes in SE Utah	129
4.4.2 Geomorphological expression of sandstone pipes	132
4.4.3 Case Studies	133
<i>4.4.31 Kodachrome Basin</i>	133
<i>4.4.32 Lake Powell region</i>	138
4.4.4 Pipe-fill grain-size, cements and evidence of fluid migration	144
<i>4.4.31 Lake Powell region</i>	144
<i>4.4.32 Kodachrome Basin</i>	145
<i>4.4.33 Cementation of pipe material</i>	146
4.5 SUMMARY OF PIPE CHARACTERISTICS	147
4.6 TIMING OF PIPE FORMATION	147
4.7 DEPTH OF PIPE FORMATION	150
4.8 DISCUSSION	151
4.8.1 Pipe Characteristics	151

4.8.2 Sources of pipe-fill material	154
4.8.3 Mechanisms of pipe genesis	156
4.8.4 Bulk transport	157
4.8.5 Triggering rapid fluid flow	158
4.8.51 Ground water flow	159
4.8.52 Upheaval Dome impact crater	160
4.8.53 Seismic shaking	161
4.9 A MODEL FOR PIPE FORMATION IN SE UTAH	164
4.10 IMPLICATIONS OF PIPE FORMATION	168
4.11 CONCLUSIONS	170
CHAPTER 5 – SOME CONSIDERATIONS ON THE FORMATION OF LARGE-SCALE SANDSTONE PIPES, SE UTAH	172
5.1 ABSTRACT	172
5.2 INTRODUCTION	173
5.3 GEOLOGICAL SETTING	174
5.3.1 Stratigraphic setting	174
5.3.2 Tectonic setting	177
5.3.3 Distribution of cylindrical sandstone pipes in SE Utah	178
5.4 PHYSICAL DESCRIPTION OF CYLINDRICAL SANDSTONE PIPES IN SE UTAH	179
5.4.1 Grain size and compositional variation	183
5.4.2 Transport direction	187
5.5 GENESIS OF SANDSTONE PIPES	187
5.6 PHYSICAL PROCESSES AND THEIR APPLICATION TO CYLINDRICAL PIPES IN SE UTAH	190
5.6.1 Transporting sand-sized grains	191
5.6.11 <i>Application of U_1 to sandstone pipes in the Lake Powell region</i>	194
5.6.12 <i>Pseudo-Fluid behaviour</i>	196
5.7 DISCUSSION	202
5.7.1 Compositional segregation of the pipe fill matrix	202
5.7.2 Transporting breccia blocks	205
5.7.3 Fluid flux and the duration of fluid flow	206

5.7.4 Applicability of homogeneous sand-water flow to the sandstone pipes of SE Utah	209
5.8 CONCLUSIONS	210
CHAPTER 6 – CONCLUSIONS	213
7.1 INTRODUCTION	213
7.2 HOST ROCK PROPERTIES	214
7.3 SAND REMOBILISATION AND FLUID FLOW	215
7.4 TRIGGERING REMOBILISATION	220
7.5 POST-EMPLACEMENT EFFECTS OF SAND INTRUSION	224
7.6 BASIN-SCALE SAND INTRUSION	225
REFERENCES	229

ACKNOWLEDGEMENTS

I would like to thank the many people that have helped me throughout my PhD, whether that be by discussing my ideas or reading my work, or by giving their support and being there when I needed them. In particular I would like to thank my supervisors, Joe Cartwright and Mads Huuse for all their help and guidance during my PhD studies. I would also like to thank Dennis Netoff and Renzo DiFelice for being so approachable and being prepared to share their specialist knowledge with me.

I am grateful to ExxonMobil and Schlumberger GeoQuest for providing seismic data and interpretation software and to Colin Harris and Keith Marshall of Robertson Research International Ltd for providing biostratigraphic analyses. Special thanks go to Dennis Netoff for sharing his knowledge on SE Utah and providing grain-size analyses and Renzo DiFelice for helping me explore the mechanics of fluidisation.

I would like to thank everyone who has helped and supported me through my PhD especially my friends, family and all the inmates of the graduate centre. Without these people around me, I seriously doubt whether I would have survived with my sanity intact! And finally, Mads, special thanks to you for giving up your time to discuss all my crazy ideas, read countless drafts of papers and listen to my rants and raves – I guess you'll be able to get on with your own research now!

LIST OF FIGURES

Figure Number	Caption	Page
Chapter 1		
1.1	A world map showing the distribution of sandstone intrusions referenced in this paper. Insets of the British Isles and North America are included to elucidate particularly dense distributions of published examples of sandstone intrusions in these regions.	4
1.2	A series of diagrams to illustrate the wide range of geometries seen in intrusive complexes: A) A highly irregular intrusive complex showing deformed sand bodies and sandstone dikes displaying varying amounts of compactional folding from Jameson Land, East Greenland (after Surlyk and Noe-Nygaard, 2001); B) A sill-dominated intrusive complex from Tabarka, Tunisia (after Parize, 1988); C) A sandstone dike swarm from the eastern side of Vancouver Island, Canada (after Rowe <i>et al.</i> , 2002).	11
1.3	Two diagrams describing different processes of dewatering and consolidation of a sand body: A) Homogeneous consolidation whereby water escapes evenly from the upper surface of the sand body resulting in an even pressure gradient across the body with depth (Terzaghi, 1943); B) Inhomogeneous consolidation whereby localisation of upward flow results in the formation of pipes of increased fluid-flow velocity, often causing fluidisation of the unconsolidated sand body, around which radial pressure gradients form (Kolymbas, 1998).	20
1.4	A diagram showing a range of unusual intrusive settings: A) Intrusion into a hot igneous sill as a result of the formation of super-critical fluids during sill emplacement before cooling and columnar jointing (Walton and O'Sullivan, 1950); B) Downward intrusion of buried sediments as a result of extensional faulting (Reeve, 1937; Vitanage, 1954; Harms, 1965; Montenant <i>et al.</i> , 1991; Beacom <i>et al.</i> , 1999). C) Post-tectonic dikes where intrusion occurs after the regional D ₁ event and S ₁ cleavage formation intrusions (Phillips and Alsop, 2000).	27
1.5	A) High fluid pressures in a sand body cause the hydraulic fracture of the body's caprock. B) If no sand is transported into the open fracture, it will heal after pressure within the sand body falls below the level required to keep the fracture dilated. C) However, if sand is transported into the fracture, when fluid pressure within the sand body falls below that required to keep the fracture open the fracture cannot close and is, in effect, propped open by the transported sand.	34
Chapter 2		
2.1	A) Location map. Study area located within area of three-dimensional seismic data (gray box). B) A regional seismic line showing stratigraphy of Eocene to Holocene strata including a complex of discordant high-amplitude reflections interpreted as sandstone intrusions emanating from Eocene sand-rich submarine fan. TWT—two-way travel time	50
2.2	A) A time-structure map (in two-way traveltime [TWT]) of intra-Neogene unconformity (INU) with superimposed outline (thick black lines) and contours, spaced every 100 ms	52

(thin black lines), of underlying sandstone intrusions mapped ~100–300 m deeper than unconformity. Topographic high (reds) of intra-Neogene unconformity surface are strongly spatially related to sandstone intrusion distribution. B) Seismic section through a topographic high showing close relationship between sandstone intrusions, forced folding of overlying sedimentary deposits, and formation of topographic highs. Note how reflections inside intrusion are upwardly domed (black dotted line), paralleling overlying intra-Neogene unconformity surface; also note that a high-amplitude package of reflections onlaps topographic high. This high-amplitude package may consist of extruded sandstone. IME—intra–middle Eocene strata. C) Schematic representation of B showing position of intruded sandstone bodies and associated uplift of overlying sedimentary deposits to form a topographic high on intra-Neogene unconformity surface. High is onlapped by later sedimentary deposits (black dotted lines).

- 2.3 A schematic diagram presenting a model for formation of conical sandstone intrusions in Faeroe-Shetland Basin. A: Pre-intrusion section and conditions. B: Formation of conical intrusions above which growth folds form and sand extrudes at surface. C: Post-intrusion burial (see text for a more detailed discussion). INU—intra-Neogene unconformity; IME—intra–middle Eocene strata; TB—top of Balder. 58

Chapter 3

- 3.1 A summary of the lithostratigraphy and tectonic history of the Atlantic margins basins, West of Britain (Holmes *et al.*, 1999). 63
- 3.2 A diagram showing the relationship between the distribution of sandstone intrusions within the study area (red semi-transparent region) and the main basement structural elements (Jowett *et al.*, 1999). Note that bulk of the sandstone intrusions seems to be closely related to the position of the Mid-Faroes Ridge and the Corona Ridge. 65
- 3.3 A) Regional 2D seismic line across the Faroe-Shetland Basin tied to three exploration wells. B) An interpreted seismic line across the Faroe-Shetland Basin showing the major basement fault blocks and overlying sedimentary strata. 67
- 3.4 Time thickness maps of: A) The Middle Eocene Strachan and Caledonian fans; B) The Eocene-Oligocene succession (between the Top Balder and INU); C) The Neogene-present contourite drift (between INU and seabed). 69
- 3.5 A) Palaeocene to Lower Eocene stratigraphy based on biostratigraphy and well log interpretation combined with seismic interpretation from Quads 214 and 206, West of Shetland (Knox *et al.*, 1997; Jowett *et al.*, 1999). B) A thickness map of Palaeocene strata showing the well-developed depocentre situated between the Rona Ridge and the Corona Ridge (Mitchell *et al.*, 1993). Sandstone intrusions in the study area (red semi-transparent area) are situated on the northern flank of the depocentre. 72
- 3.6 A) Polygonal fault plane dip with depth. Note the general trend towards shallower dips at greater depths. B) Intrusion dip with depth. Note that unlike polygonal faults, there is no systematic relationship between intrusion angle and depth. 74
- 3.7 Compaction of a fault: deeply buried sediments suffer greater levels of compaction due to increased overburden loading. Compaction of a dipping plane results in a reduced 76

angle of dip. Therefore, the greater the amount of compaction, the greater the shallowing of the plane.

- 3.8 A) Fault trace geometry for polygonal faults that do not propagate beyond the INU. Note that fault plane dip shallows with depth. Maximum fault displacements of 70 m to 100 m occur at depths of 700 m to 1000 m below the top of the fault trace. Kinks on the displacement plots in the shallow section (i.e.: more shallow than 800 m depth) are likely to be a result of interactions between closely spaced faults. B) Fault trace geometry for polygonal faults whose upper tips propagate beyond the INU into the basal units of the overlying contourite drift. There is a small growth package within the contourite drift at the upper tips of these faults. Note that the fault plane dip shallows with depth. Maximum displacements of 40 m to 50 m occur at depths of 200 m to 400 m below the top of the fault trace. Pronounced kinks or changes in gradient on the displacement plots occur in the shallow section (i.e.: more shallow than 160 m depth) these correspond to the presence of a growth package on the fault at the level of the INU. 77
- 3.9 A) Dip map of a complex array of polygonal faults (Blue marker horizon Fig.9b) showing the position of the seismic line shown in Fig.9b. B) Seismic section through the polygonally faulted Eocene-Oligocene claystone succession. Depth of variance slices in Figs.9d-h marked with dashed lines. C) Schematic of the seismic section in Fig.9b. Note how inward dipping bounding faults separate domains of high levels of brittle deformation and no brittle deformation. Zones of intense deformation become more localized with depth. D to H) Variance slices every 200 ms through the polygonally faulted section. Note how faulting becomes localized into intense segmented zones of deformation separated by regions of very little or no discernable deformation. 79
- 3.10 A) Dip map showing a complex array of polygonal faults (Blue marker horizon Fig.9b). B) Schematic diagram showing fault alignment. Downthrown hanging wall block denoted with a tick. Map of Fault intersections: Class A – Blue; Class B – Green; Class C – Red. D) Distribution of horizontal fault trace lengths. E) Comparison of fault strike and horizontal fault trace length showing a random distribution of fault lengths with fault orientation. F) Numbers of fault intersections of different classes – not the lack of Class C intersections and the dominance of Class B intersections. 80
- 3.11 Schematic diagram of the main fault intersection types for the polygonal fault system (after Lonergan *et al.*, 1988) with examples in dip map data from the Faroe-Shetland Basin. Class A – Two non-collinear faults intersecting at segment endpoints. Class B – A principal fault intersected by an adjoining fault at any angle. Class C – Three non-collinear faults intersecting at a common branch line forming intersection angles $>90^\circ$. Class D – Four or more faults intersecting. 81
- 3.12 A) Seismic section through a series of orphan conical sandstone intrusions with no observable feeder system. Note the range of different apex geometries including: pointed, rounded and flattened or bowl-shaped. Depth of variance slices marked with dashed lines. B to E) Variance slices every 100 ms through the polygonally faulted section containing the sandstone intrusions with an interpretation of the variance slice to the right (sandstone intrusions are marked in pale brown). Note how polygonal faults have a well-defined linear character whilst sandstone intrusions have a more globular texture. D) Intrusion apices are closely related to fault intersections. E) No evidence of a 84

- feeder system can be seen in the polygonally faulted section below the conical sandstone intrusions.
- 3.13 A) Location map showing the position of seismic lines X-X' and Y-Y' relative to the Caledonian and Strachan fans. B) Seismic line X-X' showing the position of two level sandstone intrusion network within the Eocene-Oligocene succession relative to the Caledonian Fan and an underlying high on the Top Balder surface. This high represents the Corona Ridge Fault block. C) Conical sandstone intrusions in the basal level of the intrusion network are physically linked to the Caledonian Fan. The top of level 1 is marked by a series of concordant high amplitude reflections likely to represent sandstone sills. Conical sandstone intrusion within level 2 are physically linked to the flat lying intrusions that mark the top of level 1. Conical sandstone intrusions in level 2 propagate upwards as far as the INU and cause uplift of the INU surface. 86
- 3.14 A time structure map (in two way travel time [TWT]) of the Top Balder surface. The elongate NE/SW orientated structural high in the north of the study represents the Corona Ridge fault block. Superimposed on this map are the positions of the Middle Eocene fans, the Caledonian Fan in the west of the region and the more highly constrained Strachan Fan in the East of the study area (semi-transparent grey areas surrounded by solid black lines) and the distribution of sandstone intrusions in the study area (pale region surrounded by a dashed black line). Note how the distribution of sandstone intrusions does not appear to closely resemble the distribution of the underlying Middle Eocene fans, but is instead appears to be more closely related to the NE/SW structural grain of the region. 88
- 3.15 A) A seismic line through a complex branching conical sandstone intrusion. The intrusion crosscuts pre-existing polygonal faults. B) A schematic drawing of the seismic section in Fig.15a. The throws of faults above and below the conical intrusion are very similar. However, the thickness of the intrusion is considerably greater than the throw on the fault implying that the whole block above the intrusion has been uplifted and the polygonal fault is crosscut by the conical intrusion. 90
- 3.16 A) Depth map of a polygonally faulted horizon below the INU (blue dashed line Fig.16c) with the position of underlying intrusions overlain. Local sub-circular highs on the mapped surface are closely spatially related to shallow conical sandstone intrusions. B) A dip map of the mapped surface above a shallow conical sandstone intrusion reveals that uplift above shallow intrusions is accommodated by the reactivation of the pervasive polygonal fault network and by the formation of reverse faults around the margins of the intrusion. C) Seismic sections through the mapped region: X-X' Shallow intrusions, underlain by deeper feeder intrusions, cause the uplift of the INU surface (green dashed line). Maximum uplift occurs above the thickest parts of the underlying intrusion (usually the apex) and the resultant extension of the overlying block is taken up by the reactivation of pre-existing polygonal faults. Note the presence of high-amplitude packages of post-INU contourite drift strata that onlap the mounded geometry on the INU formed as a result of intrusion and uplift. Y-Y' Uplift of strata overlying a shallow intrusion is not just facilitated by extension of the overlying strata, but also by the formation of reverse faults around the margins of the shallow intrusion. 94
- 3.17 A) A seismic section through a sandstone intrusion consisting only of a single limb 97

	emanating from a polygonal fault. B) A schematic drawing of the seismic section in Fig. 17a. Note that the polygonal fault from which the sandstone intrusion emanates displays normal throw beneath the intrusion, but reverse displacement above the intrusion. The total amount of throw above and below the sandstone intrusion is roughly equivalent to the thickness of the intrusion. This strongly implies that the intrusion process has resulted in the reactivation of the polygonal fault.	
3.18	Cumulative frequency plot of the dip populations of sandstone intrusions (solid black line) and polygonal faults (dashed black line) for an interval velocity of $1950 \text{ ms}^{-1} \pm 100 \text{ ms}^{-1}$ (represented by the grey envelope around each curve).	100
3.19	Schematic diagram of the effects of vertical compaction on a dipping unit. A conical sandstone intrusion (pale grey), which is V-shaped in cross-section, is hosted within a unit suffering homogenous vertical compaction of the section. This causes the rotation of the discordant limbs of the intrusion – in effect the dip of the sandstone intrusion becomes reduced with compaction.	103
3.20	A) Conical sandstone intrusions are intruded throughout a semi-compacted host rock sequence in a single intrusion event. B) After the emplacement event compaction of the host rock sequence continues. The greatest levels of compaction will occur at shallow levels where host rock porosity is greatest. Thus shallow sandstone intrusions will suffer the greatest levels of flattening due to compaction.	105
3.21	A) Conical sandstone intrusions are intruded in a series of temporally separate episodes. B) Further deposition after the initial emplacement event results in the compaction and flattening of the previous generation of conical intrusions. C) Subsequent deposition and emplacement episodes result in further compaction of the preexisting host rock sequence. Thus the discordant limbs of older intrusions will have more shallow dips than younger intrusions. It is also likely that later intrusive events will crosscut preexisting sandstone intrusions and that the feeder systems of older intrusions will become folded as a result of compaction of the host rock sequence.	107
Chapter 4		
4.1	Distribution of Jurassic rock outcrop and sandstone pipes (shown as black dots) in SE Utah (compiled from: Hannum, 1980; Hintze, 1988; Alvarez <i>et al.</i> , 1999; Netoff and Shroba, 2001; Netoff 2002)	116
4.2	(A) A simplified stratigraphic section from southwestern Utah to central Colorado showing the relation between the formations and regional unconformities discussed in this study (after Bjerrum and Dorsey, 1995). (B) A chronostratigraphic diagram of Fig. 3A (after Bjerrum and Dorsey, 1995).	123
4.3	Correlation of sections from the Paria River Valley showing the succession present within the Kodachrome Basin (Thompson and Stokes, 1970) and from Gunsight Butte (Thompson and Stokes, 1970; Baer and Steed, 2003) and Baker Ranch near Bullfrog (Doelling and Davis, 1990; Anderson <i>et al.</i> , 2003), describing the succession in the Lake Powell region. A general trend can be seen between the two regions: The Carmel Formation thins, whilst the Entrada Sandstone thickens between the Kodachrome Basin and Lake Powell. The lower members of the Carmel Formation represented in the Kodachrome basin are not present in the Lake Powell region. A) Large-scale cross-	125

- bedded sandstones and intercalated shales and mudstones within Gunsight Butte Member of the Entrada Sandstone in the Kodachrome Basin State Park. B) Large-scale cross-bedded sandstones within the Gunsight Butte Member of the Entrada Sandstone from Warm Creek Bay, Lake Powell. C) Faulted sandstone and intercalated mudstones within the Winsor Member of the Carmel Formation at Shepards Point in the Kodachrome Basin. D) Disturbed strata and possible fluid escape structures within the basal units of the Gunsight Butte Member of the Entrada Sandstone near the Henry Mountains.
- 4.4 Distribution of sandstone pipes relative to A) the underlying Page and Entrada Sandstones and B) Basement lineaments and uplifts (after Blakey, 1988). The distribution of pipes appears to be closely related to underlying basement structures. Several examples of sandstone pipes fall outside the margins of the Page Sandstone, however all recorded examples fall within the margins of the Entrada Sandstone. 127
- 4.5 Some examples of the different geomorphological expressions of sandstone pipes; (A) “Slick-rock exposures” with no topographical expression (B) Weathering pits; (C) Conical mounds; (D) Free-standing spires. In each case the contact between the host rock and the pipe is marked with a black dashed line. 131
- 4.6 (A) Chimney rock, a pipe expressed as a free sanding pipe in Kodachrome Basin State Park. The pipe sits within the Gunsight Butte member of the Entrada Sandstone (Jeg). The contact between the Gunsight Butte Member and the overlying Cannonville Member (Jec) is covered by scree slope (upper margin highlighted with a black dotted line), however the contact between the Cannonville and Escalante Members is easily identified are the J5 unconformity between the Escalante Member of the Entrada Sandstone and the Henreville Sandstone (Jh) and Tropic/Dakota Formations (Kdt) and the overlying Quaternary conglomerates (Qtco). (B) Breccia blocks within Chimney Rock display a low-angle pseudo layered fabric. (C) A large clast of chocolate brown mudstone with sand filled cracks discordant to bedding (white arrow), this distinctive block is likely to come from a bed of very similar material also showing a bedding parallel thin band of white sandstone and discordant sand filled cracks seen in a road cut at Shepard’s Point (D). This bed sits within the Winsor Member of the Carmel Formation, whilst Chimney rock has been eroded from the overlying Gunsight Butte Member of the Entrada Sandstone implying this breccia block was transported upwards from the underlying Winsor Member. 135
- 4.7 A) Large-scale collapse structure centred on a breccia pipe 15m wide within the Winsor Member of the Carmel Formation at Shepards Point near the Kodachrome Basin State Park. Person for scale (black arrow). B) Line-drawing showing strata consisting of massive sandstone intercalated with sandstone and mudstone interbeds dipping downwards towards a central pipe consisting of large breccia blocks (up to 1m in diameter) within a homogeneous sand and gravel matrix. Note that both the upper and lower terminations of the pipe have either been obscured by recent sediments or removed by erosion. 137
- 4.8 (A) “Slick-rock” exposures of lower Entrada Sandstone near the Henry Mountains with (B) a line drawing of the features seen including several sandstone pipes with little geomorphological expression or associated with weathering pits, the irregular faulted and domed contact between the Carmel Formation and the lower Entrada Sandstone and 139

- common extensional faulting within the lower Entrada. (C) The irregular contact between the brown silty Carmel Formation and the lower Entrada Sandstone. The Entrada Sandstone is heavily bleached near the contact. (D) A region with a four pipes (marked by white dashed lines) in close proximity located on the top of the hillside. Over 25 pipes were observed at this location. (E) A partially obscured pipe consisting of chocolate brown mudstone breccia fragments in a brown sandstone matrix indicative of transport of material from the underlying Carmel Formation. The pipe has a central weathering pit around which the orange Entrada Sandstone host rock is heavily bleached.
- 4.9 (A) Overview of a pipe with a highly complex geometry from Warm Creek Bay, Lake Powell. Several breccia bodies can be seen (highlighted with a black dotted line) and these are surrounded by concentrically fractured host rock blocks (white dotted lines). One breccia body can be seen to actively exploit a concentric fracture. (B) Several phases of breccia pipe emplacement can be seen at this location. In particular one small roughly circular pipe with small breccia clasts up to a few centimetres in diameter can be seen to cross cut the margins of an earlier, more irregularly shaped pipe body containing large breccia clasts several 10's of centimetres in diameter. (C) The intensity of brecciation decreases with distance along the concentric fracture from the pipe to which it is related. 142
- 4.10 A) View across Kodachrome State Park showing the stratigraphic relationship between the pipes (highlighted with white ovals) and the host sediments: the Middle Jurassic Entrada Sandstone made up of the Gunsight Butte Member (Jeg) the Cannonville Member (Jec) and the Escalante Member (Jee) which are separated from the Upper Jurassic Henrieville Sandstone (Jh) and the Cretaceous Tropic/Dakota formation by the J5 unconformity, which are in turn overlain by Quaternary gravels (Qtco). Exposures of free-standing pipes appear to be restricted to the Gunsight Butte Member of the Entrada Sandstone. B) Examples of impressive pipes standing over 20m above ground level are common in this region. C) A stratigraphic column through the rocks that outcrop within the Kodachrome Basin State Park (after Thompson and Stokes, 1970, Baer and Steed 2003) showing that pipes appear to be restricted to the Gunsight Butte Member or older rocks. 149
- 4.11 A) Small-scale faulting around a sandstone pipe within the Gunsight Butte Member of the Entrada Sandstone at Bullfrog, Lake Powell (notebook for scale). B) Movement along small-scale faults with throws of up to 40cm lends the pipe margin a ragged, stepped geometry. C) Irregular sandstone pipe and associated collapse structure situated within the Winsor Member of the Carmel Formation at Shepards Point. Strata within the collapse structure appear highly deformed. D) The collapse structure surrounding the sandstone pipe is highly irregular, its shape being locally affected by the competency of the rocks involved. The shape of the pipe is partially controlled by the collapse of material inwards towards the pipe i.e.: material within the collapse structure can protrude into the pipe body itself. 153
- 4.12 A model for pipe formation (for more detailed discussion see text): A) A liquefaction prone layer exists at depth within the section. B) In response to seismic shaking a pocket of unconsolidated sediment liquefies. Fluid pressure in the liquefied pocket equals the lithostatic pressure at the base of the pocket and a large pressure gradient exists between 165

the top of the liquefied pocket and the overburden. C) High fluid pressures within the liquefied pocket causes the hydraulic fracture and brecciation of the roof of the liquefied pocket. D) The contents of the liquefied pocket begin to settle, discrete pipes of focused upwards fluid flow form, where these reach the roof of the liquefied pocket they blast up into the overlying sediment. E) The pipe propagates to the surface. If the pressure within the liquefied pocket is not capable of sustaining high fluid velocities within the pipe solid material is not extruded onto the surface. F) The liquefied pocket settles without the formation of a collapse structure. G) The fluid pressure within the liquefied pocket is capable of sustaining high fluid velocities and solid material is extruded on to the palaeosurface. H) Extrusion of solid material leads to the depletion of the liquefied pocket and subsequent collapse of the overburden.

Chapter 5

- 5.1 Distribution of Jurassic rock outcrop and sandstone pipes (shown as black dots) in SE Utah (compiled from: Hannum, 1980; Hintze, 1988; Alvarez *et al.*, 1999; Netoff and Shroba, 2001; Netoff 2002). Most of the sandstone pipes appear to be situated within a few 10's km of underlying basement structures (distribution of basement structures after Blakey, 1988). 175
- 5.2 A) Generalised stratigraphic section through the Jurassic and Lower Cretaceous rocks of the Lake Powell region (after Anderson *et al.*, 2003) showing a marked change in drainage direction across the J3 unconformity (Bjerrum and Dorsey, 1995; Dickinson and Gehrels, 2003). B) Detailed stratigraphic log through the Entrada Sandstone in the Lake Powell region (Thompson and Stokes, 1970; Doelling and Davis, 1980). Note that there are no pipes present above the base of the Cannonville Member of the Entrada Sandstone. 176
- 5.3 A) Slick-rock section through a sandstone pipe from the Hanksville Pipe Swarm showing complex internal structure of pipe-fill, the presence of breccia blocks within the pipe and concentric faulting around the pipe margins. B) Small-scale faulting around a sandstone pipe within the Gunsight Butte Member of the Entrada Sandstone at Bullfrog, Lake Powell (notebook for scale). C) Movement along small-scale faults with throws of up to 40cm lends the pipe margin a ragged, stepped geometry. 180
- 5.4 A) Large-scale collapse structure centred on a breccia pipe 15m wide within the Winsor Member of the Carmel Formation at Shepards Point near the Kodachrome Basin State Park. Person for scale (black arrow). B) Line-drawing showing strata consisting of massive sandstone intercalated with sandstone and mudstone interbeds dipping downwards at around 30° towards a central pipe consisting of large breccia blocks (up to 1m in diameter) within a homogeneous sand and gravel matrix. Note that both the upper and lower terminations of the pipe have either been obscured by recent sediments or removed by erosion. 181
- 5.5 Average grain-size distributions from both sandstone pipe-fill matrix (solid black line) and the surrounding host rocks (dashed line) represented by the Gunsight Butte Member of the Entrada Sandstone. Diameter of clasts derived by particle size analysis (39 samples). 188
- 5.6 Compositional changes between in pipe-fill matrix relative to host rock based on 11- 189

paired samples. The amount of relative change was assessed by subtracting host rock values from pipe fill matrix values. Clast mineralogy, carbonate cement, clay coatings, interstitial clay and void space were determined petrographically by point counting (minimum of 500 counts per sample). Void space (porosity) determined by the ratio of voids to total point counts. Initial void space (initial porosity) determined by the ratio of void space + clay coatings + interstitial clay + carbonate cement to total point counts.

- 5.7 The settling velocity of spherical grains of differing composition and density within water (density 1030 kgm^{-3} , viscosity 0.0003 Pas). Grains of similar densities have similar settling velocities for a given grain size (eg: quartz, orthoclase and plagioclase). Increasing density results in a large increase in the settling velocity for a given grain size. Note that the settling velocity of magnetite is considerably higher than those of quartz or feldspar for a given grain size. 193
- 5.8 The effects of pseudo-fluid voidage (i.e.: 1-sand content) on the density and viscosity of the pseudo-fluid. Density increases linearly, however below a voidage of 0.5 the viscosity of the pseudo-fluid increases dramatically. 200
- 5.9 Settling velocities of spherical breccia blocks with diameters of 5 cm and 1 m and variable density, in a pseudo-fluid containing 54% sand. 54% sand is believed to be the highest sand content possible for fluidisation (Leva, 1959). This imparts a density of 1880 kgm^{-3} and a viscosity of 0.026 Pas . Note how the settling velocity drops dramatically as the density of the breccia block approaches that of the pseudo-fluid. 201
- 5.10 The settling velocity of spherical breccia blocks with a diameter of 1 m, but varying density in a pseudo-fluid containing 54% sand (density 1880 kgm^{-3} , viscosity 0.026 Pas) showing the differing transport domains. If $U < U_t$ the block will sink within the pipe, whilst if $U > U_t$ then the block will be entrained within the mobile fluid and transported upwards. Should the density of the pseudo-fluid be greater than that of the breccia block it will float buoyantly upwards. 203

LIST OF TABLES

Table Number	Caption	Page
1.1	Intrusion geometry	8
1.2	Propagation direction	8
1.3	Host rock depositional setting	15
1.4	Structures within sandstone intrusions	19
1.5	Sandstone intrusion cements	23
1.6	Tectonic setting of sand intrusion	23
1.7	Triggering mechanisms for sand intrusion	30
3.1	Well calibrations of sandstone intrusions	93
3.2	Examples of polygonal fault systems	101

CHAPTER 1 – INTRODUCTION AND LITERATURE REVIEW

1.1 INTRODUCTION

This PhD project used a combination of 3D seismic analysis and fieldwork to improve our understanding of some of the fundamental processes involved during the emplacement of sandstone intrusions in sedimentary basins.

Sandstone intrusions are an enigmatic class of soft-sediment deformation that have been studied for over 150 years. Sandstone intrusions originate from the remobilisation and subsequent injection of depositional sands into the surrounding host rocks. This process is commonly associated with fluid escape from the source unit. However, several aspects of the processes involved during sand intrusion including estimating the fluid flow velocity during intrusion, constraining the timing of the emplacement event, and the level dependence of sandstone intrusion geometry on pre-existing fractures are still quite poorly understood. Understanding the processes at work during the emplacement of sandstone intrusions is important because it may improve our understanding of the hydrodynamic evolution of the host sedimentary basin.

The emplacement of sandstone intrusions within a sedimentary basin is likely to have long-term effects on fluid migration within the basin because the sandstone intrusions themselves may provide high permeability conduits through otherwise low permeability caprocks. In hydrocarbon bearing basins, sandstone intrusions may act as

caprock breaches, enhance the hydrocarbon charge to shallow reservoirs, and even form reservoir sands in their own right.

This introduction chapter will introduce sandstone intrusions by reviewing the literature pertaining to sandstone intrusions and highlighting the current issues in this field of research. Background to the geological settings of the regions examined in the case studies, the data sets and methodologies employed will be provided in subsequent chapters. The aims of this study and the thesis structure is presented at the end of the chapter.

1.2 LITERATURE REVIEW

1.2.1 Introduction

Sandstone intrusions occur as concordant or discordant tabular sheets of sandstone that may branch, splitting into separate bodies or discordant sheets that may truncate primary depositional beds and structures. The process of sand intrusion involves the remobilisation of buried depositional sand and the intrusion of liquefied sand into the surrounding host rocks.

Sandstone intrusions have been studied have been studied for over 150 years (Strangeways, 1821; Murchison, 1827; Strickland, 1838; Judd, 1873; Diller, 1889; Pavlov, 1896; Ransome, 1900; Newsom, 1903) and they have been found worldwide in varied depositional and tectonic settings (Fig 1.1). Sandstone intrusions range in thickness from a few centimetres (e.g. Stephens *et al.*, 1953; Fielding and Johnson,

1987; Neef, 1991; Beacom *et al.*, 1999) to many tens of metres thick (e.g. Thompson *et al.*, 1999 Molyneux *et al.*, 2002). Individual intrusions may cross-cut hundreds of meters of host strata (e.g. Chapter 2; Molyneux *et al.*, 2002; Huuse *et al.*, 2004).

There is considerable debate over what the processes are acting during the emplacement of sandstone intrusions (e.g. Jolly and Lonergan, 2002). However previous work suggests that the initial remobilisation source body occurs in response to a triggering event such as earthquake shaking, sudden loading or the addition of fluid to the source sand Jolly and Lonergan, 2002 and references therein).

The presence of sandstone intrusions within a basin has important implications for the evolution and hydrodynamic history of the basin. Sandstone intrusions serve as a markers for important events during the evolution of the basin including large-scale fluid escape events (Chapters 3 and 4; Huuse *et al.*, 2004; Huuse and Mickleson, 2004), large-scale tectonic events (e.g. Chapters 3 and 4; Diraison *et al.*, 2000) and even individual seismic events (e.g. Obermier, 1996; Rosetti, 1999; Galli, 2000).

Therefore, if the timing of sand intrusion can be identified, the timing of fluid migration events within the host basin can be constrained. Sandstone intrusions are commonly emplaced within low-permeability fine-grained host rocks, and therefore possess high permeability relative to the encapsulating host rocks. As such they are likely to form effective fluid conduits through otherwise impermeable sequences (e.g. Hurst *et al.*, 2003). This characteristic has obvious implications for the extractive industries where fluid migration pathways are a major control on hydrocarbon prospectivity (e.g. Jenkins, 1930; Jonk *et al.*, 2003(a); Hurst *et al.*, 2003) and mineralisation (e.g. Ransome, 1900).

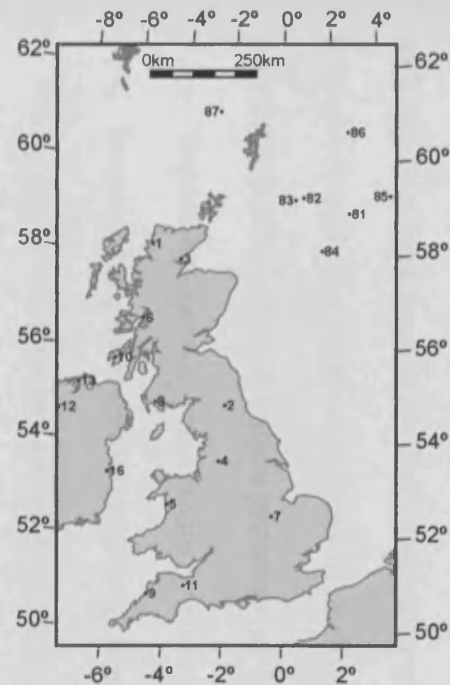
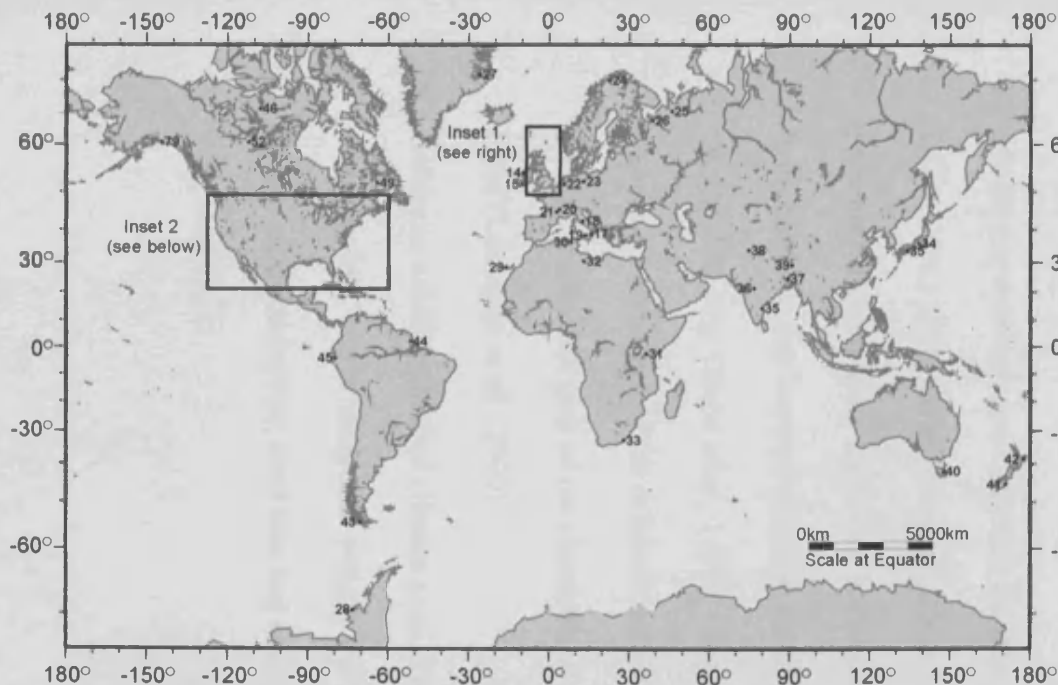
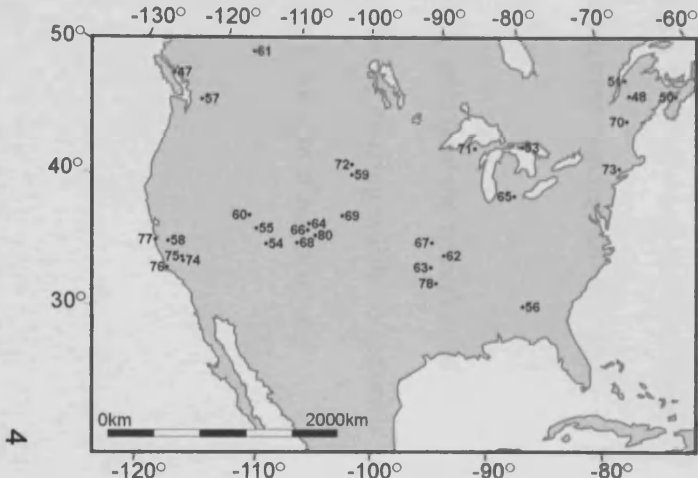


Fig 1.1 A world map showing the distribution of sandstone intrusions referenced in this paper. Insets of the British Isles and North America are included to elucidate particularly dense distributions of published examples of sandstone intrusions in these regions.



Location No.	Authors
1	Emmons et al. 1998
2	Fielding and Johnson, 1987
3	Strickland, 1938; Judd, 1973;
4	Waterson, 1980
5	Stephens et al. 1983
6	Bates, 1975
7	Smith and Rest, 1998
8	Mall and Hudson, 1989
9	Phillips and Alsop, 2000
10	King, 1970
11	Tarver, 1998
12	Muchison, 1921
13	Brandon, 1972
14	Phillips and Alsop, 2000
15	Strachen, 2002
16	Archer, 1984; Joly and Lonergan, 2002
17	Rijsdijf et al., 1999
18	Montenat et al., 1991
19	Call, 2000
20	Johansson et al., 1998; Parize et al., 1999
21	Rutten and Schönberger, 1987
22	Huang, 1988; Parize, 1998, 2001
23	Vanste et al., 1999
24	Newson, 1903
25	Williams, 1978
26	Parlov, 1998
27	Stangewiers
28	Suryk, 1957; Gjelberg et al., 2000;
29	Suryk and Nee-Nygaard, 2001
30	Taylor, 1982
31	Sturt and Furness, 1976
32	Bredden et al., 1988; Goffe, 1983
33	Reese, 1937

Location No.	Authors
32	Colomms, 1966
33	Trueman, 1972
34	Takahama et al., 2000
35	Hayashi, 1995
36	Mudholkar and Peshwa, 1998
37	Rais et al. 1985
38	Rao, 1995
39	Upadhyay, 2003
40	Clöhern and Malhe, 1972
41	Boulter, 1974
42	Lewis, 1973
43	Neal, 1991
44	Hindes, 1983
45	Anderson, 1944
46	Cecile and Campbell, 1977
47	Rose et al., 2002
48	Dionne and Shirts, 1974; Elson, 1975
49	Chown and Gobal, 1990
50	Marshall and Gibling, 1993
51	Mercot, 1979
52	Aspler and Donaldson, 1988
53	Erbacher, 1999
54	Ayres et al., 1998
55	Kriens et al., 1998
56	King, 1998
57	Carson et al., 1979
58	Diller, 1986; Paterson 1989; Joly et al., 1999
59	Boyd et al., 1999
60	Williams, 1927
61	Cherns, 1998; Wolf et al., 1998; Liu and Li, 2001

Location No.	Authors
62	Schwab and Marple 1991
63	Harris, 1985
64	Kahle, 2002
65	Vitarage, 1993
66	Brill, 1995
67	Rensom, 1900
68	McMillan, 1931
69	Moench, 1966
70	Powell, 1958; 1970; Janka, 1970
71	Rustad, 1927
72	Walton and O'Sullivan, 1960
73	Jenkins, 1930
74	Crymors and Peterson, 1971
75	Newson, 1903
76	Newson, 1903; Jenkins, 1930;
77	Thompson et al., 1999; Boehm and Bloos, 2002
78	Newson, 1903
79	Reimtz and Marshall, 1985
80	Cross, 1893
81	Tinardi, 1993; Newman et al., 1993;
82	Dixon et al., 1995
83	Donk and Stedman, 1993
84	Midyneux et al., 2002
85	Newson and Flanagan, 1993;
86	MacLeod et al., 1999; Durant and Hurst, 2002; Hillier and Cosgrove, 2002
87	Jensen et al., 1993
88	Hause et al., 2003
89	Hause et al., 2003
90	Shubert and Cartwright, In Press

In the past decade, the discovery of sandstone intrusions of sufficient volume to be economically viable as hydrocarbon reservoirs in several oil fields within the Tertiary sequences of the North Sea (e.g. Dixon *et al.*, 1995; Lonergan *et al.*, 2000; Huuse and Mickleson, 2004) has prompted a new wave of research into sandstone intrusion. Large-scale discordant sandstone intrusions are readily detectable in seismic data and well logs (e.g. Molyneux *et al.*, 2002; Duranti *et al.*, 2002). However the presence of sub-seismic scale (i.e. up to several metres thick) sandstone intrusions can also have a considerable effect on hydrocarbon prospectivity by:

- Enhancing reservoir connectivity by allowing pressure communication between different reservoir sands (e.g. Timbrell, 1993).
- Acting as seal breaches allowing migration out of potential reservoir sands (Huuse *et al.*, 2003)
- Modifying reservoir geometry and the distribution of hydrocarbons (e.g. Dixon *et al.*, 1995; Lonergan *et al.*, 2000; Huuse *et al.*, 2003). For example the presence of small-scale sandstone intrusions within the caprock may mean that hydrocarbons may become stranded within hard to access sandstones within the caprock (e.g. Dixon *et al.*, 1995). Large-scale sand intrusion may result in significant alteration of the original depositional geometry e.g. the discordant “wings” on the margins of the channelised sandstone making up the Alba Field (Lonergan *et al.*, 2000).
- Acting as a drilling hazard (Huuse *et al.*, 2005), effecting the selection of casing points, and drilling mud weight and possibly causing wellbore stability issues, sand production, mud loss and even gas blow-out if not properly mitigated for.

These factors have provided a need for field analogues to be studied and generic models for the formation of sandstone intrusions to be sought (Jolly *et al.*, 1998; Lonergan *et al.*, 2000; Surlyk and Noe-Nygaard, 2001; Jolly and Lonergan, 2002).

Neptunian dykes, which form through the passive infilling of fractures or karst structures open to the sediment surface (e.g. Smart *et al.*, 1998), will not be discussed further. This review will be restricted to forceful intrusion of sediment from a parent body into the surrounding host rocks.

1.2.2 The Physical Characteristics of Sandstone Intrusions

1.2.21 Sandstone intrusion geometry

Several broad geometrical groups of sandstone intrusions can be recognised from observations made at outcrop and in seismic data (Table 1.1): 1) sills 2) dykes 3) conical intrusions 4) cylindrical intrusions. The geometries of sandstone dykes and sills are analogous to the geometries of igneous dykes and sills in the upper crust (Johnson and Pollard, 1973; Pollard and Johnson, 1973; Delaney *et al.*, 1986; Delaney and Pollard, 1981; Hansen *et al.*, 2004; Trude, 2004). Following igneous intrusion nomenclature, a dyke is defined as a tabular body of intrusive material that cuts across the layering or structural fabric of the host rock and similarly a sill is defined as a tabular body whose boundaries are concordant with the planar structure of the host rock.

Sills

Small-scale sandstone sills that are concordant to host rock bedding have been recorded at a number of locations (e.g. Truswell, 1972; Parize, 1988). On closer inspections many sills display complex geometries. Sandstone sills may transgress to other planes within the host strata (e.g. Hiscott, 1979; Parize, 1988; Fries and Parize, 2003), split to form separate intrusive bodies (e.g. Truswell, 1972), and display highly variable thickness along strike (e.g. Surlyk and Noe-Nygaard, 2001).

Dykes

Sandstone dykes display high-angle discordance to bedding within the host rock. Dykes may be intruded upwards or downwards from the parent sand body (Table 1.2). The boundaries of sandstone dykes may be parallel (e.g. Parize, 1988; Chown and Gobeil, 1990), tapered (e.g. Rutten and Schönberger, 1957; Martill and Hudson, 1989), sinuous (Taylor, 1982) or irregular (Vaneste *et al.*, 1999). Ptygmatic folding of sandstone dykes may occur as a result of post-emplacement compaction of the host rocks (e.g. Truswell, 1972; Surlyk and Noe-Nygaard, 2001; Fries and Parize, 2003).

Conical sandstone intrusions

Large-scale, roughly conical high-amplitude anomalies, tied to discordant sand bodies tens of metres thick, have been observed using 3D seismic data in the North Sea and Faroe-Shetland Basin (Fig 2.3) (e.g. Chapters 3 and 4; Molyneux *et al.*, 2002; Huuse and Mickleson, 2004). This class of sandstone intrusion is commonly V-shaped in

1.1 Intrusion geometry

Geometry	Authors
Dykes	Ransome, 1900; Newsom, 1903; Williams, 1927; Jenkins, 1930; Reeve, 1937; Anderson, 1944; Walton and O'Sullivan, 1950; Vitanage, 1954; Brill, 1955; Rao, 1956; Rutten and Schönberger, 1957; Harms, 1965; Ookmens, 1966; Lewis, 1973; Williams, 1976; Taylor, 1982; Aspler and Donaldson, 1986; Parize, 1988; Martill and Hudson, 1989; Chown and Gobeil, 1990; Schweig and Marple, 1991; Martel and Gibling, 1993; Beacom et al., 1999; Rijdsdijk et al., 1999; Thompson et al., 1999; Phillips and Alsop, 2000; Surlyk and Noe-Nygaard, 2001; Boyd et al., 2001; Strachan, 2002.
Sills	Jenkins, 1930; Waterson, 1950; Stephens <i>et al.</i> , 1953; Truswell, 1972; Hiscott, 1979; Archer, 1984; Beaudoin, <i>et al.</i> 1986; Huang, 1988; Parize, 1988; Johansson <i>et al.</i> , 1998; Parize <i>et al.</i> , 1999; Surlyk and Noe-Nygaard, 2001; Jolly and Lonergan, 2002.
Conical Intrusions	Huuse <i>et al.</i> , 2001; Molyneux <i>et al.</i> , 2002; Gras and Cartwright, 2002; Huuse and Mickleson, 2004; Shoulders and Cartwright, 2004; Huuse <i>et al.</i> , In Press.
Cylindrical Intrusions	Hannum, 1980; Netoff, 2002; Huuse <i>et al.</i> , 2005.

Table 1.2 Propagation direction

Intrusion Direction	Authors
Upward	Williams, 1927; Jenkins, 1930; Ookmens, 1966; Lewis, 1973; Williams, 1976; Aspler and Donaldson, 1986; Martill and Hudson, 1989; Rijdsdijk <i>et al.</i> , 1999; Thompson et al., 1999; Molyneux et al., 2002; Strachan, 2002; Molyneux <i>et al.</i> , 2002; Gras and Cartwright, 2002; Shoulders and Cartwright, 2004; Huuse <i>et al.</i> , In Press(a); Huuse <i>et al.</i> , In Press(b).
Downward	Reeve, 1937; Anderson, 1944; Vitanage, 1954; Rutten and Schönberger, 1957; Harms, 1965; Parize, 1988; Chown and Gobeil, 1990; Martel and Gibling, 1993; Beacom et al., 1999
Lateral	Jenkins, 1930; Waterson, 1950; Stephens <i>et al.</i> , 1953; Truswell, 1972; Hiscott, 1979; Archer, 1984; Beaudoin, <i>et al.</i> 1986; Huang, 1988; Parize, 1988; Johansson <i>et al.</i> , 1998; Parize <i>et al.</i> , 1999; Surlyk and Noe-Nygaard, 2001; Jolly and Lonergan, 2002.

cross section and circular in plan view. Conical intrusions consist of a pointed or flattened basal apex from which discordant limbs intrude upwards.

Cylindrical intrusions

Cylindrical sandstone pipes have been observed in sandy host rock successions. Many sandstone pipes are believed to represent pillars of fluidised sand formed during fluid escape (e.g. Lowe 1975; Duranti and Hurst, 2004). However, sandstone pipes surrounded by large-scale host rock collapse structures are common in SE Utah (e.g. Chapters 4 and 5; Hannum, 1980; Netoff, 2002; Huuse *et al.*, 2005). The formation of a collapse structure implies that considerable volumes of material have been removed from the source unit and transported through the pipe (Chapters 4 and 5)

Sandstone dykes and sills are often observed in close association (Fig 1.2A, 1.2B). Sills form as branches from dykes (e.g. Stephens, 1953) or at the termini of dykes (Smyers and Peterson, 1971). Similarly, dykes may be fed from sills (e.g. Waterson, 1950; Truswell, 1972; Friès and Parize, 2003). Intrusion complexes made up of large numbers of individual intrusions dominantly consist of sills (e.g. Archer 1984; Friès and Parize, 2003), or dykes (Smyers and Peterson, 1971). The dominance of sills or dykes may vary between different regions of the same intrusion complex (Surlyk, 1987; Surlyk and Noe-Nygaard, 2001). The contacts between the sandstone intrusions and the encapsulating host rocks are commonly sharp. However, considerable variation in contact morphology has been observed. The contacts between a sandstone intrusion and its host may be irregular (e.g. Martell and Gibling, 1993; Rijdsdijk,

1999), smooth (e.g. Truswell, 1972; Parize, 1988), show striations (Waterson, 1950; Brandon, 1970), or be brecciated (Brill, 1955)

1.2.21 Intrusion scale

Sandstone dykes may be up to several tens metres thick (e.g. Thompson *et al.*, 1999) however, the majority of sandstone intrusions within the published literature are only a few centimetres thick and are usually attributed to immediate post-depositional or even syn-depositional processes. The largest observed sandstone sills are up to 50m thick (Newsom, 1903; Jenkins, 1930; Thompson *et al.*, 1999; Boehm and Moore, 2002), but with the vast majority being <2m (e.g. Waterson, 1950; Truswell, 1972). The areal dimensions of sandstone sills vary from a few square centimetres to examples covering several square kilometres (e.g. Friès and Parize, 2003; Huuse *et al.*, 2004).

Some of the largest sandstone intrusions (i.e. tens metres thickness) have been recognised using 3D seismic data (Chapters 2 and 3; Lonergan and Cartwright, 1999; Molyneux *et al.*, 2002; Huuse and Mickleson, 2004; Huuse *et al.*, 2004). Conical sandstone intrusions are commonly up to 1.5 km in diameter and cross-cut a few hundred of meters of host strata. Well data show that conical sandstone intrusions may be 10's of metres thick (e.g. Molyneux *et al.*, 2002 Huuse and Mickleson, 2004). Volumetric analysis of a conical intrusion in the Tampen Spur area (Quad 34, Norwegian North Sea) showed that it contains around 40 to 50 x 10⁶ m³ of sand (Huuse and Mickleson, 2004).

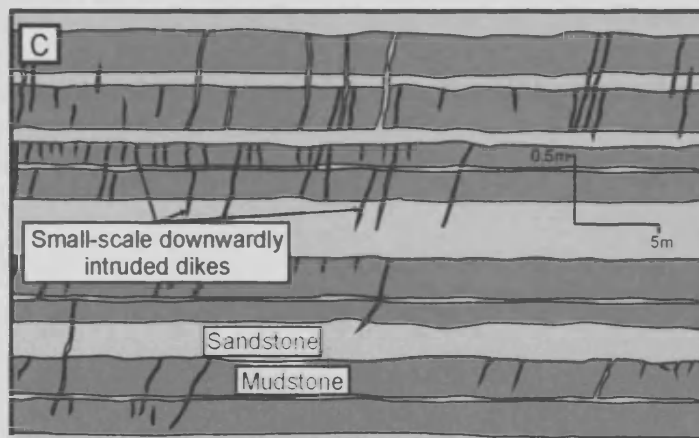
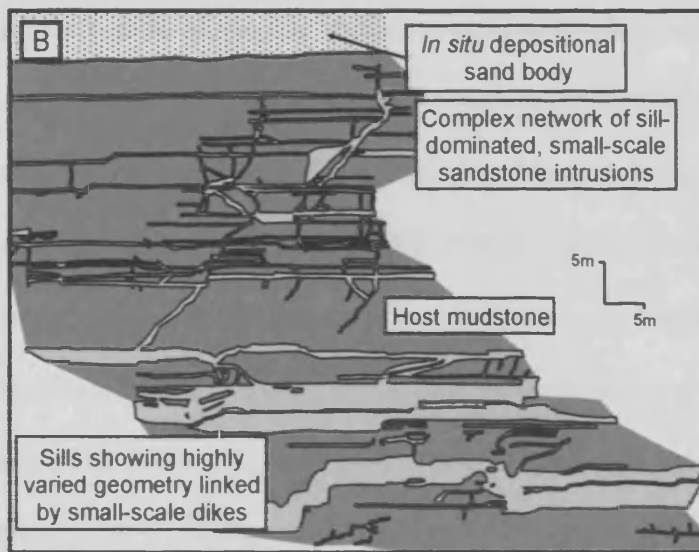
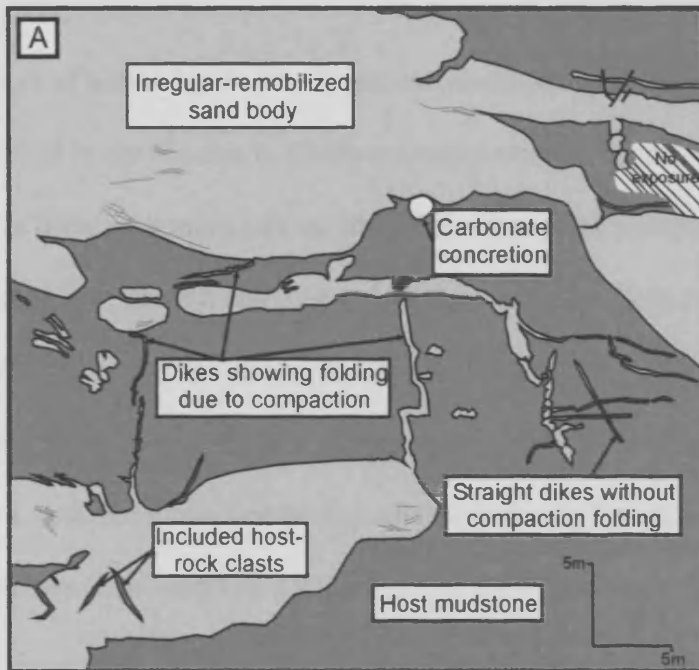


Fig 1.2 A series of diagrams to illustrate the wide range of geometries seen in intrusive complexes: A) A highly irregular intrusive complex showing deformed sand bodies and sandstone dykes displaying varying amounts of compactional folding from Jameson Land, East Greenland (after Surlyk and Noe-Nygaard, 2001); B) A sill-dominated intrusive complex from Tabarka, Tunisia (after Parize, 1988); C) A sandstone dyke swarm from the eastern side of Vancouver Island, Canada (after Rowe *et al.*, 2002).

1.2.23 Burial depth of the parent body during the intrusive event

A range of burial depths for the parent sandstone body at the time of intrusion are described in the literature. These estimates range from direct measurements of a few meters between source and surface where exceptional outcrop is found (Gill and Kuenen, 1958; Smith and Rast, 1958; Strachan, 2002), to calculated depths of up to several kilometres (Winslow, 1983; Thompson *et al.*, 1999; Phillips and Alsop, 2000). Often there may be excellent exposure of the intrusion or intrusion complex, but the parent sand body may not be identifiable or it may be unclear where the intrusion terminates (e.g. Brandon, 1972).

During the course of specific studies several methods have been developed to determine the burial depth of the source unit at the time of sand intrusion. These include: 1) Reconstruction of tectonically folded dykes and decompaction calculations (Allen 1982; Parize 1988; Hillier and Cosgrove 2002); 2) Theoretical approaches based on intrusion mechanics (Jolly and Lonergan, 2002; discussed by James, 2003; Jolly and Lonergan, 2003); 3) The use of metamorphic and hydrothermal mineral assemblages in deeply buried parent bodies (Walton and O'Sullivan, 1950; Phillips and Alsop, 2000); 4) Decompaction of host strata assuming intrusion to the palaeosurface (Huuse *et al.*, 2004). Whilst these approaches offer some opportunities for quantifying depths of the parent body at the inception of intrusion, they may only apply to particular intrusive environments.

1.2.24 Spatial distribution and orientation of sandstone intrusions

Sandstone intrusions have been used to infer the palaeostress regime or palaeoslope at the time of emplacement by examining their preferred orientations (Vitanage, 1954; Harms, 1965; Winslow, 1983; Huang, 1988; Montenat *et al.*, 1991; Jolly *et al.*, 1998; Beacom *et al.*, 1999; Diraison *et al.*, 2000; Boehm and Moore, 2002; Rowe *et al.*, 2002). Intrusions used in this way are commonly hosted in basement rocks (Vitanage, 1954; Harms, 1965; Beacom *et al.*, 1999) and are related to the forceful downward intrusion of buried sediments into extensional fractures within the basement rock. Such intrusions can be distinguished from neptunian dykes formed through the passive infill of fractures open to the sediment surface by the presence fabrics and clasts orientated parallel to the walls of the intrusion indicative of forceful intrusion.

The identification of a preferred orientation for sand intrusion has been used to imply that the intermediate effective compressive stress is very much greater than the minimum effective compressive stress (Vitanage, 1954; Harms, 1965; Huang, 1988; Jolly *et al.*, 1998; Beacom *et al.*, 1999; Diraison *et al.*, 2000; Boehm and Moore, 2002). Intrusion occurs roughly parallel to the intermediate effective stress due to dilation in the direction of minimum effective stress. This method has been applied in both extensional and strike-slip tectonic regimes.

Large-scale conical sandstone intrusions are commonly found within thick polygonally faulted claystone sequences (e.g. Lonergan *et al.*, 2000; Huuse *et al.*, 2004). The spatial distribution and geometry of the conical intrusions commonly

appears to mimic polygonal fault fabric leading to an inference of fault control on conical intrusion (Lonergan *et al.*, 2000; Gras and Cartwright, 2002; Molyneux *et al.*, 2002). However, observations of conical intrusions cross-cutting polygonal faults have been made (e.g. Chapter 3; Huuse *et al.*, 2004) and a large disparity between the dip of the discordant limbs of sandstone intrusions (Section 3.5.6) and the inclination of polygonal faults (Section 3.5.1) is present in Tranche 6 of the Faroe-Shetland Basin. These observations imply that polygonal faults may not always control the morphology of conical sandstone intrusions.

1.2.25 Intrusive materials

The composition of sandstone intrusions is dependant upon the composition of the parent sand body. Therefore, it should be expected that the composition of sandstone intrusions will be as varied as the parent sand bodies to which they are related (e.g. Table 1.3).

Clastic materials with grain sizes ranging from mud (e.g. Morely 2003; Hansen *et al.*, 2005), to grits and cobbles (e.g. Ransome, 1900; Walton and O'Sullivan, 1950; Cecile and Campbell, 1977; Rijdsijk *et al.*, 1999; Upadhyay, 2003) can be remobilised and intruded into the surrounding host rocks. However, fine and medium-grained sands are the most commonly remobilised and intruded materials (e.g. Russel, 1927; Hiscott, 1979; Neef, 1991; Jenssen *et al.*, 1993). Most sandstone intrusions consist of quartz-rich sands with varying quantities of accessory feldspar, chert, heavy minerals and lithic clasts. Intrusions containing clastic limestone or calcarenite sands are

Table 1.3 Host rock depositional setting

Depositional Setting	Authors
Lacustrine	Ookmens, 1966; Aspler and Donaldson, 1986; Martel and Gibling, 1993
Fluvio-deltaic and near shore	Stephens <i>et al.</i> , 1953; Powel, 1969, 1970; Janke, 1970; Boulter, 1974; Sturt and Furnes, 1976; Tanner, 1998; Rossetti, 1999
Deepwater systems (including Slumping)	Diller, 1889; Newsom, 1903; Jenkins, 1930; Gill and Kuenen, 1958; Smith and Rast, 1958; Peterson, 1968; Smyers and Peterson, 1971; Brandon, 1972; Truswell, 1972; Taylor, 1982; Newman <i>et al.</i> , 1993; Newton and Flanagan, 1993; Doenie and Steadman, 1993; Timbrell, 1993; Jenssen <i>et al.</i> , 1993; Dixon <i>et al.</i> , 1995; Johansson <i>et al.</i> , 1998; Jolly <i>et al.</i> , 1998; Thompson <i>et al.</i> , 1999; Parize <i>et al.</i> , 1999; MacLeod <i>et al.</i> , 1999; Surlyk and Noe-Nygaard, 2001; Boehm and Moore, 2002; Jolly and Lonergan, 2002; Huuse <i>et al.</i> , 2002; Molyneux <i>et al.</i> , 2002; Duranti and Hurst, 2002; Strachan, 2002; Shoulders and Cartwright, 2004.
Glacial Systems	Dionne and Shilts 1974; Elson 1975; Larsen and Mangerud 1992; Rijdsdijk <i>et al.</i> , 1999

observed in a small number of cases (Brill, 1955; Stewart and Furnes, 1976; Mudholkar and Peshwa, 1988; Montenant *et al.*, 1991).

The composition of the intruded material may allow the fingerprinting of the intrusion fill to a particular parent sand body (Reeve, 1937; Anderson, 1944; Rao *et al.*, 1956; Vitinage, 1954; Harms, 1965; Winslow, 1984; Johansson *et al.*, 1998; Parize *et al.*, 1999) or allow the identification of different phases of intrusion (Eisbacher, 1969; Taylor, 1982; King, 1998; Beacom *et al.*, 1999). This is achieved by close examination of the petrology of the constituents of the intrusion including the proportions of different minerals, grain-sizes, cements and in particular taking note of any heavy mineral fraction within the constituents of the intrusion (e.g. Anderson, 1944). Detailed analysis of these factors can then allow direct comparisons to be made between intrusions and possible parent bodies or other possible phases of intrusion.

Many sandstone intrusions contain breccia blocks derived from the host rocks (e.g. Diller, 1889; Newsom, 1903; Cecile and Campbell, 1977; Taylor, 1982; Dixon *et al.*, 1995; Surlyk and Noe-Nygaard, 2001). These blocks may be ripped off the walls of the intrusion through erosion and abrasion during sand emplacement, or result from the failure of the host rocks during hydrofracture at the intrusion tip. Exotic breccia blocks that can be traced to their source units can be used to trace the vertical extent of downward propagating intrusions where subsequent erosion has removed large quantities of cover rocks (Harms, 1965) or to determine the direction of emplacement (Chapters 5 and 6; Rao, 1956; Hannum, 1980). Such xenoliths can be used in a similar way to petrographic studies of the constituent sediments of the intrusion to trace source regions and the extent of intrusion where exposure is unavailable. However, it

should be noted that this method tells us about the host rocks the intrusion has passed through and not necessarily about the source of the intruded material itself. Thus the context of the data must be considered carefully before any conclusions are drawn (Kugler, 1938).

The composition of a sandstone intrusion has been observed to vary with distance from the parent sand body (Brill, 1955; Moench, 1966; Taylor, 1982). Distal parts of sandstone intrusions have been observed to display decreased grain-size (Moench, 1966; Taylor, 1982), increased mica content (Taylor, 1982), and increased frequency of host rock clasts (Brill, 1955). Observations of decreased grain-size and increased mica content towards intrusion terminations implies that such grains may be transported in preference to larger or more rounded grains during the emplacement event. Consequently platy or fine-grained grains may represent the first material entrained and sequestered from the source sand body. An increase in the frequency of host rock clasts towards the tips of dykes, relative to the main body of the intrusion, sometimes to the extent that the tips of some intrusions are more like breccias set within a reticulate vein network of sandstone intrusions can be observed in shallow marine limestones near St. Louis (Brill, 1955). This may represent a “frozen” example of how the crack tip of a sandstone intrusion propagates through the host material.

1.2.26 Internal structures and grain-size distributions

Internal structures and grain-size variations present within sandstone intrusions are well documented (Table 1.4). However, many other sandstone intrusions are homogeneous or massive (Table 1.4). Any internal structures observed within

sandstone intrusions may be formed during the emplacement of the intrusion and as a result are a product of the physical processes occurring during intrusion. Alternatively they may result from dewatering and soft sediment deformation of the intruded sand once emplacement has ceased.

Sandstone intrusions may contain dewatering structures including cylindrical fluidisation pipes (e.g. Lowe, 1975; Peterson, 1968 Duranti and Hurst 2004). It is likely that these pipe structures form due to focused fluid escape during compaction and dewatering causing localised fluidisation of the sand. During homogeneous consolidation, fluid escapes upwards through the granular sediment evenly (i.e. Terzaghi, 1943) (Fig 1.3). However, inhomogeneous velocity fields are encountered in experimental studies (Kolymbas, 1998). Thus upward fluid escape becomes localised implying that pore fluids move radially towards vertical channels of focused upwards fluid escape during dewatering, locally fluidising the sediment to form pipes (Kolymbas, 1998) (Fig 1.3).

1.2.27 Cements present within sandstone intrusions

A range of materials have been observed acting as cements in clastic intrusions exposed at the surface (Table 1.5). Some sandstone intrusions exhibit more unusual mineralisation, minerals such as zeolites (Rais *et al.*, 1985), pyrite and sphalerite (Martill and Hudson, 1989), epidote, chlorite, pyrite and garnet (Walton and O'Sullivan, 1950) and even economic deposits of frieburgite (A silver ore) (Ransome, 1900) have been observed in sandstone intrusions.

Table 1.4 Structures within sandstone intrusions

Internal Structure	Authors
Grain-size segregation and grading	Diller, 1889; Moench, 1966; Peterson, 1968; Eisbacher, 1969; Bates, 1975; Taylor, 1982; Archer, 1984; Winslow, 1983; Aspler and Donaldson, 1986; Jolly <i>et al.</i> , 1998; Rijdsijk <i>et al.</i> , 1999; Jolly and Lonergan, 2002
Flow laminations	Cecile and Campbell, 1977; Taylor, 1982; Winslow, 1983; Archer, 1984; Martill and Hudson, 1989; Neef, 1991; Beacom <i>et al.</i> , 1999; Thompson <i>et al.</i> , 1999; Rijdsijk <i>et al.</i> , 1999; Jolly and Lonergan, 2002
Alignment of platy clasts parallel to intrusion walls	Stephens <i>et al.</i> , 1953; Rao, 1956; Smith and Rast, 1958; Ookmens, 1966; Lewis, 1973; Stewart and Furnes, 1976; Surlyk, 1987; Chown and Gobiell, 1990; Gjelburg <i>et al.</i> , 2000; Surlyk and Noe-Nygaard, 2001
Dish and pillar structures	Hiscott, 1979; Montenant <i>et al.</i> , 1991; Duranti and Hurst, 2002
Fluidisation pipes	Peterson, 1968
Homogeneous/massive	Ransome, 1900; Williams, 1927; Russel, 1927; Jenkins, 1930; McMillian, 1931; Waterson, 1950; Smyers and Peterson, 1971; Brandon, 1972; Williams, 1976; Rais <i>et al.</i> , 1985; Mudholkar and Peshwa, 1988; Martell and Gibling, 1993; Johansson <i>et al.</i> , 1998; Parize <i>et al.</i> , 1999; Phillips and Alsop, 2000; Strachan, 2002

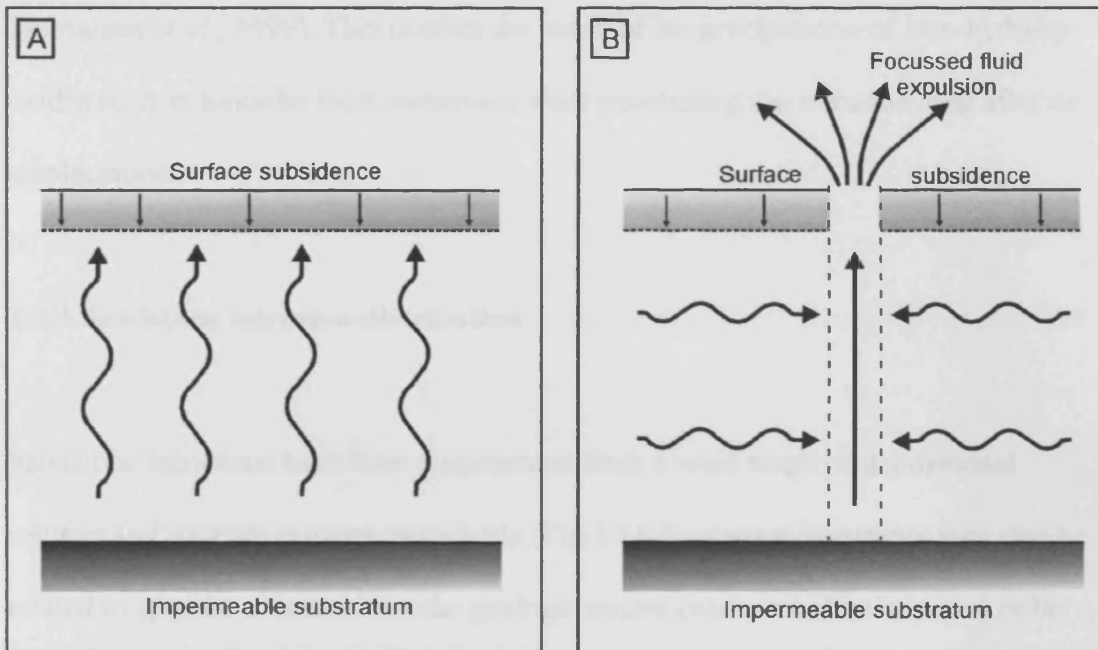


Fig 1.3 Two diagrams describing different processes of dewatering and consolidation of a sand body: A) Homogeneous consolidation whereby water escapes evenly from the upper surface of the sand body resulting in an even pressure gradient across the body with depth (Terzaghi, 1943); B) Inhomogeneous consolidation whereby localisation of upward flow results in the formation of pipes of increased fluid-flow velocity, often causing fluidisation of the unconsolidated sand body, around which radial pressure gradients form (Kolymbas, 1998).

Pseudo-structures and secondary mineral staining is often seen in field examples (e.g. Thompson *et al.*, 1999). This is often the result of the precipitation of iron-hydroxy oxides such as limonite from meteoric waters penetrating the intrusion long after its emplacement.

1.2.3 Sandstone intrusion distribution

Sandstone intrusions have been documented from a wide range of depositional settings and tectonic regimes worldwide (Fig 1.1). Sandstone intrusions may also be related to specific events within the geologic record (such as bolide impacts) or be hosted within igneous or basement rocks.

1.2.31 Tectonic setting

Sandstone intrusions are found in sedimentary basins controlled by a wide range of tectonic regimes (Table 2.6). The largest and most geometrically complex sandstone intrusions and intrusion complexes are associated with basins undergoing subsidence or are otherwise tectonically active and are therefore prone to seismic events (Jolly and Lonergan, 2002). One possible reason for this is that cyclic shear stress caused by earthquakes can cause sediment remobilisation through liquefaction (e.g. Oldham and Mallet, 1872; Plint, 1983; Obermeirer, 1996; Rossetti, 1999; Galli, 2000; Takahama *et al.*, 2000). In addition, the stresses associated with active tectonism can result in the development of high pore fluid pressures that may facilitate hydrofracture and sandstone intrusion (Jolly and Lonergan, 2002). Sandstone intrusions are found in

sedimentary basins associated with extensional, compressional or strike-slip tectonics (Table 1.6).

Sandstone intrusions are commonly found in extensional and strike-slip tectonic regimes (Table 1.6). However, observations of sandstone dyke swarms orientated perpendicular to thrust wedges in the Tierra del Fuego, within southernmost parts of the Andes, have been interpreted as sandstone intrusion during thrusting (Winslow, 1983). Emplacement of the thrust wedge was believed to have caused instantaneous loading in overpressured sediments under the thrust wedge. This resulted in the remobilisation and upward injection of sediment along pre-existing cross-joints perpendicular to the thrust front (Winslow, 1983). However, Neogene rifting orientated perpendicular to the thrust front has been identified in the Magellan Basin (Diraison *et al.*, 1997), and is associated with sandstone intrusions (Diraison *et al.*, 2000). This has led to the re-interpretation of the sandstone intrusions as occurring during Neogene rifting under an extensional regime (Diraison *et al.*, 2000) as opposed to late Mesozoic to Cenozoic thrusting (Winslow, 1983).

Table 1.5 Sandstone intrusion cements

Cementing Mineral	Authors
Calcite	Diller, 1889; Newsom, 1903; Williams, 1927; Reeve, 1937; Walton and O'Sullivan, 1950; Waterson, 1950; Rutten and Schönberger, 1957; Peterson, 1968; Powel, 1969, 1970; Janke, 1970; Winslow, 1983, Aspler and Donaldson, 1986; Martill and Hudson, 1989; Montenant <i>et al.</i> , 1991; Jolly <i>et al.</i> , 1998
Dolomite	Eisbacher, 1969; Brandon, 1972; Cecile and Campbell, 1977; Thompson <i>et al.</i> , 1999
Quartz	Walton and O'Sullivan, 1950; Cecile and Campbell, 1977; Winslow, 1983; Johansson <i>et al.</i> , 1998; Parize <i>et al.</i> , 1999;
Chlorite	Hiscott 1979; Chown and Gobeil 1990
Gypsum	Smyers and Peterson, 1971; Jolly and Lonergan, 2002

Table 1.6 Tectonic setting of sand intrusion

Tectonic Regime	Authors
Extensional	Cross, 1893; Reeve, 1937; Vitanage, 1953; Harms, 1965; Montenant <i>et al.</i> , 1991; Beacom <i>et al.</i> , 1999; Diaision <i>et al.</i> , 2000
Compressional	Winslow, 1983
Strike-slip setting	Diller, 1998; Newsom, 1903; Jenkins, 1930; Peterson 1968; Smyers and Peterson, 1971; Aspler and Donaldson, 1986; Neef, 1991; Schweig and Marple, 1991; Rossetti, 1999; Thompson <i>et al.</i> , 1999; Boehm and Moore, 2002; Jolly and Lonergan, 2002

1.2.32 Depositional environment of parent body

Sandstone intrusions can be derived from sediments deposited in a wide spectrum of depositional environments and as a result the constituent sands comprise of a range of possible compositions. Sandstone intrusions have been recorded that emanate from parent sand bodies deposited in: 1) Lacustrine sediments. 2) Fluvio-deltaic, deltaic and near shore sediments. 3) Deep-water settings. 4) Sub-glacial sediments. 5) Aeolian deposits (Table 1.3)

Sandstone intrusions are commonly found in basins containing hydrocarbon source rocks (e.g. the North Sea and Faroe-Shetland Basins). Sandstone intrusions within such basins are commonly hydrocarbon saturated at the present day (e.g. Jenkins, 1930; Lonergan *et al.*, 2000; Huuse *et al.*, In Press). It is in these depositional environments that the largest individual intrusions and intrusion complexes are found (e.g. Dixon *et al.*, 1995; Thompson *et al.*, 1999; Surlyk and Noe-Nygaard, 2001; Huuse *et al.*, 2004). Deep-water systems have moderate to high sedimentation rates and offer good opportunities for development of an efficient early seal. The very fine-grained nature of background pelagic and hemi-pelagic sedimentation produces seals which can allow overpressure to build up within suitable parent sand bodies (Jolly and Lonergan, 2002). There is a large field-based literature describing intrusions related to deep water sediments, which is augmented by a wide range of studies based on data sourced from the hydrocarbons industry, including 3D seismic surveys and data from sediment cores (Table 1.3).

A subset of the clastic intrusions observed in deep-marine facies is related to slumping. Intrusion may be a secondary effect occurring after slump emplacement, during the consolidation and dewatering of the highly disturbed slumped sediments (Gill and Kuenen, 1958; Smith and Rast, 1958; Strachan, 2002) or a response to sudden loading due to the emplacement of slump debris (Truswell, 1972; Taylor, 1982; Rowe *et al.*, 2002).

1.2.33 Exotic and unusual settings for sand intrusion

Sandstone intrusions have been discovered in some unusual settings including bolide impact craters (e.g. King, 1998; Kriens *et al.*, 1999), igneous host rocks (Walton and O'Sullivan, 1950; Lewis, 1973; Sturt and Furnes, 1976) (Fig 1.4A), crystalline basement rocks (Cross, 1893; Reeve, 1937; Vitange, 1954; Harms, 1965; Beacom *et al.*, 1999) (Fig 1.4B), and even deep below the surface *after* the first phase of regional deformation (Diraison *et al.*, 2000; Phillips and Alsop, 2000) (Fig 1.4C). Although intrusions within these exotic settings make up only a small fraction of the total number of sandstone intrusions documented, they show that the conditions required for sandstone intrusion can be met in a wide range of environments and or involve unusual triggering mechanisms.

Sandstone intrusions may be found within impact craters (King, 1998; Kriens *et al.*, 1999) where they are attributed to the moat material behaving as a Bingham plastic fluid when massive forces are applied to the wet sediment during impact (Melosh, 1989). Much more widespread regions of soft sediment deformation and sand

intrusion have also been attributed to large impacts (e.g. Alvarez *et al.*, 1988; Terry, *et al.*, 2001; Simms, 2003) although other origins are possible (Chapter 4; Netoff, 2002).

Sandstone intrusions have been observed within crystalline metamorphic and igneous rocks. The formation of such intrusion can be linked to either: 1) Extensional basement faulting (Fig 1.4B) (Cross, 1893; Reeve, 1937; Vitanage 1954; Harms, 1965; Beacom *et al.*, 1999). 2) Short-lived thermal effects associated with the emplacement of igneous bodies (Walton and O'Sullivan, 1950; Lewis, 1973; Sturt and Furnes, 1976) (Fig 1.4A). Key factors that drive sand intrusion due to thermal effects include: the thermal expansion of fluids, formation of supercritical fluids and hydrothermal activity. Sand intrusion resulting from thermal effects is distinct from peperite formation because there is no physical mixing of fractured magma and host sediment (Kokelaar, 1982; Goto and McPhie, 1996; Kano, 2002; Skilling *et al.*, 2002; Wohletz, 2002)

Sandstone intrusion may occur long after the deposition of the source sands.

Sandstone dyke swarms in Tierra del Fuego in the southern Andes resulting from Neogene extension (Dirasion, *et al.*, 2000) truncate the regional S₁ cleavage formed during the first phase of regional deformation. They are intruded perpendicular to the fold and thrust belt and contain the overprint of the regional S₂ cleavage related to later regional deformation (Winslow, 1983). Sandstone intrusions containing reworked, claystone clasts containing an S₁ cleavage intruded along and sub-parallel to the F₁ axial plane have been observed in the Dalradian successions of Scotland and Ireland (Phillips and Alsop, 2000) (Fig 1.4C).

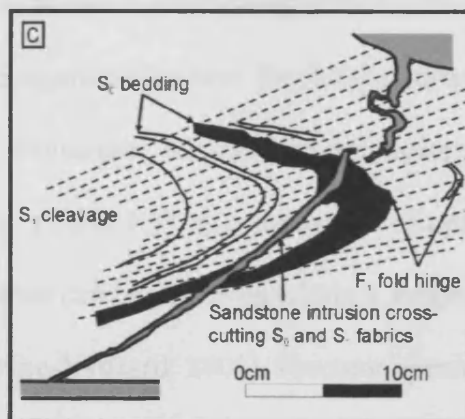
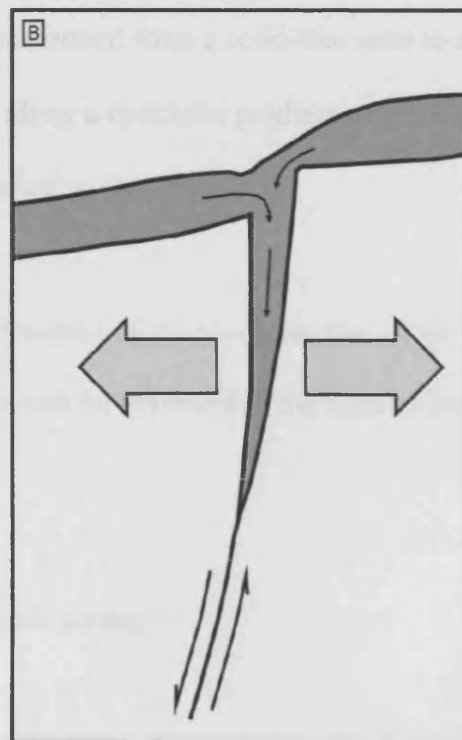
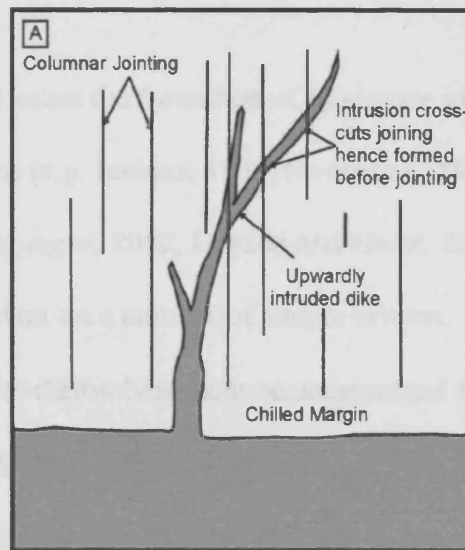


Fig 1.4 A diagram showing a range of unusual intrusive settings: A) Intrusion into a hot igneous sill as a result of the formation of super-critical fluids during sill emplacement before cooling and columnar jointing (Walton and O'Sullivan, 1950). B) Downward intrusion of buried sediments as a result of extensional faulting (Reeve, 1937; Vitanage, 1954; Harms, 1965; Montenant *et al.*, 1991; Beacom *et al.*, 1999). C) Post-tectonic dykes where intrusion occurs after the regional D_1 event and S_1 cleavage formation intrusions (Phillips and Alsop, 2000).

1.2.4 Mechanisms of sand intrusion

The processes that cause the formation of sandstone intrusions are the source of considerable debate (e.g. Jenkins, 1930; Swarbrick, 1968; Surlyk and Noe-Nygaard, 2001; Jolly and Lonergan, 2002, Duranti and Hurst, 2004). The process of sand intrusion is dependant on a number of simple criteria:

- The deposits themselves must be uncemented and therefore susceptible to remobilisation.
- There is a trigger of sufficient strength to cause the deposit to fail and/or become transformed from a solid-like state to a liquid-like state.
- Fluid flow along a hydraulic gradient must occur in order to transport sand out of the liquefied source unit.

The current understanding of the processes that occur during the emplacement of a sandstone intrusion will be reviewed in the light of these criteria in the following sections.

1.2.41 Hydrodynamic setting

An important factor in our understanding of hydrodynamic setting at the time of intrusion is the propagation direction. Sandstone intrusions may propagate upwards from the liquefied source unit, but can also propagate downwards or laterally away from the source unit (Table 1.2). A combination of upward and lateral (or downward) propagating intrusions can be observed within a single intrusive complex (e.g. Parize, 1988; Surlyk and Noe-Nygaard, 2001). Fracture opening and fluid flow will be driven

from regions of high pressure towards regions of lower pressure under most circumstances. Therefore sandstone intrusions should propagate upwards from the parent body towards the sediment surface. However, the downward propagation of sandstone dykes implies that the hydraulic gradient is reversed with lower fluid pressures present in underlying strata than in the liquefied source unit. Other factors that may conceivably result in lateral or downward propagation of sand intrusion include the presence of strata with a particularly high tensile strength through which it is very hard to drive a fracture, or the breaching of other aquifers within the section resulting in a loss of the fluid pressure. Examples where different stages of intrusion propagate in different directions (e.g. Taylor, 1982) show that the factors controlling propagation direction can vary between phases of sand intrusion.

1.2.42 Triggering mechanisms

A wide variety of mechanisms for triggering sandstone intrusion have been put forward (Table 1.7). The most commonly proposed triggering mechanisms fall into three principal groups: 1) Seismically induced liquefaction. 2) Overpressuring due to sudden loading. 3) Injection of fluid into the source sand body. However it is possible that other mechanisms such as lateral pressure transfer, clay dehydration, gas migration and the creation of biogenic gas might also trigger sand intrusion. It is likely that rather than a single triggering mechanism, several mechanisms may act in conjunction to result in sand intrusion.

Seismicity may induce liquefaction of buried sands (e.g. Obermeier, 1996). Many regions where clastic intrusions occur were seismically active (Jolly and Lonergan,

Table 1.7 Triggering mechanisms for sand intrusion

Triggering Mechanism	Authors
Seismicity	Newsom, 1903; Anderson, 1944; Reimnitz and Marshal, 1965; Williams, 1976; Plint, 1983; Rais <i>et al.</i> , 1985; Martil and Hudson, 1989; Neef, 1991; Schweig and Marple, 1991; Obermeier, 1996; Wolf <i>et al.</i> , 1998; Boyd <i>et al.</i> , 1999; Rossetti, 1999; Vanneste <i>et al.</i> , 1999; Parize <i>et al.</i> , 1999; Galli, 2000; Takahama <i>et al.</i> , 2000; Liu and Li, 2001; Surlyk and Noe-Nygaard, 2001; Jolly and Lonergan, 2002; Upadhyay, 2003
Overpressure due to loading	Rutten and Schönberger, 1957; Gill and Kuenen, 1958; Smith and Rast, 1958; Truswell, 1972; Dionne and Shilts, 1974; Elson, 1975; Hiscott, 1979; Taylor, 1982; Aspler and Donaldson 1986; Parize, 1988; Larsen and Mangerud, 1992; Martel and Gibling 1993; Rijdsdijk <i>et al.</i> , 1999; Strachan, 2002
Overpressure due to fluid migration	Jenkins, 1930; Kugler, 1938, Brooke <i>et al.</i> , 1995 Molyneux <i>et al.</i> , 2002; Løseth <i>et al.</i> , 2003
Bolide impact	King, 1998; Alvarez <i>et al.</i> , 1998; Kriens <i>et al.</i> , 1999; Terry <i>et al.</i> , 2001
Sudden heating of wet sediment	Walton and O'Sullivan, 1950; Lewis, 1973; Stuart and Furnes, 1976
Extensional tectonics	Reeve, 1937; Vitanage, 1954; Harms, 1965; Montenant <i>et al.</i> , 1991; Beacom <i>et al.</i> , 1999
Layer-parallel shortening	Ookmens, 1966; Tanner, 1998

2002) making this a strong candidate as a trigger for clastic intrusion. Soft-sediment deformation is a common response to cyclic shaking during seismic events. Seismites are formed through the liquefaction and remobilisation of soft, near-surface sediments as a response to earthquakes and may be found repeated at several levels within the same stratigraphic succession (e.g. Rosetti, 1999) as a response to different earthquakes over time. However, liquefaction at depth greater than 10 m is believed to be unlikely due to the increasing shear-strength of the source sand unit due to increasing overburden pressure with depth (e.g. Jolly and Lonergan, 2002), although recent results suggest that liquefaction may be possible at deeper levels (e.g. Benjumea *et al.*, 2003; Huuse *et al.*, 2005).

Overpressuring can be caused by loading resulting from localised depositional events such as slumping, channel sand emplacement or other factors including: glacial overstep or the effects of storm waves (Table 1.7). Such loading events produce localized overpressures within a few 10's of meters of the sediment surface and are commonly related to small-scale intrusions.

Rapid injection of fluid into the parent sand body, causing overpressuring and remobilisation of the sand body has been put forward as a trigger for sandstone intrusion (e.g. Jenkins, 1930; Brook *et al.*, 1995; Molyneux *et al.*, 2002). This process may cause the remobilisation of sands to form mounded geometries (Brook *et al.*, 1995) or result in the intrusion of sand into the overlying caprock (Molyneux *et al.*, 2002; Løseth *et al.*, 2003).

In order to link a sand intrusion event to the triggering mechanism(s) it is necessary to constrain the timing of the emplacement event. However, a robust method for dating intrusion that does not occur syn-depositionally in the shallow sediment column causing forced folding, extrusion on to or otherwise affecting the sediment surface has yet to be found. It is therefore very hard to link the emplacement of a sandstone intrusion to a particular triggering event with a high degree of confidence. Seismic events are likely to be especially hard to correlate because their far field effects may be felt a great distance from the epicentre (Eberhart-Phillips *et al.*, 2002). Commonly, multiple soft-sediment deformation events can be found within a sedimentary succession resulting from repeated slip events on a particular fault zone (e.g. Rosetti, 1999).

1.2.43 Hydraulic fracture and fracture reactivation

A sandstone dyke can be considered to be a mode 1 tensile fracture with walls that are held open by fluid pressure (acting against the confining stress) such that the flow of fluid is sufficiently rapid to transport the sand grains into the fracture (Fig 1.5). As such, the formation of a sandstone intrusion is controlled by hydraulic fracturing. During the early stages of burial the formation of hydraulic fractures is thought to be a very important way of allowing the migration of fluids through and out of partially lithified, low permeability sediments (Fyfe *et al.*, 1978; Cosgrove, 1995; Bjørlykke, 1997). To fully explain the process of sandstone intrusion, it would ideally be necessary to interlink the hydrodynamics of the fluid in the source bed in its initial state, the hydrodynamics of fluid moving through the fracture as the fracture propagates and the pressure drop within the source bed as the fluid bleeds off up the

intrusion(s) with a mechanism for sand transport within the mobile fluid. Although detailed models for hydraulic fracturing exist (e.g. Spence *et al.*, 1987; Lister 1990a, 1990b, 1991; Papanastasiou, 2000; Flekkøy *et al.*, 2002; Murdoch, 2002), a coupled system involving sand transport within the fluid has yet to be modelled successfully. This is due to uncertainties in modelling the transport mechanism and uncertainty in the in situ stress state and pressure regime in the subsurface at the time of sand intrusion. This section is thus confined to a qualitative review of hydraulic fracturing where relevant to the emplacement of clastic intrusions.

In order for fluid to escape a parent body by sand intrusion, pore pressure must reach a high enough level to cause tensile hydraulic fracture of the caprock (Cosgrove, 1995) or to dilate any favourably orientated pre-existing fractures within the caprock (Sibson, 2000). If the fluid pressure within the source body is greater than that of the capillary entry pressure of the caprock, continuous leakage may occur from an overpressured body without hydraulic fracture (Fisher *et al.*, 2001). Faults and pre-existing fractures are known to act episodically as fluid conduits (Cartwright, 1994; Roberts and Nunn, 1995; Barton *et al.*, 1995; Aydin, 2000; Eichhubl and Boles, 2000; Gudmundsson, 2001; Gay *et al.*, 2004) and therefore provide another potential mechanism for fluid escape from the parent body.

Larger overpressures are required for the formation of new hydraulic fractures than the reactivation of pre-existing fractures (Sibson, 2000). Fractures within the caprock that are ideally orientated for reactivation in the prevailing stress field are held open by the stress field and may retain high hydraulic conductivity (Barton *et al.*, 1995). As differential stress is increased, dilation of suitably orientated pre-existing fractures

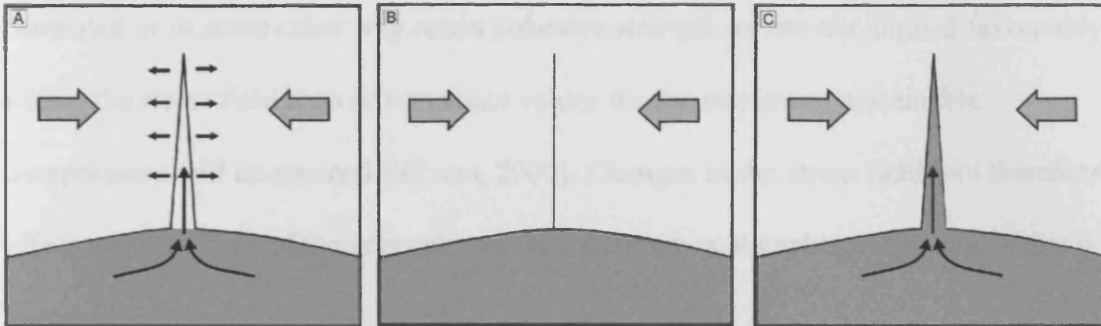


Fig 1.5A) High fluid pressures in a sand body cause the hydraulic fracture of the body's caprock. **B)** If no sand is transported into the open fracture, it will heal after pressure within the sand body falls below the level required to keep the fracture dilated. **C)** However, if sand is transported into the fracture, when fluid pressure within the sand body falls below that required to keep the fracture open the fracture cannot close and is, in effect, propped open by the transported sand.

also increases. The maximum sustainable overpressure that can be contained by a caprock is therefore likely to be controlled by fault/fracture-valve discharge rather than pure hydraulic fracture (Sibson, 2000). If any fractures in the seal are partially cemented or in some other way retain cohesive strength, or are not aligned favourably within the stress field then intermediate values for the maximum sustainable overpressure will be attained (Sibson, 2000). Changes in the stress field will therefore affect the properties of the caprock and the maximum sustainable overpressure that it may contain.

When fluid overpressure exceeds that required to dilate pre-existing fractures, or cause hydraulic fracture, fluids can escape from the overpressured parent body. Fluid escape results in a pressure drop within the parent body. Fluid flow can continue until a point is reached when the fracture may no longer be held open against the confining pressure of the caprock. At this point the fracture closes and the caprock again becomes impermeable (Fig 1.5B) (Papanastasiou, 2000). Fluid escape cannot occur again until enough overpressure can be built up to reactivate the fracture once more (Roberts and Nunn, 1995). However, if fluid migration during hydraulic fracture results in sand being transported into the open fracture before closure the walls of the fracture will be propped open by the transported sand and the conduit may retain high fluid conductivity (Papanastasiou, 2000) (Fig 1.5C).

1.2.44 Parent body remobilisation and sand transport

In order for sand to be remobilised and transported within a fluid into an open hydraulic fracture from the parent body, the solid intergranular network of the

sediment must be destroyed in order for granular sediment to be entrained within the escaping fluid. This is a process whereby the solid, grain-supported sediments of the parent body undergo a state change, liquefying to become suspension sand within a fluid. This process is described by both *fluidisation* and *liquefaction*.

Liquefaction.

Liquefaction occurs when the grains of a sediment body saturated with a fluid are disturbed so that they are no longer supported by static intergranular contacts, but separated and supported within the pore fluid instead (Allen, 1982; Nichols, 1994). The effective frictional strength of a buried sand increases as compressive stress is applied by the mass of overburden therefore the more deeply buried the sand the greater its frictional shear strength. This is opposed by the pore pressure of the fluid within the sand body, as this increases, the frictional strength of the sand and thus its resistance to deformation is reduced. When the pore pressure equals the vertical compressive stress applied by the overburden the frictional strength is reduced to zero and the sand liquefies. Multiple contributory causes of overpressure are possible including disequilibrium compaction, the introduction of more fluid to the pore space, lateral transfer, and gas migration or exsolution. Cyclic shaking during earthquakes is also known to be a common cause of the liquefaction of sands (e.g. Allen, 1982; Obermeier, 1996).

Earthquake-induced liquefaction can result in irreversible compaction, whereby the porosity of the sand body is considerably reduced after liquefaction due to pore fluid loss and tighter grain packing (Allen, 1982; Nichols, 1994; Obermeier, 1996). The

formation of sand volcanoes at the sediment surface is attributed to liquefaction (e.g. Obermeier, 1996; Galli, 2000). As fluid is expelled at the surface after the extrusive event, the extrusion vent may be prone to collapse as the liquefied source unit compacts. This may draw surface sediments down into the vent itself (Takahama *et al.*, 2000).

Fluidisation

The formation of sandstone intrusions is often attributed to the fluidisation of the parent sand body and the transport of sand into an open fracture by a *fluidised flow* of sand entrained within a mobile fluid (e.g. Surlyk and Noe-Nygaard, 2001; Duranti *et al.*, 2002; Jolly and Lonergan, 2002; Netoff 2002). Fluidisation is a response of an unconstrained bed (i.e. has no sealing layer to inhibit or focus fluid flow out of the bed) of granular material to a fluid moving vertically upwards through it. The fluid does work against gravity by exerting drag forces on the grains it passes during the upward movement of the fluid through the granular medium (Richardson, 1971; Allen, 1982; Kunii and Levenspeil, 1991; Nichols, 1994; Di Felice, 1995). The drag forces applied to each individual grain by the mobile fluid increase as fluid velocity increases. Consequently compressive stress resulting from the weight of the overlying grains and thus the shear strength of the static intergranular network becomes reduced with increasing fluid velocity. The fluid velocity at which the drag forces applied by the mobile fluid are equal to the force exacted by the weight of the individual grains, is termed the minimum velocity of fluidisation. Once this velocity is reached, the shear strength of the source sand is reduced to zero and the bed becomes fluidised.

Once fluidised, the bed may be deformed under small stresses. However, movement of the fluid and the grains is decoupled. Fluid can escape the fluidised bed, but the fluid velocities are not sufficient to transport granular sediment. In order for transport of granular sediment to occur, the fluid velocity must exceed the settling velocity of the grains. Once this occurs, grains can become fully entrained in the mobile fluid and elutriated from the system (Richardson, 1971; Kunii and Levenspeil, 1991; Di Felice, 1995 Eichubl and Boles, 2000).

Fluidisation requires that there must be fluid flow across the bed of granular material. In order to induce fluid flow a pressure gradient must exist across the bed (Jolly and Lonergan, 2002). In the case of an overpressured sand body encased within an impermeable caprock, the need for a pressure gradient strongly implies that the caprock must have failed before the inception of fluid flow and fluidisation. Caprock failure would lead to pressure release, the formation of a pressure gradient within the bed, and the induction of fluid flow. Thus caprock failure is likely to be a precondition for fluidisation within a sealed body.

Only simple single component aqueous fluids have been considered in respect to fluidisation related to sandstone intrusion. Multi-component fluids such as oil-brine and brine-gas systems have not been examined in detail but may be present during sand intrusion in hydrocarbon provinces (e.g. Jenkins, 1930; Thompson *et al.*, 1999; Molyneux *et al.*, 2002; Duranti and Hurst, 2004) or in the presence of gas hydrates (e.g. Tinivella *et al.*, 2002; Cooper and Hart, 2002; Bunz *et al.*, 2003). Experimental work has been carried out to model processes occurring during the fluidisation of a

granular material by a two-phase (gas-liquid) fluid (e.g. Song *et al.*, 1999; Li *et al.*, 2001), although these models have yet to be applied to the problem of sand intrusion.

1.2.45 Physical effects of liquefaction and fluidisation

Sandstone intrusions commonly show grain-size variations or changes in grain shape that may be the result of the physical processes and transport mechanisms that occur during the intrusion event or during post-intrusion modification during compaction, dewatering and diagenesis (Table 1.4). The settling of a poorly sorted dispersion of sediment, analogous to the consolidation of a sand body after liquefaction through irreversible compaction has been simulated in the laboratory (Druitt, 1995). It was found that segregation by grain-size and density was common, however as the concentration of sediment within the fluid was increased, segregation was inhibited. The consolidation of an enclosed liquefied bed (e.g. a buried sand body) is highly likely to involve the settling of a suspension with a very high sediment concentration and as a result segregation during liquefaction is unlikely.

1.2.46 Fluids and diagenesis

After the cessation of emplacement, sandstone intrusions may form a conduit through which fluid may later migrate if sufficient permeability is retained. Sandstone intrusions were recognised as fluid migration pathways for post-emplacement fluids early in the history of research into clastic intrusions (e.g. Ransome, 1900; Jenkins, 1930). Examples of sandstone intrusions from offshore oil fields commonly contain hydrocarbons as a pore fluid within a poorly consolidated, high porosity reservoir

sand (e.g. Dixon *et al.*, 1995; Huuse *et al.*, In Press) or as fluid inclusions in cementing minerals within the intrusion itself (Jonk *et al.*, 2003(a)). Sandstone dykes are known to act as hydrocarbon migration conduits that control the common oil water contact and pressure system within some fields (Timbrell, 1993) and therefore must retain considerable permeability long after emplacement. Episodic expulsion of hydrocarbon fluids through the Maastrichtian-Danian Moreno Shales of the Panoche Hills region of California is believed to have fed cold seeps at the palaeoseafloor for over 0.5×10^6 years (Schwartz *et al.*, 2003), similarly large-scale conical intrusions retain permeability some 30 – 40 Ma after emplacement (e.g. Huuse and Mickleson, 2004).

Sand intrusion, by definition, involves the transport of sand within a fluid medium. Two main types of fluid are commonly described within the literature: 1) Water or brine (e.g. Newsom, 1903; Harms, 1965; Taylor, 1982; Phillips and Alsop, 2000; Surlyk and Noe-Nygaard, 2001; Strachan, 2002). 2) Hydrocarbons.

Hydrocarbons may be involved during emplacement or migrate through the intrusion complex after emplacement. Dykes containing a hydrocarbon residue can clearly be seen at outcrop in the oil producing basins of California (Newsom, 1903; Jenkins, 1930; Thompson *et al.*, 1999). However, there is no direct evidence in the diagenetic record that this residue is a relic of fluid present during the emplacement of the intrusions (Thompson *et al.*, 1999). It is therefore possible that the hydrocarbons present may be the result of the secondary migration of a post-emplacement fluid (e.g. Schwartz *et al.*, 2003). In contrast, cathodoluminescence studies of samples from the North Sea have identified hydrocarbons as fluid inclusions within the calcite cements

of the sandstone intrusions (Mazzini *et al.*, 2003; Jonk *et al.*, 2003(a)). The calcite cements do not show oscillatory banding, a measure of varying geochemical environment, and instead show one phase of cement growth. This is considered to represent a single rapid cementation event soon after burial with a single fluid phase present (Mazzini *et al.*, 2003). This implies that hydrocarbons were present within the cementing fluids soon after the emplacement event and may have been present during the intrusion event itself.

Evidence from non-ferroan calcite cements within sandstone intrusions from the Kimmeridgian of Scotland implies that the temperature of fluids from which they precipitated was high (i.e. 70 °C to 100 °C) (Jonk *et al.*, 2003b). These hot fluids are believed to have migrated up the Great Glen and Helmsdale fault zones from deep within the basin and caused the remobilisation and intrusion of Oxfordian sands. These data imply that the presence of sandstone intrusions within a basin can be induced by and facilitate the migration of hot basinal fluids to more shallow levels within the basin. It is therefore possible that this may have an impact on heat flow within the basin. Aqueous fluids under high temperatures and pressures above the critical point of water (P=22.1 MPa and T=674 K) form a high-density vapour known as a supercritical fluid (Kalinichev, 2001). Clastic intrusions related to the intrusion of igneous bodies or migration of hot basinal fluids may be the result of the entrainment of sediment within a supercritical fluid.

1.2.5 Post-emplacement modification of sandstone intrusions

The host rock of a sandstone intrusion may undergo significant deformation after emplacement. This will significantly alter the original geometry. The effects of post-

intrusion deformation include: ptygmatic folding of sandstone dykes due to compaction of the host rock after early emplacement (e.g. Dott, 1966; Truswell, 1972; Parize, 1988; Phillips and Alsop, 2000; Surlyk and Noe-Nygaard, 2001; Strachan, 2002) and convergence of tectonic structures and sandstone intrusions as a result of rotation during deformation so that dyke orientations appear nearly parallel to cleavage in the host rock (Maxwell 1962; Moench 1966; Powell 1969, 1970; Dearman, 1970; Janke 1970; Bates 1975).

Ptygmatic folding of sandstone intrusions within very fine-grained host rocks had been recorded on numerous occasions (e.g. Truswell, 1972; Parize, 1988; Phillips and Alsop, 2000; Surlyk and Noe-Nygaard, 2001; Strachan, 2002). Reconstruction of ptygmatically folded dykes using decompaction calculations has been used to examine the depth and timing of emplacement. (Allen, 1982; Parize, 1988; Hiller and Cosgrove, 2002). However, the porosity profile of the sedimentary section must be known. Unlike laboratory experiments where generalised compaction curves have been produced (e.g. Taylor and Leonard, 1990; Bryant *et al.*, 1990), core data from deep-sea ODP and DSDP wells shows that rates of compaction in clay-rich sediments vary from site to site due to a number of factors including the flocculation of clay particles during deposition and the build up of overpressure. Well data from the North Sea shows that there is no elevated porosity in overpressured fine-grained rocks relative to the same rocks at similar depths that are normally pressured (Nordgård Bolås *et al.*, 2004). Therefore compaction curves based on modelling of porosity stress relationships may be unreliable (Velde, 1996; Goult, 2002) and the reconstruction of folded dykes cannot universally be used to assess sandstone intrusion depth. Field observations of ptygmatically folded sandstone dykes in close

proximity to unfolded (Surlyk and Noe-Nygaard, 2001), illustrates that heterogeneous compaction of the host rock, or the temporal spacing of separate intrusive events will result in local perturbations in the amount of compactional folding observed.

1.2.6 Summary

The geometry, scale, and composition of sandstone intrusions are well documented worldwide from a wide range of depositional and tectonic settings. Large amounts of research have been carried out into sandstone dykes, sills, conical intrusions and dyke/sill complexes whereas large-scale sandstone pipes/cylindrical sandstone intrusions appear to be either less common within the sedimentary record, or under represented within the geological literature. The largest intrusions and intrusion complexes are found in deep-water settings where the isolated nature of parent sand bodies and the fine-grained nature of background sedimentation can result in the early formation of a good seal allowing the build up of overpressure. Large-scale sandstone intrusions and intrusion complexes are commonly found in basins undergoing subsidence (e.g. the North Sea), basin inversion (e.g. The Faroe-Shetland Basin), or that are related to seismically active regions (e.g. California). In each case there is good potential for large-magnitude earthquakes providing a potential trigger for sandstone intrusion.

Whilst the physical properties of sandstone intrusions are well documented, there are significant barriers to understanding processes that cause sandstone intrusion. There is commonly some ambiguity in assessing the triggering mechanism that causes sandstone intrusion in many cases because the timing of emplacement is poorly

constrained. Identifying the timing of and triggering mechanism behind an intrusive event is likely to provide considerable insight into the processes occurring during the emplacement event itself. Similarly the fluid-flow regime during the emplacement of sandstone intrusions is poorly understood. A greater knowledge of the processes of fluid flow and sediment transport during and after the emplacement of sandstone intrusions would provide information about the fluid flux and thus improve understanding of the hydrodynamic evolution of the host basin.

The large-scale conical sandstone intrusions present in the North Sea and Faroe-Shetland Basin are not only some of the largest known sandstone intrusions, but also impact the hydrocarbons industry as they form potential reservoir sands, routes for fluid migration and even potential drilling hazards. Thus a greater understanding of the mechanisms behind their formation may provide important information to aid development of improved basin and reservoir models. In particular, the relationship between polygonal faulting within the host rock and large-scale conical sandstone intrusions in terms of both geometry, and potential feeder systems has not been fully evaluated.

1.3 AIMS OF STUDY

This PhD project addressed the issues identified within the literature review in the following ways:

- Determining the timing of large-scale sandstone intrusion in Tranche 6 of the Faroe-Shetland basin. This is achieved by examining the relationship between shallow conical sandstone intrusions and forced folds on a regional

unconformity surface. Dating of the sediments that onlap the forced folds constrains the timing of sandstone intrusion (Chapter 2)

- Undertaking a detailed examination the relationship between conical sandstone intrusions and polygonal faults in Tranche 6 of the Faroe-Shetland Basin (Chapter 3)
- Examining the distribution of conical sandstone intrusions in Tranche 6 of the Faroe-Shetland Basin and evaluating the potential sources of fluid and sand making up the intrusions and identifying feeder systems for the conical sandstone intrusions (Chapter 3).
- Characterising the physical properties of sandstone pipes in SE Utah and placing them within the context of tectonic and sedimentary evolution of southwestern USA to evaluate their importance and potential triggers for their formation (Chapter 4).
- Evaluating the fluid flow regime within sandstone pipes from the Lake Powell region of SE Utah to examine fluid flux during pipe formation and breccia block transport mechanisms (Chapter 5)

Chapters 2 to 5 are presented as papers for publication. The role that the co-authors had in production of the material presented is clearly stated at the beginning of each chapter. Each chapter contains a discussion of the material presented in it. The results of this study are clearly summarised in Chapter 6.

CHAPTER 2 – CONSTRAINING THE DEPTH AND TIMING OF LARGE-SCALE CONICAL SANDSTONE INTRUSIONS

Published as:

Shoulders, S. and Cartwright, J.A., 2004, Constraining the depth and timing of large-scale conical sandstone intrusions, *Geology*, v. 32, no. 8, p. 661-664.

Co-author role:

Joe Cartwright provided discussion of the topics presented in this chapter and support during its writing.

2.1 ABSTRACT

Kilometer-scale sandstone intrusions—a recently recognized end member of the spectrum of soft-sediment deformation structures—are important components of many deep-water sandstone reservoirs. They result from the remobilisation of considerable volumes of sand during early stages of burial. This paper uses three-dimensional seismic data, calibrated to nearby wells, to describe an extensive system of large, downward tapering conical sandstone intrusions from the Faroe-Shetland Basin, on the UK Atlantic margin. The intrusions were derived from a middle Eocene submarine fan and were injected vertically upward through overlying, highly faulted claystones to form conical bodies that interconnect across the ~700-m-thick claystone interval to feed a set of shallow intrusions located within a few hundred meters of the palaeoseabed. The forcible intrusion of these shallow sandstone bodies produced complimentary folding of the contemporaneous seabed. The subsequent onlap of these seabed domal folds took place immediately after the intrusion event, and by correlation to biostratigraphic data from nearby wells, we date these intrusions as late

Miocene. This is the first time that both the age and emplacement depth range of a system of large-scale sandstone intrusions have been constrained.

2.2 INTRODUCTION

Sandstone intrusions are an important but enigmatic class of soft-sediment deformation structure with a long history of field-based research focused on small-scale (meter-scale) intrusive bodies (see Taylor, 1982; Parize, 1988; Surlyk and Noe-Nygaard, 2001; Boehm and Moore, 2002; and references therein). More recently, research has expanded to include a number of subsurface analyses of larger-scale intrusions using seismic imaging techniques integrated with core data (Dixon *et al.*, 1995; Duranti *et al.*, 2002). This shift in emphasis has resulted from the increasing commercial significance of sandstone intrusions. Many deepwater sandstone petroleum reservoirs in the North Sea have been comprehensively remobilized and injected into overlying sediments at some stage during their burial history, and this process has a major impact on their potential as hydrocarbon reservoirs (e.g., Huuse *et al.*, 2003).

Much is known about the basinal and tectonic settings, geometries, and internal structures of sandstone intrusions (e.g., Duranti *et al.*, 2002; Jolly and Lonergan, 2002), but fundamental questions remain unanswered particularly concerning the triggering mechanism for the intrusion process (Surlyk and Noe-Nygaard, 2001; Jolly and Lonergan, 2002). A major obstacle to a better understanding of trigger mechanisms is the lack of constraint on the depth at which large-scale remobilisation of the source unit occurs, and, what is more important, the timing of the intrusion

event. It is often possible to date the intruded sedimentary host rocks and thus set a lower bound to the timing of intrusion (Taylor, 1982; Surlyk and Noe-Nygaard, 2001; Duranti *et al.*, 2002), but thus far no method has been found capable of accurately constraining the timing of the intrusion event itself.

In this paper we date large-scale sandstone intrusions for the first time by using a method adapted from a recently developed technique for dating shallow-level igneous sills (Trude *et al.*, 2003). This method is based on the seismic-stratigraphic analysis of domal folds that develop in response to the forcible intrusion of the conical sandstone bodies at a depth of a few hundred meters below the seabed. Indirect methods must be sought for dating sandstone intrusions because unlike their igneous counterparts, they cannot be dated by radiometric methods. In sandstone intrusion, direct dating of the intrusive body (e.g., by biostratigraphic methods) yields only the age of the remobilized material, which in most cases is significantly older than the intrusion event. Hence, this seismic-stratigraphic approach offers an entirely novel route to date sandstone intrusions on the basis of the folding response of the cover rocks, albeit restricted to areas of good biostratigraphic control. We demonstrate the applicability of this method with a case study from the Faroe-Shetland Basin, offshore the United Kingdom, where a suite of large-scale sandstone intrusions is imaged on three-dimensional seismic data. We are able to date these intrusions to within a time interval of a few million years, to define the depth range of the intrusions beneath the palaeoseabed, and for the first time in any study of large-scale sandstone intrusions, to constrain these key parameters.

2.3 REGIONAL GEOLOGIC SETTING

The Faroe-Shetland Basin is located between Scotland and the Faroe Islands (Fig 2.1) and is one of a series of basins that developed along the northeast Atlantic continental margin as a result of continental breakup during the Mesozoic and Paleocene (Dean *et al.*, 1999). The basin fill consists of Mesozoic clastic sedimentary deposits that accumulated during rifting and the initial stages of post rift subsidence, overlain by more laterally extensive deltaic and slope sandstones, claystones, and biosiliceous oozes deposited during the Cenozoic (Mitchell *et al.*, 1993; Davies *et al.*, 2001). Magmatically related uplift of the Scottish massif during the late Paleocene to early Eocene (White and Lovell, 1997) led to increased clastic input to the Faroe-Shetland Basin (Hall and Bishop, 2002) and the deposition of large, sand-rich deep-water fans during the early middle Eocene (Mitchell *et al.*, 1993) followed by dominantly claystone deposition during the later Eocene and Oligocene. Erosion by deep-water currents cuts down into the Eocene–Oligocene claystone sequence, forming a major regional unconformity (the intra-Neogene unconformity of Stoker *et al.*, 2002), which separates the Eocene–Oligocene claystone sequence from a largely fine-grained Neogene contourite drift succession. Inversion structures formed through compression and the reactivation of Mesozoic extensional faults throughout the basin during the middle to late Miocene (Davies *et al.*, 2004).

2.4 THREE-DIMENSIONAL SEISMIC INTERPRETATION

Our case study is focused on the Eocene to Holocene succession in the basin center and is based on ~15,000 line kilometers of regional two-dimensional and 2,600 km²

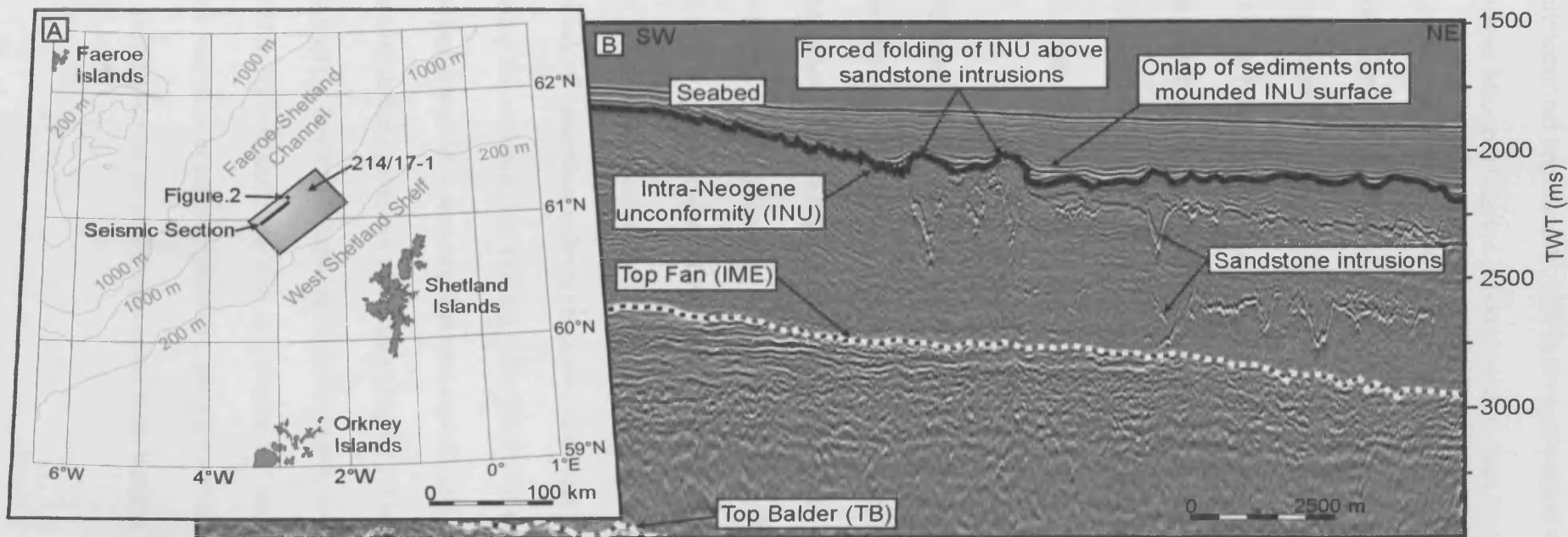


Figure 2.1. A: Location map. Study area located within area of three-dimensional seismic data (gray box). B: A regional seismic line showing stratigraphy of Eocene to Holocene strata including a complex of discordant high-amplitude reflections interpreted as sandstone intrusions emanating from Eocene sand-rich submarine fan. TWT—two-way travel time

of three-dimensional seismic data, tied to six exploration wells. In this area, the Eocene–upper Miocene interval is bounded at its base by the Top Balder horizon and at its top by the intra-Neogene unconformity (Fig 2.1). This 1–1.5-km-thick interval consists of smectite-rich claystones that are intensely deformed by a polygonal fault system that developed during early stages of burial (Cartwright, 1994). A large sand-rich submarine fan of middle Eocene age dominates the base-of-slope region and is defined at its top surface by a regionally correlatable marker horizon, the intra–middle Eocene (Fig 2.1). There is no evidence of direct hydrocarbon indicators in the study area, nor is there any evidence for methane hydrates (Davies and Cartwright, 2002).

One of the most remarkable features observed on the three-dimensional seismic data is a distinctive suite of discordant, high-amplitude reflections within the Eocene–Oligocene interval. Our mapping shows that around 5 to 10% of these discordant reflections form an interconnected system from the top fan surface (i.e., the intra–middle Eocene) up to the level of the intra-Neogene unconformity, where they can be seen to abut the locally folded surface of the intra-Neogene unconformity (Fig 2.1). This network of discordant reflections extends through 700 m of vertical section, cross-cutting the stratigraphic layering. The reflections commonly cross-cut the pervasive polygonal fault network, but also exploit polygonal faults. None of the discordant reflections cross-cut each other (Fig 2.1). The discordant reflections map as approximately downward tapering conical shapes, with diameters at their outer edges of 500–1000 m and flank dips of between 10° and 50° (Fig 2.2). There is no significant variation in conical geometry among >100 mapped cones within this interval: they have similar aspect ratios and sizes irrespective of their depth below the

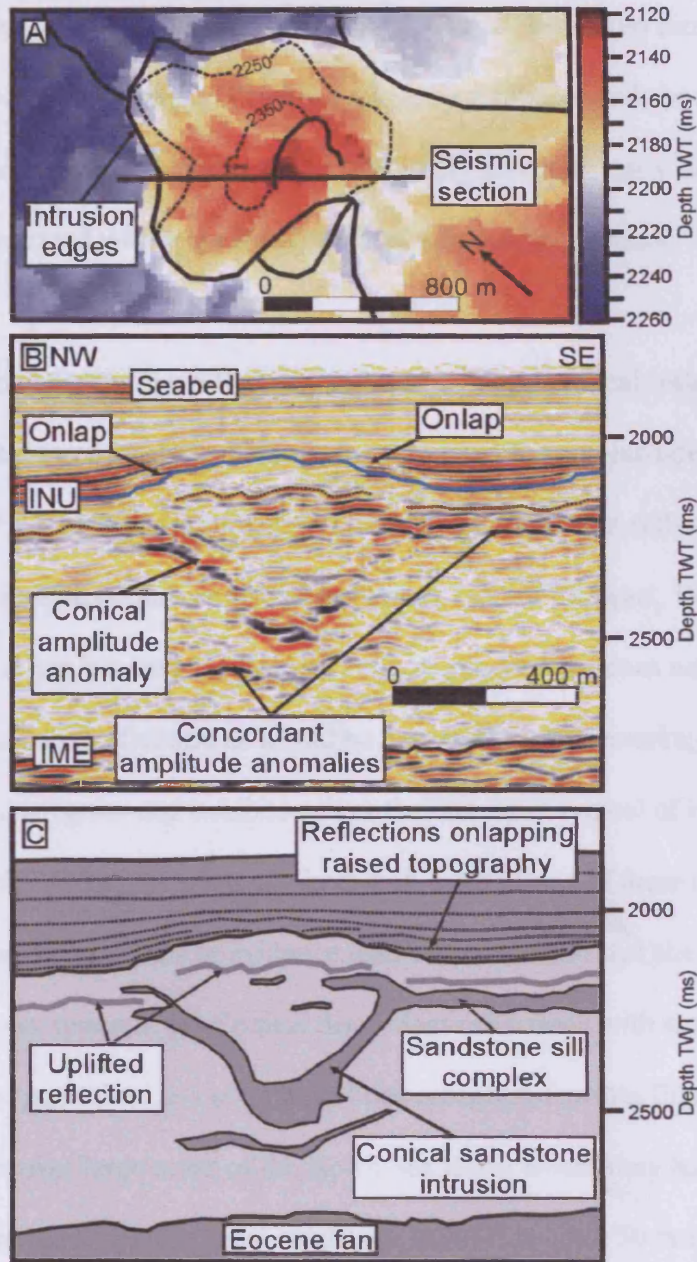


Figure 2.2. A: A time-structure map (in two-way traveltime [TWT]) of intra-Neogene unconformity (INU) with superimposed outline (thick black lines) and contours, spaced every 100 ms (thin black lines), of underlying sandstone intrusions mapped ~100–300 m deeper than unconformity. Topographic high (reds) of intra-Neogene unconformity surface are strongly spatially related to sandstone intrusion distribution. B: Seismic section through a topographic high showing close relationship between sandstone intrusions, forced folding of overlying sedimentary deposits, and formation of topographic highs. Note how reflections inside intrusion are upwardly domed (black dotted line), paralleling overlying intra-Neogene unconformity surface; also note that a high-amplitude package of reflections onlaps topographic high. This high-amplitude package may consist of extruded sandstone. IME—intra–middle Eocene strata. C: Schematic representation of B showing position of intruded sandstone bodies and associated uplift of overlying sedimentary deposits to form a topographic high on intra-Neogene unconformity surface. High is onlapped by later sedimentary deposits (black dotted lines).

intra-Neogene unconformity. This uniformity suggests that there is no direct control on geometry related to burial depth. The high seismic amplitudes and the opposite polarity of upper and lower reflections (Fig 2.2B) imply an acoustically hard (high-impedance) body encased within the low-impedance Eocene claystones.

The discordant geometry and the reflection character of these conical reflections are suggested here as being conclusive evidence for their representing intruded sediment. The only previously described features that resemble the discordant reflections are bowl-shaped or cone-shaped intrusions and pockmark craters (Stewart, 1999). We reject a pockmark origin because the detailed reflection geometry does not have a smooth, contiguous basal reflection as would be expected for pockmarks; the geometry is instead irregular and exhibits splays that are more typical of intrusive bodies (Trude *et al.*, 2003). There are no direct well calibrations of these reflections in this survey area, but several lines of evidence lead us to conclude that the intruding material is clastic, not igneous: (1) Conical discordant reflections with similar acoustic properties, geometry, and scale have been recognized within Eocene claystone packages over large areas of the North Sea Basin where they have been tied to wells and interpreted as giant conical sandstone intrusions up to 50 m in thickness (e.g., Huuse and Mickelson, 2004). (2) There is no evidence for any igneous activity within the basin later than the Paleocene–early Eocene (Gibb and Kanaris-Sotiriou, 1988), making it unlikely that these shallow intrusions, hosted in the Eocene–Oligocene section, are of igneous origin. (3) Around 5% to 10% of the discordant reflections physically connect to the top of the sand-rich middle Eocene submarine fan, which is inferred to be the most probable source for sand to form these intrusions.

(4) Seismic modeling of the reflections produces a good match with being the intruded lithology by using locally derived physical properties.

2.5 FOLDING OF THE INTRA-NEOGENE UNCONFORMITY

One of the most striking features of the discordant reflections described above is the close spatial relationship between these reflections and folds developed at the intra-Neogene unconformity surface (Fig 2.1). It was noted above that folds at the unconformity occur where the discordant reflections abut the unconformity. The close spatial correlation between folds at the unconformity and the underlying location of discordant reflections is clearly seen in Figure 2.2, a representative example drawn from the three-dimensional survey area. The low-amplitude domal fold on the intra-Neogene unconformity is sited directly above an underlying sandstone intrusion (Fig 2.2A). In profile, the fold has sharp breaks of dip defining lateral margins that lie directly above the upper margins of the underlying discordant reflections. The fold's relief (25–30 m) is similar to that of the thickness of the intruded body, as inferred from the acoustic expression of the discordant reflections.

The direct spatial correspondence between low-amplitude domal folds at the intra-Neogene unconformity and the interpreted sandstone intrusions implies a causative relationship. We propose that this relationship is the result of forced folding of the cover by the intruding sand bodies as they were emplaced into the host sedimentary deposits, in a manner analogous with forced folding of sedimentary cover by igneous laccoliths or sills (Trude *et al.*, 2003). The only possible alternative mechanism to link a fold to a subjacent intruded body would be through differential compaction of the

sandstone in the intrusion relative to the claystone of the host sequence (Hillier and Cosgrove, 2002). Folding due to differential compaction is rejected because there was no overburden load above the intra-Neogene unconformity at the time of folding. If it is accepted that the folding of the cover was due to sandstone intrusion, then by analogy with the method developed by Trude *et al.* (2003), the timing of intrusion can then be constrained by dating the growth of the fold.

The timing of fold development can be simply constrained by using standard seismic-stratigraphic relationships, provided the folds were expressed at the sediment-water interface during the deformation (e.g., Cartwright, 1989). By using this approach, we observe that in all the domal folds expressed at the intra-Neogene unconformity in our study area, the fold flanks can be seen to be onlapped by parallel-stratified (i.e., post-fold growth) base-of-slope muds and sands that immediately postdate the unconformity. We constrain the timing of folding in the study area to the late Miocene on the basis of two lines of evidence:

1. Folding postdated the erosional sculpting of the intra-Neogene unconformity surface because the unconformity surface is itself folded. The intra-Neogene unconformity represents a hiatus spanning the late Miocene to early Pliocene (Knutz and Cartwright, 2003).

2. Folding predated the parallel-stratified onlap fill succession because the geometry of onlap is not indicative of synchronous rotation and deposition. The onlap fill is dated locally by the presence of *Globergerina praebulloides* sp. as late Miocene (10.4–5.2 Ma) (Harland *et al.*, 1990) in well 214/17-1; hence the folding must have occurred within the late Miocene.

Combining these two sets of biostratigraphically derived ages allows us to derive a well-constrained relative age for the intrusive event. Thus, it is possible to say that the large-scale sandstone intrusions within the study area were all emplaced during the late Miocene.

In addition to providing a direct constraint on the timing of intrusion, the recognition that the onlap fill occurred directly after intrusion and forced folding allows us to make the important deduction that the intra-Neogene unconformity represented the seabed at the time of intrusion, because it was this surface that was subsequently overlapped. This allows us to precisely constrain the depth of intrusion (~200–300 m) for all the conical sandstone intrusions lying immediately beneath the contemporaneous seabed that forcibly folded the intra-Neogene unconformity surface. The depth range for intrusion includes the uncertainty involved in decompaction of intrusion geometry, which is small because of the relatively thin post-intra-Neogene unconformity cover sequence.

2.6 DISCUSSION

The system of discordant reflections described above is a remarkable example of pervasive intrusion of a cover sequence ~1 km thick, where for the first time; it has been possible to trace the intrusions from their source to their site of intrusion close to the palaeoseabed. We think that the intrusive process occurred in a single phase involving possibly catastrophic remobilisation of the source (the Mid-Eocene fan) because (1) the system is so interconnected, (2) there is no evidence for any cross-cutting relationships between the conical reflections, and (3) there are no examples of

forced folds related to intrusion below the intra-Neogene unconformity. The uncertainty in dating the duration of this phase of intrusion is therefore entirely due to the normal errors associated with biostratigraphic age determination.

A simplified model summarizing our preferred hypothesis of the geologic evolution of the sandstone intrusions and their associated forced folds is presented in Figure 2.3; the model is based on one of the simplest of the conical intrusions mapped in the survey area. During the late Miocene, enhanced bottom-current circulation resulted in a period of deep-water erosion leading to the cutting of what was to become the intra-Neogene unconformity surface (Fig 2.3A). Toward the end of this phase of deep-water erosion, sandstones within the middle Eocene submarine fan were remobilized as a result of a triggering event, probably a seismic event related to inversion occurring throughout the basin during the middle to late Miocene (Davies *et al.*, 2004). A fluidized flow of sand under elevated fluid pressure was transported >750 m vertically upward, exploiting polygonal faults as conduits. When the fluidized flow reached subsea depths of 200–300 m, the overpressure within the flow induced conical fractures in the upper Eocene claystones, and the sand + fluid mixture elevated the overburden above the conical intrusions. Some sand + fluid mixture might have extruded at the seabed as fracture tips propagated to the surface (Fig 2.3B). As the pressure in the conduits declined (owing to depletion of the deeper fluid source), the fluid transport system froze, large-scale sandstone intrusions were left as fracture fills, and domal forced folds were preserved as topographic features on the seabed. These folds were subsequently onlapped by upper Miocene and late Pliocene deep-water clastic sediments (Fig 2.3C), and any extruded material was buried.

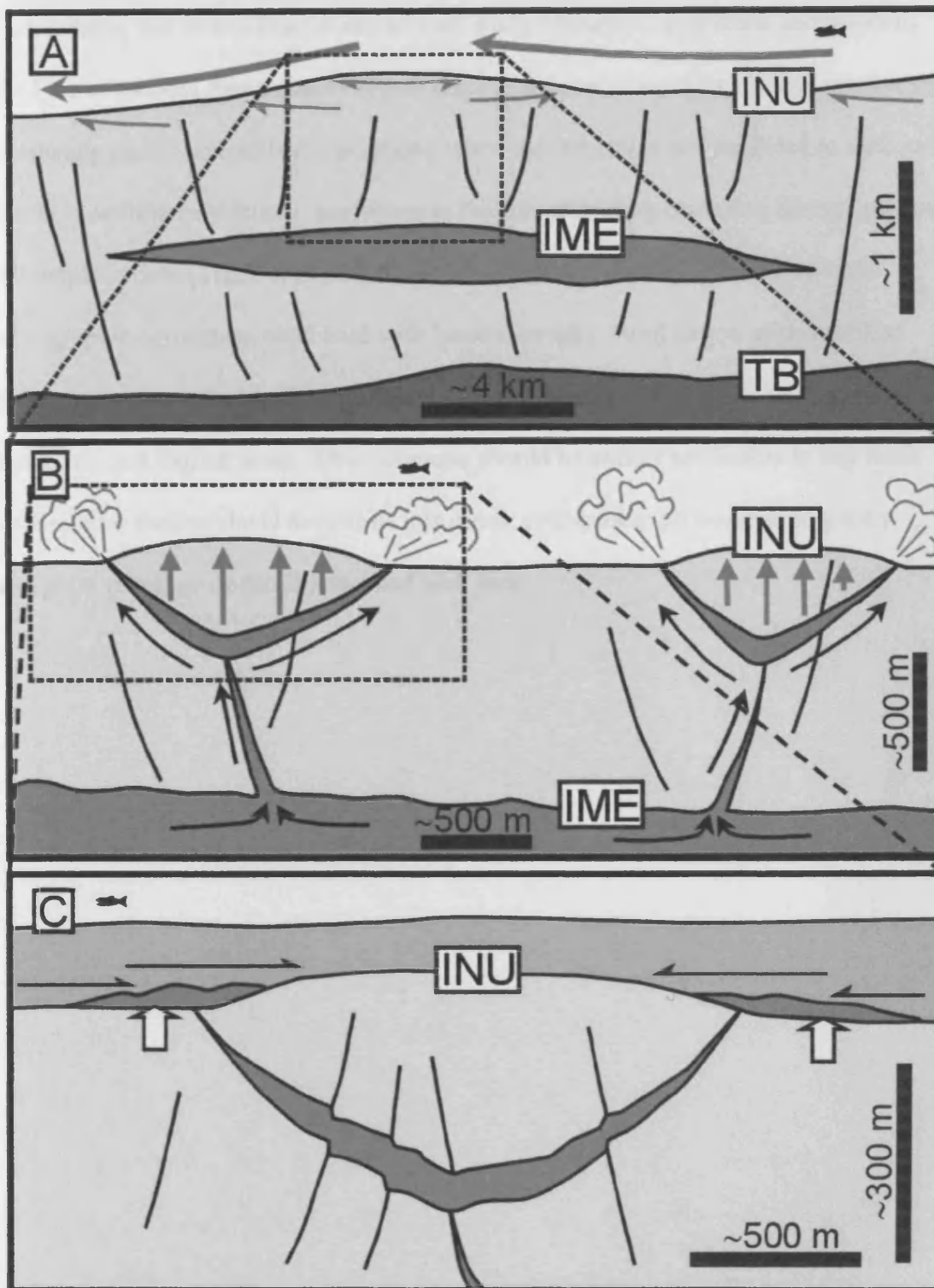


Figure 2.3. A schematic diagram presenting a model for formation of conical sandstone intrusions in Faroe-Shetland Basin. A: Pre-intrusion section and conditions. B: Formation of conical intrusions above which growth folds form and sand extrudes at surface. C: Post-intrusion burial (see text for a more detailed discussion). INU—*intra-Neogene unconformity*; IME—*intra-middle Eocene strata*; TB—*top of Balder*.

In summary, our three-dimensional seismic study of shallow-amplitude anomalies in the Faroe-Shetland Basin clearly shows that the process of sand intrusion is capable of producing significant seabed topography when the intrusions are emplaced at shallow levels in sedimentary basins, analogous to the forced folding occurring during igneous sill emplacement (Trude *et al.*, 2003). The folding can be dated by using seismic-stratigraphic correlation combined with biostratigraphy. Application of this method thus opens a route for identifying triggering mechanisms of sandstone intrusion operative on a basinal scale. This technique should be widely applicable in any basin with similar shallow-level sandstone intrusions, well-preserved cover stratigraphy, and good coverage of geophysical and well data.

CHAPTER 3 – LARGE-SCALE CONICAL INTRUSIONS AND POLYGONAL FAULT SYSTEMS IN TRANCHE 6, FAROE- SHETLAND BASIN

Submitted as:

Shoulders, S., Cartwright, J.A., and Huuse, M., 2005, Large-scale conical sandstone intrusions and polygonal fault systems in Tranche 6, Faroe-Shetland Basin, *Marine and Petroleum Geology, In Review.*

Co-author roles:

Joe Cartwright and Mads Huuse provided discussion of the topics presented in this chapter and support during its writing.

3.1 ABSTRACT

Kilometer-scale sandstone intrusions are being recognised as important components in an increasing number of deep-water clastic systems. They result from the remobilisation and injection of sand during early stages of burial, and are commonly found in fine-grained mudrocks containing a pervasive polygonal fault network. This paper uses three-dimensional seismic data from the Faroe-Shetland Basin, on the UK Atlantic margin, calibrated to nearby wells, to examine the relationship between an extensive system of large downward tapering conical sandstone intrusions to the pervasive polygonal fault network present within the surrounding encasing host mudstones. The intrusions were injected upwards during the late Miocene through Eocene/Oligocene claystones and biosiliceous sediments with a pre-existing polygonal fault network to form conical bodies up to 300 m high within the ~700-m-thick claystone sequence. Conical sandstone intrusions have previously been interpreted as exploiting polygonal faults. However, this study shows that polygonal

faults and the discordant limbs of conical sandstone intrusions form two distinct dip populations with little overlap that have average dips of 58° and 26° respectively. Polygonal faults display decreasing dip with increasing depth. However, conical sandstone intrusion dip is uniform throughout the Eocene-Oligocene succession. These observations lead us to conclude that the geometry of conical sandstone intrusions is not greatly affected by the presence of a pre-existing polygonal fault network, nor is it affected by increasing vertical effective stress with depth. Therefore the 10° to 50° dip range displayed by the limbs of conical sandstone intrusions observed within the study area is a fundamental property of this class of sandstone intrusion.

The presence of a widespread region of conical sandstone intrusions in the Faroe-Shetland Basin has important implications for vertical fluid migration in the region. The Eocene-Oligocene claystones in the region have low permeability; however the presence of large-scale conical sandstone intrusions and any possible feeder systems was likely to provide high permeability fluid conduits through this sequence. In effect, the otherwise good regional caprock provided by the Eocene-Oligocene claystone succession is breached by a network of sandstone intrusions, possibly resulting in reduced hydrocarbon potential in the region.

3.2 INTRODUCTION

Sandstone intrusions are a poorly understood class of soft-sediment deformation structure with a long history of field-based research (e.g. Newsom, 1903; Jenkins, 1930; Taylor, 1982; Parize, 1988; Surlyk and Noe-Nygaard, 2001; Boehm and Moore,

2002). Recently, research has expanded to include a number of subsurface analyses of larger-scale intrusions by using seismic imaging techniques (e.g. Chapters 2 and 3; MacLeod *et al.*, 1999; Lonergan *et al.*, 2000; Molyneux *et al.*, 2002; Huuse and Mickleson 2004; Huuse *et al.*, 2004) integrated with core data where available (Dixon *et al.*, 1995; Duranti *et al.*, 2002). This shift in emphasis has resulted from the increasing awareness of the commercial significance of large-scale sandstone intrusions. It is thus widely observed that many deepwater sandstone petroleum reservoirs in the North Sea have been comprehensively remobilized and sands are injected into overlying sediments at some stage during their burial history. 3D seismic data has facilitated the discovery of a special class of sandstone intrusion with a downward tapering conical geometry (e.g. Molyneux *et al.*, 2002). It is now recognized that post-depositional remobilisation and injection of sand has a major impact on the hydrocarbon plumbing system in the North Sea (e.g., Lonergan *et al.*, 2000; Hurst *et al.*, 2003; Huuse and Cartwright 2004).

Understanding the factors controlling the geometry of large-scale sandstone intrusions is important for a number of reasons, not least because large-scale sandstone intrusion may complicate the geometry of hydrocarbons reservoirs (e.g. Dixon *et al.*, 1995; Lonergan and Cartwright, 1998) and conical sandstone intrusions may themselves form hydrocarbons reservoirs (Huuse and Mickleson, 2004; Huuse *et al.*, In Press). The presence of high permeability injected sands within otherwise impermeable sequences may have important implications for vertical connectivity as they may provide high permeability fluid conduits long after their emplacement (Lonergan *et al.*, 2000; Hurst *et al.*, 2003; Huuse and Cartwright, 2004). This may affect the hydrocarbon prospectivity of a basin, improving it by providing effective fluid

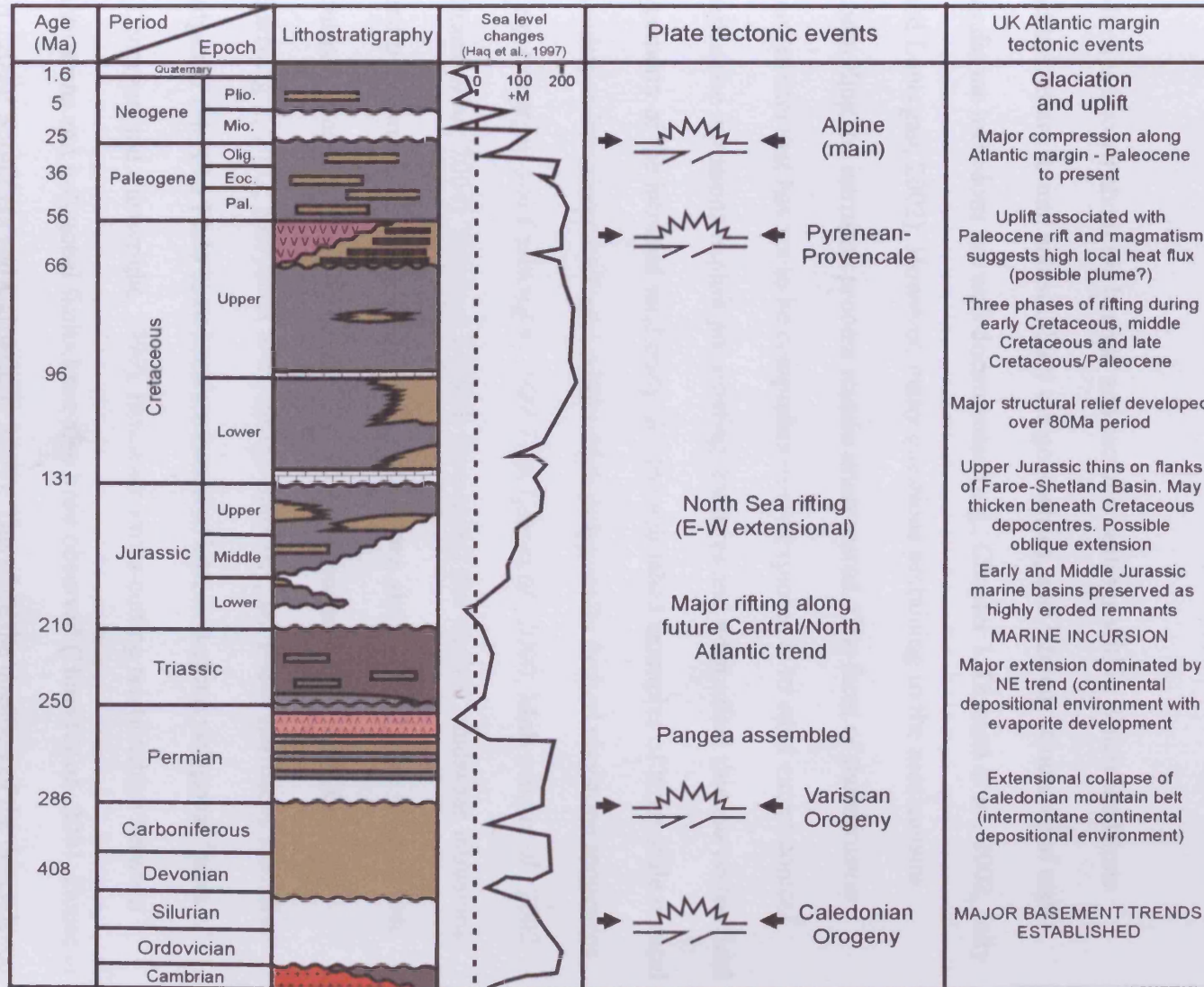


Fig 3.1 A summary of the lithostratigraphy and tectonic history of the Atlantic margins basins, west of Britain (Holmes *et al.*, 1999).

conduits to feed shallow reservoirs, or degrading prospectivity by acting as a seal breach. The presence of conical sandstone intrusions may also constitute a drilling hazard when exploring for stratigraphically deeper targets. Potential risks include mud loss and well-bore collapse or blow out and cavity formation if overpressured fluids or gas is present within the pore spaces of intruded sand bodies.

Much is known about the basinal and tectonic settings within which sandstone intrusions are found, and similarly the geometries, and internal structures of such sandstone intrusions are well documented (e.g., Chapter 1; Duranti *et al.*, 2002; Jolly and Lonergan, 2002). However, many questions pertaining to the mechanisms controlling the intrusion process remain unanswered. One facet of the intrusion mechanism that has yet to be comprehensively explored is to what extent conical sandstone intrusions exploit pre-existing fractures and what affect this has on the final geometry of the intruded sand body. All the published examples of large-scale conical sandstone intrusions are found within thick polygonally faulted claystone sequences (e.g. Lonergan and Cartwright, 1999; Lonergan *et al.*, 2000; Molyneux *et al.*, 2002 Huuse *et al.*, 2004). Previous workers have noted that conical sandstone intrusions and polygonal faults may have similar dimensions and dips and have inferred that intrusion occurs along polygonal fault planes (Lonergan *et al.*, 2000; Gras and Cartwright, 2002; Molyneux *et al.*, 2002). Similarly, wing-like intrusions from the edges of the Alba Field have been attributed to intrusion along polygonal faults (Lonergan and Cartwright, 1999). However, cross-cutting relationships between intrusions and polygonal faults have also been observed (Huuse *et al.*, 2001; Huuse *et al.*, 2004; Shoulders and Cartwright, 2004). Therefore the question of the dependence of intrusion geometry on pre-existing fractures deserves examination.

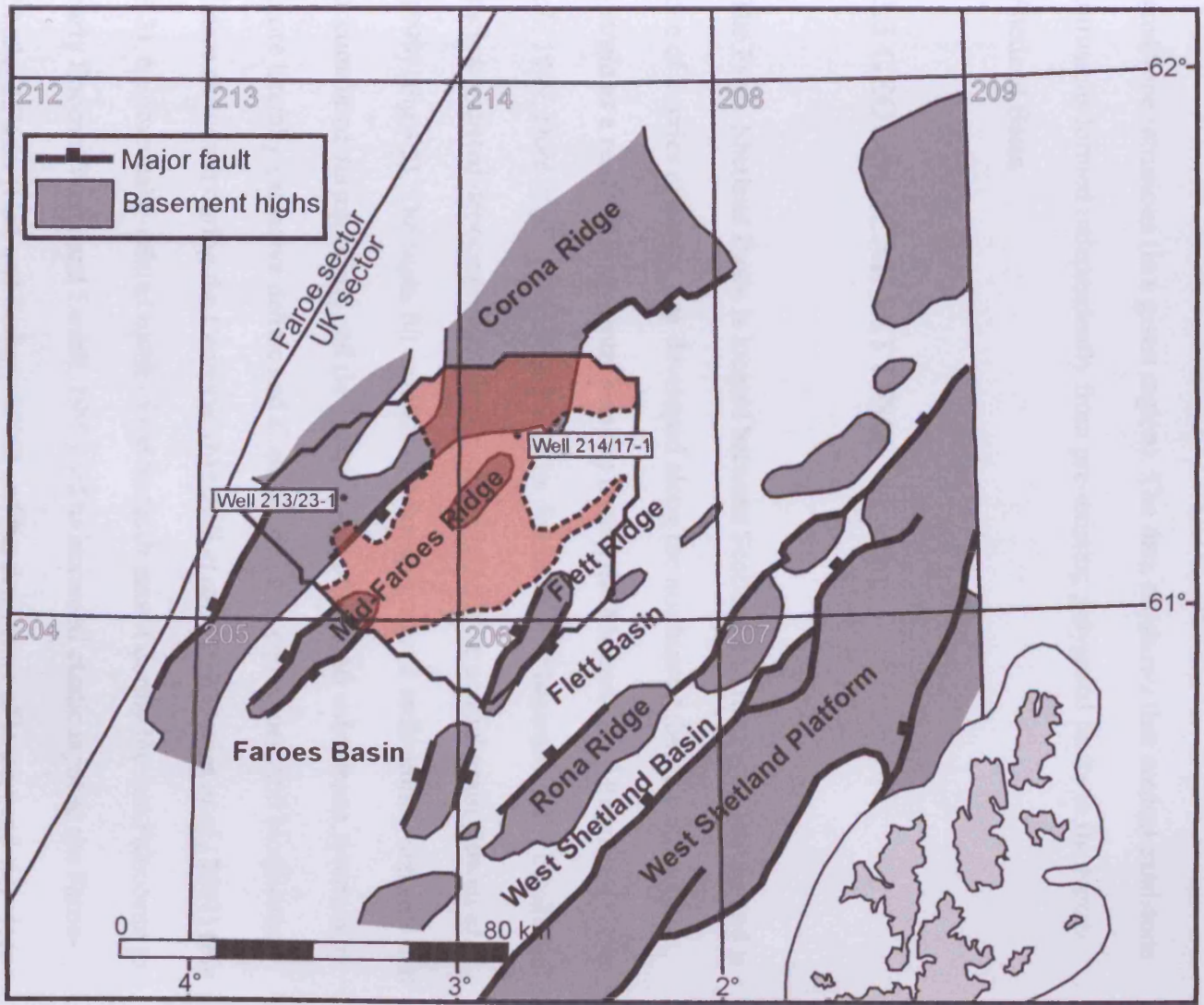


Fig 3.2 A diagram showing the relationship between the distribution of sandstone intrusions within the study area (red semi-transparent region) and the main basement structural elements (Jowett *et al.*, 1999). Note that bulk of the sandstone intrusions seems to be closely related to the position of the Mid-Faroes Ridge and the Corona Ridge.

This paper aims to assess the relationship between polygonal faults and large-scale conical sand intrusions in Tranche 6 of the Faroe-Shetland Basin. We present a large-data set of dip measurements taken from both polygonal fault planes, and discordant high amplitude reflections throughout an Eocene-Oligocene claystone succession. We will argue that these high amplitude reflections originate from large-scale conical sandstone intrusions. This is the first time that a numerical data set has been acquired specifically to explore the relationship between polygonal faults and conical sandstone intrusions (in a given region). The data set shows that conical sandstone intrusions formed independently from pre-existing polygonal faults in the Faroe-Shetland Basin.

3.3 GEOLOGICAL SETTING

The Faroe-Shetland Basin is located between Scotland and the Faroe Islands and is one of a series of basins that developed along the northeast Atlantic continental margin as a result of continental breakup during the Mesozoic and Paleocene (Dean *et al.*, 1999; Doré *et al.*, 1999) (Fig 3.1). The distribution of basement fault blocks and their associated depocentres displays a strong NE-SW structural grain (Jowett *et al.*, 1999) (Fig 3.2). The basin fill consists of Mesozoic clastic sedimentary deposits that accumulated during rifting and the initial stages of post rift subsidence, overlain by more laterally extensive deltaic and slope sandstones, claystones, and biosiliceous oozes deposited during the Cenozoic (Mitchell *et al.*, 1993; Davies *et al.*, 2001) (Fig 3.3). Magmatically-related uplift of the Scottish massif during the late Paleocene to early Eocene (White and Lovell, 1997) led to increased clastic input to the Faroe-Shetland Basin (Hall and Bishop, 2002) and the deposition of large, sand-rich deep-

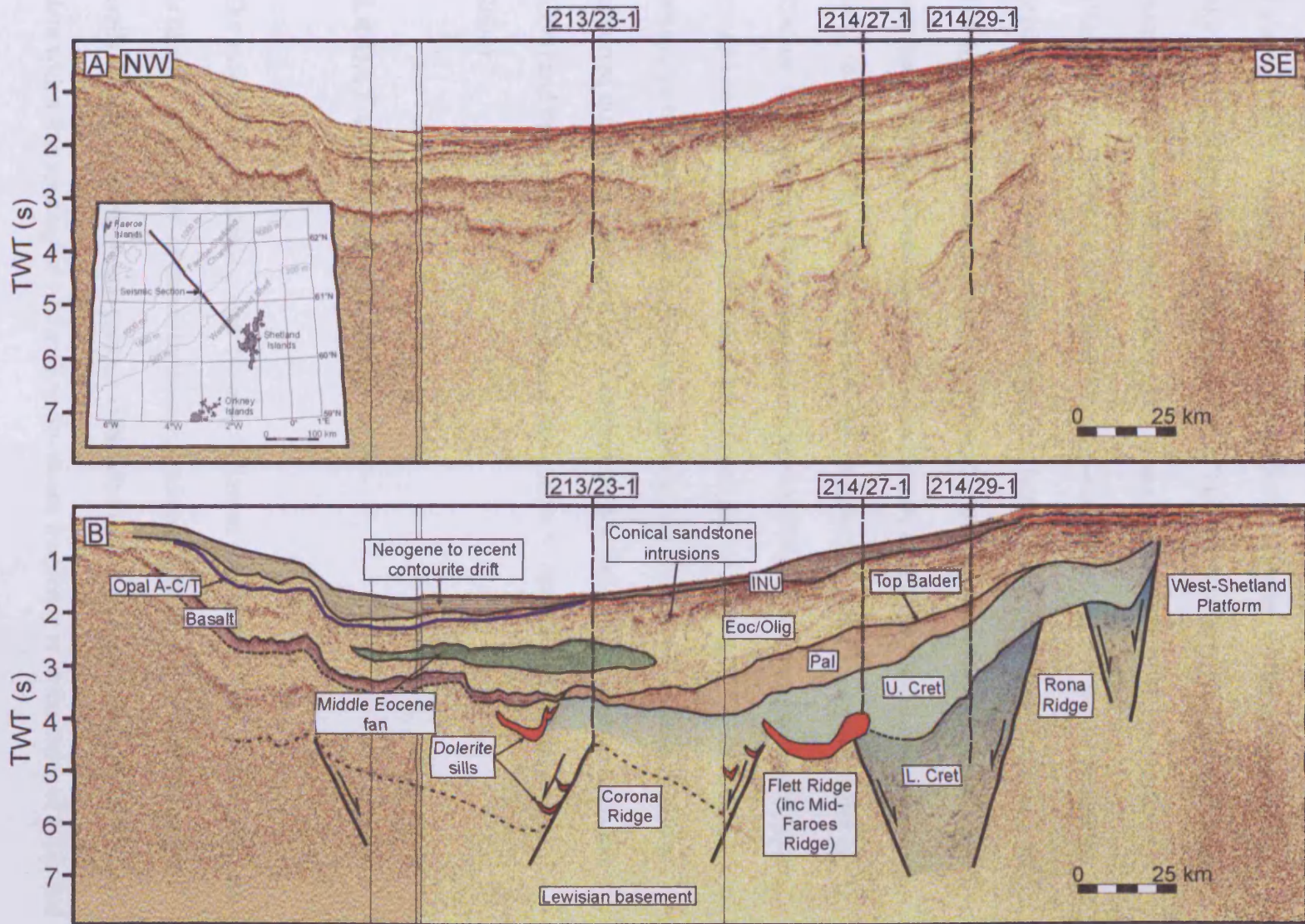


Fig 3.3 A) Regional 2D seismic line across the Faroe-Shetland Basin tied to three exploration wells. B) An interpreted seismic line across the Faroe-Shetland Basin showing the major basement fault blocks and overlying sedimentary strata. NB: INU corresponds to the intra-Neogene unconformity

water fans during the early middle Eocene (Mitchell *et al.*, 1993). Two fans are present within the study area, the Strachan Fan in the north, and the Caledonian Fan in the west of the region (Davies *et al.*, 2004) (Fig 3.4A). The impact of the proto-Icelandic plume also resulted in widespread volcanism in the region during the early Palaeogene, approximately synchronous with the inception of the opening of the North Atlantic (Ritchie and Hitchen, 1996). This resulted in the intrusion of large numbers of dolerite sills into the Upper Cretaceous and Paleocene successions (Hansen *et al.*, 2004; Trude, 2004). These events were followed by the deposition of predominantly muddy sediments during the later Eocene and Oligocene (Fig 3.4B). During the Miocene deepwater currents eroded the Eocene–Oligocene claystone sequence, forming a major regional unconformity (the intra-Neogene unconformity – INU, of Stoker *et al.*, 2002). This regional unconformity surface separates the Eocene–Oligocene claystone succession from a thin, largely fine-grained Neogene contourite drift succession (Knutz and Cartwright, 2003) (Fig 3.4C). Inversion structures formed through compression and the reactivation of extensional faults occurred during the Eocene in the southwest of the basin (Boldreel and Andersen, 1998) and throughout the basin during the middle to late Miocene (Davies *et al.*, 2004).

3.4 DATA AND METHODOLOGY

Our case study is focused on the Eocene to Recent succession in the basin centre and is based on 2,600 km² of three-dimensional seismic data, tied to several exploration wells. The three-dimensional seismic cube used during this study consists of P-wave data with a line spacing of 12.5m. The dominant frequency is in the order of 80Hz and

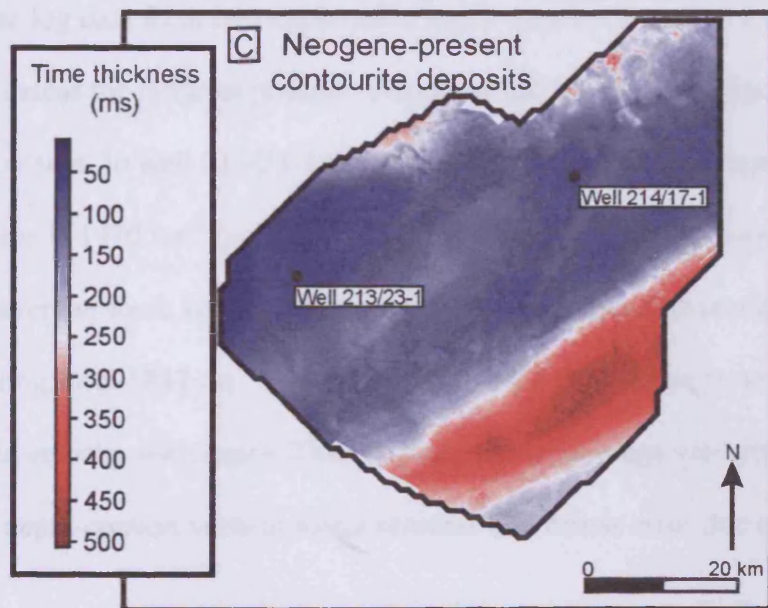
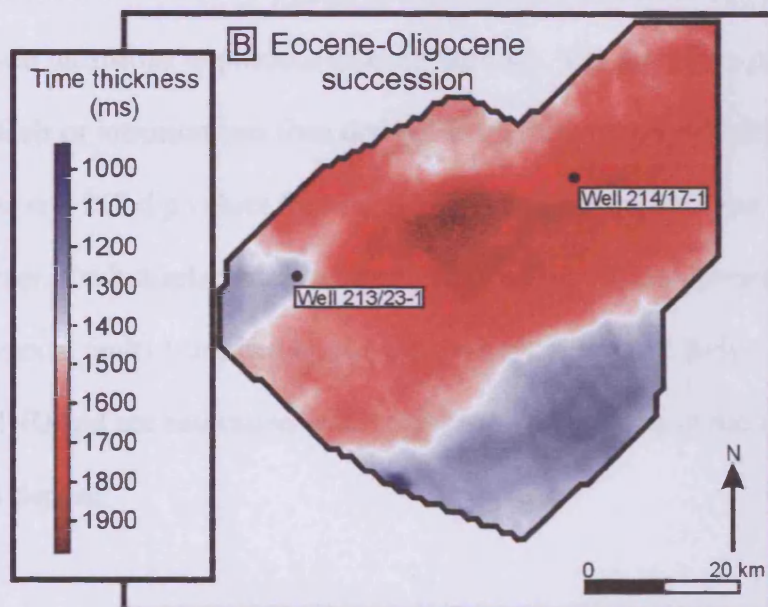
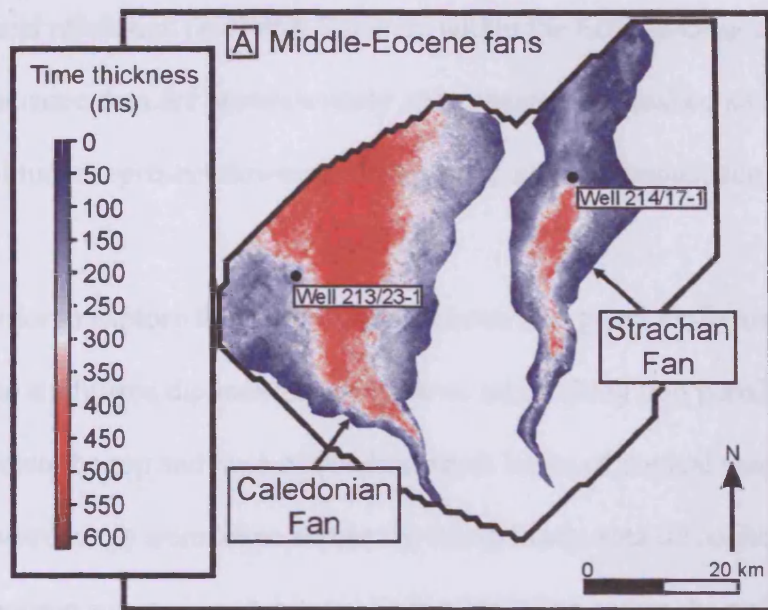


Fig 3.4 Time thickness maps of:
 A) The Middle Eocene Strachan and Caledonian fans; B) The Eocene-Oligocene succession (between the top of the Balder and INU); C) The Neogene-present contourite drift (between INU and seabed).

vertical resolution ($\lambda/4$) of 6-7 meters within the Eocene-Oligocene succession. The 3D seismic data are approximately zero-phase at the seabed and positive (red) peak amplitudes represent downward increasing acoustic impedance boundaries.

In order to explore the relationship between polygonal faults and sandstone intrusions in the study area dip measurements were taken along polygonal fault planes and between the top and base of the discordant limbs of conical sandstone intrusions. Measurements were taken across the whole study area throughout the Eocene-Oligocene succession. Arbitrary lines were taken across the polygonal faults and conical intrusions to produce true dip sections. The dip of the plane coinciding with the fault or intrusion was then derived from this section. 307 dip values for polygonal faults and 267 dip values for conical sandstone intrusions were measured in this manner. Fault displacement analysis was carried out on representative samples of polygonal faults truncated by the INU and on polygonal faults that propagate through the INU and are associated with small growth packages in the overlying contourite drift deposit.

Sonic log data from two exploration wells were used to derive the interval velocity and assess the range of possible velocities for the Eocene-Oligocene claystone succession. In well 213/23-1 the average sonic velocity through the Eocene-Oligocene section is 1970 ms^{-1} (values ranging from 1893 ms^{-1} to 2046 ms^{-1}). In well 214/17-1 the average sonic velocity through the Eocene-Oligocene section is 1966 ms^{-1} (values ranging from 1847 ms^{-1} to 2059 ms^{-1}). In both wells there is no systematic change in sonic velocity with depth. Therefore we use an average velocity of $1950 \text{ ms}^{-1} \pm 100 \text{ ms}^{-1}$ to depth-convert vertical measurements and assess error due to local variations in

sonic velocities throughout the section. These factors introduce an error of approximately $\pm 2^\circ$ for both conical sandstone intrusions polygonal faults.

3.5 SEISMIC INTERPRETATION OF THE STUDY AREA

The deepest seismically distinguishable units observed on regional 2D-reflection seismic lines across the Faroe-Shetland Basin (tied to exploration wells), are lower Cretaceous sediments overlying rifted basement fault blocks (Fig 3.3). Where drilled, the basement consists of Lewisian gneiss overlain by Devonian-Carboniferous sand-dominated strata and Triassic sandstones (Well 213/23-1). The NE-SW orientated basement fault blocks form ridges that are overlain by mudstone-dominated Cretaceous sediments. Lower Cretaceous sediments (blue strata) (Fig 3.3B) commonly infill the intra-ridge lows, whilst Upper Cretaceous sediments (pale blue strata) (Fig 3.3B) drape over the whole succession. The Paleocene succession (brown strata) (Fig 3.3B) consists of intercalated sands and muds representing a series of stacked turbidite sands that were fed from the SE margins of the basin (Fig 3.5) (Jowitt *et al.*, 1999). In well 213/23-1 only Upper Paleocene strata from the Lamba Formation, and younger formations is present (Fig 3.5A). The Paleocene sequence onlaps underlying Upper Cretaceous strata and thins to the northwest. Basalt lava flows (purple strata) (Fig 3.3B) extends from the Faroe Islands to the northwest into the basin and interfinger with the distal parts of the Upper Paleocene section. Well 214/27-1 terminated in a dolerite sill above the Flett Ridge (solid red units Fig 3.3B). Dolerite sills are common through out the Upper Cretaceous and Paleocene successions (e.g. Hansen *et al.*, 2004; Trude 2004) and are likely to have been

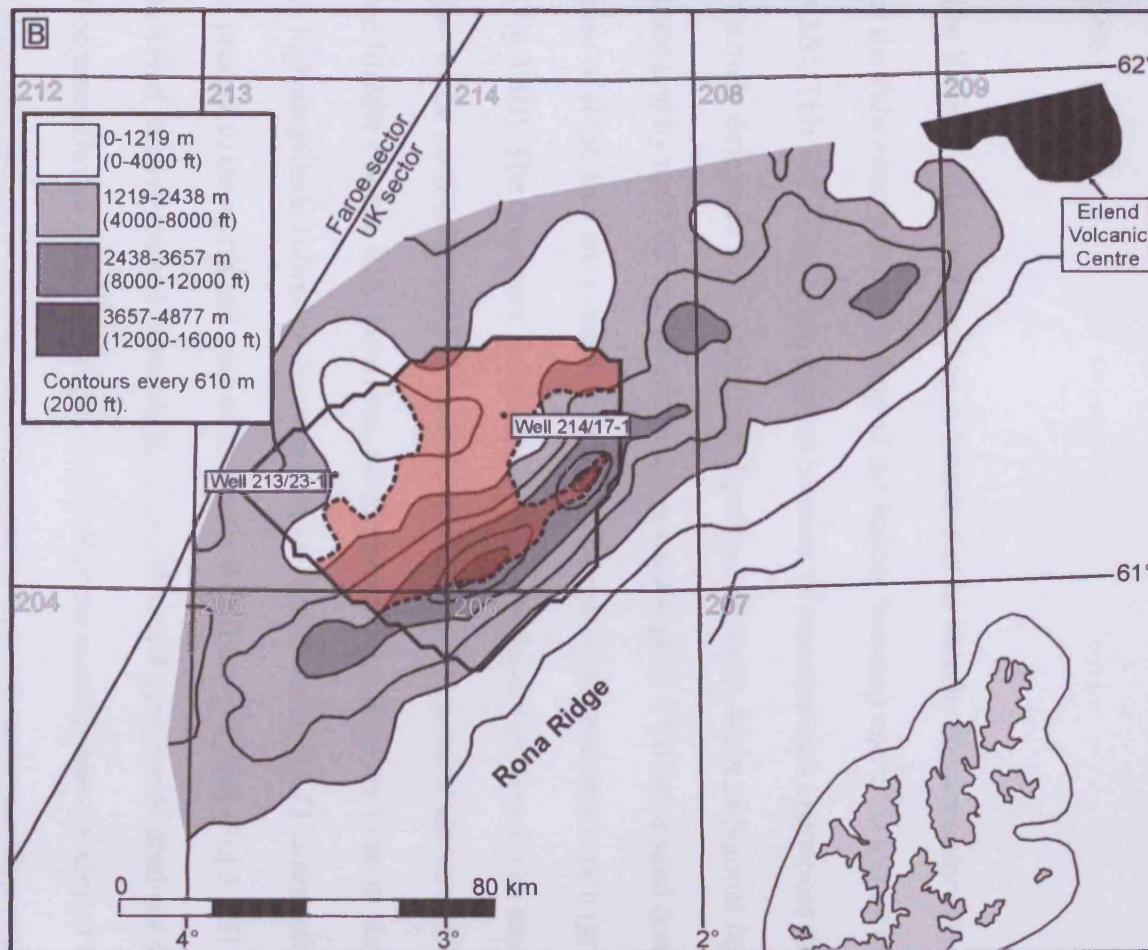
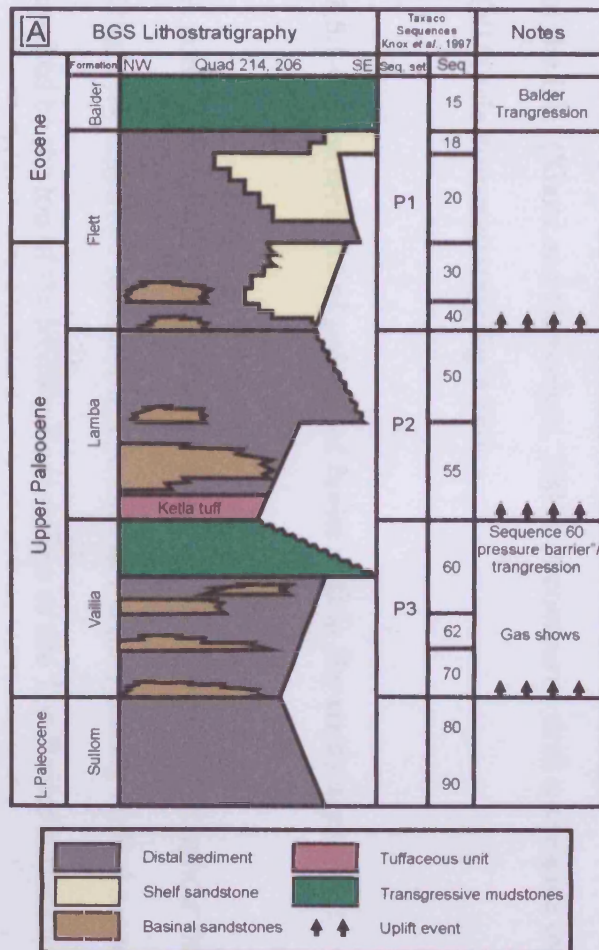


Fig 3.5 A) Palaeocene to Lower Eocene stratigraphy based on biostratigraphy and well log interpretation combined with seismic interpretation from Quads 214 and 206, West of Shetland (Knox *et al.*, 1997; Jowett *et al.*, 1999). B) A thickness map of Palaeocene strata showing the well-developed depocentre situated between the Rona Ridge and the Corona Ridge (Mitchell *et al.*, 1993). Sandstone intrusions in the study area (red semi-transparent area) are situated on the northern flank of the depocentre.

intruded during the latest Paleocene to early Eocene (55-53 Ma) (Ritchie and Hitchen, 1996).

The Eocene–Oligocene section is bounded at its base by the unconformity at the top of the Paleocene succession (top of the Balder horizon) and at its top by the INU (Fig 3.3B). This 1–1.5-km-thick interval consists of smectite-rich claystones that are intensely deformed by a single tier of polygonal faults. Most polygonal faults are truncated by the INU and do not propagate through it. Two large sand dominated, base of slope fans are present within the Eocene-Oligocene succession (green strata) (Fig 3.3B). The fans were fed from the West-Shetland Platform to the southeast and thin to the northwest. Conical sandstone intrusions are present above and adjacent to the Middle Eocene fans. However, no sandstone intrusions are present above the INU. A high amplitude reflection representing an Opal A to Opal C/T diagenetic transition is present to the north and east of the study area (blue horizon) (Fig 3.3B). This is believed to have formed in response to an enhanced geothermal gradient during the Neogene (Davies and Cartwright, 2002). Bottom currents heavily eroded the Eocene-Oligocene succession during the Oligocene to Late Miocene resulting in the sculpting of the INU (Knutz and Cartwright, 2003). A contourite drift succession overlies the INU (pale brown strata) (Fig 3.3B).

3.5.1 Characteristics of polygonal faults within the study area

A complex network of extensional polygonal faults extends throughout the Eocene-Oligocene claystone succession. The base of the polygonally faulted succession is marked by the top of the Middle-Eocene fans or the Top Balder surface where the

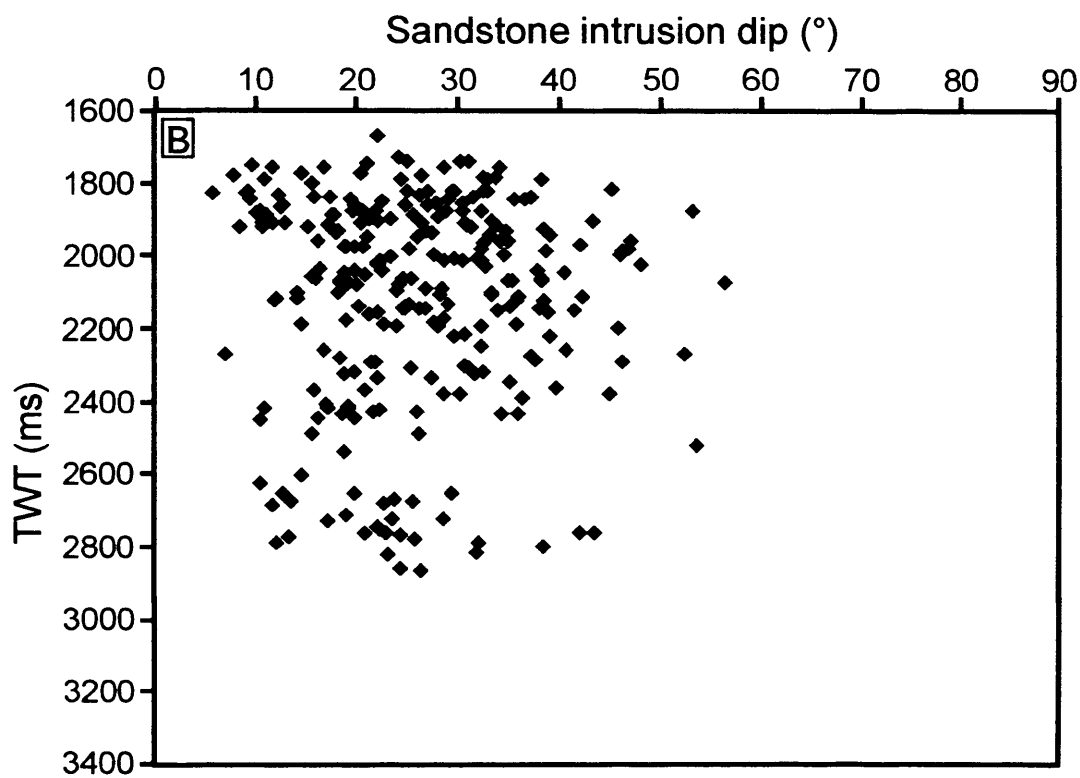
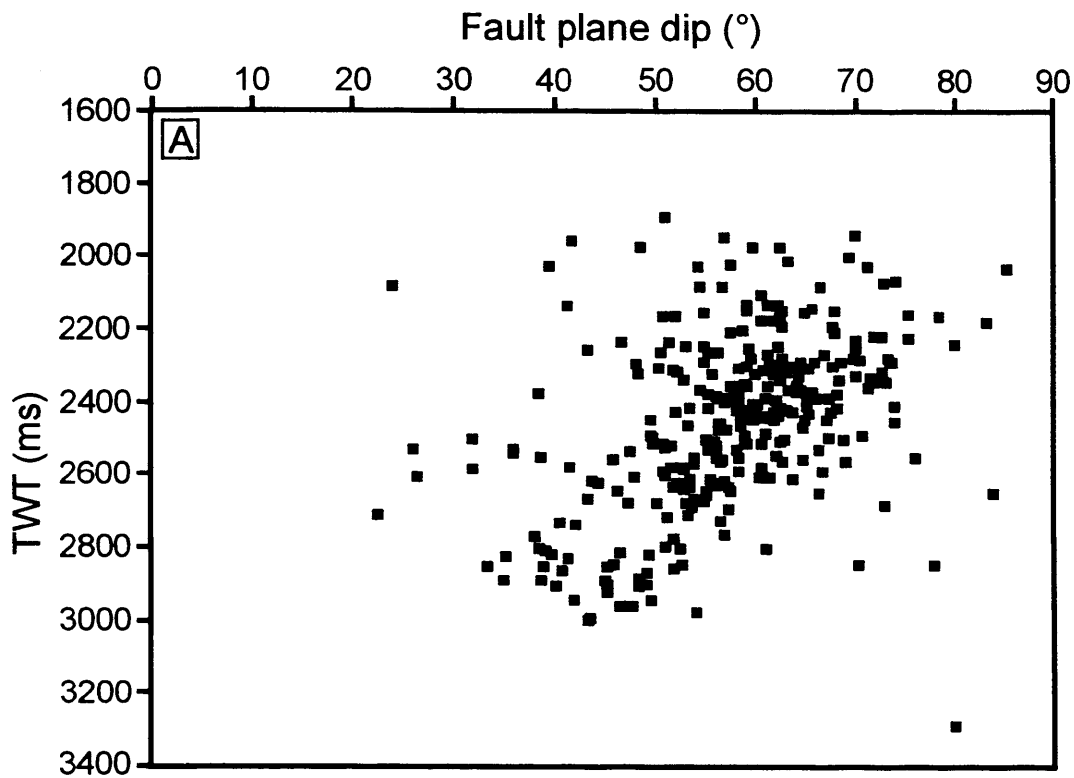


Fig 3.6 A) Polygonal fault plane dip with depth as TWT. Note the general trend towards shallower dips at greater depths. B) Intrusion dip with depth. Not that unlike polygonal faults, there is no systematic relationship between intrusion angle and depth.

Middle-Eocene fans are not present (Fig 3.3). A small number of polygonal faults propagate into the upper units of the Eocene fans. The polygonal faults are largely planar, but steepen towards the INU and shallow onto the middle Eocene fans or top Balder surface (Fig 3.6A). The average fault dip is $58^\circ (\pm 2^\circ)$. However, fault plane dip ranges from 55° and 85° at the level of the INU but shallows to between 30° and 50° at the level of the Middle Eocene fans (Fig 3.6B). The mechanisms behind the formation of polygonal faults are subject to considerable debate (Cartwright *et al.*, 2003 and references therein). However, the reduction in fault plane dip with depth may be linked to: 1) Changes in rheology with depth (such as increased smectite content) leading to a low coefficient of friction and therefore shallow angles of faulting (Gouly, 2001). However, there are no changes in sonic velocity or gamma ray log response within the study area to support this argument. 2) Divergence in the direction of maximum compressive stress (σ_1) from vertical with depth (Mandl, 2000). 3) Compaction of the host claystones after fault propagation i.e. vertical compaction causes the rotation of the dipping plane resulting in a shallower dip (e.g. Lonergan and Cartwright, 1999) (Fig 3.7).

Many of the polygonal faults sole out onto the top of the Middle Eocene fans. Displacement analysis of major polygonal faults reveals a generalized unimodal distribution with maximum displacements of 60 m to 100 m in the centre/lower centre of the faults (Fig 3.8B). Levels of displacement on the upper third of the polygonal faults are often quite irregular, but adhere to the same general displacement gradient as the surrounding faults (Fig 3.8A).

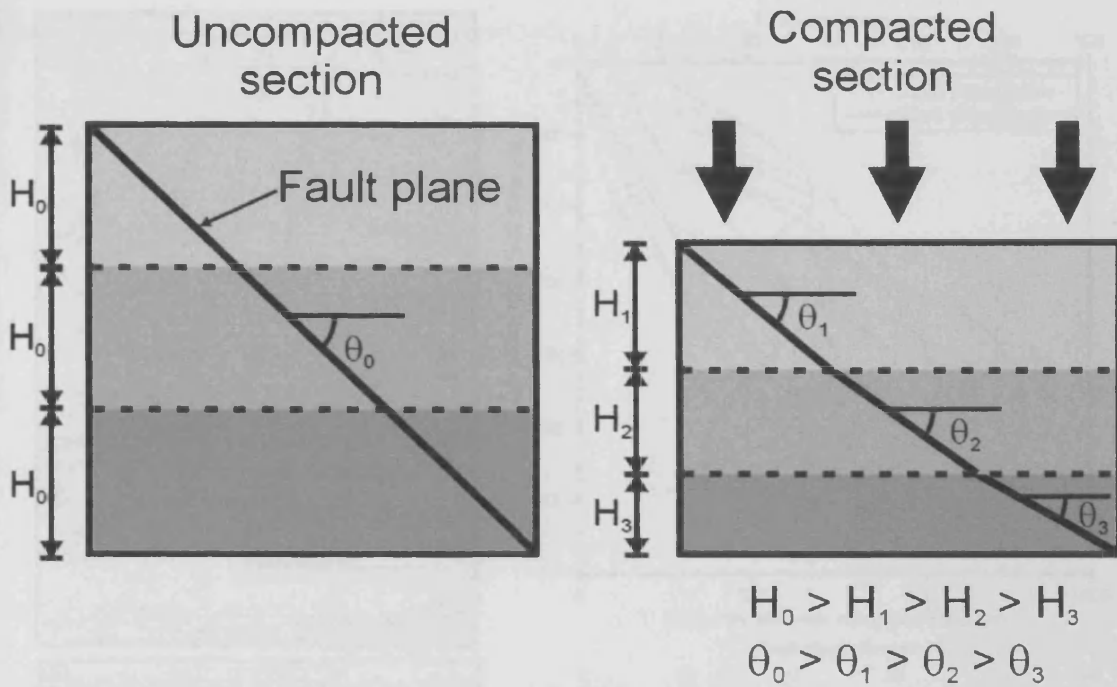


Fig 3.7 Compaction of a fault: deeply buried sediments suffer greater levels of compaction due to increased overburden loading. Compaction of a dipping plane results in a reduced angle of dip. Therefore, the greater the amount of compaction, the greater the shallowing of the plane.

Example: A fault plane dipping at 80° propagates through sediments that subsequently suffer compaction. By splitting the sediments cross-cut by the fault into three layers each with a thickness (H_0) of 200 m it is possible to examine the effects of compaction on the dip of the fault. If the upper layer suffers only 5% compaction $H_1 = 190$ m and fault dip shallows slightly to 79.5° . If the middle layer suffers 15% compaction $H_2 = 170$ m and fault dip is 78.3° . Should the basal layer have suffered 30% compaction $H_3 = 140$ m the dip of the fault plane is 75.8° .

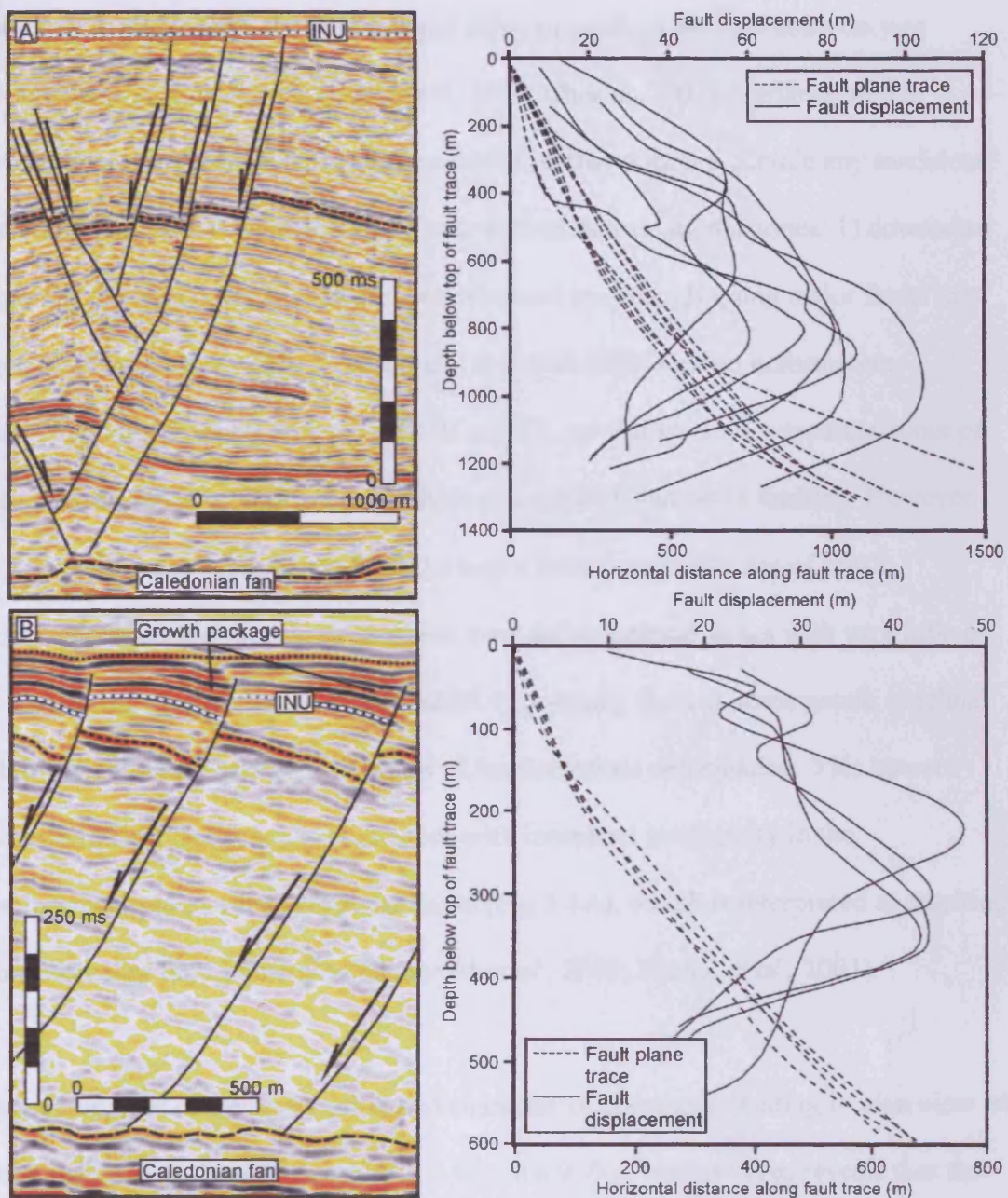


Fig 3.8 A) Fault trace geometry for polygonal faults that do not propagate beyond the INU. Note that fault plane dip shallows with depth. Maximum fault displacements of 70 m to 100 m occur at depths of 700 m to 1000 m below the top of the fault trace. Kinks on the displacement plots in the shallow section (i.e. more shallow than 800 m depth) are likely to be a result of interactions between closely spaced faults. B) Fault trace geometry for polygonal faults whose upper tips propagate beyond the INU into the basal units of the overlying contourite drift. There is a small growth package within the contourite drift at the upper tips of these faults. Note that the fault plane dip shallows with depth. Maximum displacements of 40 m to 50 m occur at depths of 200 m to 400 m below the top of the fault trace. Pronounced kinks or changes in gradient on the displacement plots occur in the shallow section (i.e. more shallow than 160 m depth) these correspond to the presence of a growth package on the fault at the level of the INU.

Polygonal fault systems are well-imaged using time slices through coherency or variance data (e.g. Bahorich and Farmer, 1995; Chopra, 2002). Variance slicing through part of the Eocene-Oligocene succession that does not contain any sandstone intrusions allows the identification of two distinct deformational zones: 1) downward tapering zones of polygonal faulting constrained by through-going major faults that dip towards each other (Fig 3.9B and C). 2) Zones of little or no deformation containing no polygonal faults (Fig 3.9B and C). At shallow levels separate zones of high intensity faulting interact to produce an even distribution of faulting. However, with increased depth below the INU the major fault-bounded zones of brittle deformation become more localized and intra-deformational zones with very little or no brittle deformation become established. Commonly there is some gentle synclinal folding in the strata between the zones of intense brittle deformation. This upward increase in fault frequency is coincident with increased irregularity in the displacement plots of the polygonal faults (Fig 3.8A), which is interpreted as resulting from increased fault interaction (Stuevold *et al.*, 2003; Nichol *et al.*, 2003).

An examination of the distribution and character of polygonal faulting in plan view on a defined horizon (blue horizon) (Fig 3.9B) in a 9.7km² sample area reveals that the polygonal faults range from straight to gently curved in shape (Fig 3.10A and B). 59 polygonal faults are present in the sample area. There are three well-defined preferred orientations a dominant NNE-SSW and NW-SE trend and a less dominant ENE-WSW trend (Fig 3.10B). Four main styles of polygonal fault intersection have previously been identified (Lonergan *et al.*, 1998) (Fig 3.11). There are 53 fault intersections present in the study area (equivalent to an intersection density of 5.5 intersections per square kilometre) (Fig 3.10C). However, only three of the

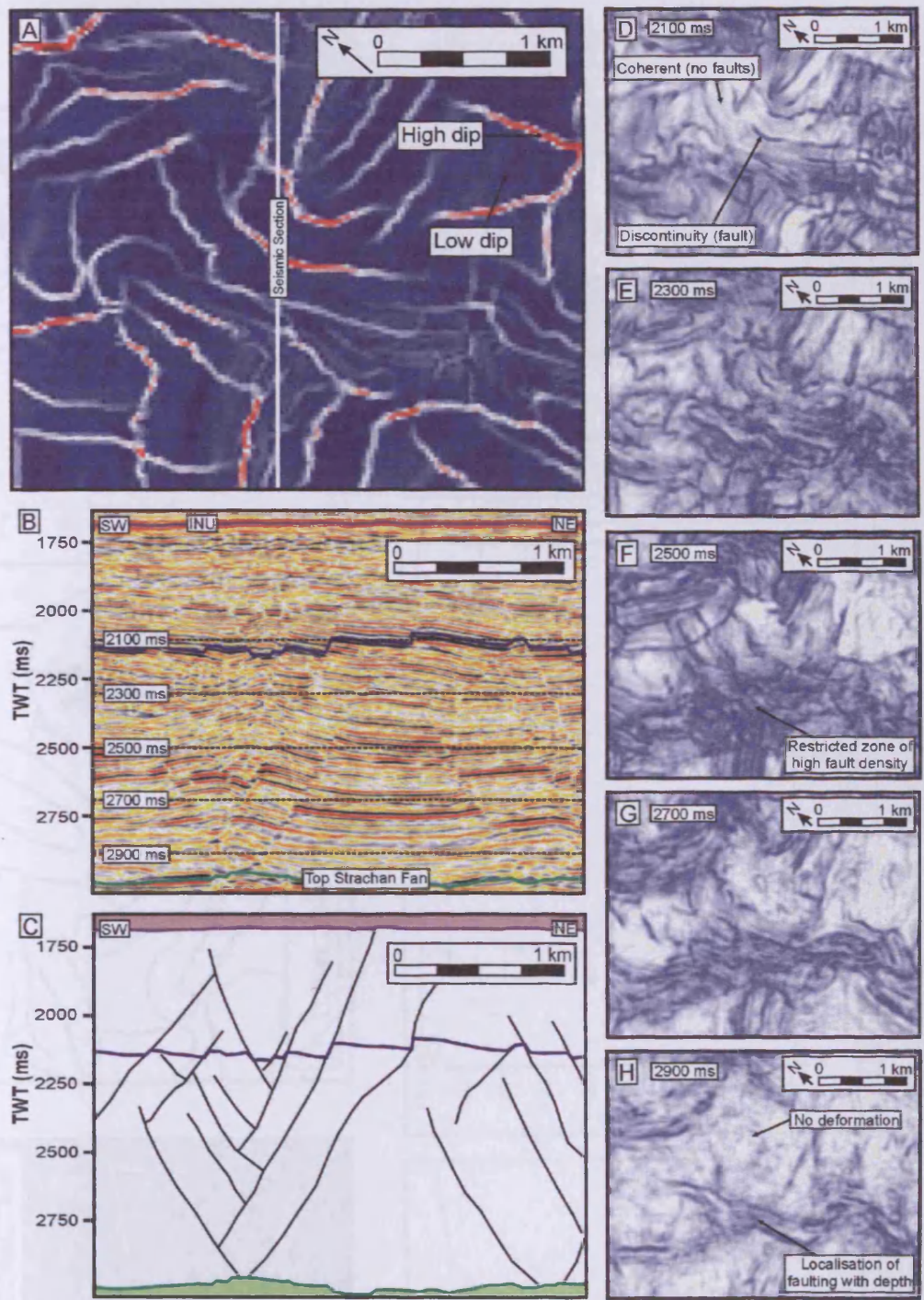


Fig 3.9 A) Dip map of a complex array of polygonal faults (Blue marker horizon Fig.9b) showing the position of the seismic line shown in Fig.9b. B) Seismic section through the polygonally faulted Eocene-Oligocene claystone succession. Depth of variance slices in Figs.9d-h marked with dashed lines. C) Schematic of the seismic section in Fig.9b. Note how inward dipping bounding faults separate domains of high levels of brittle deformation and no brittle deformation. Zones of intense deformation become more localized with depth. D to H) Variance slices every 200 ms through the polygonally faulted section. Note how faulting becomes localized into intense segmented zones of deformation separated by regions of very little or no discernable deformation.

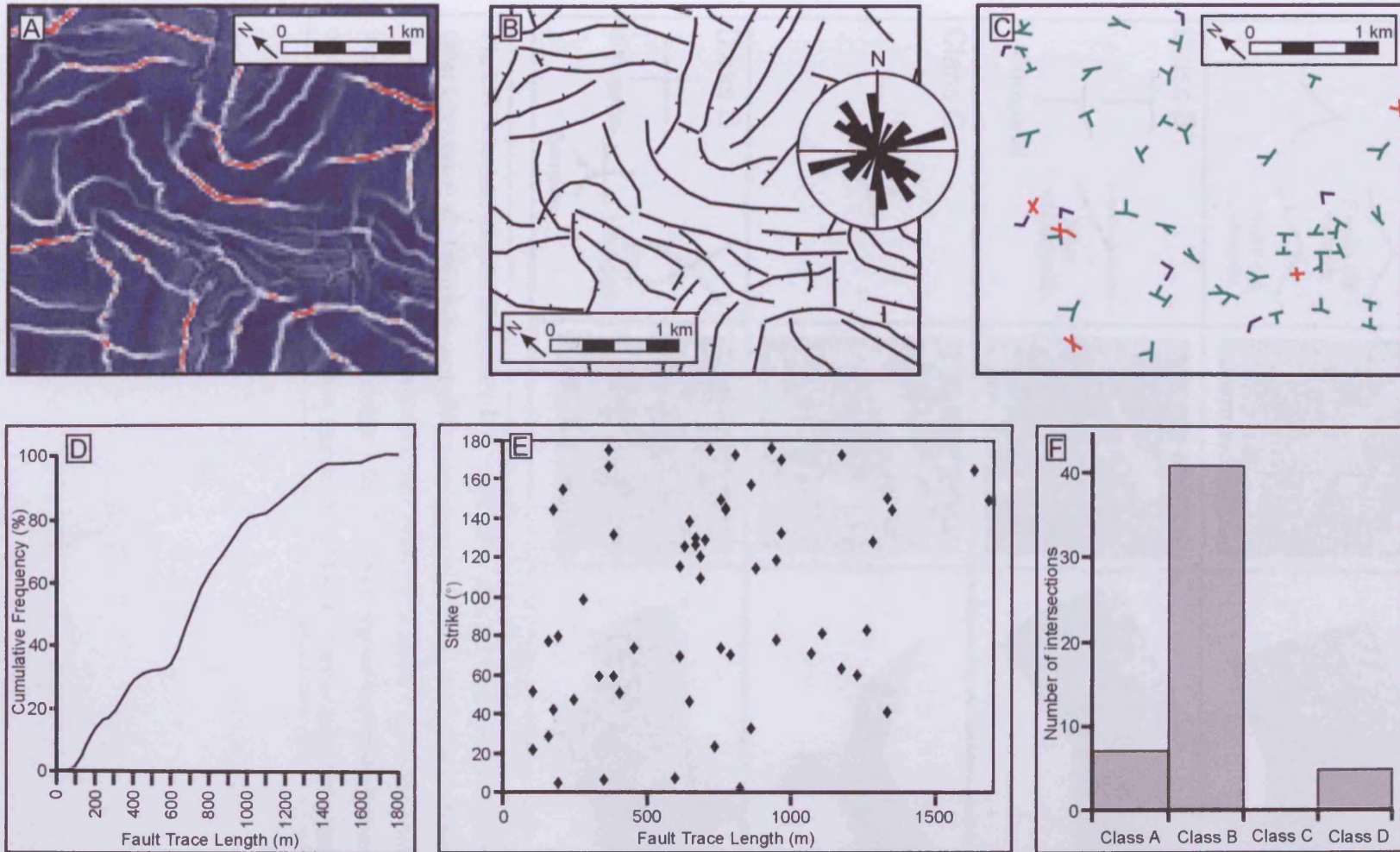


Fig 3.10 A) Dip map showing a complex array of polygonal faults (blue marker horizon Fig.9b). B) Schematic diagram showing fault alignment. Downthrown hanging wall block denoted with a tick. Map of fault intersections: Class A – Blue; Class B – Green; Class C – Red. D) Distribution of horizontal fault trace lengths. E) Comparison of fault strike and horizontal fault trace length showing a random distribution of fault lengths with fault orientation. F) Numbers of fault intersections of different classes – note the lack of Class C intersections and the dominance of Class B intersections.

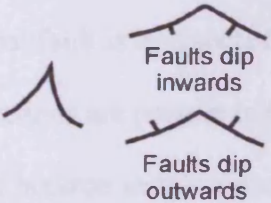
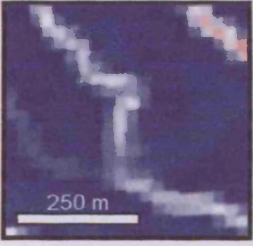
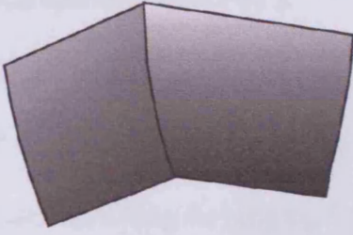
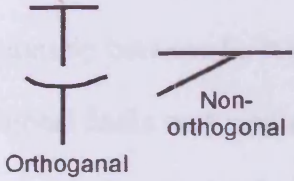
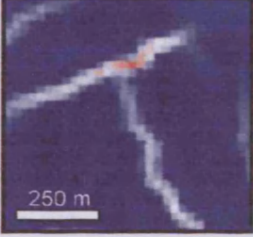
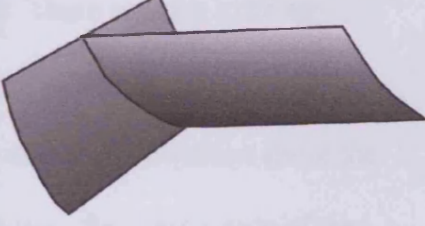
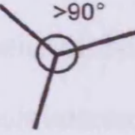
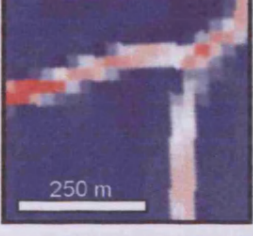
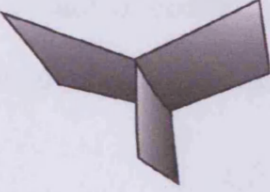
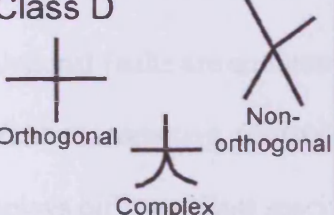
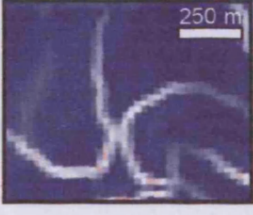
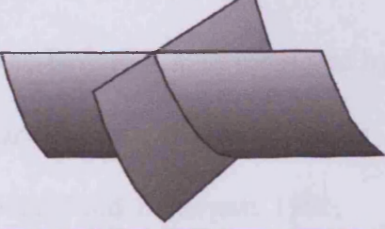
Plan view	Dip map example	3D-schematic representation
<p>Class A</p> 		
<p>Class B</p> 		
<p>Class C</p> 		
<p>Class D</p> 		

Fig 3.11 Schematic diagram of the main fault intersection types for the polygonal fault system (after Lonergan *et al.*, 1988) with examples in dip map data from the Faroe-Shetland Basin. Class A – Two non-colinear faults intersecting at segment endpoints. Class B – A principal fault intersected by an adjoining fault at any angle. Class C – Three non-colinear faults intersecting at a common branch line forming intersection angles $>90^\circ$. Class D – Four or more faults intersecting.

intersection types identified by Lonergan *et al.*, (1998) are present in the sample area (Fig 3.10F). The sample area is dominated by Class B intersections where by a principal fault is intersected by a single adjoining fault (Fig 3.10F). No Class C intersections are present in the study area. The length of the polygonal faults on the marker horizon shows a normal distribution with individual fault lengths ranging from 105 m to 1684 m (average length 714 m) (Fig 3.10D). There appears to be no relationship between fault length and orientation (Fig 3.10E). Characterising polygonal faults on a single horizon provides a great deal of information about the fault network at the level of the marker horizon. However, the distribution of the polygonal fault network changes with depth (Fig 3.9). As a result, so do the characteristics of the polygonal faults at differing levels. In particular, the character of a single fault intersection commonly varies with depth.

Polygonal faults are commonly arranged in stratigraphically bound tiers separated by unfaulted strata (e.g. Cartwright, 1994a; Cartwright and Lonergan, 1996). Each tier displays different fault spacing and orientations (Cartwright and Lonergan, 1996; Lonergan *et al.*, 1998; Dewhurst *et al.*, 1999). Separate tiers of faults commonly also show different dips, with older, more heavily compacted tiers showing shallower average dips than stratigraphically shallower, younger faults (Lonergan and Cartwright, 1999). Maximum fault displacements are commonly measured in the centre of a tier with throws decreasing towards both upper and lower tips (Dewhurst, *et al.*, 1999). Two lines of evidence point to the presence of only a single tier of polygonal faults in the study area: 1) Through-going faults are very common and there are no unfaulted units present that might represent tier boundaries. 2) The

uniformity of strain pattern with maximum displacement occurring near the middle of the polygonal faults (Fig 3.8A).

Whilst most polygonal faults terminate at the INU surface, a small subset (approximately 2-3% of the total number of faults in the study area) situated on the break of slope in the north of the study area continue through the INU in to the basal units of the overlying Neogene contourite drift succession. Fault propagation through the INU is associated with the presence of small growth packages within the contourite drift (Fig 3.8B). Displacement analysis of these faults shows a bimodal distribution with maximum displacements of up to 50 m present in the centre/lower centre of the fault and a smaller secondary peak or marked change in displacement gradient towards the upper tip of the faults in association with the growth package (Fig 3.8B). It is likely that this displacement distribution can be explained by reactivation of the upper portion of the polygonal faults during contourite drift deposition (Stuevold *et al.*, 2003).

3.5.2 Characteristics of large-scale conical amplitude anomalies within the study area

The most striking features observed on the three-dimensional seismic data are a distinctive suite of discordant, high-amplitude reflections found throughout the Eocene–Oligocene interval. The high seismic amplitudes and the opposite polarity of upper and lower reflections imply an acoustically hard (high-impedance) body encased within relatively low-impedance Eocene claystones. No conical amplitude anomalies are found above the INU. Conical amplitude anomalies are arranged in two

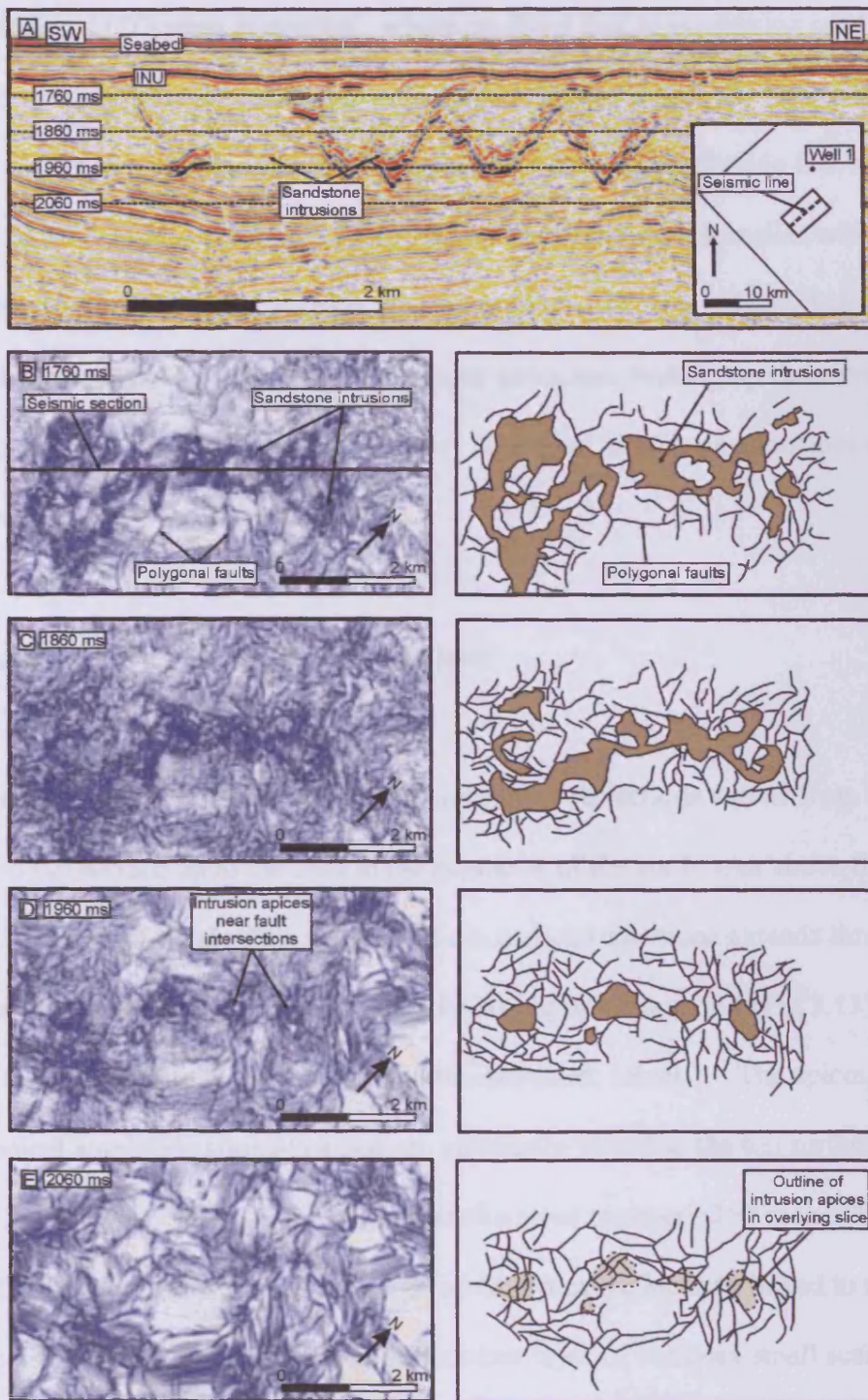


Fig 3.12 A) Seismic section through a series of orphan conical sandstone intrusions with no observable feeder system. Note the range of different apex geometries including: pointed, rounded and flattened or bowl-shaped. Depth of variance slices marked with dashed lines. B to E) Variance slices every 100 ms through the polygonally faulted section containing the sandstone intrusions with an interpretation of the variance slice to the right (sandstone intrusions are marked in pale brown). Note how polygonal faults have a well-defined linear character whilst sandstone intrusions have a more globular texture. D) Intrusion apices are closely related to fault intersections. E) No evidence of a feeder system can be seen in the polygonally faulted section below the conical sandstone intrusions.

distinct styles: 1) “Orphan anomalies” where no direct link to underlying sand units can be identified using either conventional amplitude data (Fig 3.12A) or variance slicing (Fig 3.12E). High-amplitude reflections that have no observable link to an underlying sand source make up 85% to 90% of the amplitude anomalies within the study area. 2) Interconnected systems of amplitude anomalies physically linked to the Middle-Eocene Fans (Fig 3.13). The amplitude anomalies making up these networks form around 10% to 15% of the total number of conical amplitude anomalies in the study area.

3.5.3 Networks of high-amplitude reflections

Interconnected systems of discordant high amplitude reflections extend from the level of the top fan surface up to the INU in the northeast of the study area above the Corona Ridge Fault block. This network of discordant reflections extends through up to 700 m of vertical section, cross-cutting the stratigraphic layering (Fig 3.13). Two distinct levels of amplitude anomalies can be identified: Level 1 – The apices of large-scale conical amplitude anomalies that are physically linked to the top surface of the Middle Eocene fans. These high amplitude reflections cross-cut 250 m to 300 m of strata. The upper terminations of the large-scale conical reflections linked to the fans are coincident with a stratigraphically concordant layer of complex small scale high-amplitude anomalies. Level 2 – The apices of some of the large-scale conical amplitude anomalies in this level are rooted in the stratigraphically concordant layer of small-scale amplitude anomalies that make up the top of level 1. They extend upwards for 250 m to 350 m and terminate either at the INU or at a low-amplitude hard reflection previously interpreted as the Opal CT diagenetic transition (Davies

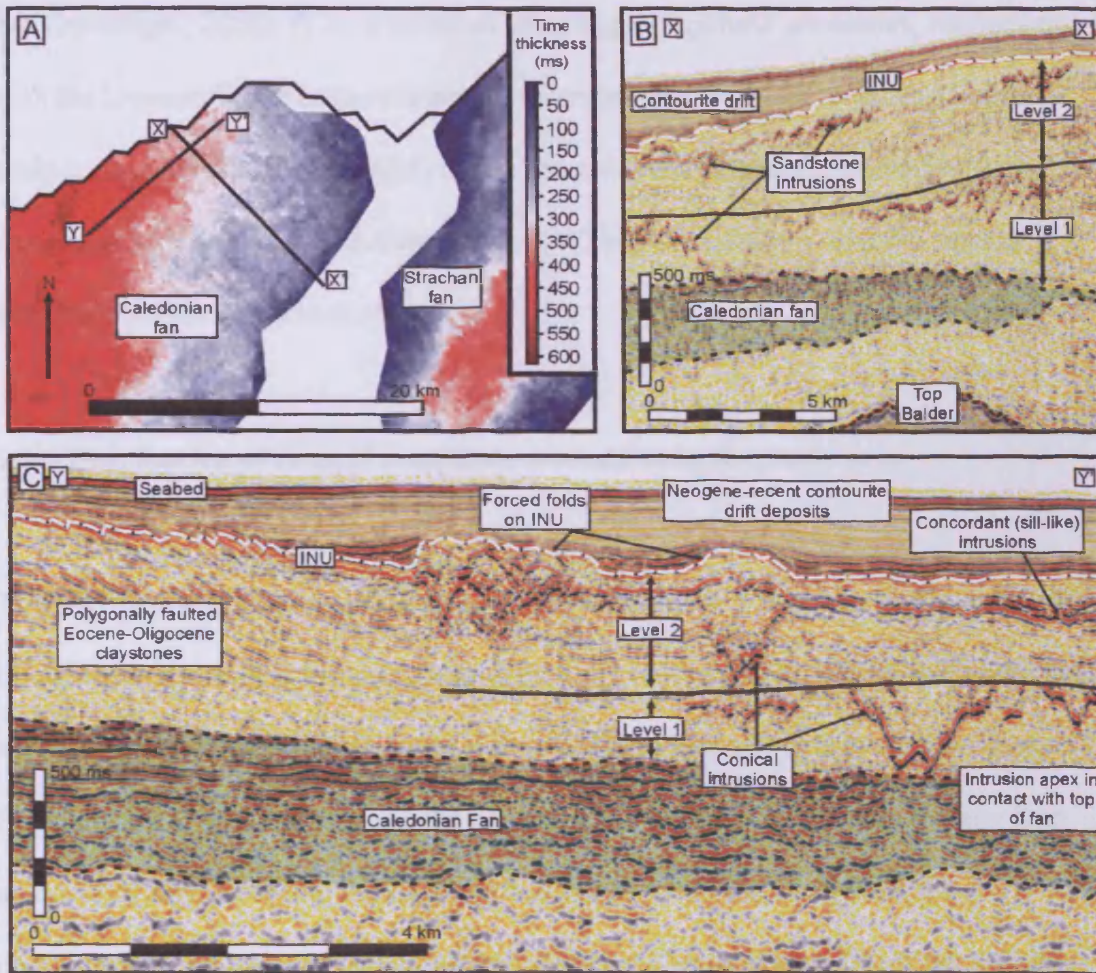


Fig 3.13 A) Location map showing the position of seismic lines X-X' and Y-Y' relative to the Caledonian and Strachan fans. B) Seismic line X-X' showing the position of two distinct levels within a sandstone intrusion network from the Eocene-Oligocene succession overlying the Caledonian Fan and possibly related to a high on the Top Balder surface. This high represents the Corona Ridge Fault block. C) Conical sandstone intrusions in the basal level of the intrusion network are physically linked to the Caledonian Fan. The top of level 1 is marked by a series of concordant high amplitude reflections likely to represent sandstone sills. Conical sandstone intrusions within level 2 are physically linked to the flat lying intrusions that mark the top of level 1. Conical sandstone intrusions in level 2 propagate upwards as far as the INU and cause uplift of

and Cartwright, 2002). A layer of small scale high-amplitude anomalies, concordant with the low-amplitude hard reflection interpreted as a diagenetic boundary. Large-scale conical amplitude anomalies in this upper level are spatially related to short wavelength (~1 km) domal folding on the INU surface (Section 2.5). No conical amplitude anomalies extend above the INU.

3.5.4 Distribution of conical amplitude anomalies in the study area

The distribution of high-amplitude anomalies in Tranche 6 forms an irregular NE-SW orientated swath across the study area (Fig 3.14). The underlying Middle-Eocene fans are orientated NW-SE in the case of the Caledonian Fan and N-S in the case of the Strachan Fan (Fig 3.14). Despite the physical link between the Middle-Eocene fans and conical amplitude anomalies identified in the NE of the study area, the distribution of high-amplitude anomalies does not closely match that of the Middle-Eocene fans. Amplitude anomalies can commonly be found several kilometres from the margins of the Middle Eocene fans.

The high-amplitude conical reflections within the study area are located above the margins of a thick NE-SW orientated Palaeocene depocentre (Mitchell *et al.*, 1993) (Fig 3.5B). Basement fault blocks at depth, and in particular the Corona Ridge fault block (represented by highs on the Top Balder surface in the NW of the study area), and Mid-Faroes Ridge (e.g. Jowitt *et al.*, 1999) (Fig 3.2) are also orientated NE-SW parallel to the distribution of the conical amplitude anomalies situated within the Eocene-Oligocene succession. This spatial relationship may imply that basement structure and the Palaeocene depocentre underlying the Eocene-Miocene succession

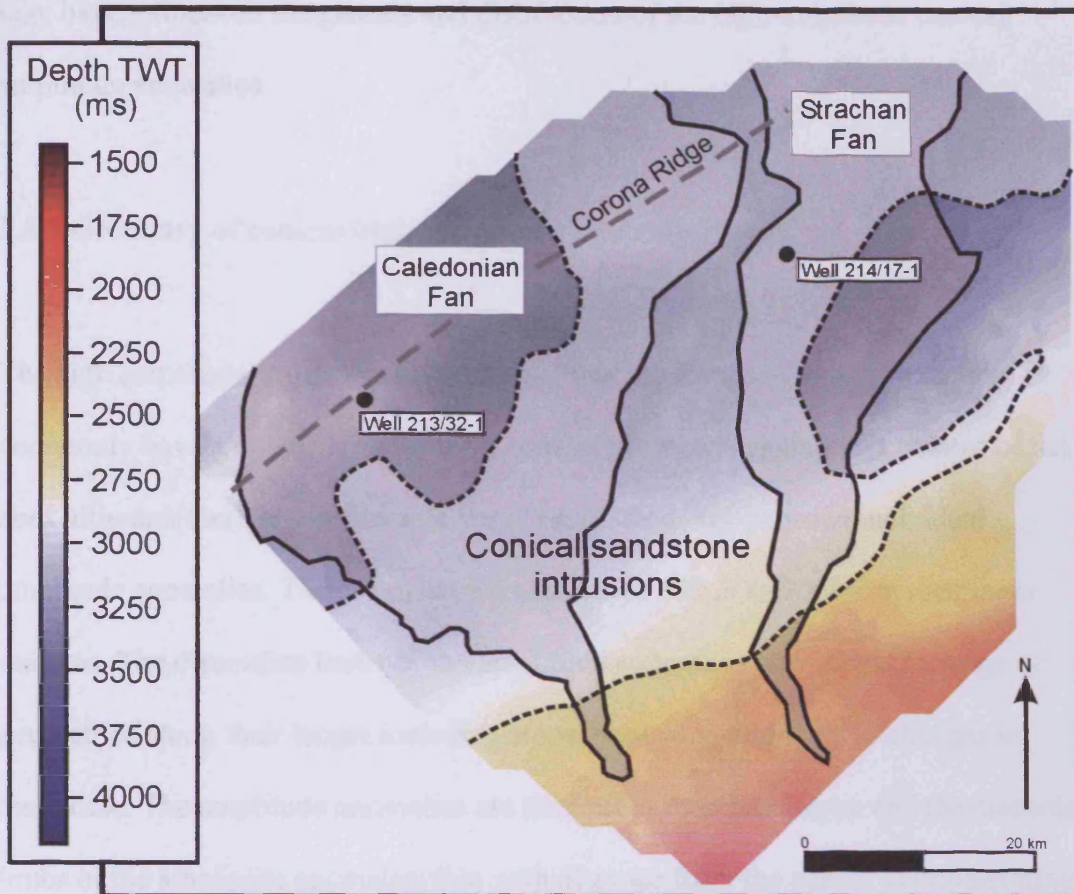


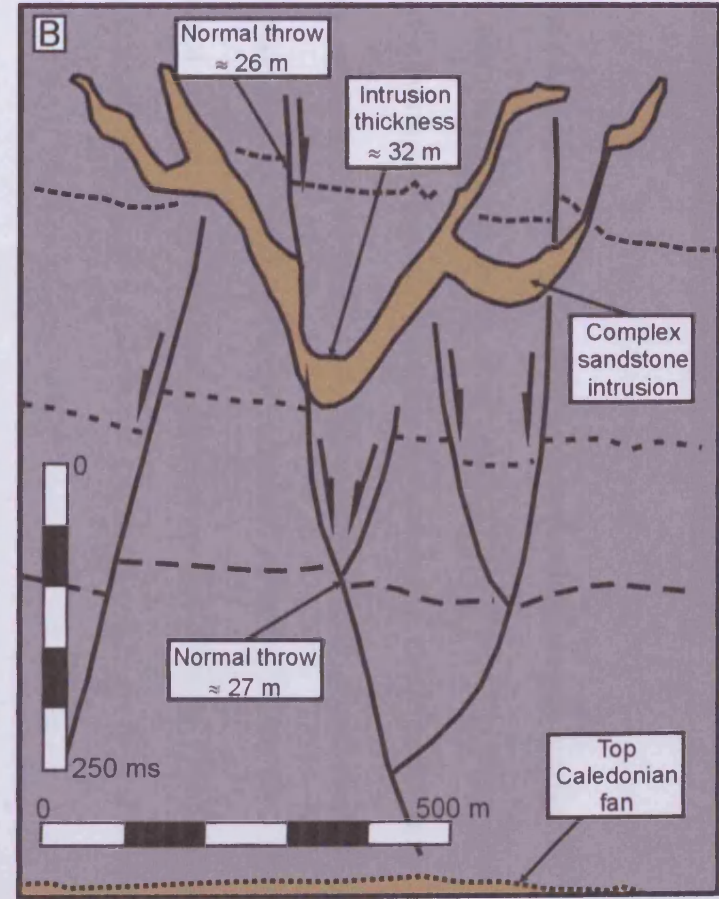
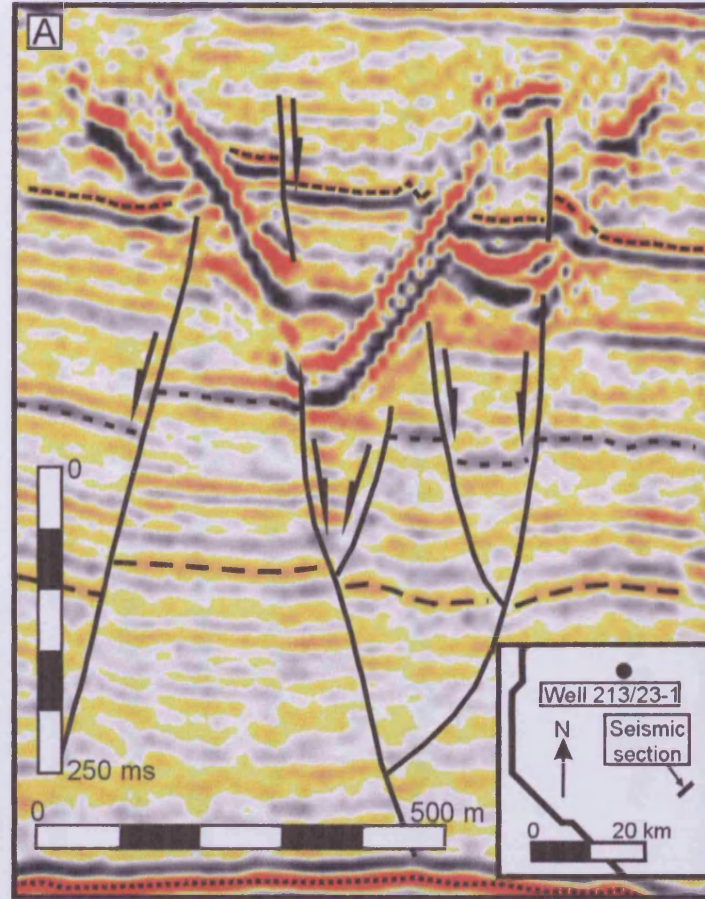
Fig 3.14 A time structure map (in two way travel time [TWT]) of the top Balder surface. The elongate NE/SW orientated structural high in the north of the study represents the Corona Ridge fault block. Superimposed on this map are the positions of the Middle Eocene fans, the Caledonian Fan in the west of the region and the more highly constrained Strachan Fan in the East of the study area (semi-transparent grey areas surrounded by solid black lines) and the distribution of sandstone intrusions in the study area (pale region surrounded by a dashed black line). Note how the distribution of sandstone intrusions does not appear to closely resemble the distribution of the underlying Middle Eocene fans, but is instead appears to be more closely related to the NE/SW structural grain of the region.

may have influenced the genesis and distribution of the high-amplitude conical amplitude anomalies.

3.5.5 Geometry of conical high-amplitude anomalies

The high amplitude anomalies found throughout the Eocene-Oligocene section commonly have a downwards-tapering conical geometry leading to a pointed or flat apex although there is considerable variation in geometry between individual amplitude anomalies. The cones have diameters of 500 m to 1000m at their outer margins. The discordant limbs of the amplitude anomalies may display a range of geometries along their length including steps, branching and marked changes in amplitude. The amplitude anomalies are thickest at their basal apex and the discordant limbs of the amplitude anomalies thin with distance from the apex. No cross-cutting relationships between conical reflections were observed. However, polygonal faults are commonly cross-cut by conical amplitude anomalies (Fig 3.15). In the example shown in Fig 3.15, the apex of a complex conical amplitude anomaly is situated over a polygonal fault. The throw on the polygonal fault can be measured at three marker horizons, two beneath the amplitude anomaly and one in the uplifted block above the amplitude anomaly. At each of the three markers, the throw on the fault is very similar (i.e. $27 \text{ m} \pm 2 \text{ m}$). The thickness of the amplitude anomaly is greater than the throw on the fault (i.e. $32 \text{ m} \pm 2 \text{ m}$). This strongly implies that the emplacement of the conical amplitude anomaly has resulted in the uplift of the overlying block without the re-activation of the fault.

Fig 3.15 A) A seismic line through a complex branching conical sandstone intrusion. The intrusion cross-cuts pre-existing polygonal faults. B) A schematic drawing of the seismic section in Fig.15a. The throws of faults above and below the conical intrusion are very similar. However, the thickness of the intrusion is considerably greater than the throw on the fault implying that the whole block above the intrusion has been uplifted and the polygonal fault is cross-cut by the conical intrusion.



3.5.6 Dip of conical high-amplitude anomalies

The discordant limbs of the amplitude anomalies have an average dip of $26^{\circ} \pm 2^{\circ}$ (with values from individual intrusions ranging from 6° to 57°). There does not appear to be any relationship between intrusion dip and depth. The 5° to 60° range in the dip of the discordant limbs of the conical high-amplitude anomalies is seen throughout the section from the level of the INU (depth of around 1700 ms TWT) to the level of the top of the Middle Eocene Fans (depth of around 2900 ms TWT). In contrast, polygonal faults show a distinct trend towards shallower dips with increased depth (Fig 3.6A). The dips of conical high-amplitude anomalies are, in general, much shallower than those displayed by polygonal fault planes (i.e. average dip of $26^{\circ} \pm 2^{\circ}$ for conical high-amplitude anomalies as opposed to $58^{\circ} \pm 2^{\circ}$ for polygonal faults) (Fig 3.6A),

3.5.7 Origin of conical high-amplitude anomalies in the Faroe-Shetland Basin

The discordant geometry and the reflection character of these conical reflections are suggested here as being evidence for an intrusive origin. The geometry of the amplitude anomalies is irregular and exhibits splays that are often seen in igneous intrusive bodies (e.g. Trude *et al.*, 2003). Whilst there are no direct well calibrations of the discordant high-amplitude reflections within the Eocene-Oligocene sequence above the base of slope fans in this survey area, several lines of evidence lead us to conclude that the intruded material is likely to be sandstone: (1) The interconnected networks of conical amplitude anomalies physically connect to the top of the sand-rich middle Eocene submarine fan (i.e. intrusions can be observed to emanate from

the upper fan surface Fig 3.13). This physical connection implies that the fans may be a probable source for sand to form at least some of the conical high-amplitude anomalies. (2) Conical discordant reflections with identical acoustic properties, geometry, and scale have been recognized within Eocene claystone packages over large areas of the North Sea Basin where they have been tied to wells and interpreted as giant conical sandstone intrusions up to 50 m in thickness (e.g.: Molyneux *et al.*, 2002; Huuse and Mickelson, 2004) (see Table 3.1). (3) Igneous intrusions are commonly represented by high amplitude reflections in seismic data (Davies *et al.*, 2002; Hansen *et al.*, 2004; Trude, 2004). However there is no evidence for any igneous activity within the basin later than the Paleocene–early Eocene (Gibb and Kanaris-Sotiriou, 1988; Ritchie and Hitchen, 1996), making it unlikely that these shallow intrusions, hosted in the Eocene–Oligocene section, are of igneous origin.

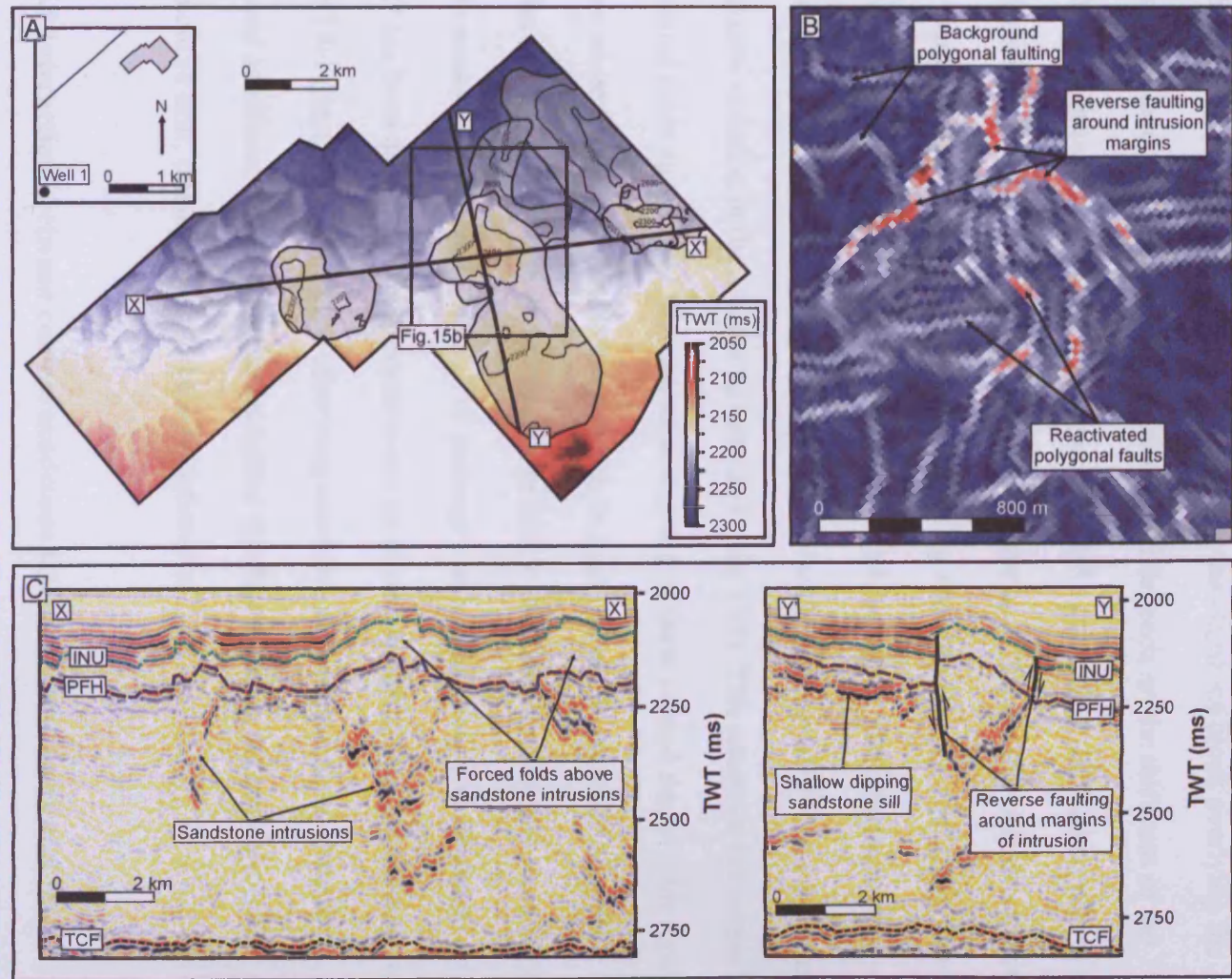
3.5.8 Folding of the INU and the timing of sandstone intrusion

Discordant high-amplitude seismic reflections, interpreted as large-scale conical sandstone intrusions are found throughout the Eocene-Oligocene claystone succession up to, but not above the level of the INU. Conical sandstone intrusions that terminate at the level of the INU show a strong spatial relationship to domal forced folding on the unconformity surface (Section 3.5) (Fig 3.16). The Eocene-Oligocene claystones above shallow intrusions are usually uplifted along curved reverse faults propagating from the tips of the discordant limbs of the underlying sandstone intrusions (Fig 3.16). The domal forced folding is interpreted as uplift rather than differential subsidence because seismic reflections inside the conical high amplitude anomalies are stratigraphically higher than in the surrounding undisturbed host rock (e.g. Fig 3.15

Table 3.1 Well calibrations of sandstone intrusions

Author	Location	Intrusion Dip	Calibration
Huuse and Mickleson, 2004	Well 34/7-9 Tampen Spur area (Norwegian North Sea Quad 34)	25° to 40°	65 m sandstone in well (therefore 50-60 m true thickness). Sandstone partially cemented and water wet.
Huuse <i>et al.</i> , 2004	Viking Graben, UK North Sea	20° to 40°	62 m thick sandstone. Seismic reflection from 2-3 m thick cemented base
Hurst <i>et al.</i> , 2003	Well N25/12-1 Norwegian North Sea	Not stated	40 m sandstone (approximately 20 m cemented)
Molyneux <i>et al.</i> , 2002	UK North Sea well 21/5-1	5° to 25°	Three blocky sandstones separated by claystones, true bed thickness 45 m
Gras and Cartwright 2002	Well 22/2a-5 Chestnut Field UK North Sea	10° - 15°	45 m thick sandstone (The Carron Sandstone)

Fig 3.16 A) Depth map of a polygonally faulted horizon below the INU (blue dashed line Fig. 16c) with the position of underlying intrusions overlain. Local sub-circular highs on the mapped surface are closely spatially related to shallow conical sandstone intrusions. B) A dip map of the mapped surface above a shallow conical sandstone intrusion reveals that uplift above shallow intrusions is accommodated by the reactivation of the pervasive polygonal fault network and by the formation of reverse faults around the margins of the intrusion. C) Seismic sections through the mapped region: X-X' Shallow intrusions, underlain by deeper feeder intrusions, cause the uplift of the INU surface (green dashed line). Maximum uplift occurs above the thickest parts of the underlying intrusion (usually the apex) and the resultant extension of the overlying block is taken up by the reactivation of pre-existing polygonal faults. Note the presence of high-amplitude packages of post-INU contourite drift strata that onlap the mounded geometry on the INU formed as a result of intrusion and uplift. Y-Y' Uplift of strata overlying a shallow intrusion is not just facilitated by extension of the overlying strata, but also by the formation of reverse faults around the margins of the shallow intrusion.



and Fig 3.17). The amount of uplift suffered by the claystone block overlying the conical sandstone intrusion is heterogeneous and depends on the thickness of the underlying intrusion. The greatest amount of uplift occurs over the thickest part of the underlying conical sandstone intrusion, usually the apex. Less uplift occurs towards the margins of the sandstone intrusion suggesting that the intrusions generally thin with distance from the basal apex. The block overlying the conical intrusion undergoes extensional faulting as a result of the heterogeneous uplift exerted by the thickness variation in the associated intrusion (Fig 3.16). This results in the formation of domal folds on the INU. The subsequent onlap of these seabed domal folds took place immediately after the intrusion event. In many cases the presence of well-defined fault scarps on the domal structures on the INU implies that there was very little erosion subsequent to uplift. The package that onlaps the domal structures on the INU has been dated as Late Miocene based on biostratigraphic data derived from well 214/17-1 (Section 2.5). It is therefore suggested that the emplacement of shallow conical sandstone intrusions occurred before the deposition of the Late Miocene contourite drift, possibly during the early Miocene.

3.5.9 Interactions between conical sandstone intrusions and polygonal faults

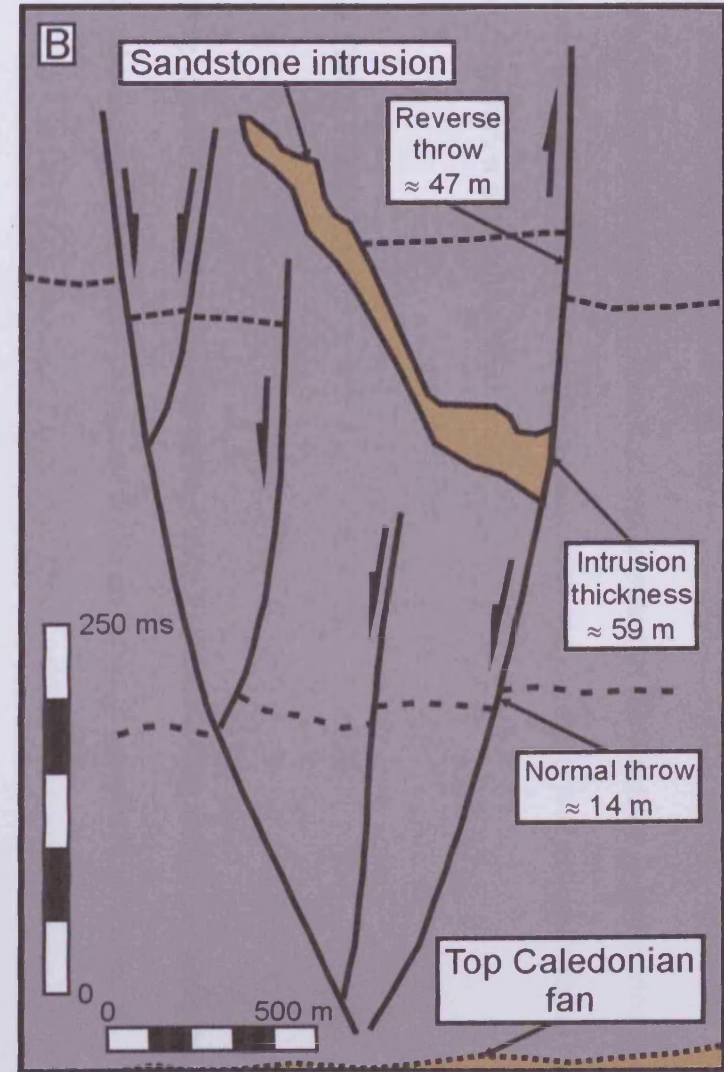
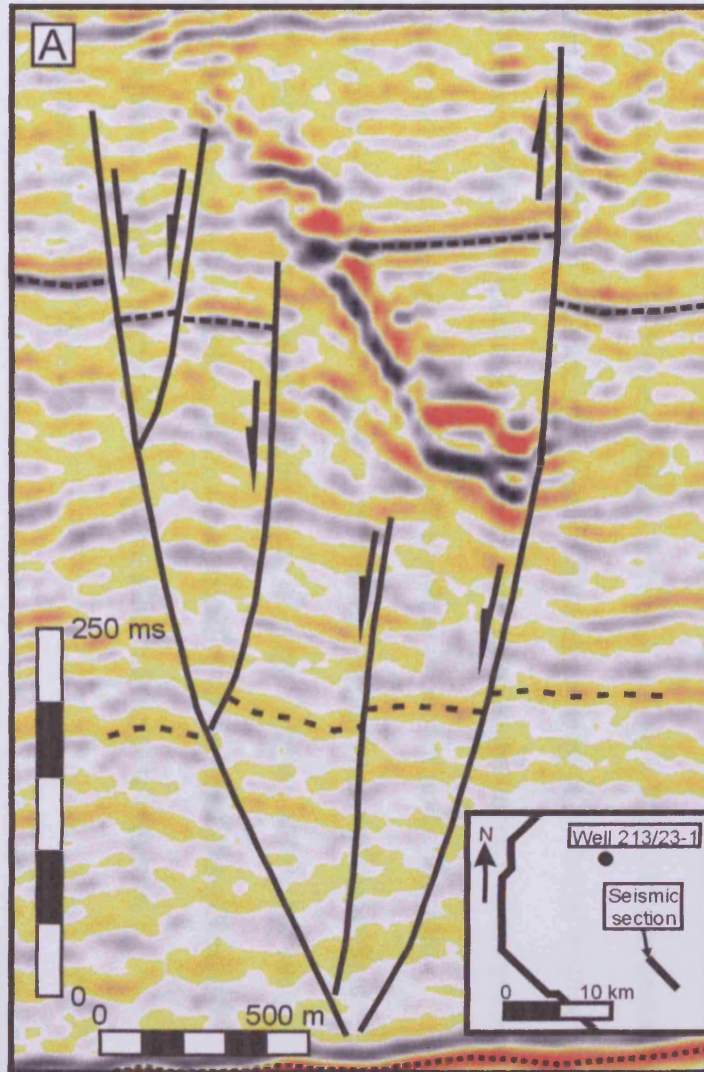
Variance slicing through a set of orphan intrusions within the polygonally faulted Eocene-Oligocene claystone sequence can be used to explore the relationship between the polygonal faults and the sandstone intrusions. A linear array of orphan conical sandstone intrusions with a range of apex geometries from pointed; to flat can be examined in this manner (Fig 3.12). The discordant limbs of the conical intrusions do not appear to be closely related to the distribution of polygonal faults at this level.



However, the apices of the conical intrusions have a close spatial relationship to the intersections of underlying polygonal faults (Fig 3.12E). This is an important observation because the intersections of polygonal faults have been recognised as conduits for enhanced fluid flow through otherwise impermeable systems (e.g. Berndt *et al.*, 2003; Stuevold *et al.*, 2003; Gay *et al.*, 2004). As with conventional amplitude seismic data, no feeder system for the orphan conical sandstone intrusions is imaged using variance slicing (Fig 3.12).

Sandstone intrusions that emanate from, or have a strong spatial relationship to, polygonal faults are common in the study area. This spatial link may take the form of the close proximity of the apex of a conical intrusion to the intersection of underlying polygonal faults (Fig 3.12) or the emplacement of a single discordant intrusion limb from a polygonal fault plane (Fig 3.17). Intrusions such as this have a sharp contact with the polygonal fault plane, which represents the basal termination of the intrusion. Generally this class of intrusion displays a single discordant limb that extends away from its basal termination, the polygonal fault plane. The intrusion is thickest at the intersection of the fault plane and the intrusion and thins with distance from the polygonal fault. The dip and dimensions of this class of intrusion are comparable to that of the conical sandstone intrusions seen throughout the study. In the example shown in Fig 3.17, the character of the polygonal fault changes from extensional, normal faulting below the intrusion, to reverse faulting above the intrusion. Material above the intrusion is uplifted relative to the surrounding host rocks. The thickness of

Fig 3.17 A) A seismic section through a sandstone intrusion consisting only of a single limb emanating from a polygonal fault. B) A schematic drawing of the seismic section in Fig. 17a. Note that the polygonal fault from which the sandstone intrusion emanates displays normal throw beneath the intrusion, but reverse displacement above the intrusion. The total amount of throw above and below the sandstone intrusion is roughly equivalent to the thickness of the intrusion. This strongly implies that the intrusion process has resulted in the reactivation of the polygonal fault.



the intrusion ($59 \text{ m} \pm 3 \text{ m}$) is very similar to the total amount of reverse movement above the fault ($60 \text{ m} \pm 4 \text{ m}$). Thus the emplacement of the intrusion is interpreted to have caused the uplift of the overlying host rock and the uplift was accommodated by the reactivation of the polygonal fault.

3.6 DISCUSSION

Using seismic and well data we have been able to examine the present-day geometries of and relationships between polygonal faults and conical sandstone intrusions in Tranche 6 in the Faroe-Shetland Basin. Post-emplacement compaction on the Eocene-Oligocene succession may have altered the geometry of both the polygonal faults and sandstone intrusions in the Faroe-Shetland Basin. However, it is possible to assess the extent of the effects of post-intrusion compaction by looking at the burial history of the Eocene-Oligocene succession, and examining the possible effects of compaction on fault and intrusion dips. Evaluating the possible effects of post-intrusion compaction provides important clues as to how the emplacement of the conical sandstone intrusions proceeded. The presence of large volumes of injected sands cross-cutting hundreds of metres of low-permeability claystones of the Eocene-Oligocene succession is highly likely to have affected the post-intrusion hydrodynamic history of the basin.

3.6.1 Key observations

Conical sandstone intrusions in the study area thin with distance from their basal apex. The discordant limbs of the conical sandstone intrusions have an average dip of

26° (with individual values ranging from 6° to 57°) whilst polygonal faults within the study area have an average dip of 58° (with individual values ranging from 23° to 85°) (Fig 3.18). The values for polygonal fault dips are consistent with previously published studies (see Table 3.2), although larger than the average of Lonergan and Cartwright (1999). The two dip populations are very distinct (Fig 3.18). The polygonal faults in the study area are arranged in a single tier and tend to display a near planar geometry but steepen towards the INU and shallow onto the top of the Middle Eocene fans or Top Balder surface. Polygonal fault dips shallow with depth with dips of 60° to 80° recorded near the level of the INU but much shallower dips of 30° to 40° at the level of the base of slope fans. In contrast, there is no relationship between depth of conical sandstone intrusion and the angles of their discordant limbs, which are within 10° to 50° throughout the Eocene-Oligocene succession.

3.6.2 Timing of polygonal faulting in Tranche 6

Most polygonal faults in the region are truncated by the INU. This implies that they formed prior or during the erosion of the unconformity surface. Similarly, where present in the study area, the Opal A-CT event is also truncated by the INU. Therefore this implies that erosion continued after this diagenetic event in this part of the basin (Fig 3.3B). Conical sandstone intrusions intruded at shallow depths below the INU caused uplift and deformation of the unconformity surface (Section 2.5) (Fig 3.16). The resultant mounded features formed on the INU are overlapped by the overlying Neogene contourite deposits, thus the INU is likely to have been the seabed at the time of conical sandstone intrusion. Sandstone intrusions commonly cross-cut polygonal faults (e.g. Fig 3.15). There is a strong spatial relationship between

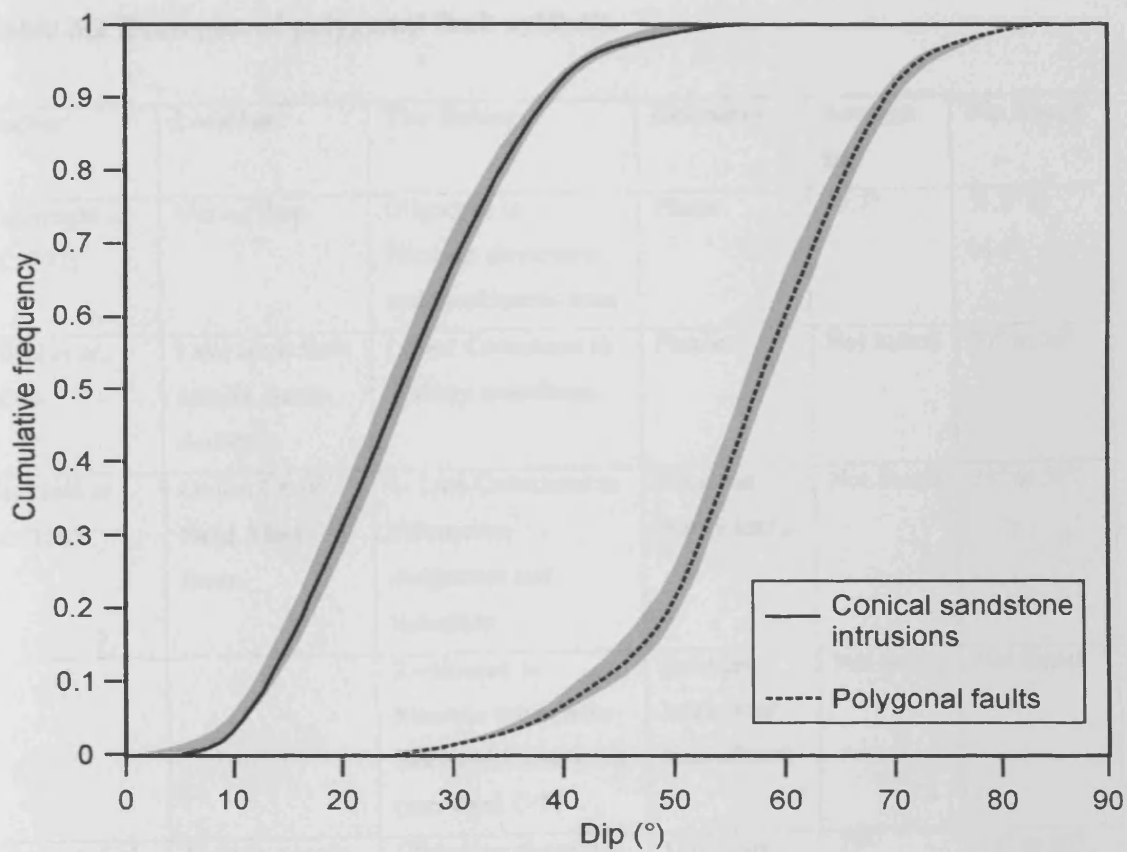


Fig 3.18 Cumulative frequency plot of the dip populations of sandstone intrusions (solid black line) and polygonal faults (dashed black line) for an interval velocity of $1950 \text{ ms}^{-1} \pm 100 \text{ ms}^{-1}$ (represented by the grey envelope around each curve).

Table 3.2 Examples of polygonal fault systems

Author	Location	Tier Setting	Geometry	Average Dip	Dip Range
Cartwright <i>et al.</i> , 2003	Vøring Basin	Oligocene to Pliocene claystones and biosiliceous ooze	Planar	59.7°	51.8° to 64.4°
Nicol <i>et al.</i> , 2003	Lake Hope fault system. South Australia	Lower Cretaceous to Tertiary mudstones	Planar	Not Stated	50° to 55°
Stuevold <i>et al.</i> , 2003	Ormen Lange Field, Møre Basin	1- Late Cretaceous to Palaeocene mudstones and turbidites	Planar to gently listric	Not Stated	25° to 50°
		2 – Eocene to Miocene mudstones and biosiliceous ooze (inc. Opal C-T)	Strongly listric near base of tier	Not Stated	Not Stated
Clausen <i>et al.</i> , 1999	Eastern margin of the Viking Graben, northern North Sea	Oligocene claystone and thinly layered sands	Generally planar, but some gently listric	73°	48° to 85°
Lonergan and Cartwright, 1998	Alba Field Central North Sea	1 – Oligocene - lower Miocene hemipelagic mudstones	Planar or gently listric	45°	27° to 67°
		2 - Eocene-lower Oligocene hemipelagic mudstones	Planar or gently listric	37°	20° to 54°
Cartwright and Lonergan, 1996	Block 16/26. UK North Sea	Two tiers - Lower Tertiary low-permeability mudrocks	Planar or gently listric	45°	30° to 70°
Cartwright, 1994	Block 30/19	Two tiers - Lower Tertiary low-permeability mudrocks	Planar to gently listric	Not Stated	30° to Subvertical

intrusion apices and the intersection of underlying polygonal faults and single-limb sandstone intrusions that emanate from polygonal faults have also been observed, implying that the polygonal fault network may have acted as a feeder system for intrusion in Tranche 6. Based on these observations, it is highly likely that the polygonal fault network was well established before the Late Miocene episode of sandstone intrusion.

3.6.3 Post intrusion compaction

One of the most difficult problems to assess within this study is the extent to which the measured dips of discordant intrusion limbs have been modified by post-emplacment compaction. This is important to establish if the dips of discordant intrusions in the Faroe-Shetland Basin are to be compared to those observed on similar intrusions in the North Sea. The discordant limbs of conical sandstone intrusions in the North Sea commonly display dips ranging from 20° to 40° (e.g. Huuse *et al.*, 2004). The dips of the discordant limbs of the conical intrusions examined during the course of this study were derived by depth-converting the modern day dimensions in seismic data. These intrusions display dips ranging from 6° to 57° (average dip 26° ±2°). Conical sandstone intrusions in the Central and Northern North Sea are commonly intruded early in the burial history into lower Eocene host rocks and are overlain by a considerable thickness of Oligocene to recent sediments (e.g. Molyneux *et al.*, 2002; Huuse and Mickleson, 2004; Huuse *et al.*, 2004). It is therefore likely that the sediments within which the conical sandstones are hosted may have undergone significant compaction since the emplacement of the sandstone intrusions. Vertical compaction of sediment containing a dipping surface or unit will

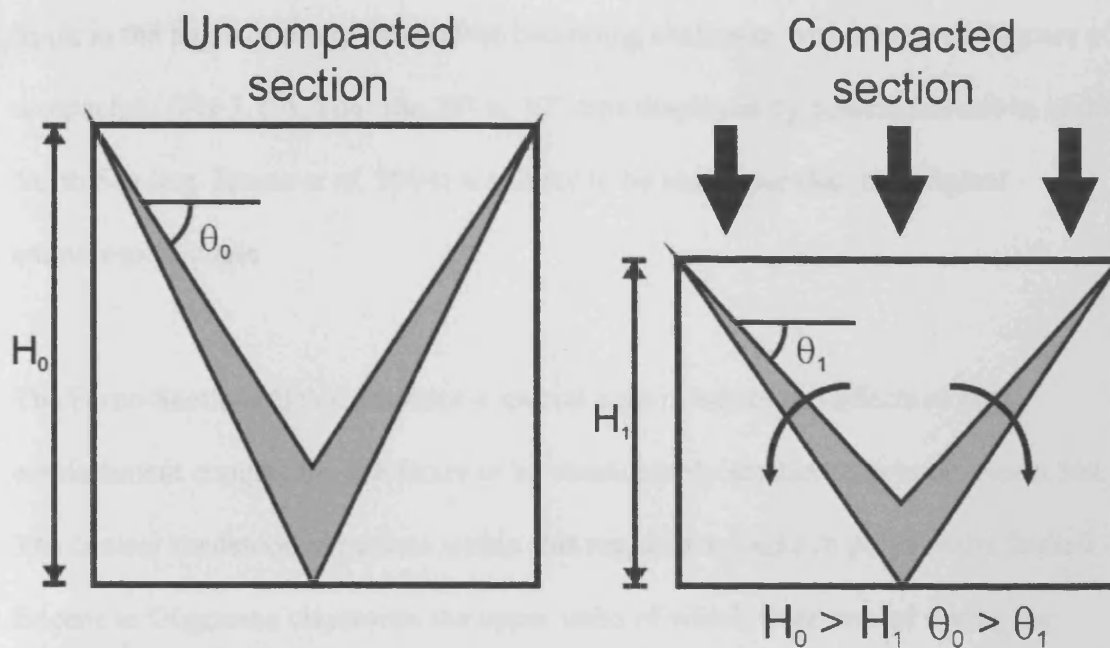


Fig 3.19 Schematic diagram of the effects of vertical compaction on a dipping unit. A conical sandstone intrusion (pale grey), which is V-shaped in cross-section, is hosted within a unit suffering homogenous vertical compaction of the section. This causes the rotation of the discordant limbs of the intrusion – in effect the dip of the sandstone intrusion becomes reduced with compaction.

Example: If the limb of a sandstone intrusion can be described as having $H_0 = 200$ m and $\theta_0 = 26^\circ$ and the host rock block suffers 20% compaction subsequent to the emplacement of the intrusion, $H_1 = 160$ m and $\theta_1 = 21^\circ$

result in the angle of dip of the surface becoming shallower with increased degrees of compaction (Fig 3.19). Thus the 20° to 40° dips displayed by conical intrusions in the North Sea (e.g. Huuse *et al*, 2004) are likely to be shallower than the original emplacement angle.

The Faroe-Shetland Basin provides a special case in which the effects of post-emplacement compaction are likely to be considerably smaller than in the North Sea. The conical sandstone intrusions within this region are found in polygonally faulted Eocene to Oligocene claystones the upper units of which were eroded during the sculpting of the INU by deep-water currents during the Early and Middle Miocene (Stoker *et al.*, 2002; Knutz and Cartwright, 2003). Very few polygonal faults within the Eocene-Oligocene succession propagate through the INU. This implies that, in general, the fault network has been inactive since the erosion of the INU. Thus the dewatering and compaction believed responsible for the formation of polygonal faults (Cartwright *et al.*, 2003) is also likely to have ceased, or at least slowed considerably. The Neogene contourite drift succession that overlies the Eocene-Oligocene claystone succession is very thin throughout most of the study area (only 67m in Well 1) (Fig 3.4A) and is therefore unlikely to contribute to the compaction of older strata. This evidence strongly implies that it is unlikely that there has been significant compaction of older strata since the erosion of the INU.

The dips of the discordant limbs of the conical sandstone intrusions do not show any dependency on depth (Fig 3.6a). This observation may provide insights into the intrusion history and the state of compaction of the host rocks at the time of intrusion. Two possible scenarios that are likely to result in systematic changes in intrusion dip

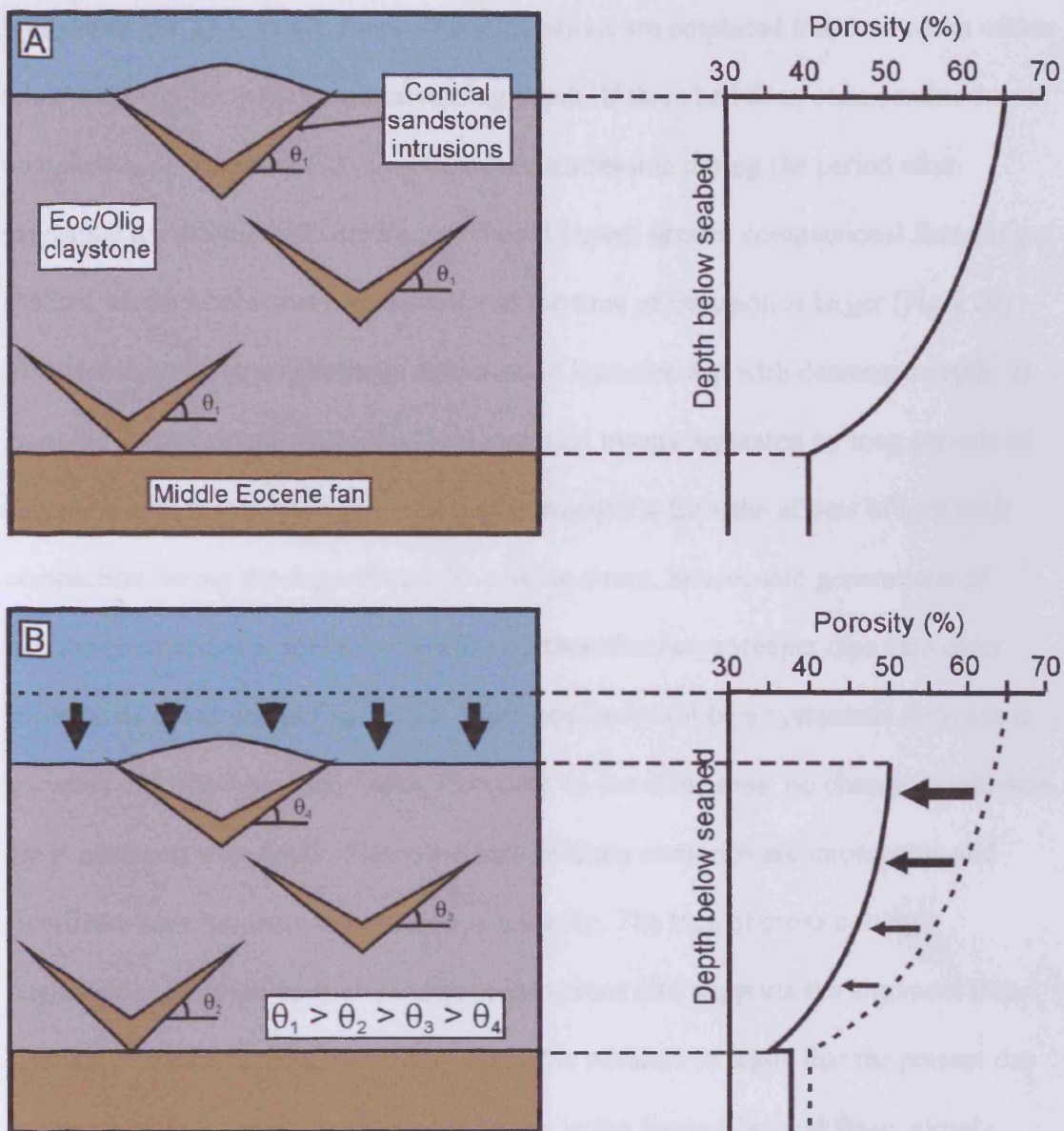


Fig 3.20 A) Conical sandstone intrusions are intruded throughout a semi-compacted host rock succession in a single intrusion event. B) After the emplacement event compaction of the host rock succession continues. The greatest levels of compaction will occur at shallow levels where host rock porosity is greatest. Thus shallow sandstone intrusions will suffer the greatest levels of flattening due to compaction.

with depth are: 1) A single event where intrusions are emplaced into host rocks within which porosity decreases with increasing depth. If there had been considerable compaction of the entire Eocene-Oligocene succession during the period after sandstone intrusion emplacement, we should expect greater compactional flattening at shallow levels where host rock porosity at the time of intrusion is larger (Fig 3.20). This would result in a systematic reduction in intrusion dip with decreased depth. 2) Episodic emplacement with individual intrusion events separated by long periods of claystone deposition. Each generation of intrusions suffers the effects of host rock compaction during the deposition of overlying strata. Subsequent generations of intrusion, emplaced at shallower levels will therefore have steeper dips than older generations of intrusions (Fig 3.21). Therefore there will be a systematic decrease in intrusion dip with increased depth. However, in the study area, no change in intrusion dip is observed with depth. Therefore both of these scenarios are improbable and significant post intrusion compaction is unlikely. The lack of cross-cutting relationships between conical sandstone intrusions also supports the argument that episodic intrusion is highly unlikely. Thus it is possible to argue that the present day geometry of the conical sandstone intrusions in the Faroe-Shetland Basin closely resembles the original late Miocene intrusion geometry and that all the sandstone intrusions within the study area were emplaced during a single intrusive episode.

3.6.4 Conical sandstone intrusions in Tranche 6

The INU is highly likely to have represented the palaeosurface at the time of conical sandstone intrusion. Therefore overburden weight would have been much greater at the level of the Middle Eocene fans than at the level of the INU. However, no depth

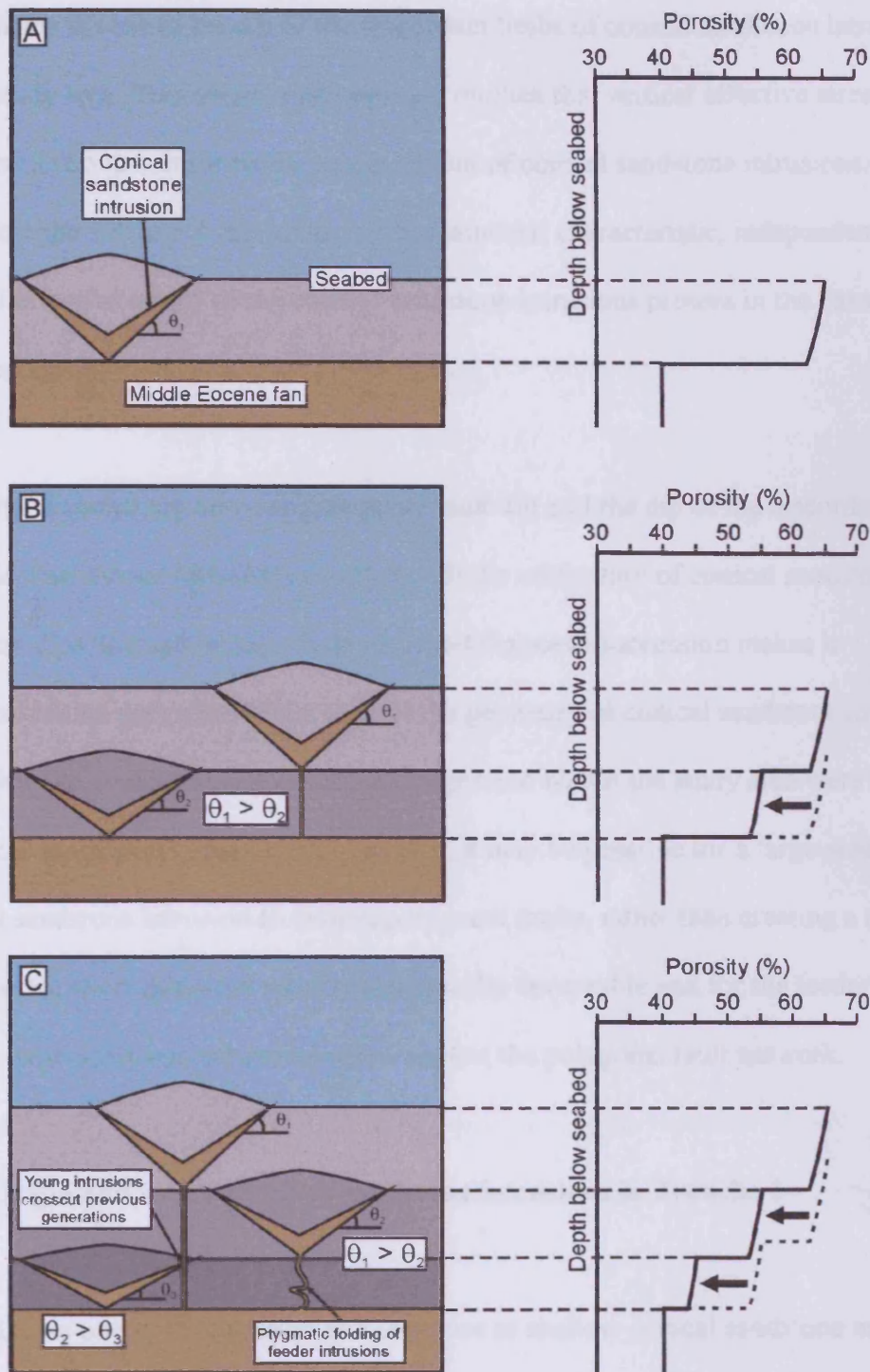


Fig 3.21 A) Conical sandstone intrusions are intruded in a series of temporally separate episodes. B) Further deposition after the initial emplacement event results in the compaction and flattening of the previous generation of conical intrusions. C) Subsequent deposition and emplacement episodes result in further compaction of the pre-existing host rock succession. Thus the discordant limbs of older intrusions will have more shallow dips than younger intrusions. It is also likely that later intrusive events will cross-cut pre-existing sandstone intrusions and that the feeder systems of older intrusions will become folded as a result of compaction of the host rock sequence.

dependency is seen in the dip of the discordant limbs of conical sandstone intrusions in the study area. This observation strongly implies that vertical effective stress does not exert a strong control on the emplacement of conical sandstone intrusions.

Therefore the 10° to 50° dip range is a fundamental characteristic, independent of vertical effective stress, of the conical sandstone intrusions present in the Faroe-Shetland Basin.

The large discrepancy between polygonal fault dip and the dip of the discordant limbs of conical sandstone intrusions coupled with the uniformity of conical sandstone intrusion dips throughout the whole Eocene-Oligocene succession makes it improbable that polygonal faults control the geometry of conical sandstone intrusions.

Therefore the conical sandstone intrusions present within the study area were not emplaced along polygonal faults. However, it may be possible for a large-scale conical sandstone intrusion to exploit polygonal faults, rather than creating a new fracture, for short distances where mechanically favourable and for the feeder systems for the large-scale conical intrusions to exploit the polygonal fault network.

3.6.5 Origin and implications of sandstone intrusions in Tranche 6

Forced folds on the INU formed as a response to shallow conical sandstone intrusion during the late Miocene (Section 2.5). This was coincident with a phase of inversion in the Faroe-Shetland Basin (Davies *et al.*, 2004). It is thus possible that inversion triggered widespread fluid migration from depth at this time. Fluids migrating upwards along faults (e.g. Holmes *et al.*, 1999) may have encountered depositional sand bodies at many different levels in the section, remobilising them and entraining

sand within the migrating fluid. In this manner sand and fluid may have been transported from great depth within the basin. It is therefore possible that conical sandstone intrusions that are situated a considerable distance from the margins of the Middle Eocene fans may contain sand derived from Palaeocene (or possibly even older) strata. However, shallower sources of sand or overpressure cannot be ruled out. It follows that the distribution of conical sandstone intrusions in the Faroe-Shetland Basin may reflect the distribution of the source of the migrating fluids and the bulk distribution of depositional sands in Palaeocene-Oligocene succession. However, it should be noted that there are no direct hydrocarbon indicators such as gas chimneys or flat spots associated with conical sandstone intrusions within the study area. Such hydrocarbon indicators are present elsewhere in the basin along the crests of inversion structures. The source of the sandstone within the intrusions can only be tested by sampling and comparative petrological analysis of both conical sandstone intrusions and possible source sands from both the Palaeocene and Middle Eocene fans. Unfortunately no such data is available at present.

Sand and fluid must have been transported through dilated fractures and faults during the fluid escape event in order to feed the large-scale sandstone intrusions examined during this study. It is likely that this transport of sand and fluid through open fractures may have left a residue of granular material in these fractures after the cessation of fluid flow. If this occurred, then it follows that a complex network of small-scale (sub-seismic resolution) sandstone intrusions is likely to have been emplaced along faults and fractures throughout the Palaeocene-Oligocene section. The presence of such a network of sand intrusions would be likely to enhance

permeability and result in a large increase in vertical connectivity and degradation of seal quality.

The low permeability claystones of the Eocene-Oligocene succession contain both polygonal faults and large-scale sandstone intrusions. Polygonal fault intersections are hypothesized to be good conduits for fluid migration (e.g. Berndt *et al.*, 2003; Stuevold *et al.*, 2003; Gay *et al.*, 2004). Three lines of evidence suggest that polygonal faults may have acted as at least part of the feeder system for orphan conical sandstone intrusions in the Eocene-Oligocene succession: 1) The close spatial relationship between intrusion apex and underlying polygonal fault intersections. 2) The presence of single-limb intrusions emanating from polygonal faults. 3) The lack of any feeder system imaged by standard seismic techniques beneath orphan conical sandstone intrusions.

3.7 CONCLUSIONS

In Tranche 6 of the Faroe-Shetland basin, conical sandstone intrusions coexist with, but share very few characteristics with a pervasive polygonal fault system within the Eocene-Oligocene succession. Polygonal faults and conical sandstone intrusions in the Faroe-Shetland Basin have distinct dip populations with little overlap. There is a strong depth dependency on the dip of polygonal faults, which may be due to a variety of factors including decreasing coefficient of friction and increased angular divergence from of the principle direction of compressive stress from the vertical with increasing depth coupled with post-propagation compaction. The conical sandstone intrusions are unlikely to have suffered significant post-emplacement compaction, and

the distribution of intrusion dips is uniform throughout the Eocene-Oligocene succession. This lack of depth dependency in conical intrusion dips implies that the overburden stress at the time of intrusion did not exert a strong control on intrusion geometry.

The polygonal fault network within the Eocene-Oligocene succession was already well developed at the time of sand intrusion. Whilst conical sandstone intrusions do not appear to be intruded along polygonal faults, it seems likely that polygonal faults, and fault intersections were utilised as a feeder system during intrusion. The presence of large-scale conical intrusions would vastly improve vertical connectivity through the Eocene-Oligocene succession and vastly degrade its potential as a sealing lithology. It is also possible that polygonal faults that acted as feeder conduits for conical sandstone intrusions are may be associated with small-scale (sub-seismic) sandstone intrusions improving vertical connectivity still further.

The distribution of conical sandstone intrusions in Tranche 6 does not closely resemble the distribution of the Middle-Eocene fans. Some intrusions can be found several kilometres from the margins of the fans. The Middle Eocene fans form the shallowest source of sand, and indeed interconnected networks of intrusions are physically linked to the fans in some areas. However, unless sand was transported laterally considerable distances from the margins of the fans, a deeper source must be appealed to source intrusions situated considerable distances from the margins of the fans. The late Miocene time emplacement of conical sandstone intrusions in Tranche 6 is coincided with a phase of basin inversion. It is therefore possible that inversion may have triggered catastrophic fluid migration from depth within the basin. Fluids

moving rapidly up through the basin, possibly utilising faults as fluid conduits, may then have been able to remobilise and entrain sand in the mobile fluid wherever depositional sand bodies were encountered. Thus the distribution of conical sandstone intrusions within the Eocene-Oligocene section may reflect the extent of overlap between the fluid source region, and the distribution of sand bodies encountered by the moving fluid throughout the section.

CHAPTER 4 – MIDDLE JURASSIC CYLINDRICAL SANDSTONE PIPES OF SE UTAH: PALAEOSEISMITES AND LONG-TERM CONDUITS FOR FLUID FLOW

Submitted as:

Shoulders, S., Huuse, M., Netoff, D., and Cartwright, J.A., 2005, Middle Jurassic cylindrical sandstone intrusions of SE Utah: Palaeoseismites and long-term conduits for fluid flow, Basin Research, *In Press*.

Co-author roles:

Mads Huuse, Dennis Netoff and Joe Cartwright all provided discussion of the topics presented in this chapter and support during its writing. Mads Huuse carried out fieldwork with me in SE Utah during November 2003. Denis Netoff provided logistical support for the fieldwork suggesting field areas to visit in the Lake Powell Region.

4.1 ABSTRACT

Sandstone pipes are a common feature of the Middle Jurassic Rocks of southeastern Utah and crop out across a region in excess of 20,000 km². This study focuses on pipes hosted within the Carmel Formation and Gunsight Butte Member of the Entrada Sandstone and form near vertical or steeply inclined cylindrical structures filled with a mixture of homogenous sand and breccia blocks of sandstone and mudstone. The sandstone pipes are interpreted to have formed in response to sudden, upward fluid migration triggered by seismic shaking and liquefaction of deeply buried sediments (up to 170 m below the palaeosurface). The sandstone pipes in SE Utah may be classified into two groups based on the presence or absence of large-scale host rock deformation and bulk sediment transport: 1) *Evacuation Pipes* display concentric dislocations and collapse structures within the host rock around a central pipe. This is a result of transport of sand and breccia blocks out of the underlying parent sand body

upwards through the pipe to form sand blows at the palaeosurface; 2) *Dewatering*

Pipes do not show large-scale host rock deformation, and bulk transport of sand and breccia blocks out of the parent body is not significant.

The presence of a widespread region of large-scale sandstone pipes in SE Utah that formed in response to earthquake shaking has several important implications:

- Once emplaced, pipes may act as conduits for fluid migration forming breaching points through permeability baffles, and increasing the potential for cross-stratal fluid flow.
- Earthquake-induced liquefaction occurred at depths up to 170 m, based on stratigraphic evidence, far greater than is usually considered in earthquake engineering.
- *Evacuation Pipes* may represent an analogue for the feeder system for large-scale conical sandstone intrusions observed in deep-water basins, such as the North Sea and Faroe-Shetland Basin, whilst *Fluidisation Pipes* may represent feeder systems for fluid escape structures such as pockmarks.

4.2 INTRODUCTION

The Middle Jurassic rocks of SE Utah form a high net to gross sand-dominated system representing a predominantly terrestrial aeolian depositional environment with subordinate fluviatile, sabkha and near-shore facies. Within these rocks, large numbers of conical landforms, weathering pits, cylindrical sandstone pillars and associated deformational structures can be found (Hannum 1980; Alvarez *et al.*, 1998; Netoff and Shroba, 2001; Netoff, 2002; Baer and Steed, 2003; Mahaney, *et al.*, 2004) (Fig 4.1).

The presence of cylindrical sandstone pipes has long been recognised in the sedimentary record (e.g. Hawley and Hart, 1934; Bailey and Newman, 1978). They are described hosted in sediments ranging in grain-size from sand to conglomerate from various depositional environments ranging from deep-marine channel sands (Mount, 1993; Davies, 2003) to terrestrial aeolian dune deposits (Deynoux *et al.*, 1990; Alvarez *et al.*, 1998; Netoff and Shroba, 2001; Netoff, 2002; Anderson *et al.*, 2003; Baer and Steed, 2003; Mahaney, *et al.*, 2004).

This paper combines recent field observations from Middle Jurassic strata from two regions, the first around the northwest shores of Lake Powell and the second from Kodachrome Basin with published data from across the region (Hannum, 1980; Alvarez *et al.*, 1998; Netoff and Shroba, 2001; Netoff, 2002; Anderson *et al.*, 2003; Baer and Steed, 2003) (Fig 4.1). When considered together, a region of large-scale soft-sediment deformation and remobilisation in excess of 20,000 km² is revealed.

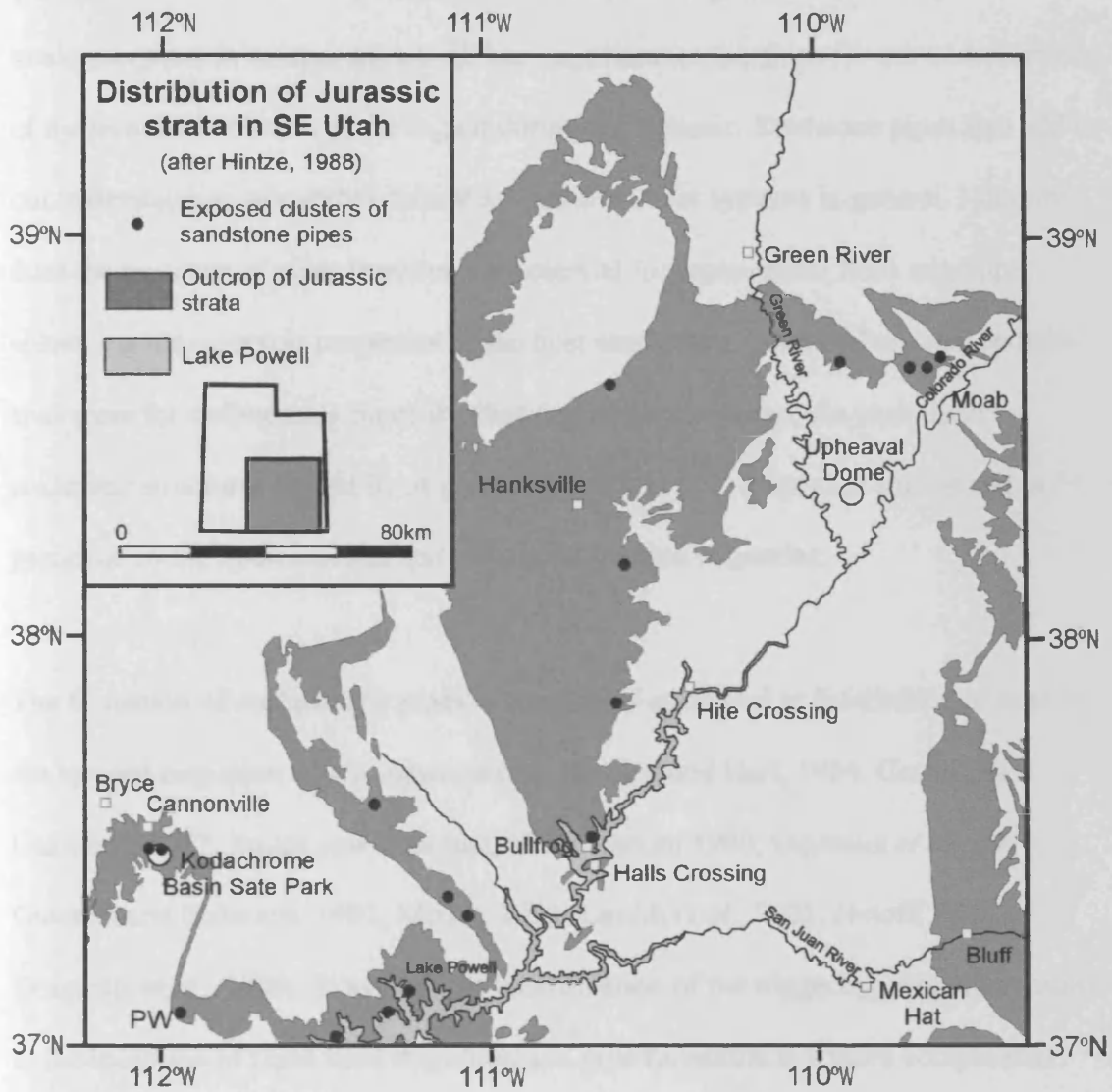


Fig 4.1 Distribution of Jurassic rock outcrop and sandstone pipes (shown as black dots) in SE Utah (compiled from: Hannum, 1980; Hintze, 1988; Alvarez *et al.*, 1999; Netoff and Shroba, 2001; Netoff 2002).

The identification and interpretation of a widespread region of seismically induced sandstone pipes in southeastern Utah has important implications for our understanding of the tectonic evolution of the region during the Jurassic. Sandstone pipes also add to our understanding of caprock failure and fluid transfer systems in general. Not only does the presence of pipes improve the potential for cross-stratal fluid migration, enhancing the reservoir properties of the host sandstones, but they may also be field-analogues for sedimentary pipes in other depositional settings. As such these enigmatic structures should be of great relevance to fluid migration studies and in particular to the hydrocarbons and mineral extraction industries.

The formation of sedimentary pipes is commonly attributed to fluidisation of sand by the upward migration of groundwater (e.g. Hawley and Hart, 1934; Cecile and Campbell, 1977; Bailey and Newman, 1978; Hanum 1980; Deynoux *et al.*, 1990; Guhman and Pederson, 1992; Mount, 1993; Løseth *et al.*, 2001; Netoff, 2002; Dragantis *et al.*, 2003). However, the identification of the triggering event that results in the inception of rapid fluid migration and pipe formation is a more complicated issue (e.g. Hannum, 1980; Alvarez *et al.*, 1998; Netoff, 2002).

4.3 GEOLOGICAL SETTING

4.3.1 Tectonic setting

The tectonic evolution of the continental interior of the western USA is both long-lived and highly complex. Several phases of compression and basin inversion have occurred across the region since the Pennsylvanian, they are controlled by subduction

along the southern and eastern margins of the North American continent (e.g. Dickinson, 2000; Dickinson and Lawton, 2001) and the formation of the Cordilleran Arc (Dickinson and Gehrels, 2003; Heller, 2003). It is important to understand the tectonic history of the region because it controls the distribution of deformation, and sedimentary deposition.

4.3.11 Jurassic shortening

Downwarp of the continental interior of the western USA triggered by shortening of the Cordilleran Arc during the Early Jurassic formed a wide topographic depression variously interpreted as a retroarc-foreland basin (Bjerrum and Dorsey, 1995), and more specifically a back-bulge basin, part of a foreland basin system (DeCelles and Currie, 1996). However, palaeoslope analysis of lower Cretaceous gravel-prone sediments suggests that only a shallow foredeep trough was present and that the region simply dipped gently to the east (Heller *et al.*, 2003) and represented a dynamic topographic low possibly formed through viscous corner flow within the mantle induced by the subducting slab (Burgess and Moresi, 1999).

During the Jurassic, large erg systems were developed and preserved within the basin during periods of increased shortening and downwarp (Allen *et al.*, 2000). Discrete pulses of increased subsidence are believed to have resulted in the preservation of both the Navajo and Entrada Ergs (Allen *et al.*, 2000). During the Middle Jurassic, western Utah and north-central Arizona were bordered to the south and west by the Jurassic Cordilleran Arc (Kowallis *et al.*, 2001) and to the east by Monument Bench (Bjerrum and Dorsey, 1995). This formed a broad elongate basin open to the north

known as the Utah-Idaho Trough (Bjerrum and Dorsey, 1995; Blakey *et al.*, 1996). Maximum subsidence of the trough occurred in northern Utah, Idaho and Wyoming, with lower rates of subsidence to the south and east. The inundation of the Utah-Idaho Trough resulted in the formation of the Middle Jurassic Carmel-Twin Creek Seaway (Imlay, 1980; Nielson, 1990), whilst the centres of erg deposition were offset up to 200 km to the south and east of the axis of the Utah-Idaho trough and were distributed around the southern and eastern margins of the basin (Blakey *et al.*, 1996).

Despite Cordilleran shortening throughout the Jurassic, the northerly or northwestern fluvial drainage pattern into the Utah Idaho Trough established during the Late Triassic, continued through the Early and Middle Jurassic until the deposition of the Middle Jurassic Romana Sandstone and Summerville Formation (e.g. Bjerrum and Dorsey, 1995; Dickinson and Gehrels, 2003). Erosional trends also followed this pattern with the J-1, J-2 and J-3 unconformities cutting down to the east and northeast (Pipringos and O'Sullivan, 1978; Bjerrum and Dorsey, 1995).

4.3.12 Early-Mid Cretaceous Cordilleran uplift and shortening

Southeast directed shortening during the Cretaceous had two major effects on the tectonics of the Colorado Plateau: easterly migration of the Cordilleran foreland system and Sevier Thrust Belt; and a phase of reactivation of basement faults causing uplift and strike-slip movement of basement arches through out the western USA (Cather, 1999; Tindall and Davis, 1999; Marshak *et al.*, 2000; Bump, 2004). Eastward migration of the Cordilleran Arc is commonly believed to have formed a foreland basin through flexural loading due to the formation of the Sevier Thrust Belt to the

west orientated roughly north south through Arizona, Utah Idaho, Wyoming and Montana during the Middle Jurassic (DeCelles and Currie, 1996; Currie, 1998). Stratigraphic and provenance studies coupled with geodynamic modelling imply that the foreland basin migrated in an eastward direction during the Middle Jurassic through to the Middle Cretaceous (DeCelles and Currie, 1996; Currie, 1998; Currie, 2002; White *et al.*, 2002). Up to 1.2 km of Lower Cretaceous eastward thinning sediments were deposited in the foredeep depozone across Colorado and Utah (Currie, 2002). However, thrusting did not propagate into western Utah until the Mid-Cretaceous (Heller *et al.*, 1986).

The widespread deposition of thin fluvial gravels during the earliest Cretaceous throughout Utah, Colorado, Wyoming, Idaho and Montana shows a distinctive eastward to northeasterly drainage pattern but is hard to reconcile with a flexural foreland basin model (Heller and Paola, 1989; Heller *et al.*, 2003). Previous interpretations suggest that these gravels were deposited in a pre-existing overfilled foreland basin that formed to the east of thrusts in Central Nevada (DeCelles and Currie, 1996; Currie, 1998). However, given that thrusting did not propagate into the region until the Mid-Cretaceous (Heller *et al.*, 1986), it seems unlikely that uplift to the west is directly related to thrusting. Gravels deposited as the result of erosion of an active orogenic source are rarely transported more than 100 km yet the Early Cretaceous gravels of the western USA were deposited over 600 km away from the nearest Cordilleran thrusts (Heller and Paola, 1989). Therefore, whilst a shallow foreland basin was present during the Jurassic and Early Cretaceous, a mechanism other than thrusting and foreland basin migration must be sought to explain extensive

eastward tilting and gravel deposition that occurred in the western USA during the Late Jurassic and Early Cretaceous.

It has been argued that dynamic loading caused by viscous mantle corner flow coupled to the subducting plate can result in long wavelength subsidence (100's kilometres) with relief of hundreds of metres (e.g. Burgess *et al.*, 1997; Burgess and Moresi, 1999; Catuneau, 2004). During the Late Jurassic and Early Cretaceous the North American continent had drifted over the Mezcalera Plate, which began subducting during the Late Triassic. Viscous corner flow within the mantle could have caused the superimposition of a long-wavelength subsidence on to the shorter wavelength flexure caused by the load of the orogenic wedge (Burgess, and Moresi, 1999; Heller *et al.*, 2002). Relaxation of this dynamic subsidence would be capable of producing the considerable gradients needed to cause widespread gravel deposition during the Early Cretaceous (Heller *et al.*, 2003).

4.3.2 Stratigraphic Setting

The field study presented focused on two areas of southeastern Utah, the Kodachrome Basin and the Lake Powell region. Sandstone pipes at those sites are restricted to the upper members of the Carmel Formation and the Lower Entrada Sandstone (e.g. Hannum, 1980; Netoff, 2002; Anderson *et al.*, 2003; Baer and Steed, 2003). It is important to examine the detailed stratigraphy of this section because there are considerable lateral facies changes over relatively small distances across the region where pipes have been recorded (Fig 4.2). Such changes will have significant effects on rock properties including the distribution of sealing lithologies.

The Middle Jurassic Page Sandstone forms the lowermost formation within the San Rafael Group. It was deposited in an aeolian dune-dominated environment and is lithologically almost indistinguishable from the underlying Navajo Sandstone (Anderson *et al.*, 2003). The Page Sandstone is present in a much smaller region of the basin than the Navajo Sandstone (Blakey, 1988). The lower Carmel Formation lies disconformably on top of the Navajo Sandstone and is, coeval to, and interfingers with the Page Sandstone (Fig 4.3). The Carmel Formation represents the incursion of the Carmel-Twin Creek Seaway (Imlay, 1980; Nielson, 1990), which extended from southwestern Utah to Canada during the Middle Jurassic.

The Carmel Formation consists of red, purple and brown siltstones and mudstones and white-grey sandstone. It represents a range of environments from mud-dominated fluvial deposits with lenses of aeolian material, to sabkha, near-shore and shallow marine deposits. The Carmel Formation is relatively thin in the Lake Powell region (southern Utah) (60 m according to Anderson *et al.*, 2003) where only the Winsor and Paria River Members are present. The Carmel formation thickens northwestward to 197 m in the Kodachrome Basin (Thompson and Stokes, 1970) (Fig 4.3) and becomes increasingly dominated by shallow marine deposits. In the Kodachrome Basin the Carmel Formation is more complete with four of the five constituent members are present (Doelling and Davis, 1989) as well as the Thousand Pockets Tongue of the Page Sandstone (Baer and Steed, 2003). The Middle Jurassic Carmel-Twin Creek Seaway was bordered to the east by an arid coastal plain leading up to the ancestral Rocky Mountains, and to the south and west by the foreland fold and thrust belt of the Cordillera Arc Mountains (Peterson, 1994).

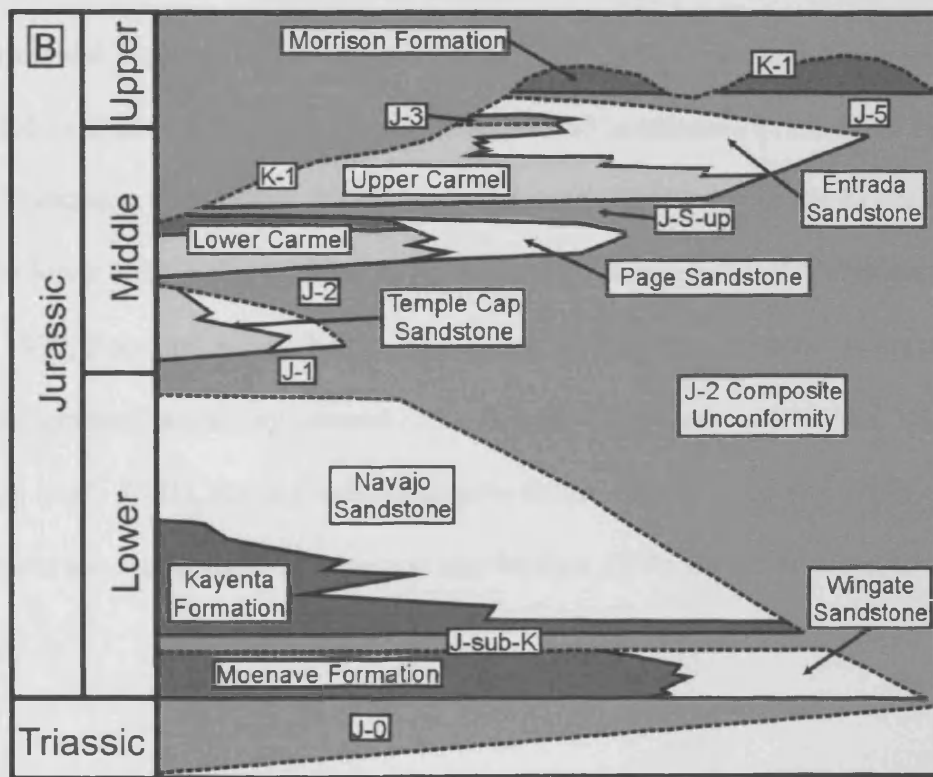
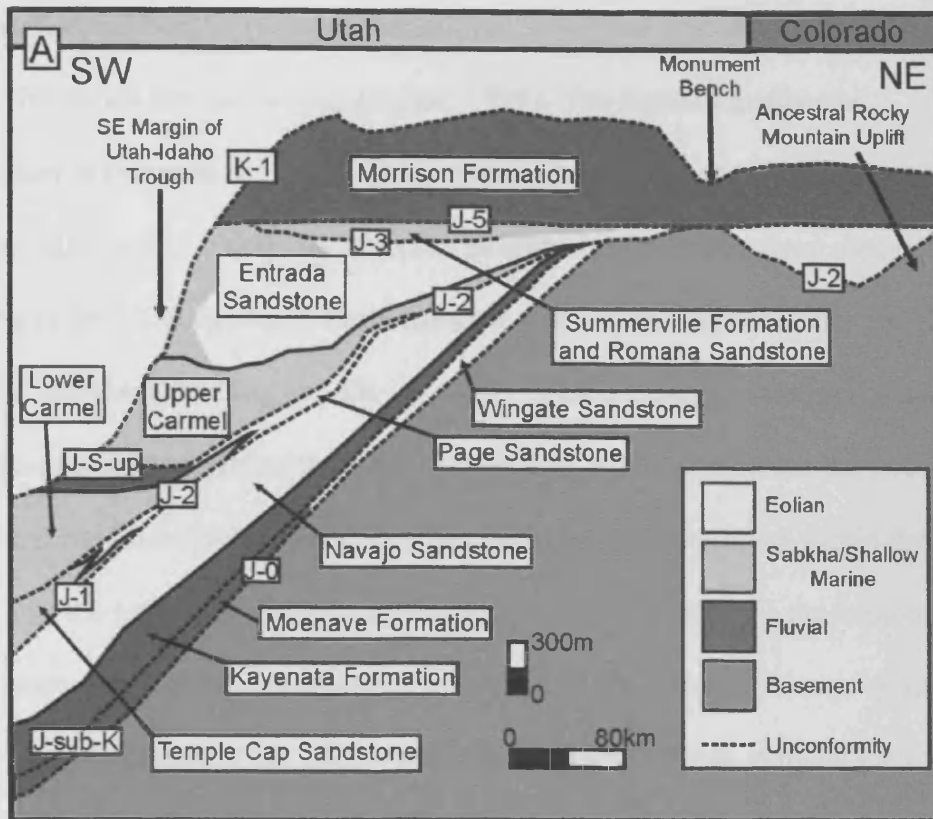
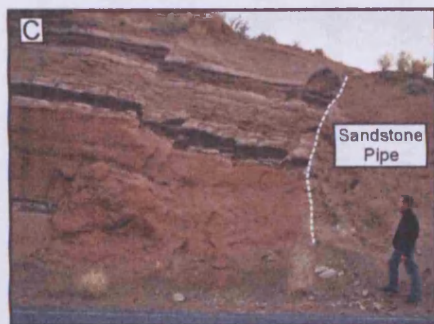


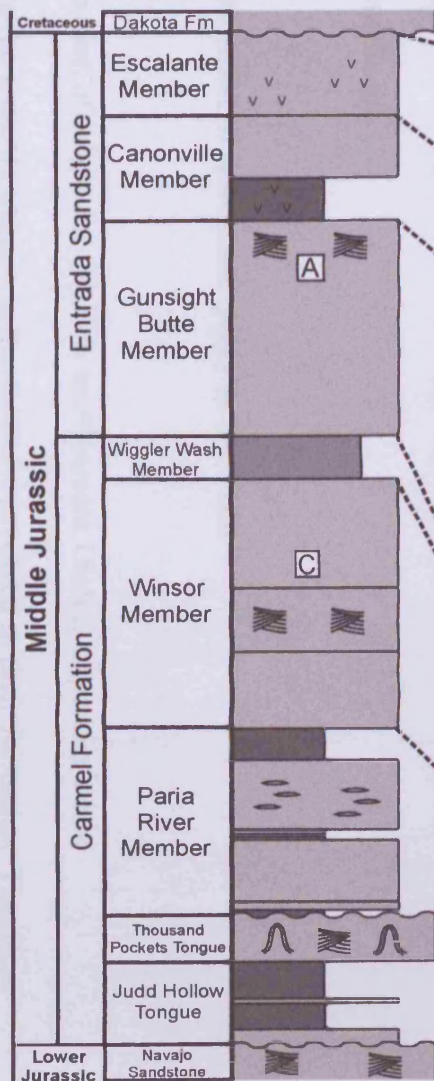
Fig 4.2 (A) A simplified stratigraphic section from southwestern Utah to central Colorado showing the relation between the formations and regional unconformities discussed in this study (after Bjerrum and Dorsey, 1995). (B) A chronostratigraphic diagram of Fig 4.2A (after Bjerrum and Dorsey, 1995).

The upper Carmel Formation has a transitional upper and lateral boundary with the Entrada Sandstone (De Gibert and Ekdale, 1999). The Entrada Sandstone accumulated in response to a pulse of increased sand supply and subsidence within the basin (Allen *et al.*, 2000). The Entrada Sandstone is split into three members (in ascending order:), the Gunsight Butte Member, the Cannonville Member and the Escalante Member (Doelling and Davis, 1989). Whilst chiefly composed of orange to white fine-grained sandstones there is considerable variation between the three members of the Entrada Sandstone and also between different areas within the basin (Fig 4.3). In the Lake Powell region the Gunsight Butte Member is made up of reddish-orange and white cross-bedded fine-grained sandstones (Thompson and Stokes, 1970, Anderson *et al.*, 2003). In the Kodachrome Basin, only 80 km to the NW, the same member has graded into silty sandstones with shale interbeds (Thompson and Stokes, 1970; Baer and Steed, 2003). The Cannonville Member is dominated by white and orange, banded fine-grained sandstones in the Lake Powell region (Thompson and Stokes, 1970; Anderson *et al.*, 2003), but in the Kodachrome Basin the lower half of this member is dominated by shales and tuffs (Thompson and Stokes, 1970; Baer and Steed, 2003). Similarly, the Escalante Member is made up of white fine-grained sandstones around Lake Powell (Thompson and Stokes, 1970, Anderson *et al.*, 2003), but in the Kodachrome Basin, interbeds of grey shale, tuffs and gypsum are also present (Thompson and Stokes, 1970; Baer and Steed, 2003).

NW

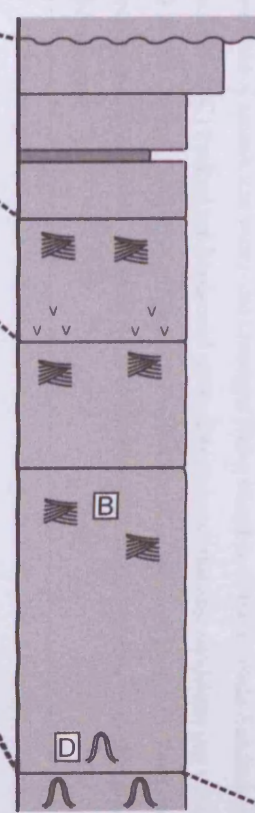


Paria River Valley
8km south of
Canonville



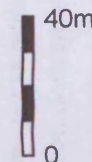
SE

Gunsight Butte,
Lake Powell

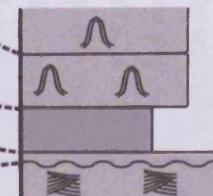


- Sandstone
- Siltstone
- Shale/
Mudstone
- Gypsum
- Limstone
- Contorted
Bedding
- Cross-
Bedding
- Tuffs
- Gypsum
Lenses

Logs compiled and
simplified from
Thompson and Stokes,
1970; Hintze, 1980;
Doelling and
Davis, 1990;
Anderson *et al.*, 2003;
Baer and
Steed, 2003.



Baker Ranch, near
Bullfrog, Lake
Powell



J5

J2

Fig 4.3 (Previous page) Correlation of sections from the Paria River Valley showing the succession present within the Kodachrome Basin (Thompson and Stokes, 1970) and from Gunsight Butte (Thompson and Stokes, 1970; Baer and Steed, 2003) and Baker Ranch near Bullfrog (Doelling and Davis, 1990; Anderson *et al.*, 2003), describing the succession in the Lake Powell region. A general trend can be seen between the two regions: The Carmel Formation thins, whilst the Entrada Sandstone thickens between the Kodachrome Basin and Lake Powell. The lower members of the Carmel Formation represented in the Kodachrome basin are not present in the Lake Powell region. A) Large-scale cross-bedded sandstones and intercalated shales and mudstones within Gunsight Butte Member of the Entrada Sandstone in the Kodachrome Basin State Park. B) Large-scale cross-bedded sandstones within the Gunsight Butte Member of the Entrada Sandstone from Warm Creek Bay, Lake Powell. C) Faulted sandstone and intercalated mudstones and sandstone pip within the Winsor Member of the Carmel Formation at Shepards Point in the Kodachrome Basin. D) Disturbed strata and possible fluid escape structures within the basal units of the Gunsight Butte Member of the Entrada Sandstone near the Henry Mountains.

These changes represent a change from dominantly aeolian deposition in the Lake Powell region to a more tidal to sub-aerial depositional environment in the Kodachrome Basin.

4.3.3 Distribution of sandstone pipes in SE Utah

The distribution of sandstone pipes in southeastern Utah is important when considering the possible triggering mechanisms involved in their formation. The pipes examined during this study and previously published studies form a northeast-southwest orientated swath through southeastern Utah. There is also evidence of the presence of pipes, which are similar in both age and character, in the San Juan Basin of New Mexico (Parker, 1933; Netoff, *unpublished data*) making this one of the largest regions of sedimentary intrusions in the sedimentary record. All the pipes examined in this study occur, in part, or entirely within the boundaries of the sandy facies of the Entrada Sandstone (Fig 4.4A). Whilst many of the pipes also lie within the boundaries of the underlying Page Sandstone, some pipes, notably those in the

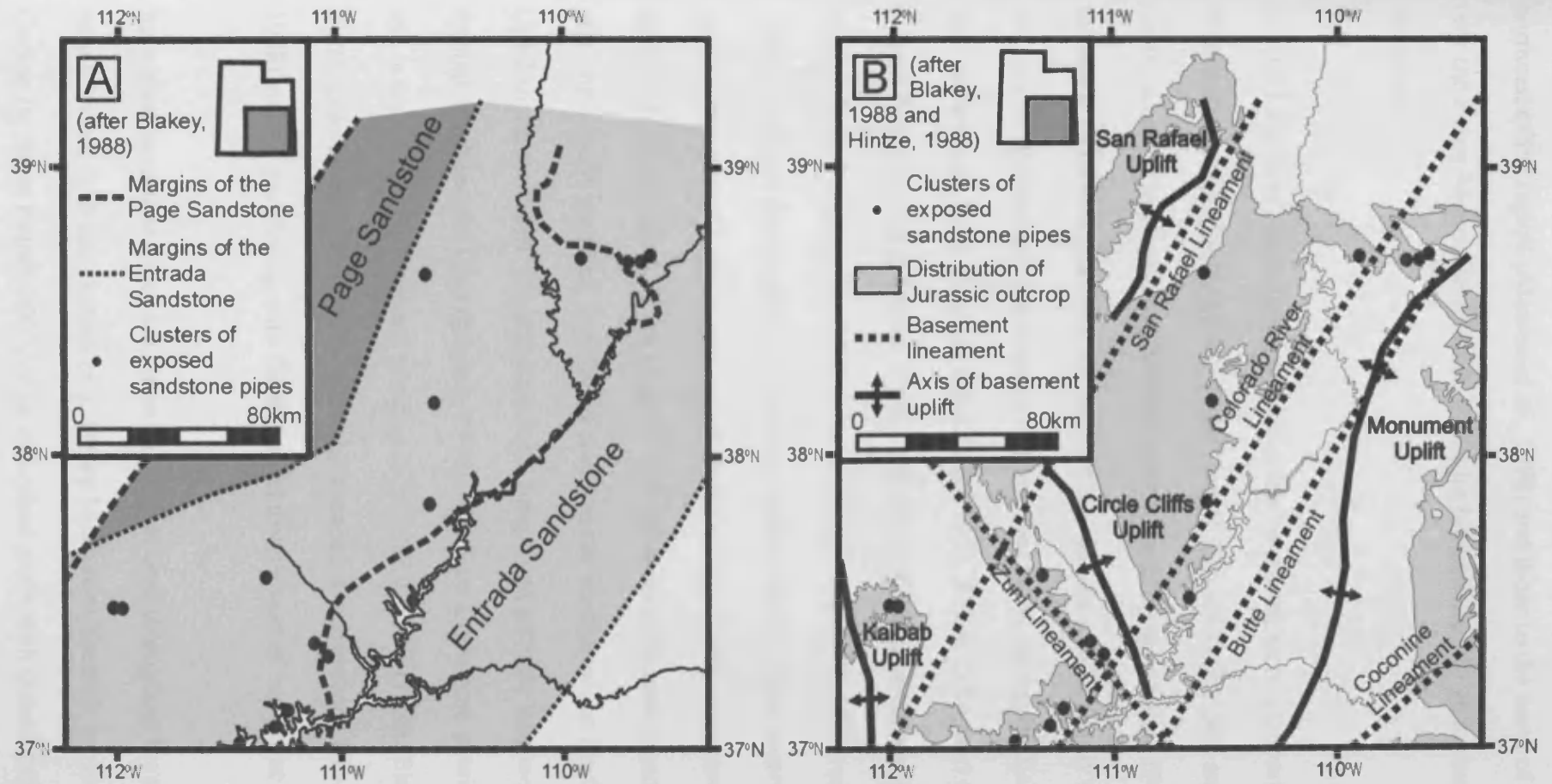


Fig 4.4 Distribution of sandstone pipes relative to A) the underlying Page and Entrada Sandstones and B) Basement lineaments and uplifts (after Blakey, 1988). The distribution of pipes appears to be closely related to underlying basement structures. Several examples of sandstone pipes fall outside the margins of the Page Sandstone, however all recorded examples fall within the margins of the Entrada Sandstone.

northeast of the region (Alvarez *et al.*, 1998) and those to the north of Lake Powell near the Henry Mountains (Netoff, 2002) lie beyond the known extent of the Page Sandstone.

Several long-lived, fault-cored, asymmetrical basement arches, in particular the Monument Bench Uplift, the San Rafael Swell, Circle Cliffs Uplift and the Kaibab Uplift, control the present day Middle Jurassic outcrop distribution (Fig 4.4B). The formation of these uplifts was the result of two phases of dominantly compressional, but also transpressional, reactivation of basement faults during the Early Carboniferous to Early Permian (Dickerson, 2003, Bump, 2004) and the Campanian to Late Palaeocene (e.g. Bump, 2004). The pipes of the Kodachrome Basin and western Lake Powell are found in a basin between the NNW-SSE trending Circle Cliffs Uplift and the roughly N-S trending Kaibab Uplift. Pipes observed towards the northeastern end of Lake Powell and further to the northeast are present within an elongate basin bounded by the roughly N-S trending Monument Bench Uplift to the east, the NE-SW trending San Rafael Swell to the northwest and the Circle Cliffs Uplift to the southeast. Several prominent long-lived tectonic lineaments also run through southeastern Utah (Blakey, 1988). The Zuni Lineament is orientated NW-SE and is situated on the southern margins of the Circle Cliffs Uplift (Blakey, 1988). The Butte, Colorado River and San Rafael Lineaments are orientated NE-SW (Blakey, 1988) crudely paralleling with the observed distribution of sandstone pipes.

Individual sandstone pipes are not evenly distributed throughout the region. Pipes may be found in dense clusters (e.g. Henry Mountains Swarm), loose clusters (e.g. Cookie Jar Butte Netoff, 2002) or as individual pipes with considerable distances

separating one pipe from another. They are not arranged in linear arrays implying that pipes do not form along joint planes or individual fault planes (e.g. Hannum, 1980).

4.4 PHYSICAL CHARACTERISTICS OF SANDSTONE PIPES

4.4.1 General characteristics of sandstone pipes in SE Utah

Sandstone pipes in southeastern Utah are circular to oval in plan view with diameters ranging from <1 metre up to >100 metres (Netoff, 2002) and form steeply dipping (70-90°) cylindrical structures (e.g. Hannum, 1980). Many of the pipes observed have straight, roughly parallel walls (Pheonix, 1958; Hannum, 1980; Netoff and Shroba, 2001; Netoff, 2002), however there is considerable variation in individual pipe morphology with some examples having a slightly sinuous or upwards tapering geometry (Hannum, 1980). Individual pipes range in exposed height from a few meters up to 100 meters (Netoff, 2002) although the terminations of individual pipes have not been described in this or other studies. The full vertical extent of individual pipes is not seen at outcrop due to erosion of the strata within which they are hosted and their continuation below the present-day land surface. The stratigraphic thickness of the host rocks, indicates that the true vertical dimensions of at least some pipes may be considerably greater than is currently exposed (e.g. Hannum 1980; Netoff, 2002).

Locally, the host rocks surrounding the pipes display a range of different deformation structures. Many intrusions are surrounded by a zone of high intensity small-scale faulting with displacements up to a few centimetres up to 3 m thick. This lends the host rock a highly shattered, partially brecciated appearance with individual blocks

displaced only a few centimetres from their original position. Large-scale host rock deformation in the form of caldera-like collapse structures (e.g. Kennedy *et al.*, 2004) that may be tens of meters in diameter, surrounding a central pipe is also observed in a limited number of examples. The central pipe is surrounded by blocks of host rock tilted down towards the pipe bounded by concentric faults. Commonly the tilted blocks are relatively undeformed and retain primary bedding and depositional structures. The collapse zone of rotated host rock blocks roughly parallels the walls of the central pipe and may be up to 150 m in diameter as seen at Shepards' Point in the Kodachrome Basin (Baer and Steed, 2003).

The material within pipes is highly variable and in general consists of homogeneous sandstone with a varied component of breccia blocks (Pheonix, 1958; Hannum, 1980; Netoff 2002; Anderson *et al.*, 2003; Baer and Steed, 2003). The breccia blocks themselves, are often highly angular and range in size from a few centimetres to over a meter in length (e.g.: Netoff, 2002). They commonly consist of dune sandstone or blocks of brown siltstone and mudstone similar to mudstones of the Carmel Formation or fine-grained sabkha-like units within the Entrada Sandstone (Netoff 2002; Hannum 1980). The blocks are easily distinguished from the matrix sandstone because they retain many original depositional fabrics and structures such as cross bedding, lamination or sand-filled desiccation cracks, whereas the surrounding sand matrix is homogeneous. Breccia blocks may be evenly distributed throughout the pipe, increase in size and frequency towards the centre of the pipe possibly indicating that flow velocity may be greater towards the centre of the pipes or form a sub-horizontal layered fabric possibly related to settling of breccia blocks within the pipe

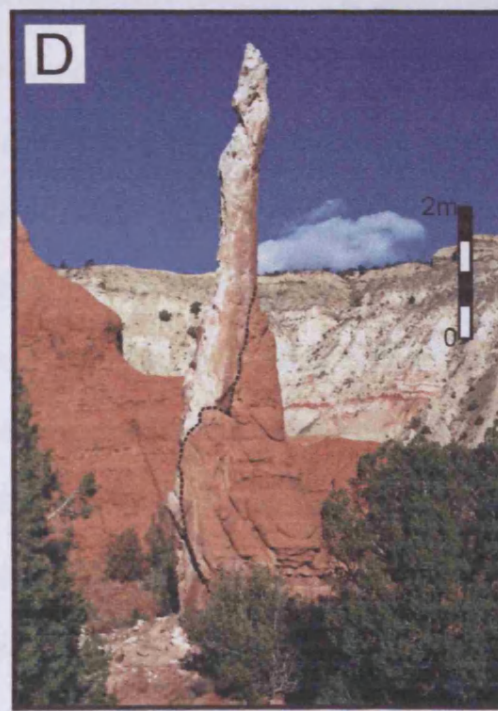
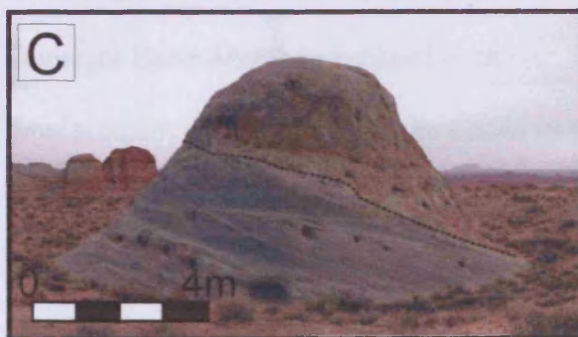
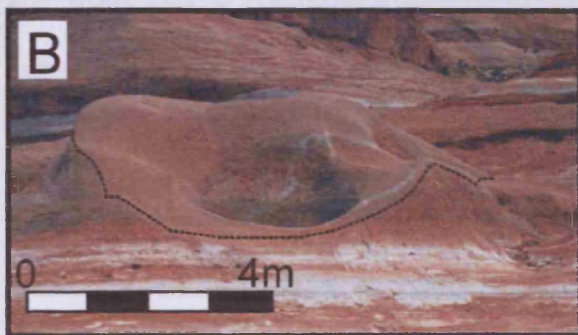


Fig 4.5 Some examples of the different geomorphological expressions of sandstone pipes; (A) “Slick-rock exposures” with no topographical expression. Black arrows highlight the margins of the pipe and grey arrows point to concentric faulting surrounding the pipe. Note how similar the pipe-fill and surrounding host rock appear. (B) Weathering pits; (C) Conical mounds; (D) Free-standing spires. The contact between the host rock and the pipe is marked with a black dashed line.

(Baer and Steed, 2003). No compositional variation of breccia blocks has been recorded along the exposed height of a pipe.

4.4.2 Geomorphological expression of sandstone pipes

The geomorphological expression of the pipes varies markedly throughout the study areas and ranges from flat, planar, “slick-rock” exposures (Fig 4.5A), “slick-rock” weathering pits (Fig 4.5B), conical mounds either with or without summit weathering pits (Fig 4.5C) and cliff sections in the Lake Powell region (Netoff and Shroba, 2001; Netoff, 2002; Anderson *et al.*, 2003) to cliff sections and cylindrical spires rising 20-30 m from the ground (Fig 4.5D) within the Kodachrome Basin (Hannum, 1980; Baer and Steed, 2003). The pipes in both study areas are partially cemented and the difference in geomorphological expression of the pipes between Lake Powell and the Kodachrome Basin appears to be an effect of the differing host rock lithologies found in these two regions. The Entrada Sandstone around Lake Powell and the material within the sandstone pipes probably had a much higher cross-stratal permeability than the fine-grained sediments of the Carmel Formation and the more silty facies of the Gunsight Butte Member exposed in the Kodachrome Basin. As a result, post-pipe emplacement fluid flow would be concentrated within the coarser facies of the Gunsight Butte Member and the intruded material of the pipes resulting in a greater level of cementation in these materials (Doelling and Davis, 1989; Chan *et al.*, 2000; Netoff and Shroba, 2001). The thick Carmel successions and silty facies of the Gunsight Butte Member exposed in the Kodachrome Basin are more easily eroded than the better-indurated pipe material leaving the sandstone pipes as freestanding spires (Hannum, 1980; Baer and Steed, 2003). In contrast, around Lake Powell where

the Carmel Formation is thin and most of the pipes are hosted within the coarser facies of the Gunsight Butte Member, there was only a minor difference in permeability between the pipe material and the host rock resulting in more even cementation. Therefore “slick-rock” exposures displaying flat or conical landforms are prevalent (Netoff and Shroba, 2001; Netoff 2002; Anderson *et al.*, 2003). The various exposures resulting from these differences provide valuable insights into the geometry of and deformation related to pipe emplacement.

4.4.3 Case studies

Individual pipes examined during the course of this investigation display a wide range of different features. In order to best illustrate the range of different features displayed by individual pipes we present a series of four individual case studies, two from the Kodachrome Basin and two from the Lake Powell region:

4.4.31 Kodachrome Basin

Pipes in the Kodachrome basin are hosted within the Winsor Member of the Carmel Formation (near Shepards’ Point) and also in the Gunsight Butte Member of the Entrada Sandstone (in the Kodachrome State Park). No pipes were observed in the overlying Cannonville or Escalante Members of the Entrada Sandstone or stratigraphically below the Winsor Formation during this study. The Winsor Member of the Carmel Formation consists of layered pale buff to purple brown fine-grained sandstones with numerous thin shale beds interbedded with dark brown mudstones and siltstones. Minor erosive surfaces are present in the section studied, which

consists of approximately 85% sandstone and 15% mudstone and siltstone. Some low amplitude folding is present in the Winsor Member of the Carmel Formation. The Gunsight Butte Member of the Entrada Sandstone that outcrops within the Kodachrome Basin State park consists of brick red-brown fine-grained sandstones and silty sandstones with cross-bedded units 2-3 m thick.

Chimney Rock

Chimney Rock is a very large free-standing pipe approximately 30 m tall with a diameter of around 18 m, situated within the Gunsight Butte Member of the Entrada Sandstone (Fig 4.6). The pipe appears to have an irregular slightly elliptical cross-section, but is heavily weathered and it is unlikely that any of the surfaces exposed at the present day represent the outer margin of the original pipe (Fig 4.6A).

Chimney rock is made up of very large breccia blocks in a matrix of sand and gravel-sized lithic clasts (Fig 4.6B). The gravel matrix is predominantly made up of lithic fragments but also contains a small proportion of black clasts identified as carbonised wood fragments (Baer and Steed, 2003) although it is unclear from where these were derived. The breccia clasts consist of highly angular sandstone, silty sandstone and dark brown mudstone. These are arranged with their long axes orientated sub-horizontally, roughly perpendicular to the margins of the pipe to form a pseudo-layered fabric.

Some of the dark brown mudstone breccia blocks also contain a thin pale fine-grained sandstone layer parallel to the long axis of the breccia block. This is associated with

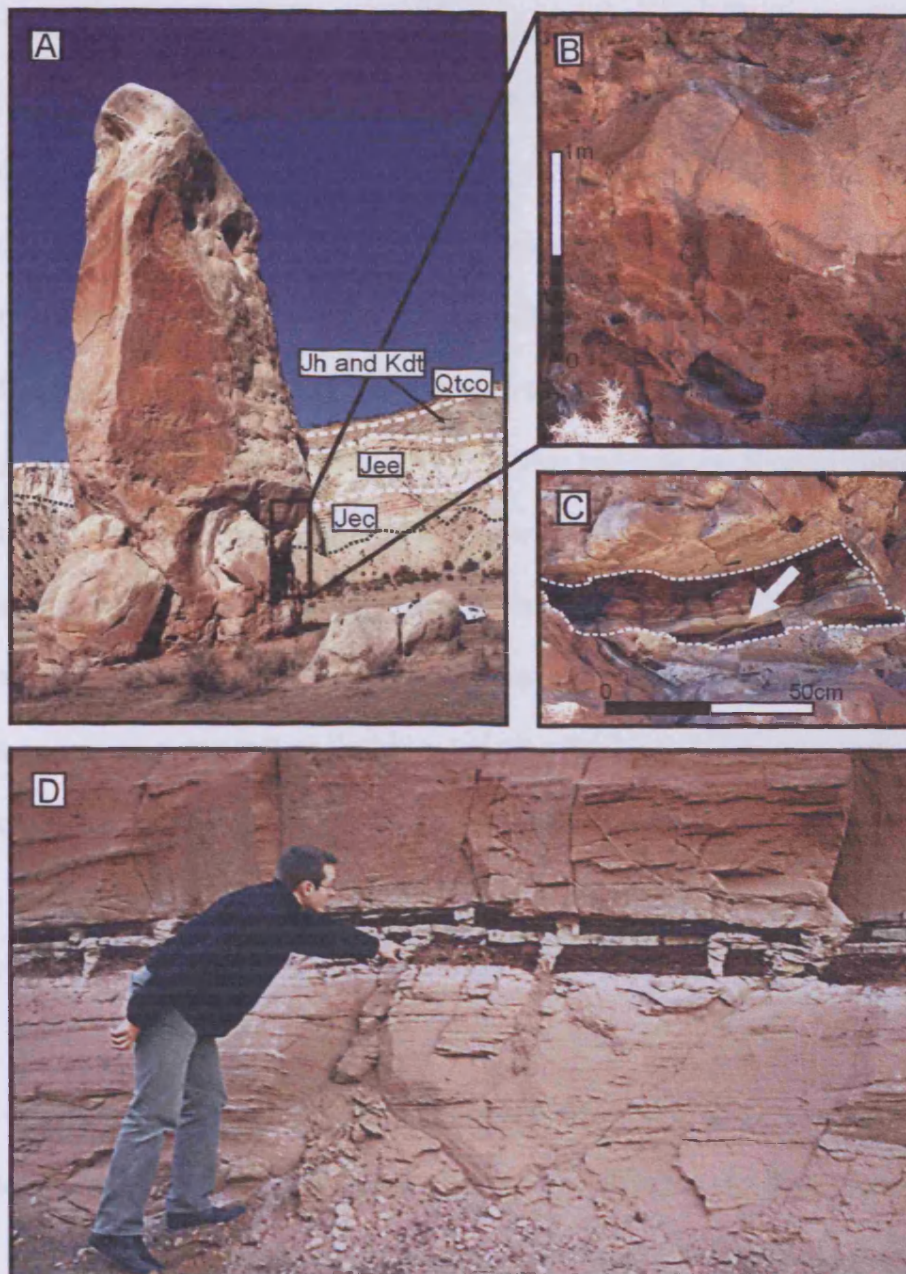


Fig 4.6 (A) Chimney rock, a pipe expressed as a free sanding pipe in Kodachrome Basin State Park. The pipe stands within the Gunsight Butte member of the Entrada Sandstone (Jeg). The contact between the Gunsight Butte Member and the overlying Cannonville Member (Jec) is covered by scree slope (upper margin highlighted with a black dotted line), however the contact between the Cannonville and Escalante Members is easily identified are the J5 unconformity between the Escalante Member of the Entrada Sandstone and the Henreville Sandstone (Jh) and Tropic/Dakota Formations (Kdt) and the overlying Quaternary conglomerates (Qtco). (B) Breccia blocks within Chimney Rock display a low-angle pseudo layered fabric. (C) A large clast of dark brown mudstone with sand filled cracks discordant to bedding (white arrow), this distinctive block is likely to come from a bed of very similar material also showing a bedding parallel thin band of white sandstone and discordant sand filled cracks seen in a road cut at Shepard's Point (D). This bed sits within the Winsor Member of the Carmel Formation, whilst Chimney rock has been eroded from the overlying Gunsight Butte Member of the Entrada Sandstone implying this breccia block was transported upwards from the underlying Winsor Member.

cracks filled with pale fine-grained sandstone orientated perpendicular to the thin sandstone layer and the long axis of the mudstone breccia blocks (Fig 4.6C). An *in situ* bed of dark-coloured mudstone observed in the Winsor Member of the Carmel Formation at Shepards' Point, stratigraphically below the Entrada Sandstone, displays very similar features (Fig 4.6D). It too has a bedding parallel band of pale fine-grained sandstone with sandstone-filled cracks that are orientated perpendicular to bedding and it is thus likely that material from this bed was transported upwards to form the dark coloured mudstone blocks observed in Chimney Rock. It is important to note that whilst the presence of distinctive breccia blocks within Chimney Rock provides information about the direction of transport, it does not conclusively identify the pipe source unit. It is only possible to say that Chimney Rock cross-cuts the depositional unit from which these blocks originate.

Shepards' Point

Shepards' Point comprises two long cliff sections, one of which contains a spectacular 18 m wide breccia-filled pipe surrounded by a large collapse structure approximately 150 m wide (Fig 4.7). The pipe and its associated collapse structure are positioned on the axis of a gentle anticline in the Winsor Member. The top of the pipe has been eroded and Quaternary conglomerates sit unconformably on top of the sandstones and mudstones of the Winsor Member, similarly the base of the collapse structure is obscured by a scree slope and vegetation.

The central pipe has straight, parallel contacts with the surrounding host rocks. These contacts are heavily eroded forming pronounced vertical clefts in the cliff. The pipe

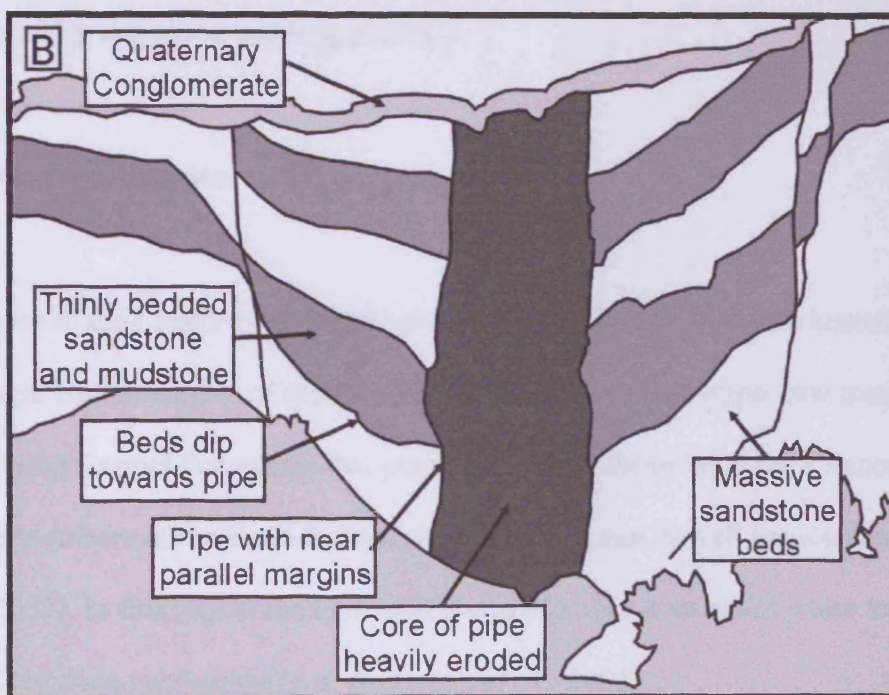
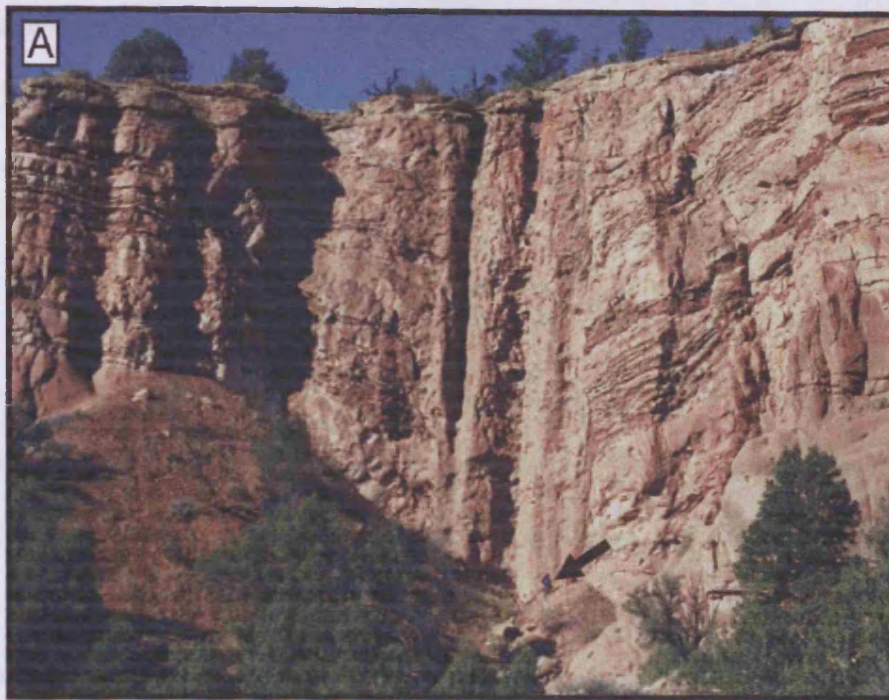


Fig 4.7 A) Large-scale collapse structure centred on a breccia pipe 15m wide within the Winsor Member of the Carmel Formation at Shepards Point near the Kodachrome Basin State Park. Person for scale (black arrow). B) Line-drawing showing strata consisting of massive sandstone intercalated with sandstone and mudstone interbeds dipping downwards towards a central pipe consisting of large breccia blocks (up to 1m in diameter) within a homogeneous sand and gravel matrix. Note that both the upper and lower terminations of the pipe have either been obscured by recent sediments or removed by erosion.

contains angular to subrounded breccia blocks of sandstone and mudstone up to a meter in diameter. They are randomly orientated with respect to the walls of the pipe and do not show any obvious layering, fabric or compositional distribution.

The pipe is positioned centrally within a symmetrical collapse structure with bounding faults dipping steeply away from the central pipe. The margins of the collapse structure are regular and well defined. Host-rock strata are not displaced across the collapse structure. Within the collapse structure, host rock beds tilt gently (~30°) downwards towards the central pipe and are otherwise not heavily deformed. It is still possible to see original bedding thickness preserved and it is likely that tilting was taken up by slip along bedding planes.

4.4.32 Lake Powell region

All the pipes in the Lake Powell region examined during this study are hosted within the Gunsight Butte member of the Entrada Sandstone or in the upper few metres of the underlying Carmel Formation. No pipes have been observed in the Cannonville or Escalante Members of the Entrada Sandstone around Lake Powell (or elsewhere) (Netoff, 2002). In this region the Gunsight Butte Member consists of white to orange cross-bedded dune sandstones (e.g. Anderson *et al.*, 2003).

Hanksville Pipe Swarm

A swarm of around 25 to 30 pipes can be seen in an extensive slick-rock exposure south of Hanksville (Fig 4.8). These pipes are situated within the Entrada Sandstone

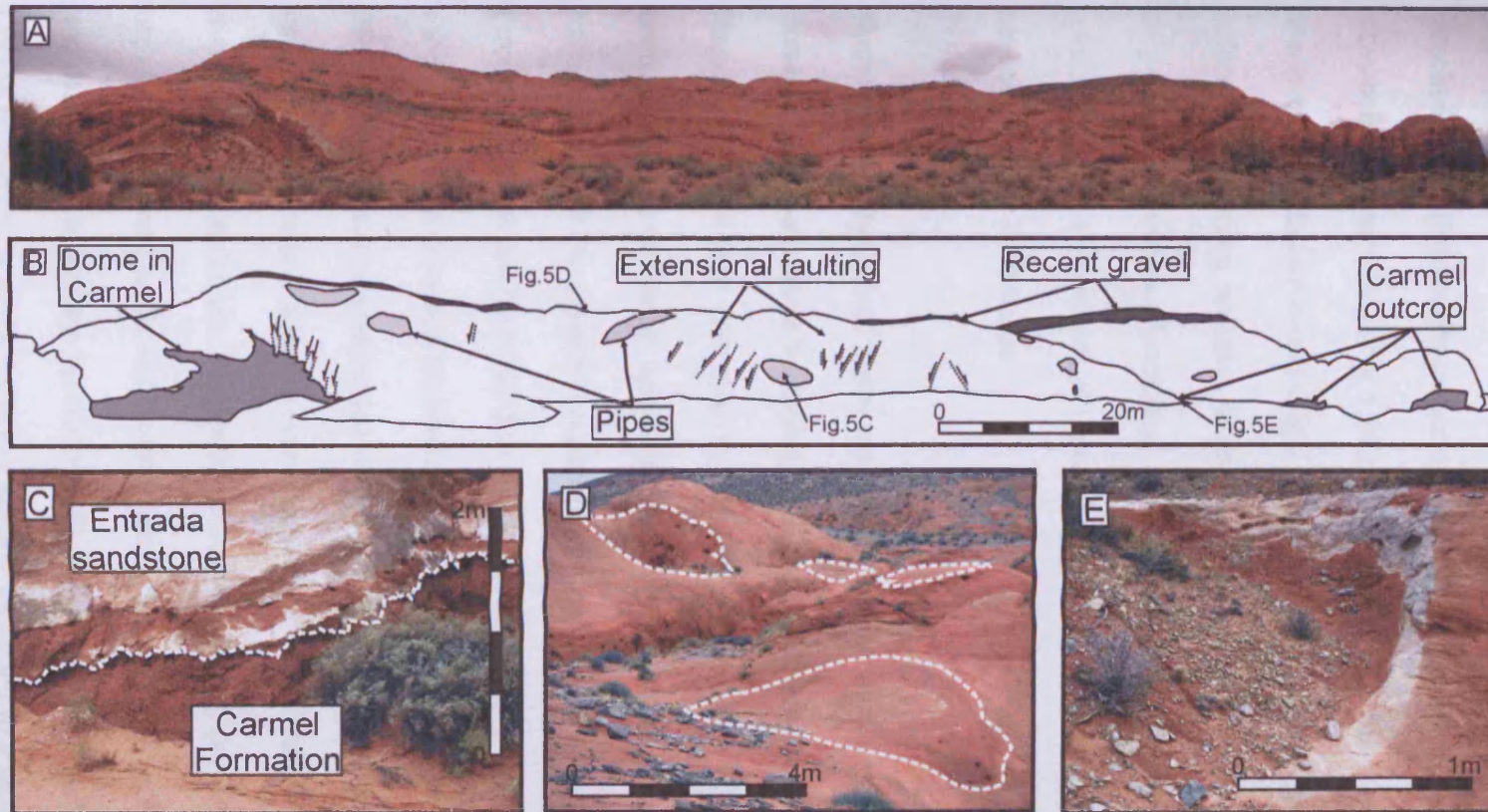


Fig 4.8 (A) “Slick-rock” exposures of lower Entrada Sandstone near the Hanksville with (B) a line drawing of the features seen including several sandstone pipes with little geomorphological expression or associated with weathering pits, the irregular faulted and domed contact between the Carmel Formation and the lower Entrada Sandstone and common extensional faulting within the lower Entrada. (C) The irregular contact between the brown silty Carmel Formation and the lower Entrada Sandstone. The Entrada Sandstone is heavily bleached near the contact. (D) A region with a four pipes (marked by white dashed lines) in close proximity located on the top of the hillside. Over 25 pipes were observed at this location. (E) A partially obscured pipe consisting of dark brown mudstone breccia fragments in a brown sandstone matrix indicative of transport of material from the underlying Carmel Formation. The pipe has a central weathering pit around which the orange Entrada Sandstone host rock is heavily bleached.

near its basal contact with the underlying Carmel Formation. The Carmel Formation is locally highly deformed and consists of dark coloured mudstones and fine-grained white to brown sandstone. The basal sands of the Entrada Sandstone are commonly bleached white; this decolouration extends up to 80 cm into the overlying orange, cross-bedded sandstones (Fig 4.8C). The contact between the Carmel Formation and overlying Entrada Sandstone displays deformation on a range of scales; large-scale deformation forming complex folds with wavelengths in excess of 50 m of which only the upper portion of anticlinal section are exposed. Small-scale extensional and reverse faulting with throws of up to about 40 cm are present along the contact between the two formations.

Numerous closely-spaced pipes are present within the Gunsight Butte Member of the Entrada Sandstone above the highly deformed basal contact. The pipes themselves range from 1 to 4 m in diameter and are separated by 1 to 15 m. They frequently occur as clusters of closely spaced pipes (Fig 4.8D). The irregular nature of the surface on which the pipes are exposed means that a wide-range of different sections through the pipes can be studied in this location. The pipe outcrops have little or no relief, or have pronounced weathering pits in their centres up to 1 m deep. Almost all of the pipes consist of homogeneous orange to white fine-grained sandstone with a variable component of angular breccia clasts of cross-bedded sandstone ranging in diameter from 1 to 25 cm. However, an example of a pipe containing homogeneous brown fine-grained sands and breccia clasts consisting of brown laminated sandstone and dark brown mudstone is also present at this locality (Fig 4.8E). It is hosted within orange Entrada Sandstone, which is heavily bleached to a pale orange to white colour along the contact with the pipe. Individual pipes show a range of internal structures

including increasing size and frequency of breccia clasts towards the centre of the pipe, fine-grained outer margins and concentric layering within the pipe.

The pipe-host contacts of individual pipes may be smooth and sub-circular or oval in shape to highly irregular. The host material is heavily fractured displaying a high intensity network of small-scale faults with throws ranging from a few millimetres to 20-30 cm. Some pipes are partially surrounded by curvilinear concentric faults, which may possibly represent collapse structures similar to those seen at Shepards' Point.

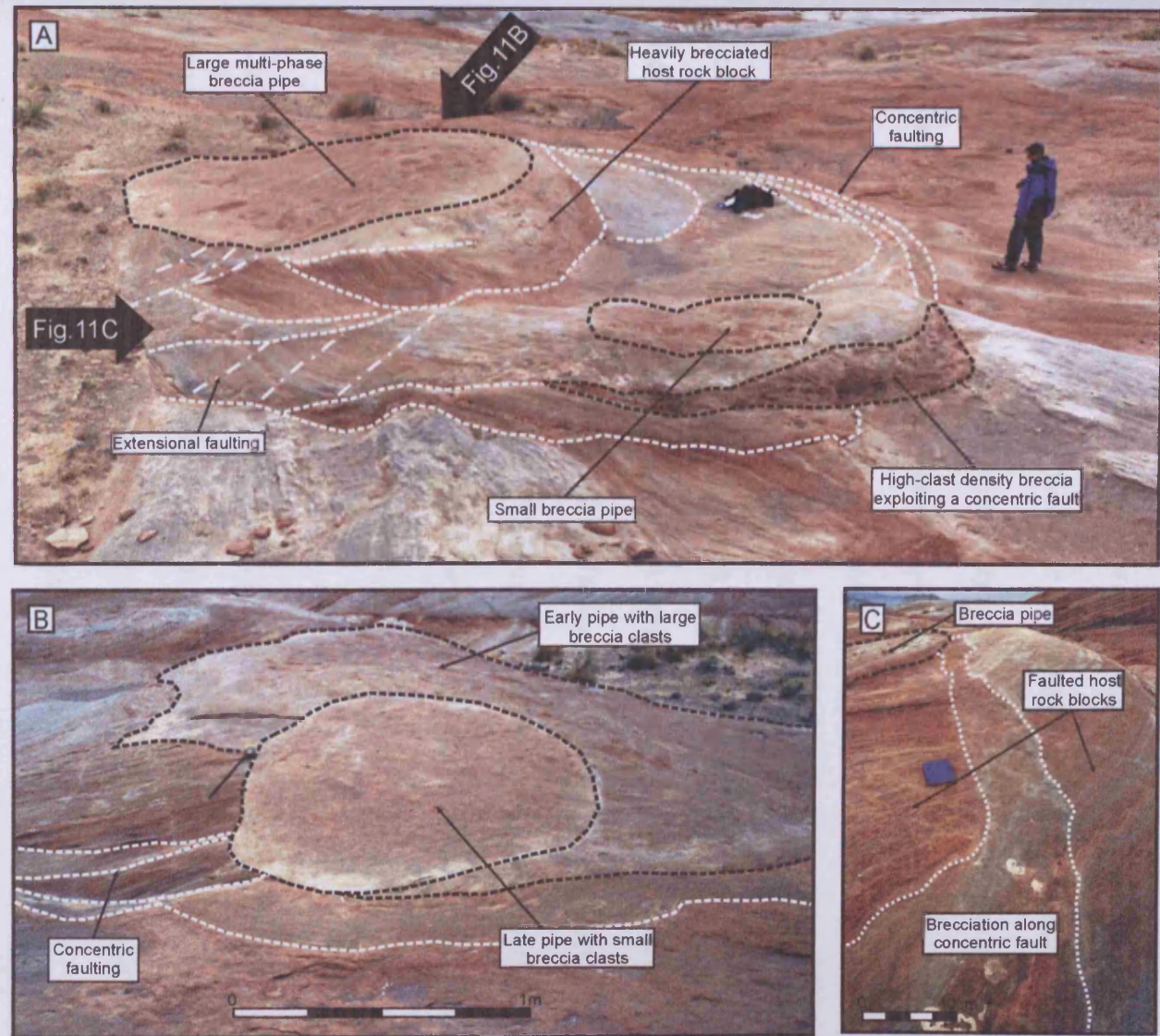
Warm Creek Bay Slick-Rock Exposures

A slick-rock exposure of a complex multi-phase pipe with a diameter of 6 to 7 m, within a zone of concentric faulting up to 6 m wide is exposed on the shores of Lake Powell in Warm Creek Bay several metres below the normal lake level (Fig 4.9A). The pipe is hosted in orange to grey and white fine-grained sandstones displaying large-scale cross beds characteristic of the Gunsight Butte Member of the Entrada Sandstone in this region.

The material making up the pipe largely consists of homogeneous sandstone and scattered angular breccia clasts made up almost exclusively of cross-bedded sandstone with a few flakes of mudstone. At least three phases of pipe formation can be identified based cross-cutting relationships and on the differing size distribution and relative abundance of breccia blocks with respect to homogeneous sandstone matrix.

A large composite pipe body is situated off centre, towards the SSW margins of the zone of concentric faulting (Fig 4.9B). Smaller more irregularly shaped breccia bodies

Fig 4.9 (A) Overview of a pipe with a highly complex geometry from Warm Creek Bay, Lake Powell. Several breccia bodies can be seen (highlighted with a black dotted line) and these are surrounded by concentrically fractured hostrock blocks (white dotted lines). One breccia body can be seen to actively exploit a concentric fracture. (B) Several phases of breccia pipe emplacement can be seen at this location. In particular one small roughly circular pipe with small breccia clasts up to a few centimetres in diameter can be seen to cross cut the margins of an earlier, more irregularly shaped pipe body containing large breccia clasts several 10's of centimetres in diameter. (C) The intensity of brecciation decreases with distance along the concentric fracture from the pipe to which it is related.



are present throughout the zone of concentric faulting. The main pipe body has two distinctive domains: an irregularly shaped outer mantle containing coarse breccia and a circular pipe approximately 1.5 m in diameter containing smaller breccia clasts. The outer irregularly shaped body contains randomly orientated breccia blocks up to 50 cm in diameter that make up around 60 to 70% intruded material. A thin mantle of breccia with clasts up to 10 cm in diameter is present along, and truncated by, the margins of the main intrusive body. The circular body cross-cuts the margins of the larger breccia body. It consists of homogeneous sandstone with breccia clasts ranging in diameter from 1 to 12 cm in diameter, which form approximately 30 to 40% of the intruded material. The contacts between the different intrusive bodies are sharp and bleaching along the contacts is common. The pipe-host contacts range from being smooth, to irregular and there may be intense faulting and considerable brecciation of the host rock in close contact to the intruded body.

The large intrusive body is partially surrounded by a zone of concentric faulting within which minor breccia bodies can be identified. These take two forms: high-density breccias and progressive zones of brecciation along fault planes (Fig 4.9C). High-density breccias form a number of irregular curved bodies and one small circular body consisting of highly angular breccia blocks up to 15 cm in diameter within a homogeneous sandstone matrix. The breccia blocks make up around 80 to 90% of the intruded volume and are randomly orientated. Progressive brecciation along fault planes forms curvilinear bodies commonly linked to pods of high-density breccia. The amount of brecciation and block rotation decreases with distance away from the high density-breccia pod and grades into thin slivers of highly faulted host rock.

The intruded bodies are partially surrounded by a zone of complex concentric and extensional faulting. These form curved fractures that range in extent from 50 cm to 8 m in length and break the host rock material up into curved blocks several meters in length and up to a meter in width. Some concentric faults display complex cross-cutting relationships and several of the curved fault blocks display arrays of extensional faults orientated roughly perpendicular to, or even cross-cutting pre-existing phases of concentric faulting.

4.4.4 Pipe-fill grain-size, cements and evidence of fluid migration

4.4.31 Lake Powell region

The lithology of the sandstone breccia blocks and matrix found within pipes in the Lake Powell region is superficially very similar to the surrounding host rocks of the Gunsight Butte Member of the Entrada Sandstone (Netoff and Shroba, 2001; Netoff, 2002; Anderson *et al.*, 2003). However, there are obvious differences in homogeneity, and presence and orientation of depositional structures between cross-bedded host-rocks and the pipes themselves. Both the pipes and host rock are made up of fine-grained quartz dominated orange to white aeolian sands. However a detailed petrographic study using 69 paired samples of host rock and pipe fill highlighted significant differences between the two rock types (Netoff and Shroba, 2001). Grain size and the initial pore volume at the time of pipe emplacement are both higher in the pipe material than in the host rock. Average grain size is 111 μm in the host sandstones but 151 μm in the pipe fill. However, the clay content and feldspar content

are lower in the pipe fill than the surrounding host rocks. Given that there are very few examples of pipes containing material derived from the underlying Carmel Formation, and the striking lithological similarities between pipe fill and host rocks noted above it is possible to infer that in the Lake Powell region, it is likely that most of the pipe fill material is derived from the Entrada Sandstone (Netoff and Shroba, 2001; Netoff, 2002).

4.4.32 Kodachrome Basin

A separate study comparing grain-size distributions in sandstone from the Winsor Member of the Carmel Formation and the Gunsight Butte Member of the Entrada Sandstone with pipe fill material in the Kodachrome Basin found a similar relationship (Hannum, 1980). The Winsor Member consists dominantly of fine-grained sands with minor medium-grained sand, silt and clay. The Gunsight Butte Member consists of sandy silts and clays (Hannum, 1980). Grain-size distributions presented from pipe fill material all contain an increased coarse fraction (medium-grained sand to gravel sized) and most have a depleted fine-grained fraction (fine-grained sand to clay sized). The grain-size distribution in some pipes strongly mirrors the distribution of sandstones within the Winsor Member of the Carmel Formation, with only a minor coarse fraction present. However, other pipes have very different grain-size distribution due to a greatly increased coarse fraction (Hannum, 1980).

The general observation that there is an increase in the coarse grain-size fraction, and depletion in the fine-grained fraction in pipe fill relative to host rock has been made independently in both studies (Hannum, 1980; Netoff and Shroba, 2001). This makes

it possible to infer that the processes involved in pipe formation may cause segregation of pipe fill material by grain-size. However, this can only be tested directly by comparing the pipe fill to its associated source bed.

4.4.33 Cementation of pipe material

The cements within pipes and the migrating fluids that precipitated them have been sparsely investigated. The sandstone and breccia in most pipes is highly friable often eroding to form weathering pits (Netoff and Shroba, 2001) indicating low levels of cementation. Pipes and the cross-bedded host rocks encasing them in the Lake Powell region have low levels of calcite and clay mineral cements at the present day (Netoff and Shroba, 2001). Under cathodoluminescence calcite crystals appear to show two or even three phases of growth and clay mineralogies are dominated by smectite with minor illite. Further to the east, in the Moab region of the Paradox Basin, fluid inclusion studies have found evidence of hydrocarbons in calcite cements within Jurassic sandstones (Chan *et al.*, 2000).

The contacts, or outer margins of many pipes, both in the Lake Powell region and in the Kodachrome Basin are more resistant than either host rock, or pipe fill due to increased levels of calcite cementation relative to both the host rock and pipe centre (Hannum, 1980; Netoff and Shroba, 2001). Increased concentrations of calcite cements at the contacts of pipes in the Lake Powell region gives the contact a lighter colour, positive relief and a much-reduced porosity (Netoff and Shroba, 2001). Host rocks in contact with pipes in the Kodachrome commonly show bleaching interpreted as evidence for reducing conditions associated with pipe fluids or hydrocarbon

volatiles (Hannum, 1980; Chan *et al.*, 2000; Baer and Steed, 2003; Beitler *et al.*, 2003).

4.5 SUMMARY OF PIPE CHARACTERISTICS

The general characteristics of the sandstone pipes of SE Utah may be summarised as:

- Tubular or upwards tapering geometry with roughly circular or elliptical cross sections and with straight or slightly sinuous, near parallel walls.
- Pipe diameters ranging from 1 to 75 m and individual pipes may cross-cut a considerable thickness of host strata.
- Contacts between host rocks and pipe fill are usually sharp.
- Pipe fill consists of breccia blocks up to 1 m in length with similar lithologies to the surrounding host rock or underlying units set within a matrix of sand and gravel.
- Many pipes (especially in the Lake Powell Region) are surrounded by a zone of high-intensity, small-scale normal faulting up to 3 m wide producing margins with a ragged step-like geometry.
- Some pipes are surrounded by large-scale collapse structures within which, faulted host rock strata dip towards the pipe axis in a manner reminiscent to caldera collapse.

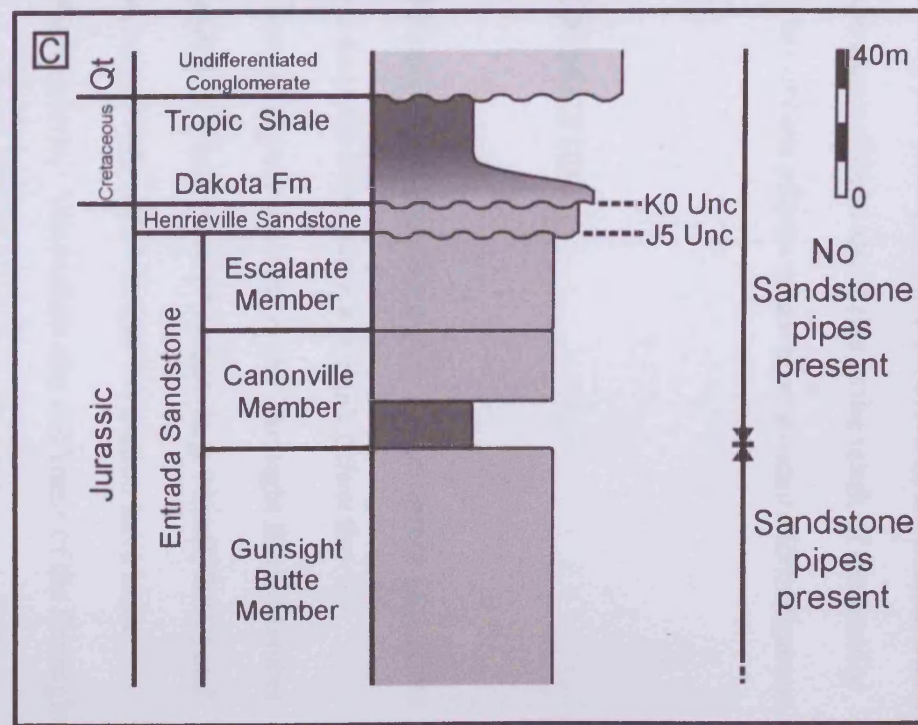
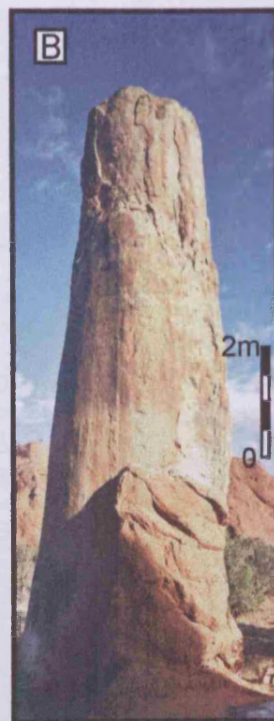
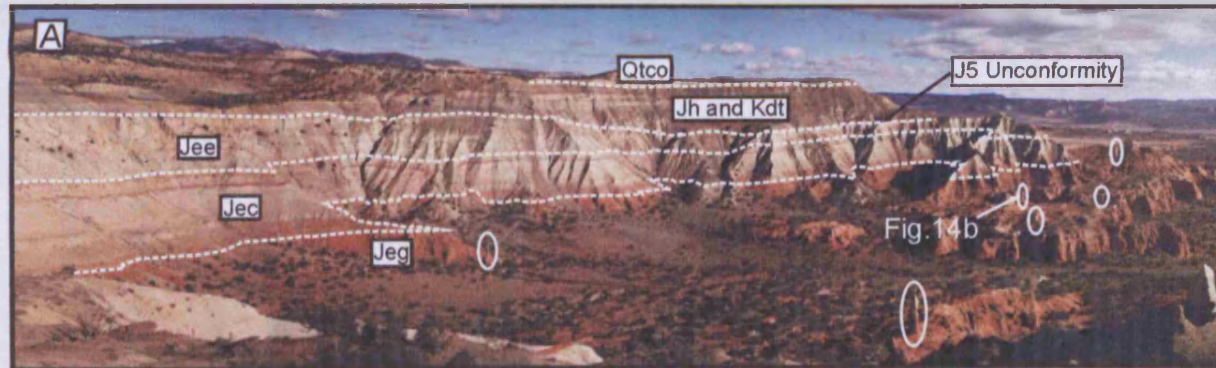
4.6 TIMING OF PIPE FORMATION

Dating sandstone intrusion events is inherently difficult because unlike igneous intrusions, radioactive isotopes cannot be used. Dating the intrusion fill or breccia

blocks within an intruded body dates merely the age of the units through which the intrusion has passed and sequestered material and not the emplacement event itself. Dating is further complicated by the predominantly terrestrial nature of the sediments examined during this study. Dating becomes possible where sandstone intrusions affect a datable depositional surface by sand extrusion (Netoff, 2002) or topographic deformation that can be dated by stratigraphic methods (e.g. Chapter 2)

Two lines of evidence can be used to constrain the timing of pipe formation in southeastern Utah: Pipes are found within the Carmel Formation and the Gunsight Butte member of the Entrada Sandstone (e.g. Netoff, 2002; Anderson *et al.*, 2003; Baer and Steed, 2003). No pipes have been observed above the Gunsight Butte Member of the Entrada Sandstone in either the Kodachrome Basin (e.g. Fig 4.10) or in the Lake Powell region. Secondly, a possible large-scale, sand volcano, or “mega-sandblow” associated with underlying sandstone pipes has been identified at the top of the Gunsight Butte Member of the Middle Jurassic Entrada Sandstone at Rock Creek Bay, Lake Powell (Netoff, 2002). The lack of intrusions above the base of the Cannonville Member of the Entrada Sandstone implies that pipe formation did not occur during the deposition of this unit. When this observation is combined with the presence of a large-scale sand-volcano at the top of the Gunsight Butte Member of the Entrada Sandstone it appears likely that this surface represents the palaeo-surface at the time of pipe formation and that at least some of the sandstone pipe propagated to this surface. This is consistent with previous estimates of the timing of pipe formation (Hannum, 1980; Alvarez *et al.*, 1998; Netoff, 2002). However, it is impossible to distinguish whether all the sandstone pipes formed in a single event, or during multiple events occurring over a short time period. Examples of pipes displaying

Fig 4.10 A) View across Kodachrome State Park showing the stratigraphic relationship between the pipes (highlighted with white ovals) and the host sediments: the Middle Jurassic Entrada Sandstone made up of the Gunsight Butte Member (Jeg) the Cannonville Member (Jec) and the Escalante Member (Jee) which are separated from the Upper Jurassic Henrieville Sandstone (Jh) and the Cretaceous Tropic/Dakota formation by the J5 unconformity, which are in turn overlain by Quaternary gravels (Qtco). Exposures of free-standing pipes appear to be restricted to the Gunsight Butte Member of the Entrada Sandstone. B) Examples of impressive pipes standing over 20m above ground level are common in this region. C) A stratigraphic column through the rocks that outcrop within the Kodachrome Basin State Park (after Thompson and Stokes, 1970, Baer and Steed 2003) showing that pipes appear to be restricted to the Gunsight Butte Member or older rocks.



multiple, cross-cutting phases of intrusion are present in SE Utah (e.g. Warm Creek Bay). Although, in this case, it is impossible to say if this is the result of temporally separate phases of intrusion, or merely the effects of collapse structure formation on the geometry of the axial pipe.

4.7 DEPTH OF PIPE FORMATION

If we consider the top of the Gunsight Butte Member as the palaeosurface at the time of pipe emplacement it becomes possible to estimate the depth below the palaeosurface at which pipes formed. Pipes are found in the Gunsight Butte Member of the Entrada Sandstone throughout the Lake Powell region (e.g. Netoff, 2002) and pipes that are likely to have originated within the Carmel Formation have been observed (e.g. the Hanksville Pipe Swarm). The present day thickness of the Gunsight Butte Member is 145 m thick at Gunsight Butte, Lake Powell and the total thickness of the Carmel Formation is 33 m near Bullfrog (Thompson and Stokes, 1970).

Therefore assuming that the maximum distance a pipe could propagate is from the base of the Carmel Formation to the top of the Gunsight Butte Member of the Entrada Sandstone, remobilisation and pipe formation may have occurred at a maximum depth of 178 m below the palaeosurface in the Lake Powell region. Note that this is a maximum estimate and it is possible that not all pipes propagate to the palaeosurface, or emanate from the base of the Carmel Formation. The stratigraphic thicknesses presented are compacted present-day values.

In the region around the Kodachrome Basin State Park, pipes may be observed throughout the Gunsight Butte Member of the Entrada Sandstone and also within the

Winsor Member of the Carmel Formation (e.g. Hannum 1980; Baer and Steed, 2003). Therefore the maximum distance a sandstone pipe can propagate based on these observations, is from the base of the Winsor Member of the Carmel Formation to the top of the Gunsight Butte Member of the Entrada Sandstone. In this area the present day thickness of the Gunsight Butte Member of the Entrada Sandstone is considerably thinner than around Lake Powell (72 m, Thompson and Stokes, 1970) and is underlain by both the Wiggler Wash and Winsor Members of the Carmel Formation. In the Paria River Valley 8 km south of Canonville, the base of the Winsor Member is 169 m below the top of the Gunsight Butte Member (based on stratigraphic thickness logged by Thompson and Stokes, 1970). Note this is a maximum estimate based on the stratigraphic thickness of the sediments within which pipes were observed and that the thicknesses presented are compacted present-day values.

4.8 DISCUSSION

4.8.1 Pipe characteristics

The sandstone pipes examined during this study display a wide array of features. Often the level of variation is greater between different pipes in a single area, than between groups of pipes seen in different regions. However, a number of general characteristics can be recognised in every pipe: A vertically orientated cylindrical geometry with a subcircular to ellipsoid cross section is common to all pipes. Pipes are filled with fine-grained homogeneous sandstone and angular breccia blocks resembling the host strata are present within almost all pipes.

Breccia blocks are present in every intrusion examined and many display primary depositional fabrics such as lamination and cross bedding. This implies that the host rocks were cohesive at the time of pipe formation and that they were not transported far and therefore did not suffer significant attrition. The high level of angularity of the breccia blocks also implies that very little attrition of these blocks occurred during pipe emplacement. This may indicate transport processes within the pipe were relatively low energy and did not cause significant attrition, or that the pipe formation process was short-lived and that there simply was not enough time or transport distance was too short to allow significant erosion of breccia blocks present during pipe formation.

The host rock strata that encapsulate the sandstone pipes may or may not show deformation related to the pipes (Fig 4.11). Where present, two distinct styles of host rock deformation can be distinguished: small-scale deformation and large-scale collapse structures. Small-scale deformation affects the host rocks within 1-3 m of the pipe/host contact. It consists of high intensity, closely spaced, but small-scale extensional faulting (Fig 4.11A-B). The resultant irregular or step-like pipe geometry is likely to form during the latest stages of pipe formation because otherwise any irregularities on the pipe walls are likely to have been eroded during the emplacement process. This style of deformation was more commonly observed around pipes in the Lake Powell region (possibly due to easier identification in slick rock exposure) where the host rock consisted of fine-grained cross-bedded sandstone as opposed to the more cohesive silty facies present in the Kodachrome Basin. It is possible that this style of deformation only formed if the surrounding host rocks were relatively weak.

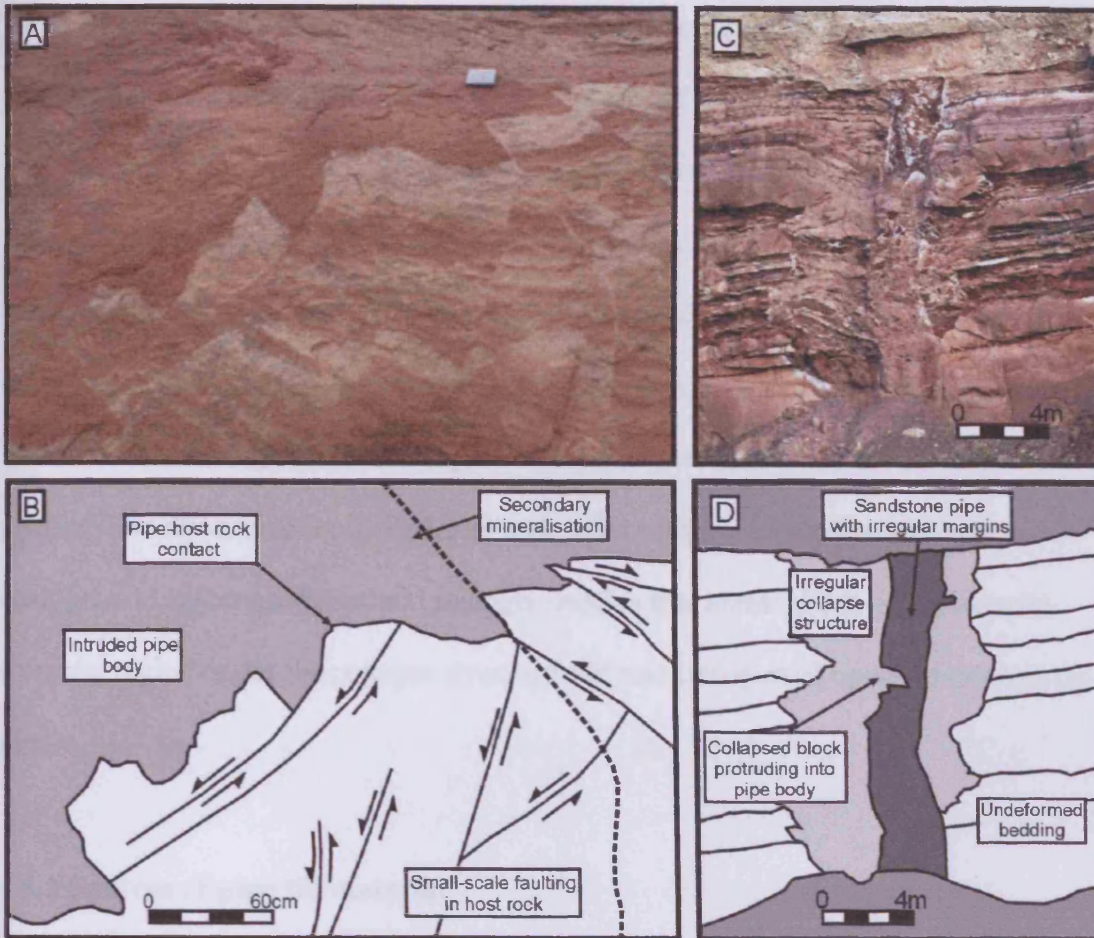


Fig 4.11 A) Small-scale faulting around a sandstone pipe within the Gunsight Butte Member of the Entrada Sandstone at Bullfrog, Lake Powell (notebook for scale). B) Movement along small-scale faults with throws of up to 40cm lends the pipe margin a ragged, stepped geometry. C) Irregular sandstone pipe and associated collapse structure situated within the Winsor Member of the Carmel Formation at Shepards Point. Strata within the collapse structure appear highly deformed. Note that the upper termination of the pipe has been eroded and Quaternary gravels sit unconformably on top of the Winsor Member of the Carmel Formation. D) The collapse structure surrounding the sandstone pipe is highly irregular, its shape being locally affected by the competency of the rocks involved. The shape of the pipe is partially controlled by the collapse of material inwards towards the pipe i.e. material within the collapse structure can protrude into the pipe body itself.

After the cessation of pipe formation the pipe walls collapsed in to the pipe forming a halo of step-like extensional faults and slumps around the pipe. Large-scale deformation can be seen in both the Lake Powell region and in the Kodachrome Basin and is therefore not dependant on the host rock facies. Large-scale deformation consists of a collapse structure with a well-defined outer margin within which deformed beds dip downwards towards a sandstone pipe (Fig 4.11C-D). The pipe may be central or offset towards the margins of the collapse structure, but is always present. The downward motion of host rock units within the collapse structure is analogous to caldera collapse and strongly implies that material has been removed from the region under the collapse structure and was transported upwards through the pipe.

4.8.2 Sources of pipe fill material

The pipe fill material provides information about the strata the pipe has penetrated and the source strata from which the pipe originated. The pipe-fill matrix is likely to be derived from the remobilised source unit or the pipe walls. The breccia blocks found within the pipes are likely to be derived from the roof of the remobilised source unit and the walls of the pipe itself. In general, white to orange fine to very fine-grained sandstone is characteristic of the Gunsight Butte Member of the Entrada Sandstone and it is likely that a large component of the material within the pipes is derived from this formation. A small number of distinctive pipes consisting of very fine-grained dark brown sands and silts encased within white to orange Entrada Sandstone were observed during the course of this study. The dark colour and fine grain size are characteristic of the upper members of the Carmel Formation and it is

likely that these pipes contain material originating from the Carmel Formation (e.g. Fig 4.8E).

In the Lake Powell region both the pipe matrix and breccia blocks have a very similar composition to the surrounding Entrada Sandstone host rock (e.g. Netoff and Shroba, 2001). Breccia blocks within the pipes consist of cross-bedded sandstone with a very minor mudstone/shale component in a few examples. This strongly implies that most of the material within the pipes around Lake Powell was derived from the surrounding Entrada Sandstone with only a minor component introduced from the underlying Carmel Formation. No breccia blocks indicative of overlying strata were found. In the Kodachrome Basin region pipe fill material is considerably more variable. Mudstone and sandstone breccia blocks are present in all pipes in the Kodachrome Basin, whether they are hosted in the Entrada Sandstone or the Carmel Formation. This implies that both matrix and breccia blocks were derived from both these formations.

The grain-size of pipe matrix is typically coarser than the host rock in both the Kodachrome Basin (Hannum, 1980) and in the Lake Powell region (Netoff and Shroba, 2001). Sandstone units with larger grain sizes than those present in the Entrada Sandstone can be found at deeper levels in the Triassic to Jurassic succession (e.g. the Navajo Sandstone at Red Breaks, east of the Kaiparowits Plateau, has an average grain-size of 169 μm), however, no evidence of pipes emanating from below the Carmel formation was observed study or has been published previously. The implication of these observations is that material is unlikely to have been transported upwards from the Navajo Sandstone. Therefore grain-size variation between pipe fill matrix and host rock is likely to be a function of the pipe formation process.

4.8.3 Mechanisms of pipe genesis

Various mechanisms have been put forward to explain the formation of sandstone pipes. These mechanisms fall into two distinct groups: dissolution collapse (e.g. Sweeting, 1972; Hunter *et al.*, 1992; Weinrich *et al.*, 1992; Walsh and Zacharz, 2001) and forceful upward fluid flow and remobilisation of granular sediments (e.g. Hawley and Hart, 1934; Hannum, 1980; Deynoux *et al.*, 1990; Guhman and Pederson, 1992; Mount, 1993; Netoff, 2002; Dragantis *et al.*, 2003).

During dissolution collapse, local dissolution of soluble rocks such as evaporite or carbonate deposits causes cylindrical failure and down dropping of the overlying beds (Hunter *et al.*, 1992). If the soluble unit is deeply buried, this leads to the formation of sub-cylindrical pipes that are filled with structureless sedimentary rock or breccia, derived from the overlying units, or down dropped unbroken strata similar to that surrounding the pipe (Hunter *et al.*, 1992). The largest dissolution collapse pipes may be up to 75 m in diameter and have a vertical extent of up to 1220 m (Weinrich *et al.*, 1992) but most are considerably smaller (Hunter *et al.*, 1992; Walsh and Zacharz 2001). During dissolution collapse material is transported downwards and at no level is material from deeper stratigraphical units observed (Weinrich *et al.*, 1992).

Strong evidence of upwards transport of material within pipes can be found in the Middle Jurassic rocks of Utah (e.g. Mudstone blocks in Chimney Rock derived from the underlying Carmel Formation). This is incompatible with a dissolution collapse origin for the sandstone pipes of SE Utah. Several other lines of evidence suggest that

a dissolution collapse origin for the pipes is unlikely: a) No sizable deposits of evaporites are present in the rocks underlying the section studied (Baars and Stevenson, 1982). b) Dissolution collapse does not explain the presence of breccia filled pipes that do not show collapse structures. c) Dissolution collapse may simply lead to the downdropping of overlying beds without the formation of a sandstone/breccia pipe (Hunter *et al.*, 1992). Therefore, we interpret the sandstone pipes of southeastern Utah to have formed as a result of forceful vertical fluid migration and sediment remobilisation rather than by dissolution collapse.

4.8.4 Bulk transport

Despite the considerable variation shown by individual pipes, two broad categories can be identified based on the presence, or lack of collapse structures in the host rock surrounding the pipes:

- *Dewatering Pipes.* If no collapse structures are observed fluid may have escaped the parent unit with little or no solid material being transported out of the pipe. Fluid velocities within the pipe and source unit may have been fast enough to allow the fluidisation and homogenisation of granular sediment within the pipe, but were not fast enough to cause the elutriation of granular sediment from the pipe. In effect fluid is able to escape from the pipe, but sediment is not. The pipe seen at outcrop at the present day consists of homogeneous sand and breccia blocks representing the column of fluidised sand formed during fluid escape. The pipe represents a fluid escape pathway to a more shallow level in the sequence and possibly to the palaeosurface.

- *Evacuation Pipes*. The presence of collapse structures implies that sediment has been transported out of the parent unit forming a depleted zone within the parent unit from which the pipe emanated. Fluid velocities within the pipe were great enough to entrain and transport granular sediment out of the pipe/source unit. In order for a collapse zone to form, the radius of the depletion zone within the source unit must be greater than the radius of the pipe. In effect the pipe has acted as a feeder system to sand volcanoes or sand blows at the palaeosurface and removal of material from the parent unit has undermined the overlying strata causing their collapse. It is therefore logical to argue that the amount of displacement of host material within the collapse structure is equal to the volume of sand transported out of the parent unit.

4.8.5 Triggering rapid fluid flow

Three different mechanisms for triggering pipe formation through forceful fluid flow and fluidisation of granular sediment have been proposed by previous workers: steady state artesian ground water flow (Hannum, 1980; Guhman and Pederson, 1992), liquefaction due to the Upheaval Dome impact (Alvarez *et al.*, 1998) and liquefaction due to seismic shaking (Hannum 1980; Netoff, 2002). We propose that because all the pipes examined in southeastern Utah have similar characteristics and timing, therefore their formation is also likely to have been triggered by the same processes.

4.8.51 Ground water flow

Artesian ground water flow has been invoked to explain springs and pipes in both ancient examples (e.g. Hawley and Hart, 1934; Allen, 1961; Hannum, 1980; Dragantis *et al.*, 2003) and modern analogues (e.g. Guhman and Pederson, 1992).

Boiling sand springs observed along the shores of the Dismal River, Nebraska, the result of artesian groundwater discharge, display many features analogous to the fluidisation pipes seen in southeast Utah (Guhman and Pederson, 1992) including: cylindrical geometry with a diameter of up to 10 m and depth of up to 44 m.

Commonly the springs have firm sides at the surface although the subsurface geometry of the pipe walls is not known. The boiling sand springs are found within 30 m of the river. The springs commonly occur in bowl shaped depressions and contain mobile sand displaying a churning (or boiling) motion which has a distinct interface with an overlying clear water layer, which drains into the nearby Dismal River (Guhman and Pederson, 1992). The observation that a layer of clear water sits on top of a boiling sand layer is important because it implies that fine-grained solid material is not currently being elutriated in abundance from the pipe, but that water is able to escape. Thus the fluid velocity in the pipe is currently below the settling velocity of the suspended grains within the pipe and transport does not occur. However, it is possible that any fine-grained component in the pipe fill has previously been winnowed away leaving a coarser fraction that has a settling velocity greater than the fluid velocity within the pipe. These springs form in response to artesian ground water flow in close proximity to an incised river channel. If the pipes seen in southwest Utah were to have formed in this manner we would expect them to be distributed parallel to the courses of any ancient rivers present. Rivers did flow from the south

and east during the Jurassic (Dickinson and Gehrels, 2003), however the distribution of pipes in southwest Utah appears to parallel the margins of the Carmel-Twin Creek Seaway rather than any northwesterly flowing palaeo-river system. There is no recorded sedimentological evidence for fluvial channels associated with the top of the Gunsight Butte Member of the Entrada Sandstone. Also the observation that there is no sediment transport out of the pipes driven by artesian groundwater flow (Guhman and Pederson, 1992) is incompatible with the presence of pipes which display collapse structures.

4.8.52 Upheaval Dome impact crater

The presence of widespread seismites and or regions of sandstone intrusions have been attributed to specific impact events (e.g. South Dakota, the UK) (Terry *et al.*, 2001; Simms, 2003 respectively). Upheaval Dome is a suspected impact crater situated within the northern part of the Canyon Lands National park in southeastern Utah (Kanbur *et al.*, 2000). The crater is 5.5 km in diameter (Huntoon, 2000) with a rim monocline, and ring syncline, and a 2.5 km wide central uplift making up the main structural elements (Kenkman, 2003). The timing (e.g. Shoemaker and Herkenhoff, 1984; Alvarez *et al.*, 1998; Kriens *et al.*, 1999; Kenkman and Scherler 2002; Kenkman, 2003) and even origin (Smith, 2004; Jackson *et al.*, 1988) of Upheaval Dome is currently the subject of considerable debate. Whilst it is possible to say that impact occurred after the deposition of the Navajo Sandstone (the youngest rocks exposed in the crater) it is hard to constrain the date further. Estimates for the timing of the Upheaval Dome impact range from Middle Jurassic (Alvarez *et al.*, 1998; Kriens *et al.*, 1999) to Cretaceous or Tertiary (Shoemaker and Herkenhoff, 1984;

Kenkman and Scherler, 2002; Kenkman, 2003). Therefore we conclude that whilst it is possible that an impact may have triggered pipe formation during the Middle Jurassic in SE Utah, the timing of Upheaval Dome is too poorly constrained to conclusively link it to the sandstone pipes.

4.8.53 Seismic shaking

Liquefaction and fluidisation induced by seismic shaking has been tentatively proposed as the trigger for pipe formation in the Kodachrome Basin (Hannum, 1980) and has also been invoked to account for the formation of pipes in the Lake Powell region (Netoff, 2002). Local site conditions such as basement structure and large thicknesses of unconsolidated, fluid saturated, sandy sediments may lead to amplification of earthquake shaking by an order of magnitude or more (Aki, 1993; Benjumea *et al.*, 2003), which may increase the depths at which remobilisation of buried sand can occur to in excess of 100 metres (Benjumea *et al.*, 2003). Our analysis shows that sandstone pipes in Utah may originate at depths of up to 169 m below the palaeosurface at the time of intrusion. This is considerably deeper than liquefaction triggered by historic earthquakes (e.g. Obermier *et al.*, 2002).

Two regional tectonic events can be envisaged as possible causes of Middle Jurassic earthquakes in Utah: a phase of accelerated Cordilleran shortening (Allen *et al.*, 2000) and rebound of dynamic topography due to a change in the subductive regime of the Falleron Slab. The Entrada Sandstone was deposited in a retro-arc foreland basin during a period of accelerated shortening and downwarp (Allen *et al.*, 2000).

Therefore, pipe formation occurred at the same time as an increase in the northeast-

southwest orientated stress field. This would be likely to cause an increase in seismicity throughout the region as long-lived tectonic elements may have become reactivated (Blakey, 1988). It should be noted that the Lower Jurassic Navajo Sandstone was also deposited in a similar period of accelerated shortening and downwarp (Allen *et al.*, 2000), and it too is associated with at least localised pipe formation (Mahaney, *et al.*, 2004) but that pipes are not seen throughout the Entrada Sandstone, but only in the basal Gunsight Butte Member.

Previous studies have suggested that the subsidence of the retro-foreland basin was partially controlled by the formation of dynamic topography due to mantle flow around the descending plate (Heller and Paola, 1989; Burgess, and Moresi, 1999; Heller *et al.*, 2003). Uplift to the west of the study area due to the relaxation of this dynamic topography occurred during the Late Jurassic and Early Cretaceous and resulted in the deposition of widespread gravels on the K-0 unconformity (Heller *et al.*, 2003). However, a marked change from the long-lived westerly and north-westerly drainage pattern established during the Triassic, to an easterly drainage pattern recorded in the Middle Jurassic Romana Sandstone and Summerville Formation and Late Jurassic Morrison Formation (e.g. Bjerrum and Dorsey, 1995; Dickinson and Gehrels, 2003) seems to imply that uplift to the west of the study area began in the Middle Jurassic. Erosion responded to this easterly tilting in a similar manner and a marked change from the down cutting of the J-1, J-2, and J-Sup unconformities to the east and northeast, to westerly down cutting on the J-5 and K-0 unconformities (Pipringos and O'Sullivan, 1978) resulted. Regional tilting may also have affected ground water flow, increasing the hydraulic pressure of pore fluids in the study area. An increase in pore fluid pressure would result in a net decrease in the

effective shear stress of the sediments increasing their susceptibility to liquefaction.

Whilst pipes may form in response to artesian ground water flow (e.g. Guhman and Pederson, 1992), it is highly unlikely that this mechanism is capable of bulk sediment transport and the formation of collapse structures.

Both increased rates of shortening (Allen *et al.*, 2000) and relaxation of dynamic topography (Heller *et al.*, 2003) occurred during the deposition of the Entrada Sandstone. It is possible that both of these events could have altered the stress state of the rocks of the Colorado Plateau thus providing at least circumstantial evidence for increased earthquake activity. Evidence from historical earthquakes implies that only earthquakes with moment magnitude greater than 6.9 trigger liquefaction at epicentral distances in excess of 100 km (Ambraseys, 1988). This implies that either the earthquake capable of causing basin-wide liquefaction was very large (i.e. in excess of magnitude 8) or that widespread reactivation of basement faults occurred through out the region or that local site amplification had a major role in causing widespread liquefaction. Widespread basement faults have been reactivated at least twice in the tectonic history of the Colorado Plateau (e.g. Dickerson, 2003, Bump, 2004). It is highly likely that the major change in stress state observed during the Middle Jurassic caused widespread re-adjustment of these long-lived faults and this may have resulted in large-scale seismicity. Much of the post-rift activity on these faults has been compressional inversion, however there is also a strong transpressional component on most of the basement faults (e.g. Cather, 1999; Tindall and Davis, 1999; Bump, 2004). Both compressional and strike-slip earthquakes commonly have high magnitudes (i.e. in excess of M_w 7) (Trifonov, 2004) making seismic events resulting from the reorganisation of stress on these faults a likely candidate for pipe formation.

4.9 A MODEL FOR PIPE FORMATION IN SE UTAH

Based on the sequence of events and analysis of Middle Jurassic pipe outcrops in SE Utah presented above we propose the following model for the formation of sandstone pipes in SE Utah. Increased rates of southwesterly shortening coupled with the inception of easterly tilting of the region due to the rebound of dynamic topography considerably altered the palaeo stress field across the western USA during the Middle Jurassic. This resulted in the reactivation of long-lived blind basement faults. The resulting high magnitude compressional and strike-slip earthquakes caused remobilisation of water-saturated Middle Jurassic sediments within the Carmel Formation and the basal Gunsight Butte Member of the Entrada Sandstone. The uneven distribution of pipes seen across both the study areas implies that liquefaction and pipe formation did not occur evenly across the region and occurred in more localised pockets. Pockets of liquefied sand within larger sand bodies have been observed on a smaller scale in the field and in experimental systems (Lowe, 1975). In order for a liquefied pocket to form, the sand within it must be more prone to remobilisation than the surrounding material. It is likely that a range of different factors such as depositional fabric (e.g. clay content and grain-size), presence or absence of sealing lithologies, degree of lithification, and local amplification of seismic waves may contribute to the sands susceptibility to remobilisation.

In order for liquefaction to occur within the Middle Jurassic sediments they must have been water saturated, and therefore below the water table. The absence of evidence for liquefaction and water escape structures (other than large-scale pipes) within the

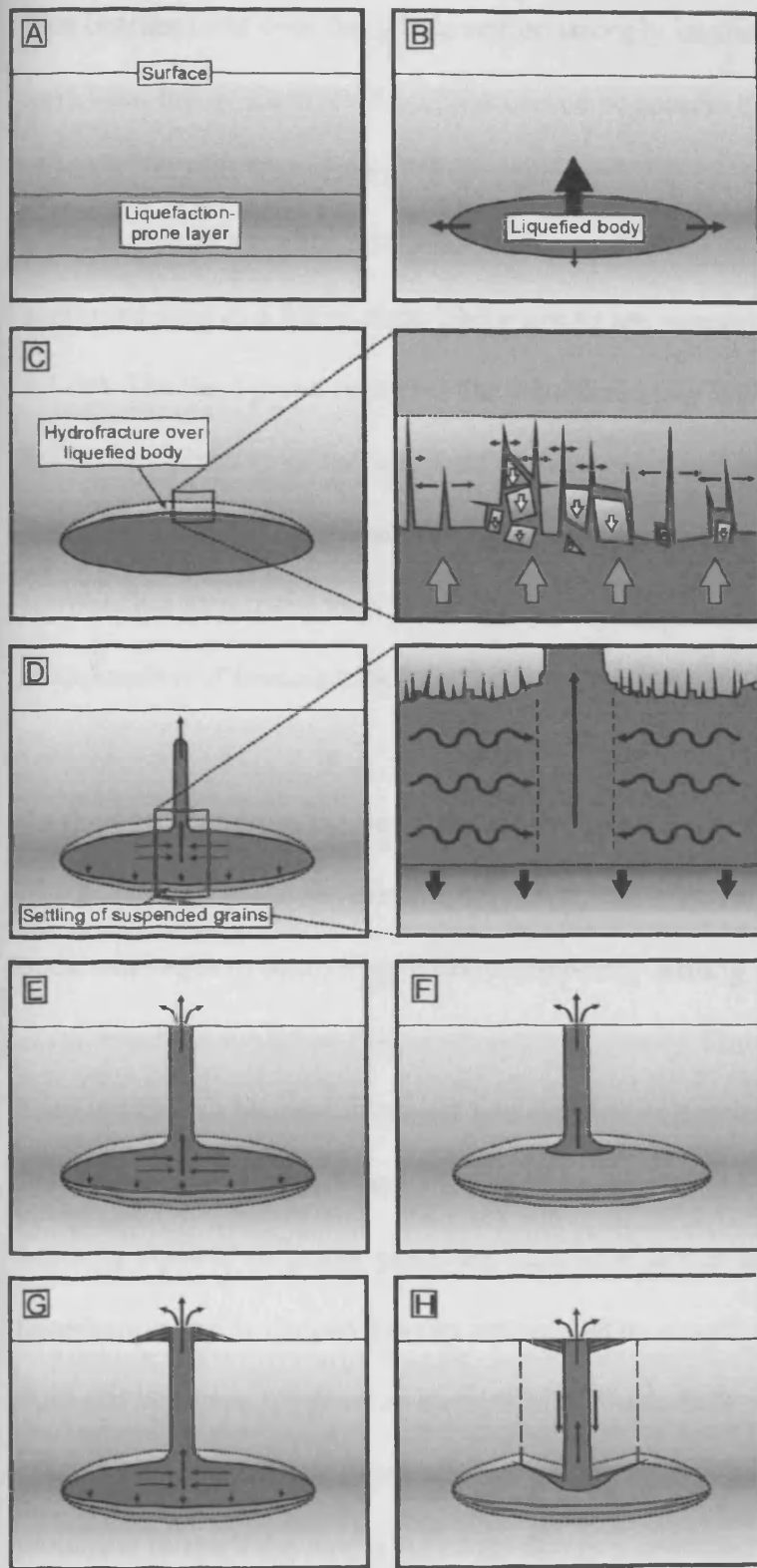


Fig 4.12 A model for pipe formation (for more detailed discussion see text): A) A liquefaction prone layer exists at depth within the section. B) In response to seismic shaking a pocket of unconsolidated sediment liquefies. C) High fluid pressures within the liquefied pocket causes the hydraulic fracture and brecciation of cohesive sediments around the liquefied pocket. D) The contents of the liquefied pocket begin to settle, discrete pipes of focused upwards fluid flow form within the liquefied sand, where the focused fluid flow reaches the roof of the liquefied pocket they propagate up into the overlying sediment. E) The pipe propagates to the surface. If the pressure within the liquefied pocket is not capable of sustaining high fluid velocities within the pipe solid material is not extruded onto the surface. F) The liquefied pocket settles without the formation of a collapse structure. G) The fluid reservoir within the liquefied pocket is large enough to sustain high fluid velocities for prolonged periods of time and solid material is extruded on to the palaeosurface. H) Extrusion of solid material leads to the depletion of the liquefied pocket and subsequent collapse of the overburden.

pipe bearing units over the whole region strongly implies that the water table may have been below these levels. The presence of breccia blocks in many of the pipes observed implies that some of these sediments were at least partially lithified.

Liquefaction of a pocket of buried sediment changes its state from a solid grain supported state to a liquid state where grains are supported by the pore fluid (Fig 4.12B). The fluid pressure within the liquefied body will be much greater than the hydrostatic pressure of the surrounding host rocks and fluids may begin to drain from the liquefied body. If the fluid pressure is greater than the lithostatic pressure of the surrounding host rocks then hydraulic fracture may occur possibly resulting in the incorporation of breccia blocks into the liquefied body (Fig 4.12C) (Morley, 2003).

As fluid escapes from the liquefied source unit into the host rocks pore spaces or open hydraulic fractures, overpressure dissipates, the granular sediment within the liquefied body will begin to settle (Fig 4.12D). However, settling and fluid expulsion does not occur evenly in liquefied bodies (Kolymbas, 1998). Fluid escape within the liquefied body is likely to become localised into discrete cylindrical channels fed by radial flow from the surrounding sediments (Kolymbas, 1998). Sediment within these dewatering pipes is no longer passively supported within the pore fluid as a result of liquefaction, but is instead heavily influenced by drag forces applied by the escaping fluid and becomes fluidised as a result of the high fluid velocity within the pipe.

When such a dewatering pipes reaches the top of the liquefied body it is able to propagate through the overlying rocks due to a combination of the high fluid pressure within the liquefied body and the added momentum of a column of upwardly flowing water. More breccia blocks may be incorporated into the pipe by stoping of the pipe ceiling. The cylindrical geometry of the pipes seen in SE Utah may therefore be

inherited from dewatering pipes within the liquefied source units and it is likely that the spacing of sandstone pipes observed in the field (e.g. Hanksville Pipe Swarm) may represent the distribution of dewatering channels within the liquefied source unit.

If the volume and fluid pressure within the liquefied pocket is sufficient, pipes may propagate upwards to the palaeosurface (Fig 4.12E). In SE Utah, the top of the Gunsight Butte Member of the Entrada Sandstone represents the palaeosurface at the time of pipe formation. It is likely that the pipe will begin to widen as through flow of fluid and sediment causes plucking of material from the pipe walls. If pressure within the fluid reservoir represented by the liquefied pocket is not great enough to sustain fluid velocities above the fluidisation velocity of the entrained grains within the pipe, but not greater than the settling velocity of the entrained grains, then the movement of the escaping fluids and the movement of the sand grains within the pipe is decoupled. Sediments within the pipe are fluidised, but not elutriated from the system; however fluid does escape from the system (Fig 4.12F). In this case fluid is expelled onto the palaeosurface, but there is no bulk transport of sediment out of the liquefied source unit or the associated pipe. Pressure dissipation continues and the system “freezes” without the formation of a collapse structure and thus a *dewatering pipe* results.

Should the pressure within the fluid reservoir, represented by the liquefied source unit, be great enough to sustain fluid velocities within the pipe greater than the settling velocity of the sand grains within the pipe then grains will be transported out of the source unit, through the pipe and extruded on to the palaeosurface. Bulk transport of sediment out of the source unit results in depletion in the volume of the source unit and the undermining of the overburden around the pipe. This results in the

collapse of the overlying units into the source unit and the formation of an *evacuation pipe* (Fig 4.12H).

As pressure drops within the liquefied source unit fluid flow will wane and eventually cease. Fluid loss may result in a bulk reduction in pipe fill volume. Where the surrounding host rocks were weak, the pipe walls collapsed in to the pipe forming a halo of extensional faults around the pipe rendering the margins of the pipe with an irregular or step-like geometry.

4.10 IMPLICATIONS OF PIPE FORMATION

Sandstone pipes are found within Middle Jurassic across SE Utah. They are likely to have formed during seismically triggered, fluid escape event across the region at this time. Previous authors have suggested a potential link between seismicity and pipe formation (e.g. Hannum, 1980; Netoff 2002), but the severity and widespread nature of the pipe formation event(s) has not previously been recognised. The scale of this event adds considerably to our understanding of the hydrodynamic and tectonic history of the basin. Pipe formation is considered here to represent the response of the sedimentary column to a basin tectonic event, namely a major change in stress direction resulting in a redistribution of strain on basement faults and widespread fault reactivation and seismicity. Thus by linking pipe formation to this event we constrain the timing of regional stress reorientation to the Middle Jurassic.

In general the sandstone pipes examined during this study have a coarser grain-size and increased porosity relative to the surrounding sandstone host rocks. They also

cross-cut siltstone/mudstone interbeds that may have acted as permeability baffles to vertical fluid flow. The enhanced vertical permeability and connectivity that results, enables sandstone pipes to act as pathways for fluid flow long after their emplacement. A good example of this characteristic can be observed where sandstone pipes cross-cut very fine-grained sediments within the Carmel Formation within the Kodachrome Basin. Evidence of pipes acting as fluid conduits comes from the identification of multiple phases of carbonate cements within pipes and increased cementation of pipe margins. This implies that fluids with differing chemistries and therefore differing sources migrated through the pipes and were able to react with host rock pore fluids resulting in increased cementation near pipe margins. Bleaching of host rocks in close proximity to pipe walls also implies that hydrocarbons or mineralising fluids enriched in elements such as uranium may have migrated through the pipes.

Similar pipe-like structures have been identified beneath sea-floor collapse structures (Davies, 2003) and pockmarks (Hovland and Judd, 1988; Løseth *et al.*, 2001; Bünz *et al.*, 2003) in hydrocarbon prone basins using commercial seismic data. It is also possible that sandstone pipes may act as feeder systems for large-scale conical sandstone intrusions such as those seen in the in the North Sea and Faroes-Shetland Basin (e.g. Chapters 3 and 4; Molyneux *et al.*, 2002; Huuse and Mickleson, 2004). Unlike the Middle Jurassic sediments of Utah, fine-grained sediments dominate both the systems described above. However, the conditions that control the formation of large-scale sandstone intrusions are often poorly constrained and further study of these field analogues may provide important information about large-scale fluid escape events and as such could be of considerable interest to the hydrocarbons

industry and to palaeoclimatology if hydrocarbons such as methane are allowed to escape into the atmosphere during fluid escape.

4.11 CONCLUSIONS

Sandstone pipes are found across a region in excess of 20,000 km² in the SE Utah. They are found in the sand-dominated, high net to gross rocks of the upper members of the Carmel Formation and the Gunsight Butte member of the Entrada Sandstone. They formed in response to earthquakes triggered by a sudden change in the tectonic regime during the Middle Jurassic at a time coincident with the top of the Gunsight Butte Member of the Entrada Sandstone. Increased southeasterly shortening and uplift of the west of the region possibly due to relaxation of dynamic subsidence during the Middle Jurassic may have resulted in a bulk redistribution of strain on long-lived basement faults causing an episode of widespread high-magnitude seismicity across the region.

Sands buried to considerable depth were locally remobilised in response to earthquake shaking. Fluid escape from liquefied source sands caused localised fluidisation and pipes formation in overlying host rocks that may have expelled fluids and sediment onto the palaeosurface. Two distinct forms of sandstone pipe have been identified: *Evacuation pipes* where there was bulk transport of material out of the parent unit forming a depleted zone within the parent unit into which overlying sediments collapsed. *Dewatering pipes* where little or no bulk sediment transport out of the parent unit occurred, a depleted zone did not form in the source unit, and there was no collapse of overlying material.

The cylindrical geometry of these sandstone intrusions is important because it is in direct contrast to the more commonly recognised tabular sandstone intrusions, which are found within cohesive fine-grained host rocks rather than sandy host rocks.

Sandstone pipes may cross-cut permeability baffles in reservoir sands enhancing vertical permeability and connectivity.

CHAPTER 5 – SOME CONSIDERATIONS ON THE FORMATION OF LARGE-SCALE SANDSTONE PIPES, SE UTAH

Submitted as:

Shoulders, S., Netoff, D., DiFelice, R., Huuse, M., and Cartwright, J., 2005, Some considerations on the formation of large-scale sandstone pipes, SE Utah, *Journal of Sedimentary Research*, In Review.

Co-author role:

Dennis Netoff kindly provided grain-size analyses of sandstone pipes in the Lake Powell Region. Renzo DiFelice provided technical support in the form of detailed discussion of the application of the pseudo-fluid model to sandstone pipes and confirmation that the formulae and principles applied were applicable to sandstone pipes. Mads Huuse undertook fieldwork with me in SE Utah in November 2003 and along with Joe Cartwright provided discussion of the topics presented in this chapter and support during its writing.

5.1 ABSTRACT

Sandstone pipes are commonly believed to form through the remobilisation of a sandy source unit and fluid escape through the overlying material. We utilize a novel method to evaluate the emplacement of fluidisation pipes in terms of fluid velocity and flow regime. This study uses grain-size and compositional data from a widespread region of sandstone pipes hosted within the Middle Jurassic Entrada Sandstone of SE Utah to explore the genesis of sandstone pipes in the Lake Powell region. Our results indicate that the average fluid velocity during pipe emplacement was 1.6 cms^{-1} (with calculated values from individual pipes ranging from 0.8 cms^{-1} to 2.1 cms^{-1}). These results rely on the basic assumption that the source of the material for the sandstone pipe has similar grain size and compositional characteristics to the surrounding host sandstones at the time of pipe formation and that sorting during pipe formation caused any variation seen at the present day. Knowing the fluid velocity

present during pipe formation enables the fluid flux during pipe formation and the duration of the pipe formation event to be estimated. Our calculations suggest that the volume of fluid expelled during the Middle Jurassic pipe formation event in SE Utah is comparable to, or may even exceed the volumes of water released at the surface during modern magnitude 7-7.5 earthquakes.

5.2 INTRODUCTION

Cylindrical sandstone intrusions, or sandstone pipes, have long been recognised in the geological record (e.g. Hawley and Hart, 1934; Bailey and Newman, 1978; Deynoux *et al.*, 1990; Mount, 1993; Netoff and Shroba, 2001; Netoff, 2002; Davies, 2003).

They usually consist of a vertical, roughly cylindrical mass of homogeneous sand (and sometimes breccia) set within a sandy host rock (e.g. Chapter 4; Netoff, 2002).

Sandstone pipes observed at outcrop in SE Utah may be up to 75 m in diameter (Netoff, 2002) and may cross cut up to 170 m of strata (Section 4.8). Pipe formation has been attributed to a range of different processes related to rapid vertical fluid escape including: artesian ground water flow (Guhman and Pederson, 1992); impact induced liquefaction and fluidisation (Alvarez *et al.*, 1998) and seismically induced liquefaction and fluidisation (Section 4.9.5; Hannum, 1980; Netoff, 2002; Huuse *et al.*, 2005).

The presence of sandstone pipes within a basin may represent (one or more) catastrophic vertical fluid escape event(s) and they may act as conduits for enhanced cross-stratal fluid migration long after the original emplacement event. Therefore understanding the processes involved in the formation of sandstone pipes may

improve our understanding of the hydrodynamic history of the host basin. The processes, conditions and fluid flow regime present during the emplacement of large-scale sandstone pipes are still poorly understood (Netoff, 2002; Huuse *et al.*, 2005). This paper uses field observations derived from a widespread region of large-scale sandstone pipes in SE Utah (Chapter 4; Hannum, 1980; Netoff, 2002; Anderson *et al.*, 2003; Baer and Steed, 2003; Huuse *et al.*, 2005) (Fig 5.1) and grain-size data from sandstone pipes west of Lake Powell (Netoff and Shroba, 2001) to estimate the fluid flow regime present during pipe formation within SE Utah.

5.3 GEOLOGICAL SETTING

5.3.1 Stratigraphic setting

In SE Utah, sandstone pipes are found within the sand-dominated rocks of the Middle Jurassic San Rafael Group (Fig 5.2). The San Rafael Group is bounded by two major regional unconformities. The basal J-2 unconformity separates the San Rafael Group from the underlying Glen Canyon Group and older rocks (Pipringos and O'Sullivan, 1978). The J-3 forms the upper boundary of the San Rafael Group and represents a partial marine transgression, which separates the San Rafael Group from the predominantly fluvial deposits of the overlying Upper Jurassic Romana Sandstone and Summerville Formation (Pipringos and O'Sullivan, 1978).

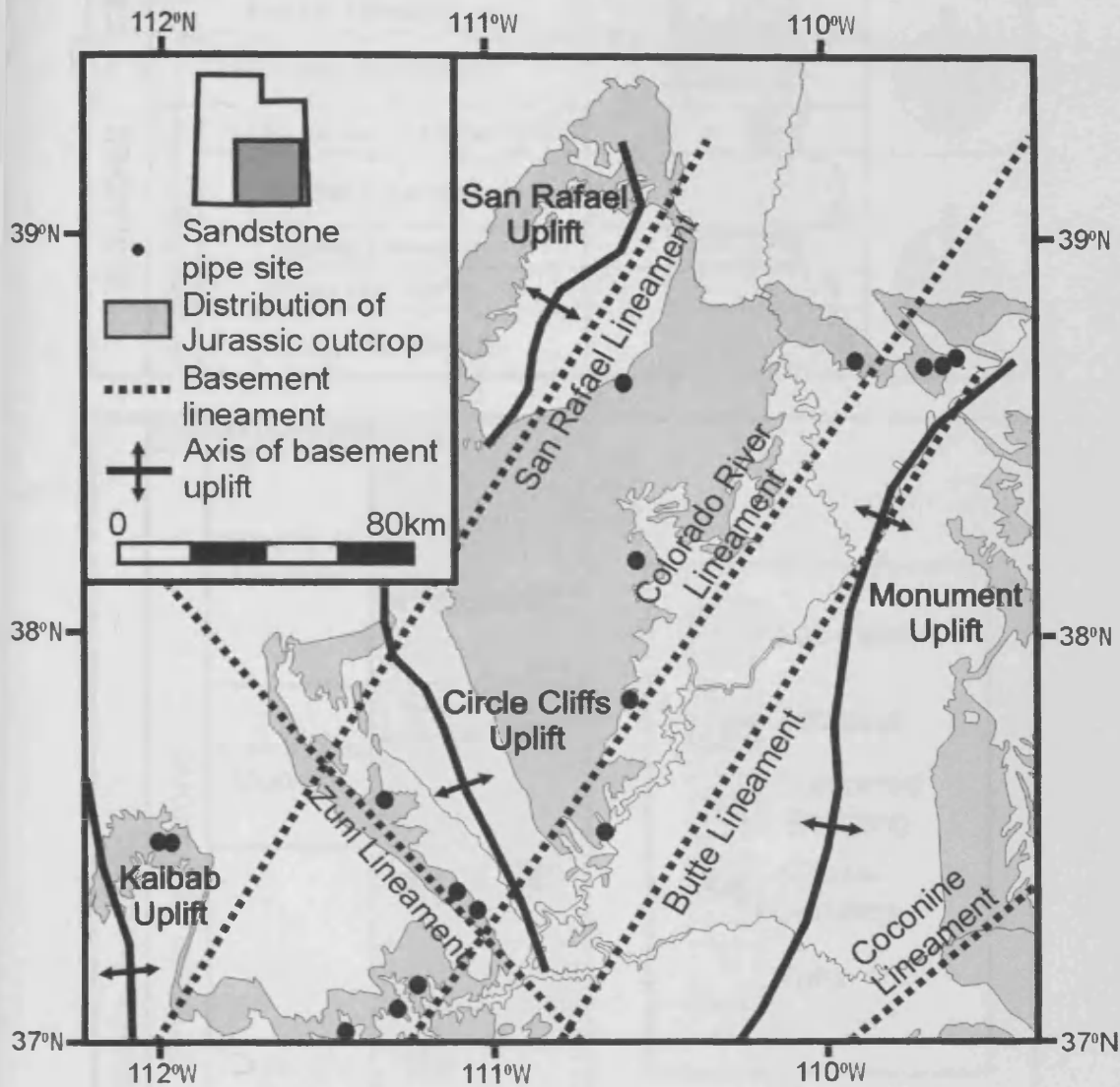


Fig 5.1 Distribution of Jurassic rock outcrop and sandstone pipes (shown as black dots) in SE Utah (compiled from: Hannum, 1980; Hintze, 1988; Alvarez *et al.*, 1999; Netoff and Shroba, 2001; Netoff 2002). Most of the sandstone pipes appear to be situated within a few 10's km of underlying basement structures (distribution of basement structures after Blakey, 1988).

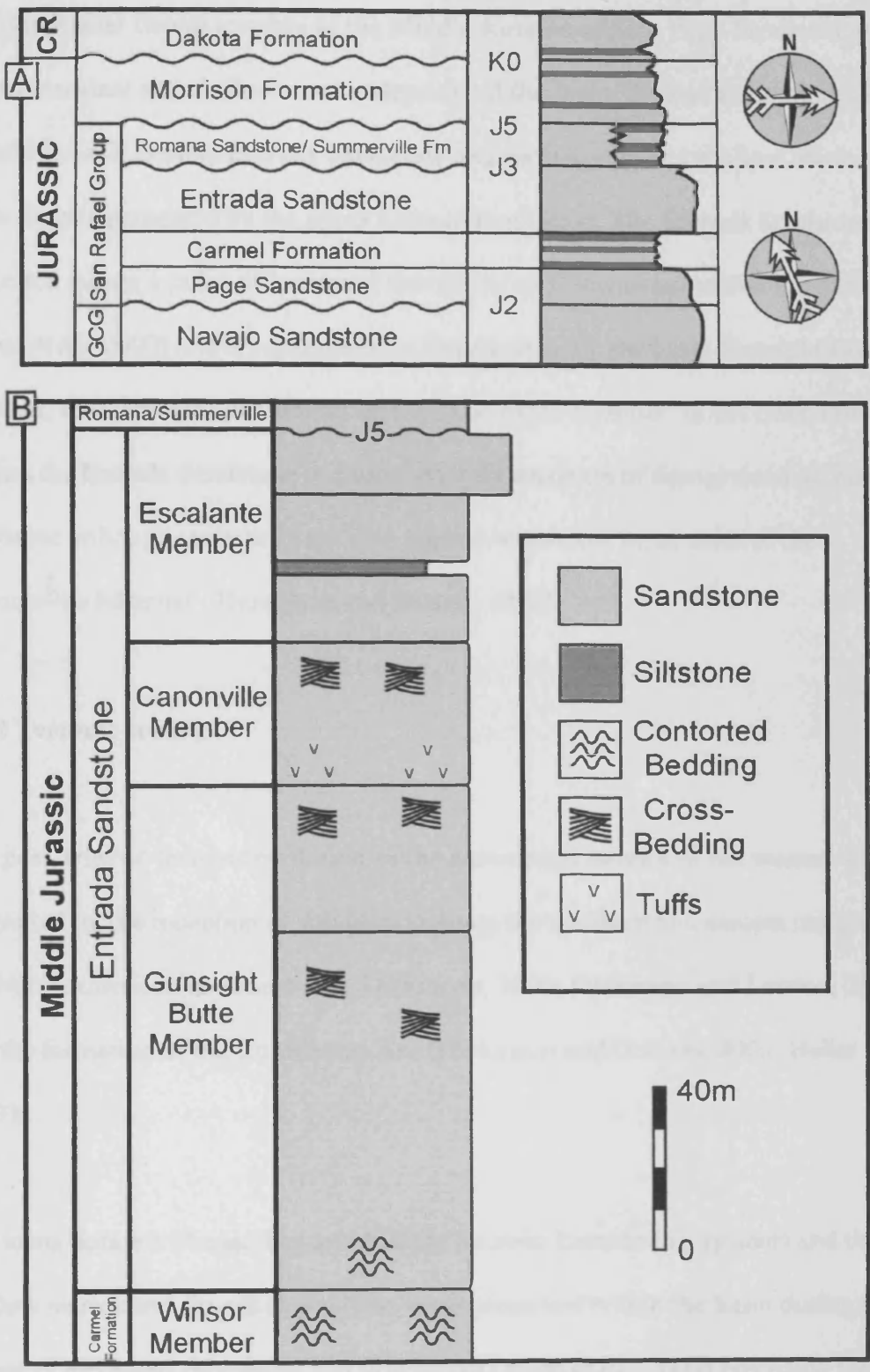


Fig 5.2 A) Generalised stratigraphic section through the Jurassic and Lower Cretaceous rocks of the Lake Powell region (after Anderson *et al.*, 2003) showing a marked change in drainage direction across the J3 unconformity (Bjerrum and Dorsey, 1995; Dickinson and Gehrels, 2003). B) Detailed stratigraphic log through the Entrada Sandstone in the Lake Powell region (Thompson and Stokes, 1970; Doelling and Davis, 1980). Note that there are no pipes present above the base of the Cannonville Member of the Entrada Sandstone.

The San Rafael Group consists of the Middle Jurassic aeolian Page Sandstone the coeval marginal and shallow marine deposits of the lower Carmel Formation, the Middle Jurassic aeolian Entrada Sandstone and its marginal and shallow marine equivalents represented by the upper Carmel Formation. The Entrada Sandstone was deposited during a pulse of increased shortening and downwarp within the basin (Allen *et al.*, 2000) and is separated into three members: the basal Gunsight Butte Member, the Cannonville Member and the Escalante Member. In the Lake Powell Region the Entrada Sandstone is almost entirely made up of fine-grained aeolian sandstone although some tuffs are also present within the basal units of the Cannonville Member (Thompson and Stokes, 1970).

5.3.2 Tectonic setting

The post-Triassic tectonic evolution of the continental interior of the western USA is controlled by the inception of subduction along the southern and eastern margins of the North American continent (e.g. Dickinson, 2000; Dickinson and Lawton, 2001) and the formation of the Cordilleran Arc (Dickinson and Gehrels, 2003; Heller *et al.*, 2003).

The lower Jurassic Navajo Erg and Middle Jurassic Entrada Erg systems and their shallow marine and fluvial equivalents were preserved within the basin during two phases of increased shortening and downwarp (Allen *et al.*, 2000) preceding the inception of major NW-SE orientated shortening during the Early Cretaceous, which had a major effect on the tectonics of the Colorado Plateau. It resulted in the easterly migration of the Cordilleran foreland system and Sevier Thrust Belt; and

transpressional inversion of Ancestral Rocky Mountain basement faults causing uplift and strike-slip movement of basement arches throughout the western USA between the Campanian and Late Palaeocene (Cather, 1999; Tindall and Davis, 1999; Marshak *et al.*, 2000; Bump, 2004)

Uplift of the Cordilleran Arc to the west of the study area occurred long before the propagation of the Sevier thrust Belt into central Utah. There is a marked change from northerly fluvial drainage within the Middle Jurassic Page and Entrada Sandstones (Dickinson and Gehrels, 2003) to easterly drainage within the Upper Jurassic Romana and Summerville Formations (Bjerrum and Dorsey, 1995) representing eastwards tilting of the region (Fig 5.2A). This uplift may represent the relaxation of long wavelength dynamic subsidence formed through viscous mantle corner flow coupled to the subducting Falleron Slab (Heller *et al.*, 2003)

5.3.3 Distribution of cylindrical sandstone pipes in SE Utah

Sandstone pipes crop out in a northeast-southwest orientated swath through southeastern Utah covering in excess of 20,000 km² of the Colorado Plateau.

Sandstone pipes are found in only a small portion of the succession observed in the region. In particular they are restricted to the upper members of the Carmel Formation and the Gunsight Butte Member of the Entrada Sandstone (Chapter 4; Hannum, 1980; Alvarez *et al.*, 1998; Netoff, 2002; Anderson *et al.*, 2003; Baer and Steed, 2003; Huuse *et al.*, 2005). Several long-lived fault-cored, asymmetrical basement arches, in particular the Monument Bench Uplift, the San Rafael Swell, Circle Cliffs Uplift and the Kaibab Uplift, control the present day outcrop distribution. A number of

prominent long-lived tectonic lineaments also run through southeastern Utah (Blakey, 1988) (Fig 5.1). The cylindrical sandstone pipes commonly appear within a few 10's km of the basement lineaments and their mapped distribution appears to mirror the distribution of these long-lived basement structures.

5.4 PHYSICAL DESCRIPTION OF CYLINDRICAL SANDSTONE PIPES IN SE UTAH

The sandstone pipes observed in SE Utah generally have a cylindrical geometry. However, individual intrusions may show varied geometries and taper upwards, or display a slightly sinuous geometry. All the sandstone pipes observed are roughly circular or elliptical cross-sections and with straight, near-parallel walls. Pipe diameters range from 1 to 75 metres (e.g. Netoff, 2002) and individual pipes may cross-cut considerable thicknesses of host strata (up to 170 m, Section 4.8). The contacts between the host rock and the pipe fill are always sharp and well defined (Fig 5.3).

Many of the sandstone pipes in SE Utah are surrounded by zones of brittle deformation within the encapsulating host rocks. This brittle deformation takes two main forms: small-scale extensional deformation (Fig 5.3B and C) and large-scale collapse structures (Fig 5.4). Small-scale deformation usually forms of a halo up to 3 m wide of high-intensity extensional faulting. Maximum throws are up to 40 cm, but most faults only have throws of a few centimetres. The incursion of fault blocks into the pipe fill lends the pipe margin a ragged step-like geometry.

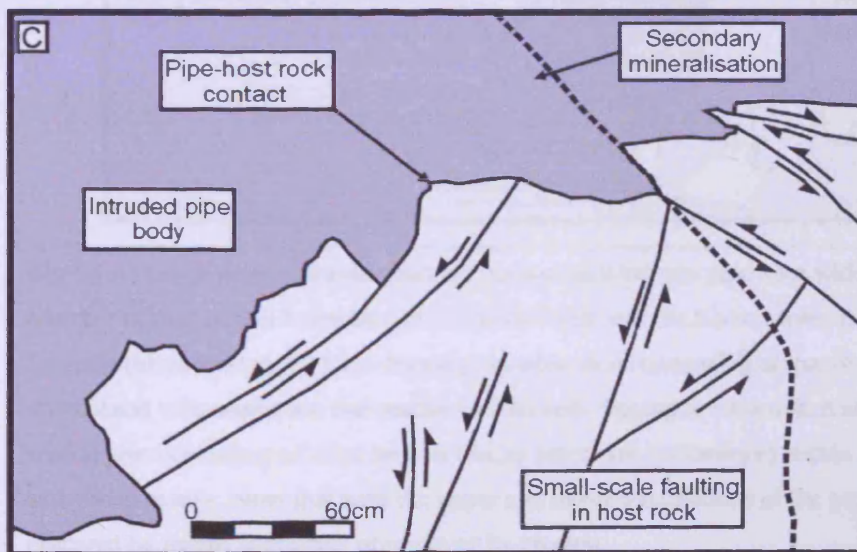
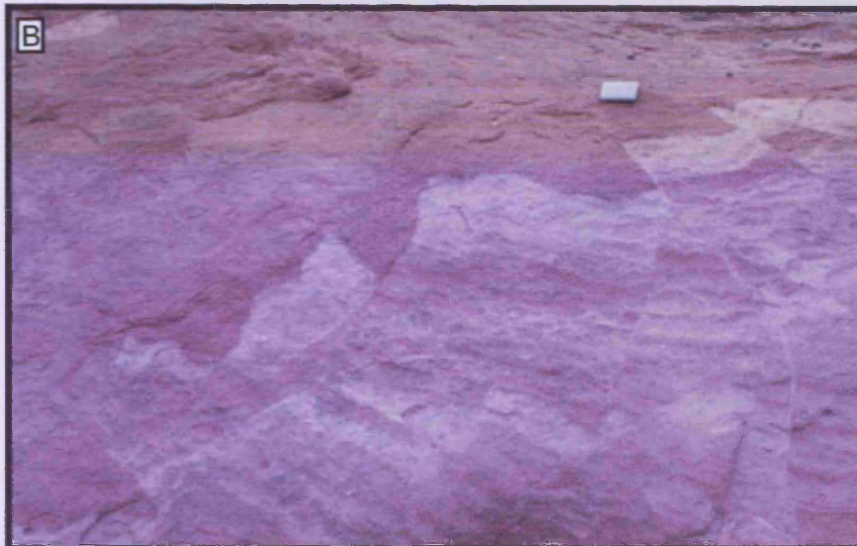
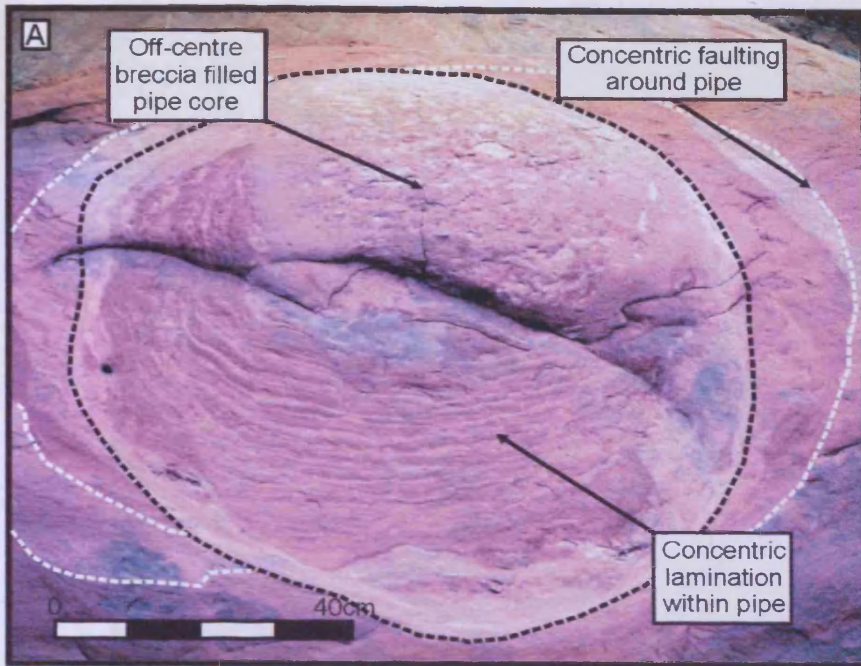


Fig 5.3 A) Slick-rock section through a sandstone pipe from the Hanksville Pipe Swarm showing complex internal structure of pipe-fill, the presence of breccia blocks within the pipe and concentric faulting around the pipe margins. B) Small-scale faulting around a sandstone pipe within the Gunsight Butte Member of the Entrada Sandstone at Bullfrog, Lake Powell (notebook for scale). C) Movement along small-scale faults with throws of up to 40cm lends the pipe margin a ragged, stepped geometry.

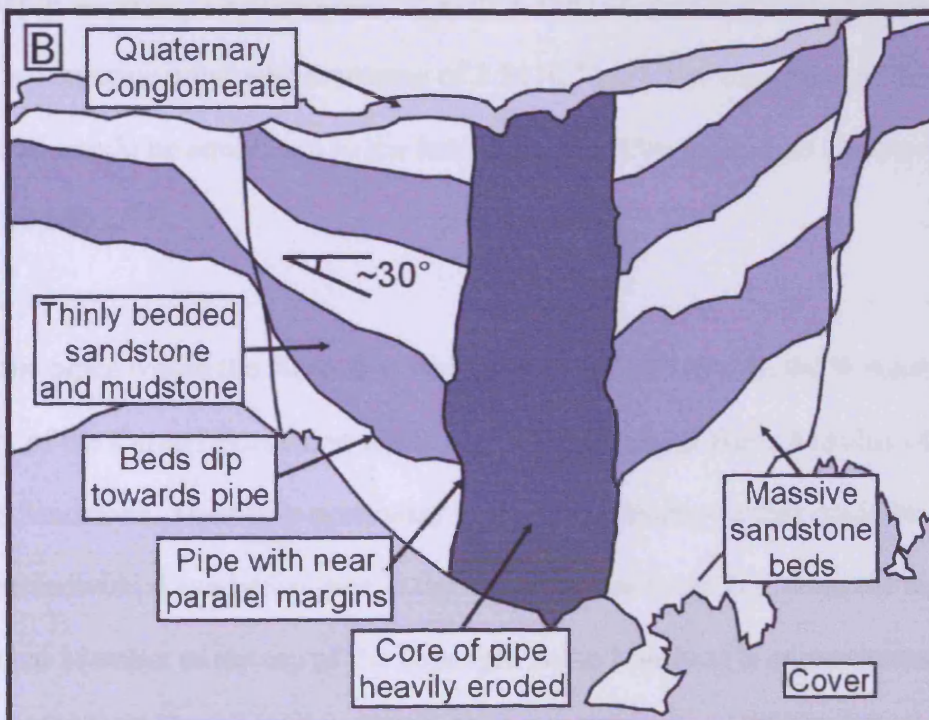


Fig 5.4 A) Large-scale collapse structure centred on a breccia pipe 15m wide within the Winsor Member of the Carmel Formation at Shepards Point near the Kodachrome Basin State Park. Person for scale (black arrow). B) Line-drawing showing strata consisting of massive sandstone intercalated with sandstone and mudstone interbeds dipping downwards at around 30° towards a central pipe consisting of large breccia blocks (up to 1m in diameter) within a homogeneous sand and gravel matrix. Note that both the upper and lower terminations of the pipe have either been obscured by recent sediments or removed by erosion.

Large-scale collapse structures consist of a zone of faulted host rock strata that are tilted downwards towards a (central) cylindrical intrusion. The margins of the collapse structures are well defined by concentric faults. One of the largest observed examples of a sandstone pipe surrounded by a collapse structure can be observed in a cliff section at Shepard's Point, just outside the Kodachrome Basin State Park (Fig 5.4). In this example, a collapse structure 150m in diameter containing host units dipping at around 30° surrounds a sandstone pipe approximately 15 m in diameter (Section 4.5.21). Collapse of host strata strongly implies that volume reduction must have occurred at depth. The volume of the collapse structure is therefore likely to be equivalent to the volume of material expelled from the source unit. In this example, if the collapse structure is assumed to be circular, the collapse structure forms a downward tapering cone with a volume of $2.5 \times 10^{-4} \text{ km}^3$. The expulsion of this volume of material would be equivalent to the formation of a 25m thick sand blow over an area of 10,000 m^2 .

Sandstone pipes within the Kodachrome Basin are found between the Winsor Member of the Carmel Formation to the top of the Gunsight Butte Member of the Entrada Sandstone. Therefore maximum stratigraphic thickness that could be cross-cut by an individual sandstone pipe in the Kodachrome Basin (i.e. from the base of the Winsor Member to the top of the Gunsight Butte Member) is approximately 170 m (Thompson and Stokes, 1970). However, it should be noted that the terminations of pipes have not been observed in this region. If the sandstone pipe at Shepards Point is assumed to have a cylindrical geometry of constant radius and is assumed for the purpose of this calculation to have a vertical extent of 170 m, the maximum volume of the sandstone pipe associated with the Shepard's Point collapse structure is 3.0×10^{-5}

km³. Thus a considerable volume of material (i.e. nearly 10 times the volume of the pipe itself) is likely to have been transported through the pipe to be expelled at the surface and the pipe should be considered as a sandstone intrusion. However, in examples of sandstone pipe where the collapse structure has a small diameter, or is absent as is commonly seen in the Lake Powell region (Section 4.5.22; Netoff, 2002), it is likely that the volume of material expelled at the surface is considerably less than the total volume of the sandstone pipe (i.e. fluid has passed through the pipe but there has not been bulk transport of solid material through the pipe). If there has been no bulk transport, these pipes cannot be considered as intrusions (*sensu stricto*) and therefore the solid material within such pipes must primarily be derived from the surrounding host rocks rather than an underlying source unit.

Pipe fill generally consists of a varying component of breccia blocks in a fine sand matrix (occasionally with a gravel component). Breccia blocks may be up to 1 m in length and are composed of aeolian cross-bedded sandstone and mudstone with very similar lithologies to the surrounding host rock or underlying units (Hannum, 1980; Netoff, 2002).

5.4.1 Grain size and compositional variation

Two studies have been carried out comparing the grain-size distributions in sandstone samples taken from both the sandy pipe fill matrix and the surrounding host rock (Hannum, 1980; Netoff and Shroba, 2001). In the Kodachrome Basin, sandstone pipes are hosted within the Winsor Member of the Carmel Formation and the Gunsight Butte Member of the Entrada Sandstone (Section 5.5.21; Hannum, 1980; Baer and

Steed, 2003). The Winsor Member of the Carmel Formation consists dominantly of fine-grained sands with minor medium-grained sand, silt and clay whilst the Gunsight Butte Member consists of sands, sandy silts and clays (Hannum, 1980). Grain-size distributions presented from pipe fill matrix all contain an increased coarse fraction (medium-grained sand to gravel sized) and a depleted fine-grained fraction (fine-grained sand to clay sized) relative to the surrounding host rocks (Hannum, 1980). Gravel sized clasts observed within pipes in the Kodachrome Basin are commonly made up of lithic clasts of similar lithology to the surrounding host rocks.

In the Lake Powell region sandstone pipes are only found in the Gunsight Butte Member of the Entrada Sandstone (Section 4.5.22; Netoff and Shroba, 2001; Anderson *et al.*, 2003). A study using 69-paired samples of cross-bedded host rock and pipe fill matrix taken from surface or near surface cores (0-10 cm depth) within the Gunsight Butte Member of the Entrada Sandstone in the Lake Powell region found that grain size and initial pore volume (before cementation and compaction) were both higher in the pipe matrix than in the host rock (Netoff and Shroba, 2001). Average grain size is 111 μm in the host sandstones and 151 μm in the pipe fill matrix. Similarly, the average initial porosity of the host rocks is 34.1% (actual values ranging from 26.2 to 41.3%), whereas the initial porosity of the pipe matrix was 36.9% (actual values ranging from 30.9% to 42.7%) (Netoff and Shroba 2001). However, the clay content, and feldspar content are lower in the pipe fill than the surrounding host rocks.

The observation that there is an increase in the coarse grain-size fraction, and depletion in the fine-grained fraction in between pipe fill and host rock was made in

both previous studies (Hannum, 1980; Netoff and Shroba, 2001). A distinct change in composition between pipe fill and host rock has also been identified (Netoff and Shroba, 2001). Assuming that there is little vertical variation within the host sequence (e.g. Thompson and Stokes, 1970; Doelling and Davis, 1989) these differences may be attributed to the transport process involved in pipe formation. However, systematic sampling across a pipe, or vertically down its exposed length has not yet been carried out. It is not possible to test whether the process of pipe formation causes segregation by grain size or composition unless the pipe source unit, is compared to the pipe fill. Unfortunately the source bed for a particular sandstone pipe has yet to be confidently identified (Chapter 4; Hannum, 1980; Netoff, 2002; Huuse *et al.*, 2005) and a proxy for the source unit composition must therefore be sought.

Three main lines of evidence suggest that the bulk composition of the Gunsight Butte Member of the Entrada Sandstone is a good proxy for the source unit of the sandstone pipes in the Lake Powell region: 1) Large collapse structures which imply that considerable volumes of material derived from a deep source unit passed through the sandstone pipe during its formation, are not present in the Lake Powell region.

Therefore it is likely that the greater majority of material within the pipes was derived from the host rocks surrounding the pipes rather than from a deep source unit. 2) Very few examples of pipes containing material derived from the Carmel Formation are seen within the Gunsight Butte Member of the Entrada Sandstone in the Lake Powell region (Chapter 4) Therefore it appears unlikely that the sandstone pipes in the Lake Powell region contain material derived from the Carmel Formation or from deeper in the succession. 3) In the Lake Powell Region, the Gunsight Butte Member of the Entrada Sandstone shows very little vertical lithological variation (e.g. Thompson and

Stokes, 1970; Doeling and Davis, 1990) and there are striking lithological similarities between pipe fill and host rocks (Chapter 4; Netoff and Shroba, 2001; Huuse *et al.*, 2005).

A subset of the data collected around Lake Powel (Netoff and Shroba, 2001) consisting of 39 samples of host rock and pipe fill matrix and 11-paired samples of host rock and pipe fill matrix from individual pipes were examined during this study. Grain size analysis was carried out by the USGS and point counting and compositional analysis was carried out by Denis Netoff at Sam Houston State University. Analysis of the data examined showed that the average grain-size in the host sandstones is 114 μm (with values from individual samples ranging from 82 μm to 139 μm) and 148 μm (with values from individual samples ranging from 100 μm to 174 μm) within the pipe fill matrix (Fig 5.5). The initial pipe-fill matrix porosity was derived through point counting from the ratio of the sum of present day void space, clay coatings, interstitial clay and carbonate cement to total point counts. It was found that the initial porosity of the pipe fill matrix is considerably greater than that of the host rock (Fig 5.6). The grain size of each host rock sample had a smaller average grain-size than the pipe fill matrix sample to which it is paired. There are marked compositional variations between the pipe fill matrix and the surrounding host rocks derived through point counting (Fig 5.6): The pipe fill matrix is depleted in polycrystalline quartz, orthoclase, plagioclase and oxide minerals relative to the host rocks, but is considerably enriched in monocrystalline quartz. Feldspars observed in thin section were heavily weathered and altered to clay minerals.

5.4.2 Transport direction

It is impossible to discern the fluid and sediment transport direction in many of the sandstone pipes in SE Utah. Most of the breccia blocks present within the pipes consist of material that is lithologically very similar to the surrounding host rocks. However, three lines of evidence suggest that both fluids and granular material were transported upwards through the sandstone pipes: 1) collapse structures imply that material was removed from below the stratigraphical level of the pipe exposure and expelled upwards (See section 4.9.1) 2) characteristic breccia blocks present in Chimney Rock, a pipe in the Kodachrome Basin State Park, can be traced to a depositional unit deeper within the section (Section 4.5.21); 3) pipes containing material derived from the Carmel Formation can be found within the basal units of the overlying Gunsight Butte Member of the Entrada Sandstone in the Hanksville Pipe Swarm (Section 4.5.22).

5.5 GENESIS OF CYLINDRICAL SANDSTONE PIPES

The sandstone pipes of SE Utah are believed to have formed in response to earthquake shaking during the Middle Jurassic (e.g. Section 4.9.53; Hannum, 1980; Netoff, 2002; Huuse *et al.*, 2005). This argument is based partly on the spatial relationship between sandstone pipes and long-lived basement structures in SE Utah (Fig 5.1), the close temporal link between Middle Jurassic pipe emplacement and the inception of major regional uplift to the west (Section 4.5.93) and increased shortening and downwarp of the Utah Idaho trough (Allen *et al.*, 2000). Where local conditions were suitable, earthquakes are believed to have caused the

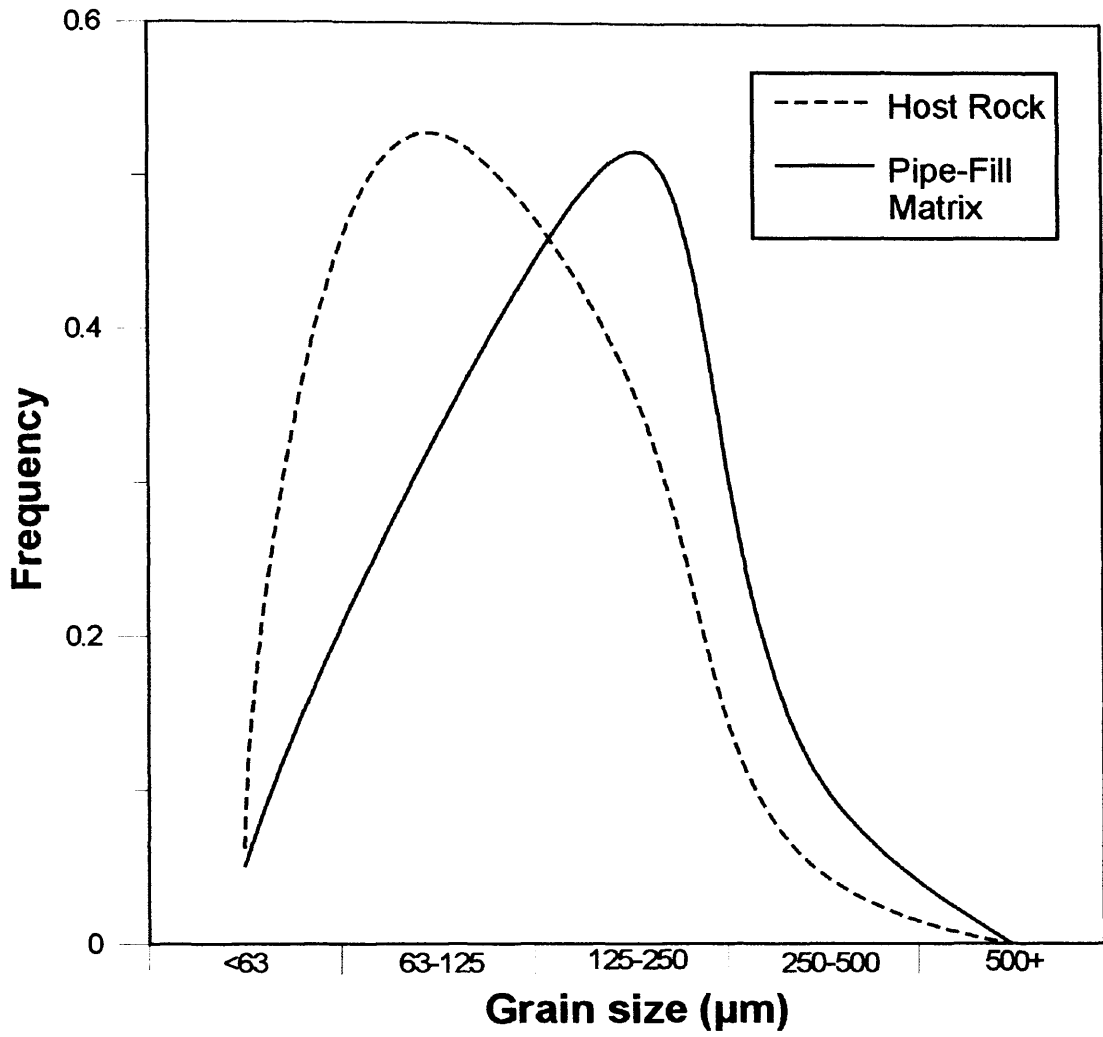


Fig 5.5 Average grain-size distributions from both sandstone pipe-fill matrix (solid black line) and the surrounding host rocks (dashed line) represented by the Gunsight Butte Member of the Entrada Sandstone. Diameter of clasts derived by particle size analysis of 39 samples (i.e. sieving of disaggregated samples).

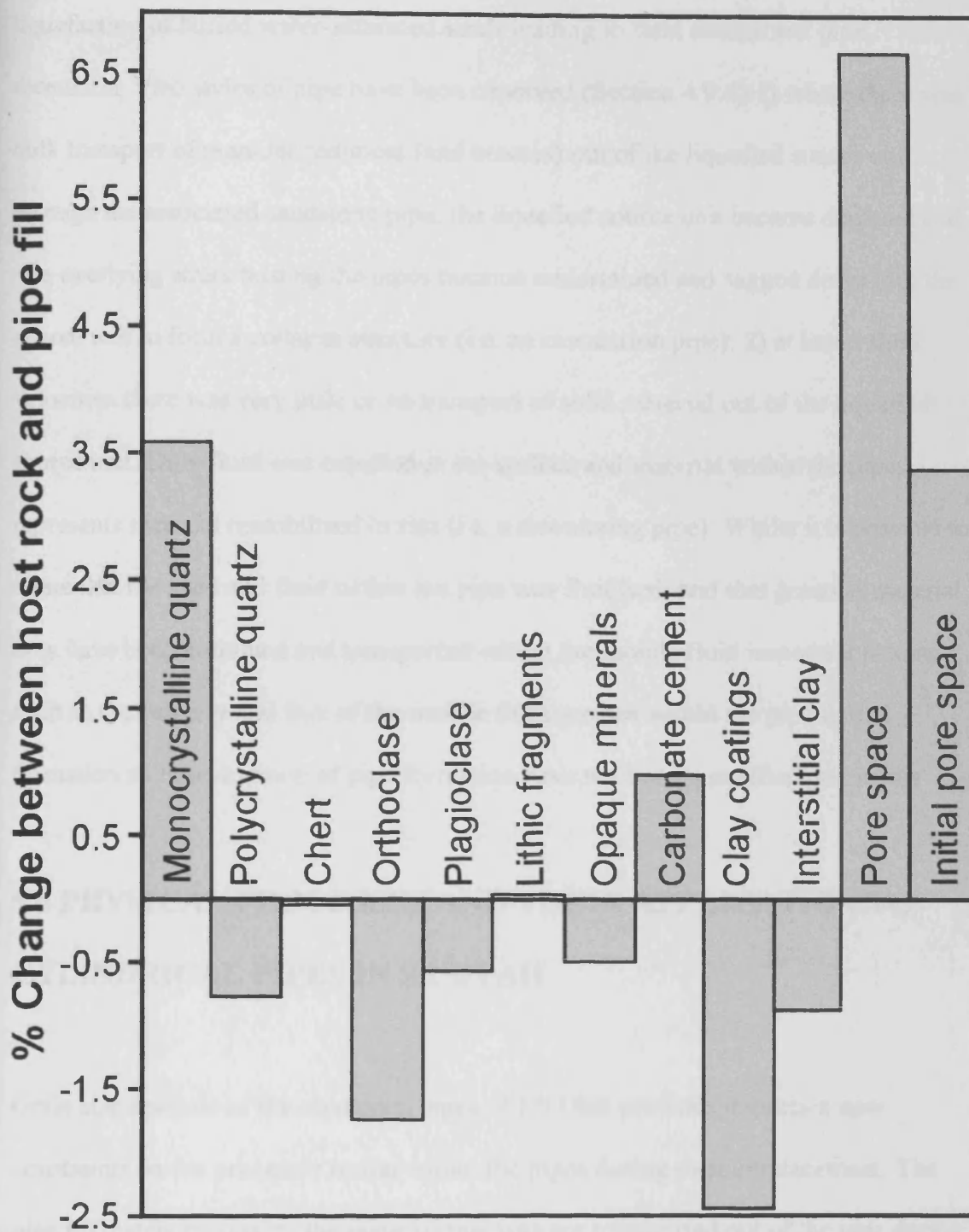


Fig 5.6 Compositional changes between in pipe-fill matrix relative to host rock based on 11-paired samples. The amount of relative change was assessed by subtracting host rock values from pipe fill matrix values. Clast mineralogy, carbonate cement, clay coatings, interstitial clay and void space were determined petrographically by point counting (minimum of 500 counts per sample). Void space (porosity) determined by the ratio of voids to total point counts. Initial void space (initial porosity) determined by the ratio of void space + clay coatings + interstitial clay + carbonate cement to total point counts.

liquefaction of buried water-saturated sands leading to fluid escape and pipe formation. Two styles of pipe have been observed (Section 4.9.4): 1) where there was bulk transport of granular sediment (and breccia) out of the liquefied source unit through the associated sandstone pipe, the liquefied source unit became depleted and the overlying strata hosting the pipes became undermined and sagged down into the source unit to form a collapse structure (i.e. an evacuation pipe). 2) at lower fluid velocities there was very little or no transport of solid material out of the liquefied source unit. Only fluid was expelled at the surface and material within the pipes represents material remobilised in situ (i.e. a dewatering pipe). Whilst it is possible to argue that the sand and fluid within the pipe was fluidised, and that granular material may have been entrained and transported within the mobile fluid important factors such as the velocity and flux of the mobile fluid present within the pipe during formation and the duration of pipe formation have not been quantified previously.

5.6 PHYSICAL PROCESSES AND THEIR APPLICATION TO CYLINDRICAL PIPES IN SE UTAH

Grain size analysis of the sandstone pipes of SE Utah provides important new constraints on the processes acting within the pipes during their emplacement. The pipe fill matrix represents the material that was not transported out of the pipe during its formation, and as such provides evidence for the maximum fluid velocity within the pipe during its formation. A model assuming that upwards flow of a sand-fluid mixture through a vertical conduit is driven by overpressure at the base of the conduit and opposed by gravity, viscous resistance and turbulent drag has recently been proposed to explain vigorous sand eruptions resulting from drilling into shallow,

highly overpressured aquifers above deep-water oil fields (Gallo and Woods, 2004). Such a model may be analogous to the processes occurring during pipe formation in SE Utah. The model considers that for high fluid velocities (i.e. 10 times the settling velocity of the granular sediment) and small sand fractions (i.e. 80% fluid and 20% granular solids) flow through the conduit will be homogeneous and volume within the conduit will be conserved. At higher sand fractions, or slower fluid velocities flow ceases to be homogeneous and becomes two phase (i.e. motion of fluids and solids becomes decoupled) or does not develop (Gallo and Woods, 2004).

The applicability of such a model to the sandstone pipes of SE Utah may be examined by calculating the fluid velocity within the pipe during its formation. The approach taken here is to derive the settling velocity of the pipe fill matrix from a grain size analysis of the pipe fill. If the upward fluid velocity exceeds the settling velocity of a suspended grain with a given diameter and density, the grain will become entrained within the fluid and transported out of the system (Richardson, 1971; Kunii and Levenspiel, 1991; De Felice, 1995; Eichhubl and Boles, 2000). The pipe fill matrix within the sandstone pipes was not transported out of the pipe and therefore was too large or too dense to be removed. Therefore by calculating the settling velocity of the pipe fill matrix it is possible to constrain the maximum fluid velocity within the sandstone pipes of SE Utah.

5.6.1 Transporting sand-sized grains

Fluid moving upwards through granular sediment exerts a drag force on the particles it passes. The necessary fluid flow velocity required to support a particle against

gravity is equal to its settling velocity (U_t). The settling velocity based upon Stoke's Law is suitable for small clast sizes (Allen, 1985; Kunii and Levenspiel, 1991) and is defined as:

$$U_t = \left\{ \frac{18\mu}{(\rho_s - \rho_f)gd^2} + \left[\frac{\rho_f(2.335 - 1.744\psi)^2}{(\rho_s - \rho_f)gd} \right]^{0.5} \right\}^{-1} \quad (5.1)$$

Where:

- U_t = settling velocity (ms^{-1})
- μ = the viscosity of the fluid (Pas)
- ρ_s = the density of the grain (kgm^{-3})
- ρ_f = the density of the fluid (kgm^{-3})
- g = acceleration due to gravity (9.81 ms^{-2})
- d = grain diameter (m)
- ψ = an dimensionless empirical value describing the shape of the grain (1=Spherical, based on Bear 1972: p. 134)

The density of the material making up the granular sediment (ρ_s) exerts a major control on the settling velocity given grain. The aeolian sandstone of the Gunsight Butte Member consists mostly of highly rounded, frosted quartz grains with minor orthoclase and plagioclase and very small amounts of accessory opaque minerals (likely to be magnetite). Quartz (2630 kgm^{-3}), orthoclase (2680 kgm^{-3}) and plagioclase (2560 kgm^{-3}) all have similar densities and thus the settling velocity of a spherical grain of quartz will be very similar to that of orthoclase or plagioclase (Fig 5.7). Magnetite has a considerably higher density than these minerals (i.e. 5150 kgm^{-3}) and as a result its settling velocity is considerably higher (Fig 5.7). It is therefore likely that for a given grain size, there will be segregation by grain density between

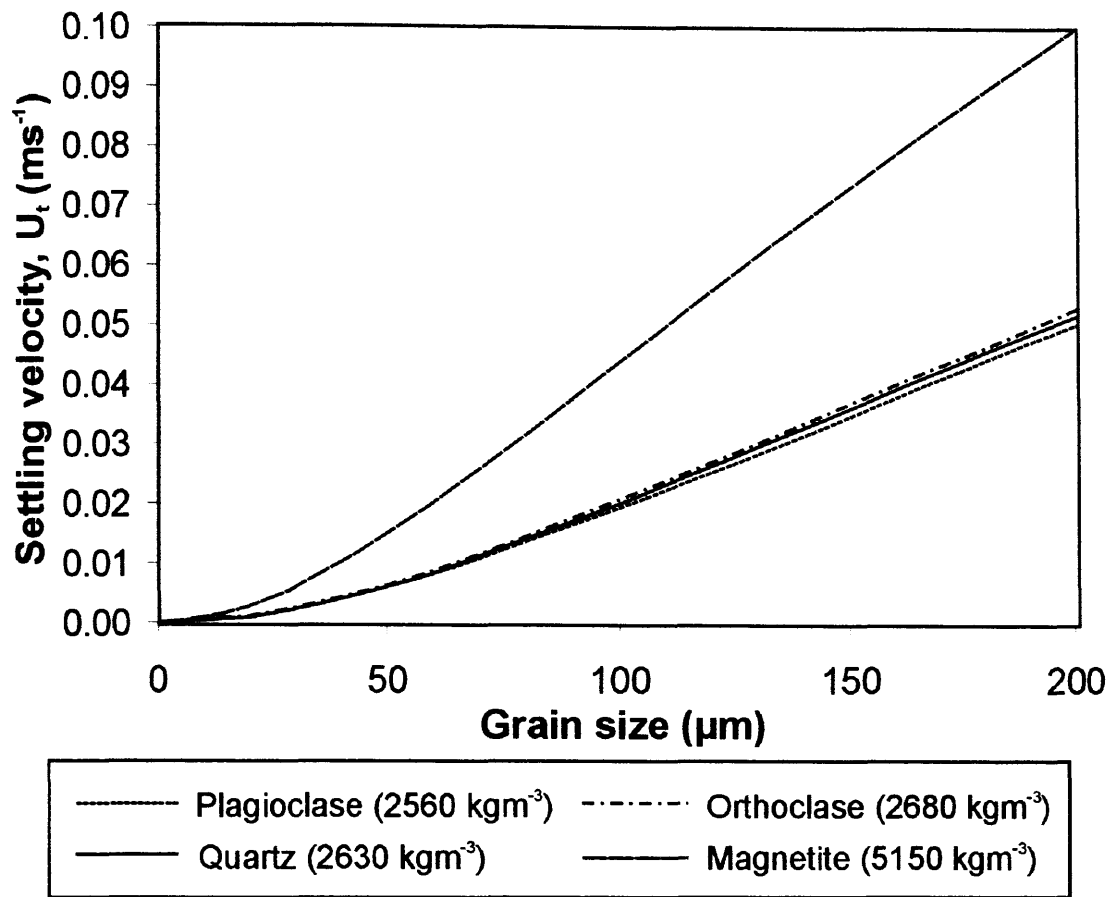


Fig 5.7 The settling velocity of spherical grains of differing composition and density within water (density 1030 kgm^{-3} , viscosity 0.0003 Pas). Grains of similar densities have similar settling velocities for a given grain size (e.g. quartz, orthoclase and plagioclase). Increasing density results in a large increase in the settling velocity for a given grain size. Note that the settling velocity of magnetite is considerably higher than those of quartz or feldspar for a given grain size.

magnetite and non-magnetite grains resulting in compositional variation between the pipe fill matrix and the source unit.

5.6.11 Application of U_c to sandstone pipes in the Lake Powell region

The fluid flow regime within sandstone pipes is likely to be highly complex, however based on the following observations we propose a simple model for sand transport within sandstone pipes: There is an increase in average grain-size of pipe fill matrix relative to host rock in both the Lake Powell region and in the Kodachrome Basin (Hannum, 1980; Netoff and Shroba, 2001). Given that the bulk properties of the Gunsight Butte Member of the Entrada Sandstone represent the source material for the pipe fill matrix, sorting by grain-size within the pipe fill matrix is likely to be a primary effect of the processes acting during pipe formation. Sorting by grain-size may represent the elutriation of fine-grained material during fluidisation leaving a coarser residue (e.g. Richardson, 1971; Kunii and Levenspeil, 1991; DiFelice, 1995; Eichubl and Boles, 2000). We assess the fluid flow regime during pipe formation by making the assumptions that: 1) The relative increase in grain size between the pipe fill matrix and the host rocks represents sorting during steady state flow conditions. 2) Fluid velocity is uniform throughout the vertical extent of the pipe. Thus the settling velocity of the average grain-size of the pipe fill matrix can be used as an estimate of the maximum fluid velocity present within the pipes during their formation. Should the fluid velocity within the pipes have been higher than this value, larger grains would have been elutriated. Therefore the average grain-size of pipe fill matrix would have been forced upwards. It is unlikely that post-emplacement processes would have

altered this grain-size signature unless the whole system suffered another phase of remobilisation.

Two limitations are intrinsic to this approach: 1) it does not take into account any possible change in fluid velocity across the whole vertical extent of the pipe (such as variations in pipe width altering fluid flux and therefore velocity); 2) It is possible that the pipe formation was very short-lived, and therefore the pipe fill matrix is only partially sorted and steady state conditions were not reached. In order to test the extent to which these factors influence grain-size variation in the pipe fill matrix vertical sampling along the whole extent of a sandstone pipe would be required.

The average grain size of the pipe fill matrix in sandstone pipes in the Lake Powell region is 148 μm (with values from individual samples ranging from 100 μm to 174 μm). A spherical grain of quartz (2630 kgm^{-3}) of average grain-size (148 μm) for pipe fill matrix has a settling velocity of 1.6 cms^{-1} in water (density 1000 kgm^{-3} , viscosity 0.001 Pas) (Equation 5.1). The range in grain-sizes displayed by individual samples (100 μm to 174 μm) equates to a range in maximum settling velocities between 0.8 cms^{-1} and 2.1 cms^{-1} . These values constitute an estimate of the maximum fluid velocity during pipe formation. If fluid velocities within the sandstone pipes were greater than 0.8 cms^{-1} and 2.1 cms^{-1} then the average grain size of the pipe fill matrix would be forced upwards as more fine-grained material was elutriated.

Assuming that the bulk properties of the Gunsight Butte Member of the Entrada Sandstone represent the properties of the source unit for the sandstone pipes in the Lake Powell region it is possible to estimate the minimum fluid velocity during pipe

formation. The average grain size of the host rocks surrounding the sandstone pipes is 114 μm (with values from individual samples ranging from 82 μm to 139 μm). In order for the average grain-size of the pipe fill matrix to be greater than this value, elutriation of the fine-grained component must have occurred. This requires fluid velocities in excess of the settling velocity of the average host rock grain size. A spherical grain of quartz (2630 kgm^{-3}) of average grain-size (114 μm) for pipe fill matrix has a settling velocity of 1.0 cms^{-1} in water (density 1000 kgm^{-3} , viscosity 0.001 Pas) (Equation 5.1). The range in grain-sizes displayed by individual samples (82 μm to 139 μm) equates to a range in possible settling velocities between 0.6 cms^{-1} to 1.6 cms^{-1} (Equation 5.1).

5.6.12 Breccia blocks and Pseudo-Fluid behaviour

The addition of a solid granular component to a fluid will significantly alter the basic properties of the bulk fluid (e.g. Van Der Weilen *et al.*, 1996; DiFelice, 1998). The fluid-sand suspension present within a sandstone pipe during its formation can be considered as a multi-component system consisting of a fluid and a component of suspended solids. In order to consider the behaviour of large breccia blocks within sandstone pipes in the Lake Powell region it is necessary to consider the bulk properties of the sand/fluid mixture within the sandstone pipe (e.g. Van Der Weilen *et al.*, 1996; DiFelice, 1998). This approach has previously been used to examine the transport of centimetre-sized breccia blocks in sandstone intrusions (Duranti and Hurst, 2004). If this multi-component system is considered to behave as the equivalent homogeneous fluid (i.e. a *pseudo-fluid*) (Di Felice, 1991; 1998), it is then possible to model the behaviour of large clasts within a sand/fluid suspension. The

pseudo-fluid model performs well in predicting the settling velocity of a large grain (i.e. with a diameter several times greater than the fine grains in the suspension) within a fluid/solid suspension (Van Der Weilen *et al.*, 1996) The addition of granular solids to a fluid will result in differing density (ρ_{pf}) and viscosity (μ_{pf}) when compared to the original solid-free fluid. Density and viscosity can be represented by the following formulae (Di Felice *et al.*, 1991):

Density of pseudo fluid:

$$\rho_{pf} = \rho_f \varepsilon + \rho_s (1 - \varepsilon) \quad (5.2)$$

Where:

- ρ_{pf} = density of pseudo-fluid (kgm^{-3})
- ρ_f = density of the pore fluid (kgm^{-3})
- ρ_s = density of suspended solids (kgm^{-3})
- ε = pseudo-fluid voidage (i.e. proportion by volume of suspension which is not solids)

Viscosity of pseudo fluid:

$$\mu_{pf} = \mu_f [1 + 2.5(1 - \varepsilon) + 10.05(1 - \varepsilon)^2 + 0.0027 \exp[16.6(1 - \varepsilon)]] \quad (5.3)$$

Where:

- μ_{pf} = pseudo-fluid viscosity (pas)
- μ_f = pore fluid viscosity (pas)
- ε = pseudo-fluid voidage (i.e. proportion by volume of suspension which is not solids)

Equation 5.3 is the empirical relation proposed by Thomas (1965) for the effective viscosity of a narrow size distribution suspension and is frequently cited because of its accuracy (Usui *et al.*, 2001).

It is not possible to calculate the terminal flow velocity of large clasts using Stoke's Law (as presented in Equation 5.1). Instead the square root law, which is suitable for grains over a few millimetres in diameter, is applied (Allen, 1985):

$$U_t = k \left(\frac{(\rho_s - \rho_f)}{\rho_f} g d \right)^{1/2} \quad (5.4)$$

Where:

- U_t = settling velocity (ms^{-1})
- ρ_s = the density of the grain (kgm^{-3})
- ρ_f = the density of the fluid (kgm^{-3})
- g = acceleration due to gravity (9.81 ms^{-2})
- d = grain diameter (m)
- $k = \left(\frac{4}{3} C \right)^{1/2}$

The drag coefficient for a solitary sphere in motion (C) is constant at 0.45 over a wide range of Reynolds Numbers (i.e. from 10^3 to 3×10^5) (Allen, 1985).

The maximum concentration of suspended granular material within a fluidised bed is around 54% based on experimental evidence (Leva, 1959). The presence of 54% quartz sand grains (2630 kgm^{-3}) within the sand/fluid suspension imparts a density of 1880 kgm^{-3} (Equation 5.2) and viscosity of 0.026 Pas (Equation 5.3) to the pseudo-fluid. Lower concentrations of solid granular material within the sand/fluid suspension will result in correspondingly lower pseudo-fluid density and viscosity (Fig 5.8). Examining the settling velocity of breccia blocks within a pseudo-fluid containing 54% solid granular material therefore provides a minimum estimate of the settling velocity of the breccia blocks. The minimum settling velocity thus provides a

measure of the relative behaviour of breccia blocks of varying size and density within a sandstone pipe (Fig 5.9).

Increasing the size and density of the breccia block results in an increase in the settling velocity of the block (Fig 5.9). Given that for upward transport of a breccia block, the fluid flow velocity must exceed the settling velocity of the block, high fluid velocities (in the order of 10's cms^{-1}) are required in order to induce the upward transport of large or dense breccia blocks. These fluid velocities are considerably larger than the 1.6 cms^{-1} maximum fluid velocity calculated from the settling velocity of the pipe fill matrix. It is therefore highly likely that breccia blocks with densities greater than that of the sand/fluid suspension would have not been supported by upwards fluid motion and would have sunk within a pseudo-fluid moving at the velocities calculated. Given that there is good evidence that upward transport of large breccia blocks does occur, either the calculated fluid velocities based on grain size and the assumptions behind these calculations are incorrect, or that an alternative mechanism for breccia block transport should be sought.

However, as the density of the breccia block approaches that of the pseudo-fluid the settling velocity of the block decreases rapidly. Should the density of the breccia block have been equal to, or less than that of the pseudo-fluid the block would have achieved neutral or positive buoyancy. If positive buoyancy was achieved, the breccia block would have floated upwards within the pseudo-fluid irrespective of fluid flow velocity (Fig 5.10). If the breccia blocks have a diameter more than three times that of the particles within the pseudo-fluid then the effects of drag caused by the shape of

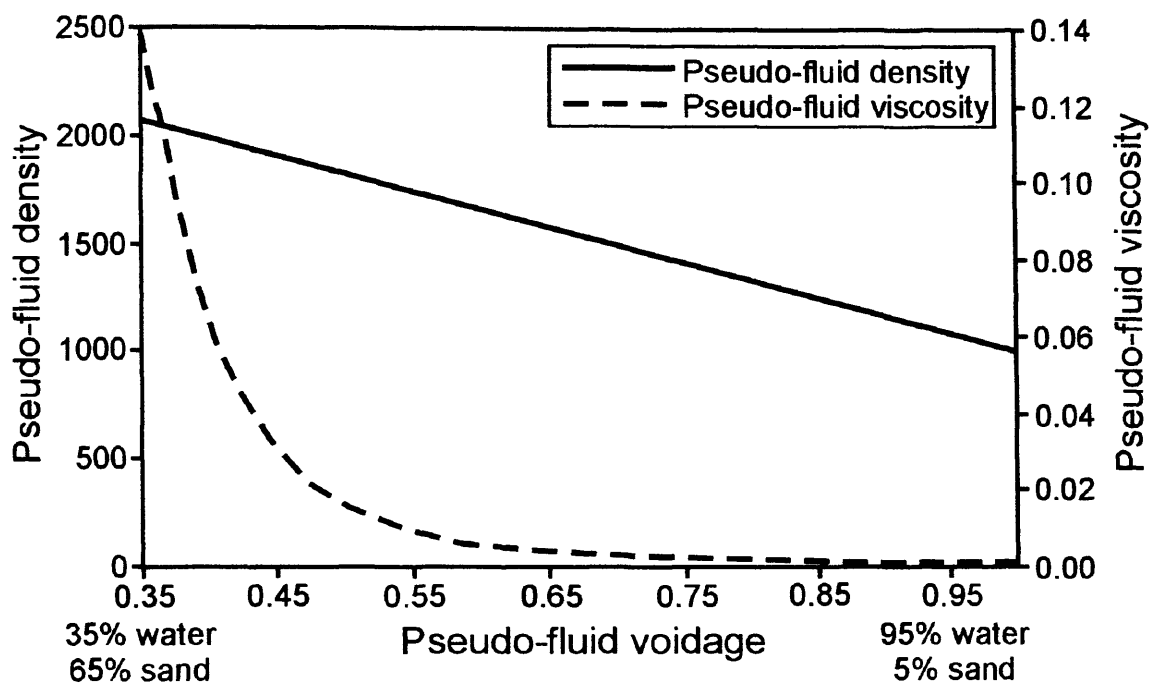


Fig 5.8 The effects of pseudo-fluid voidage (i.e. 1-sand content) on the density and viscosity of the pseudo-fluid. Density increases linearly, however below a voidage of 0.5 the viscosity of the pseudo-fluid increases dramatically.

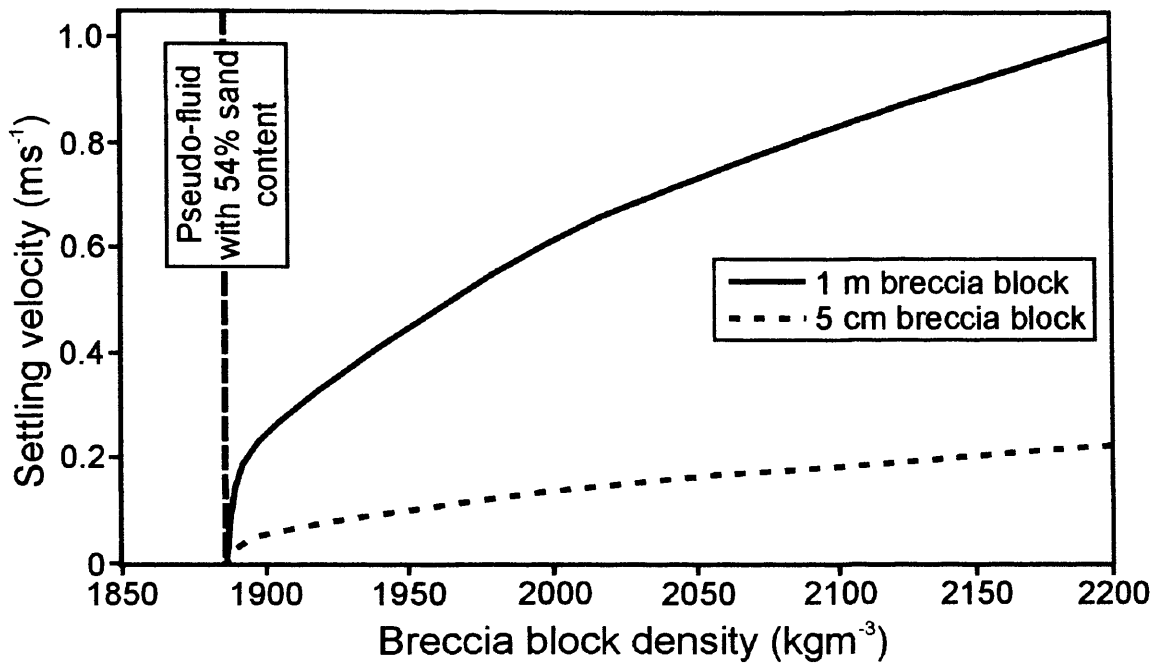


Fig 5.9 Settling velocities of spherical breccia blocks with diameters of 5 cm and 1 m and variable density, in a pseudo-fluid containing 54% sand. 54% sand is believed to be the highest sand content possible for fluidisation (Leva, 1959). This imparts a density of 1880 kgm^{-3} and a viscosity of 0.026 Pas . Note how the settling velocity drops dramatically as the density of the breccia block approaches that of the pseudo-fluid.

the block becomes unimportant (DiFelice *et al.*, 1989) assuming that individual blocks do not interfere with each other. Therefore the actual shape and associated drag coefficient of the breccia blocks within the sandstone pipes is unimportant in the case of buoyant transport. If relatively small fluid velocities calculated from the grain size of the pipe fill matrix are correct it implies that large breccia blocks could not have been supported by the sand/fluid suspension present within the sandstone pipes. Therefore buoyancy driven transport may have been the main mechanism for upwards transport of blocks.

5.7 DISCUSSION

5.7.1 Compositional segregation of the pipe fill matrix

There is systematic compositional variation between the Gunsight Butte Member of the Entrada Sandstone and the pipe fill matrix. As previously discussed, the bulk properties of the Gunsight Butte Member are highly likely to be a good proxy for the characteristics for the pipe source unit(s). The pipe fill matrix therefore represents the material left behind after the pipe formation process has ceased. Oxide minerals, feldspar and polycrystalline quartz are all depleted in pipe fill matrix relative to host rock (Fig 5.4). Assuming that the source unit for the sandstone pipe fill is of similar composition to the bulk properties of the Gunsight Butte Member of the Entrada Sandstone it is possible to examine compositional segregation in terms of the pipe formation process.

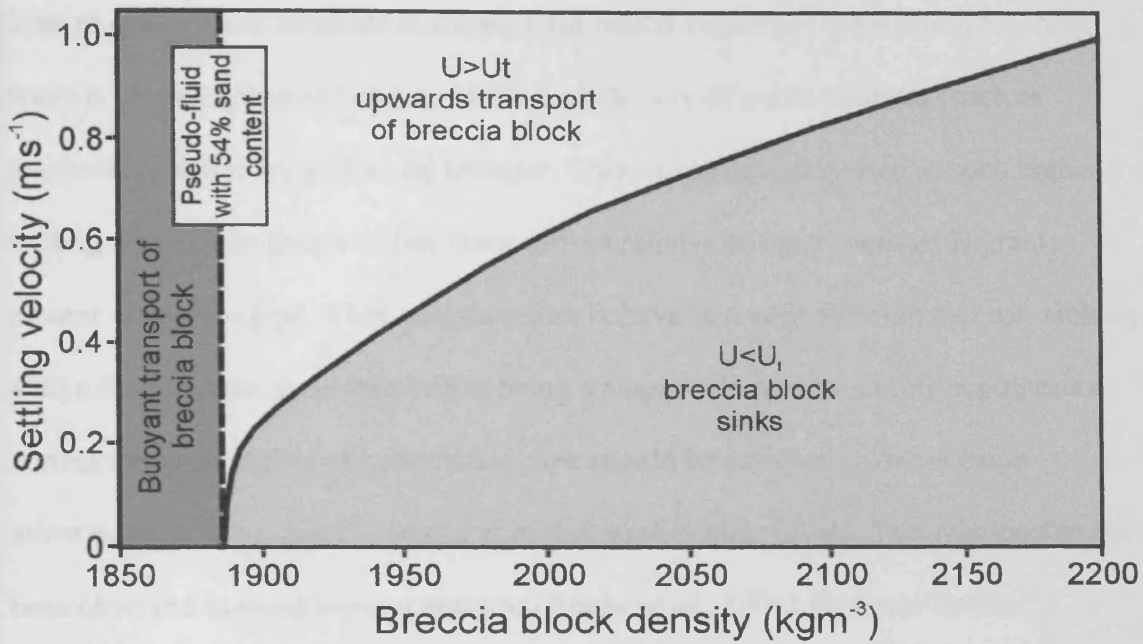


Fig 5.10 The settling velocity of “spherical” breccia blocks with a diameter of 1 m, but varying density in a pseudo-fluid containing 54% sand (density 1880 kgm⁻³, viscosity 0.026 Pas) showing the differing transport domains. If $U < U_t$ the block will sink within the pipe, whilst if $U > U_t$ then the block will be entrained within the mobile fluid and transported upwards. Should the density of the pseudo-fluid be greater than that of the breccia block it will float buoyantly upwards.

Loss of dense oxide minerals in the pipe fill matrix relative to the surrounding host rocks is easily explained because of the high density of oxide minerals (such as magnetite) relative to quartz and feldspar. This would have imparted a much higher settling velocity on grains of this composition relative to other, non-oxide grains present within the pipe. They will therefore behave in a very different manner, sinking within the fluidised mass rather than being transported upwards. If this hypothesis is correct the basal region of a sandstone pipe should be enriched in dense oxide minerals relative to pipe fill matrix at higher stratigraphic levels. This relationship has been observed in experimental systems (Roche *et al.*, 2001) However further sampling throughout the full vertical extent of a sandstone pipe would be required to confirm this hypothesis.

Depletion in orthoclase and plagioclase in pipe fill matrix relative to the surrounding host rocks cannot be explained by segregation by density because the density of these minerals (and thus their settling velocity) is very similar to monocrystalline quartz. However, much of the feldspar present in the samples was highly weathered and, is therefore mechanically weak when compared to monocrystalline quartz. Attrition of these weak grains during pipe formation would result in a reduction in grain-size and thus lower settling velocities. These smaller fragments would be more likely to be elutriated from the system resulting in the observed depletion in these grain-compositions.

5.7.2 Transporting breccia blocks

Sandstone breccia blocks are present in almost every sandstone pipe examined in the lake Powell region and there is good evidence for the upwards transport of these blocks. The density of a water-saturated sandstone breccia block with a porosity of 34% (equivalent to the initial porosity of the host rocks derived through point counting) is around 2080 kgm^{-3} . This is well in excess of the density-range of the pseudo-fluid present within a sandstone pipe containing a sand/fluid suspension with maximum 54% sand (1880 kgm^{-3}). Therefore, such blocks could not have been supported within the pseudo-fluid and would have sunk within the pipe. However, it is highly likely that the sediments of the Gunsight Butte Member of the Entrada Sandstone have undergone significant compaction since deposition. Modern aeolian dune sands buried to depths of up to 17 m have porosities ranging between 40% and 58% (Atkins *et al.*, 1991). These values are significantly higher than those observed within the pipe host rocks. The density of water-saturated breccia blocks derived from sandstones with these porosities ranges between 1680 kgm^{-3} to 1980 kgm^{-3} . Increased porosity of breccia blocks at the time of pipe formation, relative to modern-day porosities makes the buoyant upward transport of breccia blocks more likely.

There is good evidence to suggest that mudstone blocks within sandstone pipes from the Kodachrome Basin have been transported upwards relative to the stratigraphic level of their source depositional unit (Section 4.4.31). Mudstones with 40% to 60% porosity, consistent with burial of up to 200 m (i.e. similar to that achieved by the host rocks at the time of pipe formation), have a density of between 1700 kgm^{-3} and 2000 kgm^{-3} . It is therefore possible that mudstone blocks with densities towards the lower

end of this range were buoyant within the sand/fluid suspension present within the pipes and could have been transported upwards within the sandstone pipes.

5.7.4 Fluid flux and duration of fluid flow

Using the average velocity of fluid movement within the sandstone pipes in the Lake Powell region it is possible to assess the fluid flux. This can then be compared to proposed modern day analogues for the sandstone pipes of SE Utah. One possible analogue for the sandstone pipes of SE Utah may be found in the boiling sand springs found on banks of the Dismal River in Nebraska. In the case of the boiling sand springs, fluid flow is driven by artesian groundwater flow and boiling refers to the churning motion displayed by sand within the spring (Guhman and Pederson, 1992). Two closely spaced spring pits had a combined discharge rate of 50 litres of water per second (i.e. $0.05 \text{ m}^3 \text{ s}^{-1}$). Water was discharged, but no suspended granular sediment was expelled with the water although sands within the spring pit were seen to display a churning motion, likely to represent spouting behaviour seen in fluidised beds (e.g. Allen 1985; McCallum 1985). The two roughly circular spring pits on the banks of the Dismal River had a cross-sectional area of approximately 90 m^2 (equivalent to a single spring pit with an approximate diameter of 11 m). Therefore fluid velocities within the boiling sand springs must have been around 0.06 cms^{-1} . If we compare the discharge rate to that occurring during pipe formation in SE Utah, where fluid the maximum average fluid velocity was 1.6 cms^{-1} (with a calculated range of possible velocities between 0.8 cms^{-1} and 2.1 cms^{-1}) the flux from a pipe with a cross-sectional area of 90 m^2 would be $1.4 \text{ m}^3 \text{ s}^{-1}$. The fluid flux from the sandstone pipes of SE Utah during the Middle Jurassic was thus a maximum of 30 times greater than the fluid

discharge related to artesian groundwater flow in the boiling sand springs of Nebraska at the present day, and the latter are probably not an appropriate analogue for the sandstone pipes of SE Utah.

If the grain-size and compositional sorting seen within the pipe fill matrix of the sandstone pipes in the Lake Powell area is considered a direct result of steady state flow through a cylindrical sandstone pipe it is possible to make an estimate of the minimum time for which a sandstone pipe was active. During pipe formation, fluid was transmitted from a remobilised source unit at depth below the palaeosurface, to the palaeosurface. Therefore a conservative minimum estimate of the duration of pipe activity is given by the length of time it takes fluid to migrate from the source unit to the surface. In the Lake Powell area the Gunsight Butte Member of the Entrada Sandstone is 145 m thick (Thompson and Stokes, 1970). The lack of evidence for material within the pipes derived from the Carmel Formation or older strata implies that the maximum distance between source unit and the palaeosurface is 145 m. The maximum average flow velocity through the sandstone pipes present in the study area is 1.6 cm s^{-1} (with a calculated range of possible velocities between 0.8 cm s^{-1} and 2.1 cm s^{-1}). Therefore the minimum duration of pipe activity was about 2.5 hours. A pipe of diameter 10 m would therefore expel around 11400 m^3 ($1.14 \times 10^{-5} \text{ km}^3$) of fluids during this period. However, this is a conservative estimate of the duration of pipe activity, and therefore the volume of fluid expelled because it does not take into account the size of the fluid reservoir or the length of time required for a pipe to propagate through the host strata. It is likely that the duration of pipe activity may have been much longer and thus volume of water expelled onto the palaeosurface may have been considerably greater.

Large-scale sandstone pipe formation is believed to be a response to widespread liquefaction and fluid escape resulting from seismic activity (Section 4.9.53; Netoff; 2002; Huuse *et al.*, 2005). Coseismic increases in stream flow resulting from fluid expulsion to the surface during modern earthquakes have previously been observed (e.g. Muir Wood, 1994; Wang *et al.*, 2004). The magnitude 7, normal fault, Hebgen Lake earthquake occurred in 1959 in Montana and resulted in the expulsion of 0.3 km³ to 0.5 km³ of water measured as increased fluid flux in streams in the Hebgen Lake region (Muir Woods, 1994). Similarly the magnitude 7.5, 1999 Chi Chi earthquake in Taiwan released around 0.7 km³ of water (Wang *et al.*, 2004). The estimated maximum volume of fluid expelled from a single sandstone pipe in the Lake Powell region with diameter 10 m, over a period of 2.5 hours, is about 1.14×10^{-5} km³. This is a conservative estimate of the volume fluid expelled from a sandstone pipe in the Lake Powell region. It is therefore likely that the volume of fluid expelled during the Middle Jurassic sandstone pipe formation event in SE Utah may be comparable, or possibly even greater than the volumes of water expelled during each of the two earthquakes discussed above. As such the Middle Jurassic sandstone pipe formation event in SE Utah represents a volumetrically significant, seismically triggered fluid-escape event that may rival or possibly surpass modern earthquake induced fluid escape events in terms of scale.

5.7.4 Applicability of homogeneous sand-water flow to the sandstone pipes of SE Utah

During homogeneous sand-water flow the movement of the fluid and the entrained sand grains is coupled and volume is preserved. This will occur at relatively high fluid velocities (i.e. 10 times the settling velocity of the granular sediment) and small sand fractions (i.e. 80% fluid and 20% granular solids) (Gallo and Woods, 2004). Whilst this model may be applicable to vigorous sand eruptions, it appears that it is not suitable to explain the formation of the sandstone pipes of SE Utah based on the calculations presented above.

The depletion of the fine-grained fraction observed in sandstone pipe fill matrix relative to the surrounding host rocks suggests that whilst fine grains may be elutriated from the system, coarser material is left behind. Two distinct styles of remobilisation and transport of granular sediment are present within the sandstone pipes: 1) A fluidised coarse granular solid component. Sand grains were not elutriated from the pipe and made up the pipe fill matrix after the cessation of fluid flow. 2) A fine-grained component that was entrained within the moving fluid. These entrained grains were transported upwards within the fluid. The calculated maximum average fluid velocity based on the average grain-size of pipe-fill matrix is 1.6 cms^{-1} (with a range in possible velocities from 0.8 cms^{-1} to 2.1 cms^{-1}). Fluid velocities of ten times U_t of the pipe fill matrix (i.e. 0.08 ms^{-1} to 0.21 ms^{-1}) are therefore incompatible with the presence of the observed range of grain sizes present within the pipes ($100 \text{ }\mu\text{m}$ to $174 \text{ }\mu\text{m}$).

Conservation of volume within the conduit during pipe formation by homogeneous sediment/fluid-flow implies that there must be bulk transport of solid material out of the source unit. Whilst field examples of sandstone pipes associated with large-scale collapse structures are observed (Fig 5.4), many sandstone pipes in the Lake Powell region are not associated with large-scale collapse structures. Moreover, evidence for the elutriation of a fine-grained component within the sandstone pipes strongly implies that sediment/fluid flow during pipe formation was inhomogeneous.

5.8 CONCLUSIONS

We estimate the fluid flow regime within the sandstone pipes of the Lake Powell region by making the following assumptions: 1) The bulk properties of the Gunsight Butte Member of the Entrada Sandstone are a valid proxy for the source unit(s) for the pipes. 2) The grain-size and compositional variation between the pipe fill matrix relative to the surrounding host rocks represents sorting resulting from steady-state fluid flow through the sandstone pipes. 3) The fluid velocity throughout the vertical extent of the sandstone pipes is uniform. 4) The pseudo-fluid model can be applied to the sand/fluid suspension present within the pipes during their formation in order to explore the behaviour of breccia blocks within the sandstone pipes.

Given these assumptions, we constrain the average maximum fluid velocity present during pipe formation to 1.6 cms^{-1} (with values derived from individual sandstone pipes ranging from 0.8 cms^{-1} to 2.1 cms^{-1}). Two distinct styles of remobilisation of granular sediment are present within the sandstone pipes during their formation: 1) A fluidised coarse granular solid component. These grains were not elutriated from the

pipe and represent the pipe fill matrix left after the cessation of fluid flow. 2) A fine-grained component that was entrained within the moving fluid. These entrained grains were transported upwards within the fluid and may have been expelled at the palaeosurface.

At the fluid velocities and viscosities calculated from the pipe fill matrix, the upward transport of breccia blocks can only occur if their density approaches, or is less than that of the sand/fluid suspension (pseudo-fluid) within the pipe. The upward transport of dense breccia blocks is incompatible with low fluid velocities calculated from the pipe fill matrix, therefore it is likely that buoyancy driven transport may be the main mechanism behind breccia block transport. In particular it is unlikely that fluid saturated sandstone breccia blocks could be transported upwards within a sandstone pipe due to their high relative density when compared to the maximum density of the pseudo-fluid present within the pipe. The likelihood of upward transport of sandstone breccia blocks increases if the porosity of the blocks was greater than that observed within the host rock at the present day.

A conservative estimate of the minimum duration of the pipe formation based on considerations of stratal thickness and the calculated fluid velocity within the pipes is 2.5 hours. Depending on fluid reservoir size and duration of time required for a sandstone pipe to propagate from source to surface, it is possible that the duration of the pipe formation event was considerably longer. A single sandstone pipe in the Lake Powel region with a diameter of 10 m could expel $1.14 \times 10^{-5} \text{ km}^3$ over a 2.5-hour active period (equivalent to a flux of $1.4 \text{ m}^3 \text{ s}^{-1}$). Given that numerous sandstone pipes are found across SE Utah and that the total volume of fluid expelled is likely to be

very large (in the order of km^3), sandstone pipe formation may rival, or possibly surpass the scale of two modern examples of fluid escape resulting from earthquake events. Therefore the Middle Jurassic sandstone pipe formation event is likely to represent a large-scale fossil example of earthquake-triggered fluid escape.

CHAPTER 6 - CONCLUSIONS

6.1 INTRODUCTION

The objectives of this chapter are to summarise the results of this PhD project and place the results obtained within the context of the published literature in order to highlight the main advances afforded by this study and outline some of the remaining problems.

The global distribution of sandstone intrusions and their presence in a wide range of depositional environments (Table 1.3) and tectonic settings (Table.1.6) illustrates the importance of sand intrusion as a geologic process. The process of sand intrusion is still poorly understood, but requires that a number of preconditions are met:

- Sand is deposited and subsequently buried. The surrounding rock within which sandstone intrusions will later be hosted, is commonly, but not always a sealing lithology allowing build up of overpressure.
- The sand must be prone to remobilisation (i.e. uncemented).
- A triggering event capable of causing the remobilisation of the source sand unit must occur. Possible triggering events include earthquake shaking and fluid migration.

The following sections examine these conditions and discuss the effects and controls of basin-scale sand intrusion:

6.2 HOST ROCK PROPERTIES

The largest intrusions are found in deep-water settings where the isolated nature of the parent sand bodies and the fine-grained nature of background sedimentation allows the early formation of a good seal allowing the build up of overpressure to begin at relatively shallow burial depths (e.g. Jolly and Lonergan 2002). The Faroe-Shetland basin case study is a good example of sand intrusion in this setting (Chapters 2 and 3). The large-scale conical sandstone intrusions present in Tranche 6 are hosted within a thick, polygonally faulted claystone succession (Section 3.3). The claystones have low permeability and good potential to form a regional seal. In contrast, the only sealing lithologies present in SE Utah are thin mudstones within the Carmel Formation (Section 4.4). Whilst these have the potential to form local seals, most of the Middle Jurassic succession is sand dominated (Section 4.4), and therefore a poor seal possessing high porosity (Netoff 2002) and good permeability (e.g. Chan *et al.*, 2000).

Tabular sandstone intrusions are found almost exclusively in fine-grained (and low permeability) host rocks (e.g. Truswell, 1972; Taylor, 1982; Dixon *et al.*, 1995; Friès and Parize, 2003). In contrast sandstone pipes are commonly found in sandy host rocks (e.g. Hannum, 1980; Deynoux *et al.*, 1990; Mount, 1993; Netoff, 2002; Huuse *et al.*, 2005). It is therefore likely that the host rock properties may affect the mechanism of intrusion propagation and thus intrusion geometry.

6.3 SAND REMOBILISATION AND FLUID FLOW

The source sand must be unlithified (e.g. Parnell and Kelly, 2003) at the time of intrusion in order for remobilisation to occur. The processes of liquefaction and fluidisation are commonly invoked to explain sand intrusion (e.g. Obermeier, 1996; Jolly and Lonergan, 2002 and references therein). However, there are problems with the application of both of these processes to sand intrusion.

Liquefaction of granular sediment become more unlikely as burial depth increases due to increased sediment shear-strength with increasing overburden load (e.g. Seed and Idriss, 1971; Obermeier, 1996; Jolly and Lonergan, 2002). However, sandstone intrusions have been recorded related to source units buried to depths in excess of several hundred metres (e.g. Section 4.5; Phillips and Alsop, 2000; Duranti and Hurst, 2004). Factors that may increase the probability of liquefaction at substantial burial depths include local site amplification of seismic waves and high fluid overpressures resulting in reduced sediment shear strength (eg; Aki, 1993; Benjumea *et al.*, 2003). Instantaneous liquefaction of a buried sand body results in a state change from solid (grain-supported) to fluid (pore fluid-supported). The fluid pressure within the liquefied body will equal the lithostatic pressure at the base of the liquefied body. The fluid pressure of the liquefied body may therefore be high enough to cause the hydraulic fracture of the surrounding host rock (e.g. Sibson, 2000).

The escape of fluid from a sand body may result in fluidisation if fluid flow is vigorous (e.g. Di Felice, 1995). In order for fluidisation to occur the drag forces exerted by the mobile fluid must be greater than the weight of the grains. By

definition, fluidisation acts against gravity (Allen, 1985; Kunii and Levenspiel, 1991; Di Felice, 1995). Fluid flow from the source unit is required as a precondition to fluidisation (e.g. Jolly and Lonergan, 2002) and therefore it would seem most likely that fluid escape from the source unit is a precondition for fluidisation.

The formation of sandstone intrusions other than neptunian dykes requires that sand must be transported into an open fracture held open by the pressure exerted by the mobile fluid. Lower fluid overpressures are required to dilate pre-existing fractures than to create new hydraulic fractures (e.g. Sibson, 2000) if such fractures are present within the caprock. It is therefore likely that caprock failure and fluid flow (and thus sand intrusion) is likely to be driven by the reactivation of pre-existing fractures within the caprock rather than the formation of new hydraulic fractures (e.g. Sibson, 2000). However, this observation is inconsistent with the formation of large-scale conical sandstone intrusions, the discordant limbs of which commonly cross-cut pre-existing polygonal faults within the host rock (e.g. Fig 3.15; Huuse *et al.*, 2001; Huuse *et al.*, 2004). This observation suggests that the fluid pressures involved during upward sand intrusion are so large that the difference between the reactivation of pre-existing fractures and the formation of new hydraulic fractures is negligible.

Whilst hydraulic fracture or the reactivation of pre-existing fractures readily explains the formation of tabular sandstone intrusions in fine-grained sediments, the fracture of sediments with high permeability (i.e. sand) and the formation of a cylindrical geometry through hydraulic fracture is much more problematic. Should the host rock be highly permeable it is likely that transient high fluid pressures cannot be sustained because of fluid bleed off into the surrounding host rock and it is therefore highly

unlikely that hydraulic fractures can propagate for any great distance in this medium. The cylindrical geometry of sandstone pipes is similarly problematic. According to Mohr-Coulomb theory, hydraulic fractures form tabular shapes the orientation of which is controlled by the fluid pressure and host rock stress state (e.g. Cosgrove, 1995; Mendel, 2000). It is therefore hard to envisage the formation of cylindrical hydraulic fractures. It may be possible to form a cylindrical intrusive geometry if the migrating fluids exploit joint intersections and enlarge the fluid flow conduit through wall rock plucking. However, in the case of the sandstone pipes of SE Utah, no systematic distribution, reflecting exploitation of pre-existing joint sets or fault planes is observed (Section 4.3.4) and other mechanisms for the formation of a cylindrical geometry must be sought. Self-organisation of fluid escape into pipe-like structures is commonly observed during the setting of liquefied sediment (e.g. Druitt, 1995; Kolymbas, 1998). Therefore, one possibility for forming a cylindrical geometry is that the superimposition of pipe-like fluid escape within the source sand onto the host sandstones around the liquefied body may promote the formation of pipes in the host rock by focusing fluid flow out of the remobilised source sand body.

The analysis of grain size data derived from the matrix of the sandstone pipes in the Lake Powel region enables the average maximum fluid velocity during pipe formation to be constrained to a maximum average fluid velocity of 1.6 cm s^{-1} (with calculated fluid velocities for individual pipes ranging from 0.8 cm s^{-1} to 2.1 cm s^{-1}) (Section 5.6.11). This is the first time that the fluid velocity within a sandstone pipe has been constrained in this manner. Unfortunately, no exploration wells have penetrated the conical sandstone intrusions within Tranche 6 of the Faroe-Shetland Basin and their source sand has not been conclusively identified. Therefore it is currently impossible

to apply the techniques developed in Chapter 5 to conical sandstone intrusions in the Faroe-Shetland Basin.

The sandstone pipes in SE Utah commonly contain large breccia blocks of sandstone and mudstone up to 1 m in length (e.g. Hannum, 1980; Netoff 2002; Huuse *et al.*, 2005) and there is good evidence for the upward transport of breccia blocks of this size (Section 4.4.31). The settling velocities of such blocks are much higher than the fluid velocities calculated from the pipe-fill matrix grain size. However, if a pseudo-fluid model (Di Felice, 1991; 1998) is applied to the sand/fluid suspension present within the pipe during its formation it becomes possible to transport breccia blocks upwards within the sandstone pipe if the density of the breccia block approaches, or is less than that of the pseudo-fluid within the pipe (Section 5.7.3). It is therefore possible that buoyant upward transport of breccia blocks may have been the major mechanism for the upward transport of breccia blocks in the sandstone pipes of SE Utah.

Constraining the fluid velocity within the sandstone pipes enables the fluid flux during pipe formation to be assessed. The minimum fluid flux from an individual sandstone pipe with a diameter of 10 metres during its formation is $1.14 \times 10^{-5} \text{ km}^3$ (Section 5.7.4). It is therefore likely that the amount of fluid expelled during the pipe formation event across the whole region within which pipes are found is likely to be equivalent to, or possibly in excess of fluid expulsion observed as increased stream flux during modern day earthquakes (Muir Wood, 1994; Wang *et al.*, 2004).

During sand intrusion, fluid escapes the remobilised source unit resulting in a pressure drop. Eventually a point will be reached where fluid flow ceases. The presence of sand within the hydraulic fracture opened during sand intrusion will prop open the fracture (e.g. Papanastasiou, 2000). The sandstone intrusion can now act as a fluid conduit allowing fluid migration to other parts of the host succession, other aquifers or to the palaeosurface.

One possible example of the effect that a network of sandstone intrusion may have on hydrocarbon migration is represented by the large-scale conical sandstone intrusion of the Faroe-Shetland basin. The overall distribution of conical sandstone intrusions within the study area does not follow the extent of the Middle Eocene fans, the shallowest possible source of sand beneath the conical sandstone intrusions (Fig.3.3). Instead the distribution of conical sandstone intrusions seems more strongly related to the NE-SW orientated tectonic fabric of the basin (Fig 3.2 and Fig 3.14) and the distribution of the underlying Palaeocene turbidite succession (Fig.3.5). It is therefore possible that the fluids (and possibly some of the sands) involved in the emplacement of the conical sandstone intrusion in the Eocene-Oligocene succession may have been derived from sources deep within the basin. A possible candidate for source sands stratigraphically deeper than the Middle Eocene fans, are the stacked turbidite sands present within the Palaeocene succession (Jowitt *et al.*, 1999). However, the possibility of shallower sources of sand and overpressure cannot be completely ruled out.

There are no hydrocarbon shows within the stacked turbidite sands of the Upper Palaeocene succession in the study area, despite active hydrocarbon migration from

the Cretaceous onwards (Jowitt *et al.*, 1999; Sullivan *et al.*, 1999). Whilst it is possible that this succession was never charged, or that any seals were breached during basin inversion this observation may provide circumstantial evidence for the presence of vertical fluid migration pathways from the Palaeocene succession. If a portion of the sand present within the conical sandstone intrusions within the Eocene-Oligocene succession is derived from Upper Palaeocene turbidites it is likely that there may be small-scale (sub-seismic resolution) sandstone intrusions throughout the Palaeocene-Oligocene succession. The presence of such intrusions would provide an effective bypass route from the Palaeocene to the INU allowing hydrocarbon migration to the palaeoseabed effectively draining the Palaeocene-Oligocene succession of hydrocarbons within Tranche 6.

6.4 TRIGGERING REMOBILISATION

A wide range of triggering events has been proposed for sandstone intrusions (Table 1.7). Most triggering mechanisms fall in to three broad categories: overpressuring due to seismic shaking; overpressuring due to sudden loading, and the migration of fluid into the source rock from an exterior source (Section 1.5.2). Most of the proposed triggering events, with the notable exception of hydrocarbon migration, share the important characteristic of being geologically instantaneous. Therefore, in order to tie a sand intrusion event to a particular triggering event with a high degree of certainty, the timing of both the intrusion event and the proposed trigger must be tightly constrained. This is rarely achieved, and the case studies presented in Chapters 2 to 5 represent some of the best examples of temporally constrained intrusion events.

Large-scale conical sandstone intrusions and large-scale intrusion complexes are found in basins undergoing subsidence (e.g. the North Sea, Huuse and Mickelson, 2004) basin inversion (e.g. the Faroe-Shetland Basin, Chapters 2 and 3;) or that are located in seismically active regions (e.g. California, Thompson *et al.*, 1999; Boehm and Moore, 2002). Commonly, the only evidence for many ancient earthquakes is the occurrence of seismites, such as intruded/extruded sand bodies (e.g. Obermeier, 1996; Rossetti, 1999). This leads to a circular argument within which earthquakes trigger sand intrusion and/or seomite formation, but the only evidence for the earthquake is the presence of sandstone intrusions or seismites. Given the inherent difficulties of constraining the timing of palaeo-earthquakes without relying on inferred palaeoseismites, it is important to seek independent evidence for tectonic activity that is coeval with the sand intrusion event if seismicity is proposed as the triggering mechanism.

In the Faroe-Shetland Basin, the emplacement of conical sandstone intrusions in the shallowest section of the Eocene-Oligocene claystone succession caused the formation of forced folds on the INU in the study area (Fig.2.2). Dating of sediments that onlap these forced folds constrains the timing of emplacement to the Late Miocene based on biostratigraphical data. This is the first time that emplacement of large-scale conical sandstone intrusions has been dated with such a level of confidence. A phase of basin inversion occurred in the Faroe-Shetland basin during the Late Miocene (Davies *et al.*, 2004). It is therefore possible that seismic activity and fluid migration associated with basin inversion resulted in the emplacement of conical sandstone intrusions in the Faroe-Shetland Basin during the Late Miocene. The distribution of sandstone intrusions lies along a Late Cretaceous/Palaeocene to

recent hydrocarbon migration pathway from the Kimmeridgian hydrocarbon kitchen at depth (Jowitt *et al.*, 1999) and it is possible that hydrocarbon migration may be partially responsible for the emplacement of the conical sandstone intrusions in Tranche 6. However, the basin is considered to be over mature with most vertical hydrocarbon migration occurring during the Palaeocene (Ilfie *et al.*, 1999), long before the Late Miocene emplacement of the conical sandstone intrusions in Tranche 6. However, if sand and fluids were derived from the Palaeocene succession it is possible that a pulse of hydrocarbon leakage resulting from Late Miocene inversion may be responsible for sand intrusion.

Several mechanisms for triggering pipe formation in Jurassic sediments of the Colorado Plateau have been proposed including bolide impact (Alvarez *et al.*, 1999), dissolution collapse (Hunter *et al.*, 1992), artesian ground water flow (Hannum, 1980) and seismic activity (Section 5.9.5; Hannum, 1980; Netoff, 2002; Huuse *et al.*, 2005). Bolide impact was suggested as a trigger for sandstone pipe formation because of the presence of Upheaval Dome impact crater within Middle Jurassic sediments in SE Utah (Alvarez *et al.*, 1999). However the timing of the impact event is very poorly constrained (e.g. Shoemaker and Herkenhoff, 1984; Kriens *et al.*, 1999; Kenkman and Scherler, 2002). Therefore, although it is impossible to rule out impact-induced liquefaction as the trigger for pipe formation it is also impossible to directly correlate the timing of impact with the timing of pipe formation. Dissolution collapse to form breccia pipes is relatively common in karstic terrain or where evaporites are present within the sedimentary succession (e.g. Weinrich *et al.*, 1992; Hunter *et al.*, 1992; Walsh and Zachraz 2001). However, evidence for the upward transport of breccia blocks within sandstone pipes from the Kodachrome Basin (Section 4.4.31) and the

lack of extensive evaporite deposits within the Middle Jurassic succession present in the study area (e.g. Section 4.3.11; Thompson and Stokes, 1970; Doelling and Davis, 1989) preclude this mechanism from forming the sandstone pipes present in SE Utah. Artesian ground water flow has also been invoked as a triggering mechanism for sandstone pipe formation (Hannum, 1980). However, the fluid flux from modern-day boiling sand springs related to artesian ground water flow on the banks of the Dismal River in Nebraska (Guhman and Pederson 1992) is 30 times smaller than the fluid flux calculated from the sandstone pipes in SE Utah (Section 5.7.4).

Seismically induced liquefaction has been invoked as the triggering mechanism for pipe formation in SE Utah (e.g. Section 4.9.53; Hannum, 1980; Netoff, 2002; Huuse *et al.*, 2005). Sandstone pipes are not found above the top of the Gunsight Butte Member of the Entrada Sandstone. The top of the Gunsight Butte Member of the Entrada Sandstone is associated with a large sand blow in the Lake Powel region (Netoff, 2002). It is therefore most likely that pipe formation occurred before the deposition of the overlying Cannonville Member of the Entrada Sandstone. However, seismites, other than the sandstone pipes, are not present in the Middle Jurassic succession to support this hypothesis (e.g. Anderson *et al.*, 2003). Pipe formation is coincident with uplift to the west of the Colorado Plateau began during the deposition of the Entrada Sandstone. This resulted in a marked change in drainage direction from northwards (Bjerrum and Dorsey, 1995; Dickinson and Gehrels, 2003) to eastward drainage after the deposition of the Entrada Sandstone (Dickinson and Gehrels, 2003). Uplift to the west, and increased shortening during the Middle Jurassic (Allen *et al.*, 2000) was highly likely to have caused the reactivation of long-lived basement structures within the region and increased seismicity at a time coincident with pipe

formation. Therefore it is likely that pipe formation was a product of the remobilisation of buried sands in response to seismic activity.

6.5 POST-EMPLACEMENT EFFECTS OF SAND INTRUSION

The emplacement of sandstone intrusions commonly results in the formation of high permeability conduits through otherwise low permeability strata. Therefore sandstone intrusions can form efficient fluid conduits through otherwise effective sealing rock units long after their initial emplacement. The presence of large-scale sandstone intrusions is thus highly likely to improve vertical connectivity between separate aquifers and even the palaeosurface. The presence of sandstone intrusions may therefore allow the migration of hot fluids or hydrocarbons from depth within the basin (e.g. Jonk *et al.*, 2003(b)). In hydrocarbon prone basins sandstone intrusions may enhance reservoir potential by increasing connectivity between reservoir sands (e.g. Jenkins, 1930; Timbrell *et al.*, 1993; Huuse *et al.*, In Press) or may themselves be potential reservoir sandstones (e.g. Lonergan *et al.*, 2000; Huuse *et al.*, 2004).

However sandstone intrusions may also act as effective seal breaches or constitute drilling hazards and thus also be detrimental to hydrocarbon prospectivity. Therefore the identification, characterisation and prediction of large-scale sandstone intrusions is important during hydrocarbon exploration.

The Eocene-Oligocene claystone succession within Trance 6 of the Faroe-Shetland Basin is a good candidate for a regional caprock. However, conical sandstone intrusions are present within this succession and form interconnected networks (Fig 3.13) or “orphan” intrusions beneath which no feeder system is imaged using seismic

data (Fig 3.12). There is a good spatial relationship between the basal apices of the orphan conical sandstone intrusions and the intersections of underlying polygonal faults (Fig 3.12 D and E). This implies that the polygonal fault network may have acted as the feeder system for the conical sandstone intrusions in the study area. It is therefore likely that polygonal faults utilised as feeder conduits, may be associated with small-scale sandstone intrusions along the fault planes at scales below seismic resolution, or are too steeply dipping to be imaged using conventional exploration seismic data. The presence of an extensive network of sandstone intrusions within the Eocene-Oligocene claystone succession would have a major effect on vertical connectivity within the claystone succession. The sandstone intrusions could form routes for fluid migration bypassing the otherwise effective caprock formed by the Eocene-Oligocene claystones.

6.6 BASIN SCALE SAND INTRUSION

The study regions examined during this PhD project are some of the most widespread regions of sandstone intrusion ever recorded. The large-scale conical sandstone intrusions of the Faroe-Shetland Basin cover a region of around 10,000 km², whereas the sandstone pipes of SE Utah cover a region of around 20,000km².

Previous studies have identified similarly widespread regions of sandstone intrusions (e.g. Fries and Parize, 2003, Huuse and Mickleson, 2004), and the regions examined in this study add to this catalogue of basinwide sandstone intrusion occurrences.

However, this study is important because is the first to constrain the timing of intrusion thus allowing the probable triggering events to be identified. This allows sand intrusion to be placed within the tectonostratigraphic context of the basin. In the

Faroe-Shetland basin the emplacement of conical sandstone intrusions occurs during the Late Miocene (Section 2.5) coincident with a major phase of basin inversion (Davies *et al.*, 2004). The formation of sandstone pipes in SE Utah coincides with a time of increased shortening (Allen *et al.*, 2000) and tilting of the whole basin as a result of uplift to the west (Section 3.9.53). In both the Faroe-Shetland Basin and SE Utah the formation of sandstone intrusions is coincident with basin wide inversion and the reactivation of long-lived basement structures. It is highly likely that high magnitude compressional or strike-slip earthquakes were associated with these inversion events and are likely to have occurred at the same time as both the intrusion events further strengthening the link between sandstone intrusion and seismicity.

Sand intrusion is generally considered as a process whereby high fluid pressures result in caprock failure and granular sediment is transported into fractures as a sand/fluid suspension. The fluid velocities required to transport sand-sized grains are in the order of centimetres per second (e.g. Section 5.6.11, Eichhubl and Boles, 2000; Jolly and Lonergan, 2002; Gallo and Woods 2004). Large-scale sandstone intrusions, or regions containing numerous sandstone intrusions are therefore likely to record large-scale catastrophic transient fluid migration events. Thus the presence of numerous sandstone intrusions emplaced simultaneously across a widespread region is likely to represent a very important event in the hydrodynamic evolution of a basin.

Sandstone intrusion is an often-overlooked geologic process, however recent interest has sparked a new wave of research. It is possible that large-scale, basinwide sandstone intrusions may be more common and important than presently realised.

Whilst there have been significant improvements in our understanding of this process

over the past decade there are still several important problems remaining. These include identifying the source sand unit, identifying the fluid present during intrusion and understanding the mechanics of hydraulic fracture with respect to sand intrusion and in particular understanding the geometry of conical sandstone intrusions and sandstone pipes.

6.7 SUGGESTIONS FOR FURTHER WORK

The results of this study strongly imply that large-scale sand intrusion events record catastrophic fluid escape events triggered by large-scale tectonic events. Several avenues for further research can be used to explore some of the more problematic aspects of the issues presented in this study:

1) Petrological fingerprinting of conical sandstone intrusions within the Faroe-Shetland Basin – There is no data linking the conical sandstone intrusions within the Faroe-Shetland Basin to a particular source sand. Sampling of conical sandstone intrusions from the Faroe-Shetland Basin would allow comparison of the mineralogy and grain-size to potential source sands such as the Middle Eocene fans, or Palaeocene turbidite sands possibly constraining the provenance of the sand. If the source sand of a conical sandstone intrusion could be identified this would provide important information about the depth of the source unit during intrusion and the vertical distance across which sand and fluid may be transmitted during an intrusion event. Grain-size analysis of both source and intruded sand may allow the fluid velocity during intrusion to be constrained allowing estimates of fluid flux to be made.

2) Looking deeper into Tranche 6– The Tranche 6 data set used during this study were cropped to a depth of 3.5 seconds two way travel time. Therefore the distribution of Palaeocene sands and basement structures in the study area could not be mapped using 3D data. 3D mapping and comparison of these features to the distribution of the conical sandstone intrusions in the Eocene-Oligocene succession would provide insight in to the possible sources of sand and fluid involved in the Late Miocene intrusion event.

3) Detailed sampling of sandstone pipes in SE Utah – The sandstone pipes of SE Utah provide an excellent opportunity to study the fluid-flow regime present during sand remobilisation and intrusion. Whilst it is possible to constrain the average fluid velocity from single samples from a number of pipes, a more focused sampling strategy could provide important information. Detailed mapping of sandstone pipes coupled with an examination of grain-size from a series of samples taken across a pipe, and down the vertical length of a pipe may provide important information about heterogeneities in fluid flow regime within the pipe.

REFERENCES

- Aki, K., 1993, Local site effects on weak and strong ground motion: *Tectonophysics*, v. 24, p. 93-111.
- Allen, J. R. L., 1985, *Principles of sedimentary geology*: George, Allen and Unwin, London.
- Allen, J.R.L., 1961, Sandstone-plugged pipes in the lower old red sandstone of Shropshire, England: *Journal of Sedimentary Petrology*, v. 31, iss. 3, p. 325-335.
- Allen, P.A., Verlander, J.E., Burgess, P. M., and Audet, D.M., 2000, Jurassic giant erg deposits, flexure of the United States continental interior, and timing of the onset of Cordilleran shortening: *Geology*, v. 28, no. 2, p. 159-162.
- Alvarez, W., E. Staley, D. O'Connor, and M. A. Chan, 1998, Synsedimentary deformation in the Jurassic of southeastern Utah – A case of impact shaking?: *Geology*, v. 26, no. 7, p. 579-582.
- Ambraseys, N.N., 1988, *Engineering Seismology: Earthquake Engineering and Structural Dynamics*, v. 17, p. 1-105.
- Anderson, J. L., 1944, Clastic dykes of the Chira and Verdun Formations Northwestern Peru: *Journal of Geology*, v. 32, p. 250-263.
- Anderson, P.B., Chidsey, T.C., Jr, Sprinkel, D.A. and Willis, G.C., 2003, *Geology of Glen Canyon National Recreation Area, Utah-Arizona*: In: *Geology of Utah's National Parks and Monuments* (Eds D.A. Sprinkel, T.C. Chidsey and P.B. Anderson), p. 301-335. Publication 28. Utah Geological Association, Salt Lake
- Anketell, J.M., Cegla, J., and Dzulynski, S., 1970, On the deformational structures in systems with reversed density gradients: *Annales de la Societe Geologique de Pologne*, v. XL, p. 3-29.
- Archer, J. B., 1984, Clastic intrusions in deep-sea fan deposits of the Rosroe Formation, lower Ordovician, western Ireland: *Journal of Sedimentary Petrology*, v. 54, p. 1197-1205.
- Aspler, L. B., and J. A. Donaldson, 1986, Penecontemporaneous sandstone dykes, Noacho Basin (early Proterozoic, Northwest Territories): Horizontal injection in vertical, tabular fissures: *Canadian Journal of Earth Sciences*, v. 23, p. 827-838.
- Atkins, J.E., and McBride, E.F., 1991, Porosity and packing of Holocene river, dune, and beach sands: *AAPG Bulletin*, v. 75, iss. 3, p. 335.

Aydin, A., 2000, Fractures, faults, and hydrocarbon entrapment, migration and flow: *Marine and Petroleum Geology*, v. 17, p. 797-814.

Baars, D.L., 2003, Geology of Canyonlands National Park, Utah. In: *Geology of Utah's National Parks and Monuments* (Ed by D.A. Sprinkel, T.C. Chidsey and P.B. Anderson), Utah Geological Association, Salt Lake, v. 28, p. 61-83.

Baars, D.L., and Stevenson, W.R., 1982, Subtle stratigraphic traps in the Palaeozoic rocks of the Paradox Basin. In: *The deliberate search for the stratigraphic trap* (Ed by Halbouty, M.T.), American Association of Petroleum Geologists Memoir 32, p. 131-158.

Bachrach, R., A. Nur, and A. Agon, 2001, Liquefaction and dynamic poroelasticity in soft sediments: *Journal of geophysical Research*, v. 106, no. B7, p. 13515-13526.

Baer, J.L. and Steed, R.H. 2003, Geology of Kodachrome Basin State Park, Utah, in Sprinkel, D.A., Chidsey, T.C., and Anderson, P.B., ed., *Geology of Utah's National Parks and Monuments 2nd Edition*: Utah Geological Association Publication, v. 28, p. 449-463.

Bailey, R. E., and W. A. Newman, 1978, Origin and significance of cylindrical sedimentary structures from the Boston Bay Group, Massachusetts: *American Journal of Science*, v. 278, p. 703-714.

Bahorich, M., and Farmer, S., 1995, 3D seismic discontinuity for faults and stratigraphic features: The coherence cube: *The Leading Edge*, v. 14, p. 1053-1058.

Barbeau, D.L., 2003, A flexural model for the Paradox Basin: implications for the tectonics of the Ancestral Rocky Mountains: *Basin Research*, v. 15, p. 97-115.

Barton, C. A., M. D. Zoback, and D. Moos, 1995, Fluid flow along potentially active faults in crystalline rocks: *Geology*, v. 12, p. 683-686.

Bates, D. E. B., 1975, Slaty cleavage associated with sandstone dykes in the Harlech Dome, North Wales: *Geological Journal*, v. 10, p. 167-175.

Beacom, L. E., T. B. Anderson, and R. E. Holdsworth, 1999, Using basement-hosted clastic dykes as syn-rifting palaeostress indicators: an example from the basal Stoer Group, NW Scotland: *Geological Magazine*, v. 136, p. 301-310.

Bear, J., 1972, *Dynamics of fluids and porous media*: American Elsevier Publishing Company, New York.

Beaudoin, B., O. Parize, G. Fries, M. Pinault, and H. Bensalem, 1986, Sills et dykes sédimentaires du flysch numinien du Tunisie septentrionale: étude préliminaire du secteur de Tabarka: Notes Service Géologique, Tunisie, v. 51, p. 3-37.

Beitler, B., Chan, M.A., and Parry, W.T., 2004, Bleaching of Jurassic Navajo Sandstone on the Colorado Plateau Laramide Highs: Evidence of exhumed hydrocarbon supergaints?: *Geology*, v. 31, iss. 12, p. 1041-1044.

Benjumea, B., Hunter, J.A., Aylesworth, J.M., and Pullan, S.E., 2003, Application of high-resolution seismic techniques in the evaluation of earthquake site response, Ottawa Valley, Canada: *Tectonophysics*, v. 386, p. 193-209.

Beutner, E., 1980, Slaty cleavage unrelated to tectonic dewatering: The Siamo and Michigamme Slates revisited: *Geological Society of America Bulletin*, v. 91, p. 171-178.

Bilodeau, W.L., 1986, The Mesozoic Mogollon Highlands, Arizona: and Early Cretaceous rift shoulder: *Journal of Geology*, v. 94, p. 724-735.

Bjerrum, C. J., and Dorsey, R. J., 1995, Tectonic controls on deposition of Middle Jurassic strata in a retroarc foreland basin, Utah-Idaho trough, western interior, United States: *Tectonics*, v. 14, no. 4, p. 962-978.

Bjølykke, K., 1997, Lithological control on fluid flow in sedimentary basins, in B. Jamtveit and B. W. D. Yardley, eds., *Fluid Flow and Transport in Rocks*, Chapman and Hall, New York, p. 15.

Blakey, R., Havholm, K., and Jones, L.S., 1996, Stratigraphic analysis of aeolian interactions with marine and fluvial deposits, Middle Jurassic Page Sandstone and Carmel Formation, Colorado Plateau, USA: *Journal of Sedimentary Research*, v. 66, p. 324-342.

Blakey, R., 1988, Basin tectonics and erg response: *Sedimentary Geology*, v. 56, p. 127-151.

Boehm, A., and J. C. Moore, 2002, Fluidised sandstone intrusions as an indicator of Palaeostress orientation, Santa Cruz, California: *Geofluids*, v. 2, p. 147-161.

Boldreel, L.O. and Andersen, M.S., 1998, Tertiary compressional structures on the Faroe-Rockall Plateau in relation to northeast Atlantic ridge-push and Alpine foreland stresses: *Tectonophysics*, v. 300, p. 13-28.

Bons, P. D., 2001, The formation of large quartz veins by rapid ascent of fluids in mobile hydrofractures: *Tectonophysics*, v. 336, p. 1-17.

Borradaile, G. J., 1982, Particulate flow, folds cleavage and magnetic fabrics: *Journal of Structural Geology*, v. 4, no. 2, p. 231.

Boulter, C. A., 1974, Tectonic deformation of soft sedimentary clastic dykes from the Precambrian rocks of Tasmania, Australia, with particular reference to their relations with cleavages: *Geological Society of America Bulletin*, v. 85, p. 1413-1420.

Boyd, D. W., D. E. Nice, and N. D. Newell, 1999, Silt injection as a mode of fossilization: a Triassic example: *Palaios*, v. 14, p. 545-554.

Brandon, A., 1972, Clastic Dykes in the Namurian shales of Co. Leintrim Republic of Ireland: *Geological Magazine* v. 109, p. 361-367.

Brill, K. G., 1955, Clastic limestone dykes, Ste. Genevieve County, Missouri: *Geological Society of America Bulletin*, v. 66, p. 1535.

Brooke, C.M., Trinble, T.J., and Mackay, T.A., 1995, Mounded shallow gas sands from the quaternary of the North Sea: analogues for the formation of sand mounds in deep water Tertiary sediments?, in A. J. Hartley, and D. J. Prosser eds., *Characterization of Deep Marine Clastic Systems: Geological society Special Publication*, No.94, p. 95-101.

Bump, A. P., 2004, Three-dimensional Laramide deformation of the Colorado plateau: competing stresses from the Sevier thrust belt and the flat Falleron Slab: *Tectonics*, v. 23, TC1008, doi: 10.1029/2002TC001424, 15 p.

Bunz, S., J. Meinert, and C. Berndt, 2003, Geological controls on the Storegga gas-hydrate system of the mid-Norwegian continental margin: *Earth and Planetary Science Letters*, v. 203, no. 3-4, p. 291-307.

Burgess, P.M., and Moresi, L.N., 1999, Modelling rates and distribution of subsidence due to dynamic topography over subducting slabs: is it possible to identify dynamic topography from ancient strata?: *Basin Research*, v. 11, p. 305-314.

Burgess, P.M., Gurnis, M., and Moresi, L., 1997, Formation of sequences in the cratonic interior of North America by interaction between mantle, eustatic, and stratigraphic processes: *Geological Society of America Bulletin*, v. 108, no. 12, p. 1515-1535.

Caputo, M.V., 2000, Geology of the Paria Canyon-Vermilion Cliffs wilderness, Utah and Arizona. In: *Geology of Utah's National Parks and Monuments* (Ed by D.A. Sprinkel, T.C. Chidsey & P.B. Anderson), Utah Geological Association, Salt Lake, v. 28, p. 531-561.

Carman, P. C., 1937, Fluid flow through a granular bed: *Transactions of the Institution of Chemical Engineers*, v. 15, p. 150-167.

Carson, R. J., C. F. McKhann, and M. H. Pizey, 1978, The Touchet beds of the Walla Walla Valley, in V. R. Baker and D. Nummedal eds., *The Channeled Scablands*.

Cartwright, J.A., and Lonergan, L., 1996, Volumetric contraction during the compaction of mudrocks: a mechanism for the development of regional scale polygonal fault systems: *Basin Research*, v. 8, p. 183-193.

Cartwright, J.A., 1994, Episodic basin-wide fluid expulsion from geopressured shale sequences in the North Sea basin: *Geology*, v. 22, no. 5, p. 447-450.

Cartwright, J.A., 1989, The kinematics of inversion in the Danish central graben: In: Cooper, M.A., and Williams, G.D. (eds.), *Inversion tectonics: Geological Society [London] Special Publication 44*, p. 153-175.

Cather, S. M., 1999, Implications of Jurassic, Cretaceous and Proterozoic piercing lines for Laramide oblique-slip faulting in New Mexico and rotation of the Colorado Plateau: *Geological Society of America Bulletin*, v. 111, no. 6, p. 849-868.

Catuneau, O., 2004, Retroarc foreland systems – evolution through time: *Journal of African Earth Sciences*, v. 38, p. 225-242.

Ceciele, M. P., and F. H. A. Campbell, 1977, Large scale stratiform and intrusive sedimentary breccias of the lower Proterozoic Goulburn Group, Bathurst Inlet, N.W.T: *Canadian Journal of Earth Sciences*, v. 14, p. 2364-2387.

Chan, M.A., Parry, W.T., and Bowman J.R., 2000, Diagenetic hematite and manganese oxides and fault-related fluid flow in Jurassic sandstones, southeastern Utah: *AAPG Bulletin*, v. 84, p. 1281-1310.

Chopra, S., 2002, Coherence cube and beyond: *First Break*, v. 20.1, p. 27-33.

Chown, E. H., and A. Gobeil, 1990, Clastic dykes of the Chibougamau Formation: Distribution and origin: *Canadian Journal of Earth Sciences*, v. 27, p. 1111-1114.

- Cole, D., S. A. Stewart, and J. A. Cartwright, 2000, Giant pockmark craters in the Palaeogene of the outer Morray Firth Basin, UK North Sea: *Marine and Petroleum Geology*, v. 6, p. 275-285.
- Cooper, A. K., and P.E. Hart, 2002, High-resolution seismic-reflection investigation of the northern Gulf of Mexico gas-hydrate-stability zone: *Marine and petroleum Geology*, v. 19, no. 10, p. 1275-1293.
- Cosgrove, J. W., 1995, The expression of hydraulic fracturing in rocks and sediments, in: M. S. Ameen, ed., *Fractography: fracture topography as a tool in fracture mechanics and stress analysis*, Geological Society Special Publication, No.92, p. 187-196.
- Crabaugh, M., and Kockurek, G., 1993, Entrada Sandstone: an example of a wet aeolian system, In Pye, K., (ed.), *The dynamics and Environmental Context of Aeolian Sedimentary Systems: Geological Society Special Publication 72*, p. 103-126.
- Cross, W., 1893, Intrusive sandstone dykes in granite: *Bulletin of the Geological Society of America*, v. 5, p. 225-230.
- Currie, B.S., 1998, Upper Jurassic-Lower Cretaceous Morrison and Cedar Mountain Formations, NE Utah-NW Colorado: Relationships between nonmarine deposition and early Cordilleran foreland-basin development: *Journal of Sedimentary Research*, v. 68, no. 4, p. 632-652.
- Das, M. B., 1993, *Principles of Soil Dynamics*: PWS-Kent, Boston, Massachusetts.
- Dearman, W. R, E. E. Freshney, A. F. King, M. Williams, and M. C. McKeown, 1970. *Geological Association Guides*, no.10, *The North Coast of Cornwall*: Geological Association, London.
- Davies, R., Cloke, I., Cartwright, J., Robinson, A., and Ferrero, C., 2004, Post break-up compression of a passive margin and its impact upon hydrocarbon prospectivity: An example from the Tertiary of the Faroe-Shetland Basin, UK: *American Association of Petroleum Geologists Bulletin* 88-1, p. 1-20.
- Davies, R. J., 2003, Kilometer-scale fluidisation structures formed during early burial of a deep-water slope channel on the Niger Delta: *Geology*, v. 31, no. 11, p. 949-952.
- Davies, R., and Cartwright, J., 2002, A fossilized opal A to opal C/T transformation on the northeast Atlantic margin: Support for a significantly elevated palaeogeothermal gradient during the Neogene?: *Basin Research*, v. 14, p. 467-486.
- Davies, R.J., Bell, B., Cartwright, J.A., and Shoulders, S., 2002, Three-dimensional seismic imaging of dyke-fed submarine volcanoes: *Geology*, v. 30, p. 223-226.

- Davies, R., Cartwright, J., Pike, J., and Line, C., 2001, Early Oligocene initiation of North Atlantic Deep Water formation: *Nature*, v. 410, p. 467–486.
- Dean, K., McLachlan, K., and Chambers, A., 1999, Rifting and the development of the Faroe-Shetland Basin, In Fleet, A.J., and Boldy, S.A.R., eds., *Petroleum geology of Northwest Europe: Proceedings of the 5th conference*: London, Geological Society, p. 533–544.
- De Celles, P.G., and Currie, B.S., 1996, Long-term sediment accumulation in the middle Jurassic- early Eocene Cordilleran retroarc foreland-basin system: *Geology*, v. 24, no. 7, p. 591-594.
- De Gibert, J.M., and Ekdale, A.A., 1999, Trace fossil assemblages reflecting stressed environments in the Middle Jurassic Carmel Seaway of central Utah: *Journal of Palaeontology*, v. 73, no. 4, p. 711-720.
- Delaney, P. T., and D. D. Pollard, 1981, Deformation of host rocks and flow of magma during growth of minette dykes and breccia bearing intrusions near Ship Rock, New Mexico: US Geological Survey Professional Paper, 1202.
- Delaney, P. T., D. D. Pollard, J. I. Ziony, and E. H. McKee, 1986, Field relations between dykes and joints: emplacement processes and palaeostress analysis: *Journal of Geophysical Research* v. 91, p. 4920-4938.
- Dewhurst, D.N., Cartwright, J.A., and Lonergan, L., 1999, The development of polygonal fault systems by syneresis of colloidal sediments: *Marine and Petroleum Geology*, v. 16, p. 793-810.
- Deynoux, M., J. N. Proust, J. Durand, and E. Merino, 1990, Water-transfer cylindrical structures in the Late Proterozoic aeolian sandstones in the Taoudeni Basin, West Africa: *Sedimentary Geology*, v. 66, p. 227-242.
- Dickerson, P.W., 2003, Intraplate mountain building in response to continent-continent collision – the Ancestral Rocky Mountains (North America) and inferences drawn from the Tien Shan (Central Asia): *Tectonophysics*, v. 365, p. 129-142.
- Dickinson, W. R. and Gehrels, G. E., 2003, U-Pb ages of detrital zircons from permian and Jurassic aeolian sandstones of the Colorado Plateau, USA: palaeogeographic implications: *Sedimentary Geology*, v. 163, p. 29-66.
- Dickinson, W. R., and Lawton, T. F., 2001, Sequential intercontinental suturing as the ultimate control for Pennsylvanian Ancestral Rocky Mountain deformation: *Geology*, v. 31, no. 7, p. 609-612.

Dickinson, W. R., 2000, Geodynamic interpretation of Palaeozoic tectonic trends orientated oblique to the Mesozoic Klamath-Sierran continental margin in California, In: Soreghan, M. J., and Gehrels, G. E., (eds), Palaeozoic and Triassic palaeogeography and tectonics of western Nevada and northern California: Geological Society of America Special Paper 347, p. 209-245.

DiFelice, R., 1995, Hydrodynamics of Liquid Fluidisation: *Chemical Engineering Science*, v. 50, no. 8, p. 1213-1245.

DiFelice, R., 1998, The applicability of the pseudo-fluid model to the settling velocity of a foreign particle in a suspension: *Chemical Engineering Science*, v. 53, no. 2, p. 371-375.

DiFelice, R., Foscolo, P.U., Gibilaro, L.G., and Rapagna, S., 1991, The interaction of particles with a fluid-particle pseudo-fluid: *Chemical Engineering Science*, v. 46, p. 1873-1877,

DiFelice, R., Foscolo, P.U., and Gibilaro, L.G., 1989, The experimental determination of the interaction force on spheres submerged in liquid fluidised beds: *Chemical Engineering and Processing*, v. 25, p. 27-34.

Diller, J. S., 1889, Sandstone dykes: *Geological Society of America Bulletin*, v. 1, p. 411-442.

Dionne, J. C., and Shilts, 1974, A Pleistocene clastic dyke, Upper Chaudiere Valley, Quebec: *Canadian Journal of Earth Sciences*, v. 11, v. 1594-1605.

Diraison, M., Cobbald, P.R., Gapais, D., Rossello, E.A., and Le Corre, C., 2000, Cenozoic crustal thickening, wrenching and rifting in the foothills of the southernmost Andes: *Tectonophysics*, v. 316, p. 91-119.

Diraison, M., Cobbald, P.R., Gapais, D., and Rossello, E.A., 1997, Magellan straight: part of a Neogene rift system: *Geology*, v. 25, no. 8, p. 703-706.

Dixon, R. J., K. Schofield, R. Anderton, A. D. Reynolds, R. W. S. Alexander, M. C. Willaims, and K. G. Davies, 1995, Sandstone diapirism and clastic intrusion in the Tertiary Submarine fans of the Burce-Beryl Embayment, Quad 9, UKCS, in A. J. Hartley, and D. J. Prosser eds., *Characterization of Deep Marine Clastic Systems: Geological society Special Publication, No.94*, p. 77-94.

Doelling, H. H., and Davis, F. D., 1989, The geology of Kane County Utah: *Utah Geological and Mineral Survey Bulletin*, v. 124, 192p.

Domenico, P. A., and F. W. Schwartz, 1990, *Physical and chemical hydrogeology*: John Wiley and Sons, Inc, 824 p.

Doré, A.G., Lundin, E.R, Jensen, L.N., Birkeland, O., Eliassen, P.E., and Fichler, C., 1999, Principal tectonic events in the evolution of the Northwest European Atlantic Margin, In Flett, A.J., and Boldy, S.A.R., (eds.), *Petroleum geology of northwest Europe: Proceedings of the 5th conference*: Geological Society, London, p. 41-61.

Dott, R. H., 1966, Cohesion and flow phenomena in clastic intrusions: *AAPG Bulletin*, v. 50, p. 610-611.

Downie, R. A., and C. L. Stedman, 1993, Complex deformation and fluidization structures in Aptian sediment gravity flow deposits of the Outer Moray Firth, in J. R. Parker, ed., *Petroleum geology of NW Europe: proceedings of the 4th Conference*, v. 1, p. 185-188.

Dragantis, E., Grasmann, B., and Schmid, H.P., 2003, Fluidisation pipes and spring pits in a Gondwana barrier-island environment: ground water phenomenon, palaeo-seismicity or a combination of both? In: *Subsurface sediment Mobilization*. Ed by Van Rensburgen, P., Hillis, R.R., Maltman, A. J., & Morley, C. K.), Geological Society, London, Special Publication 216, p. 109-137.

Druitt, T. H., 1995, Settling behaviour of concentrated dispersions and some volcanological applications: *Journal of Volcanology and Geothermal Research*, v. 65, p. 27-39.

Duranti, D., and Hurst, A., Fluidization and injection in the deep-water sandstones of the Eocene Alba Formation (UK North Sea), 2004, *Sedimentology*, v. 51, p. 503-529.

Duranti, D., A. Hurst, C. Bell, S. Groves, and R. Hanson, 2002, Injected and remobilized Eocene sandstones from the Alba Field, UKCS: core and wireline log characteristics: *Petroleum Geoscience*, v. 8, p. 99-107.

Eichhubl, P., and J. R. Boles, 2000, Rates of fluid flow in fault systems - evidence for episodic rapid fluid flow in the Miocene Monterey Formation, coastal California: *American Journal of Science*, v. 300, p. 571-600.

Eisbacher, G. H., 1969, Contemporaneous Faulting and Clastic intrusions in the Quirke Lake Group, Elliot Lake, Ontario: *Canadian Journal of Earth Sciences*, v. 7, p. 215-225.

Elbert-Phillips, D., P. J. Haeussler, J. T. Freymueller, A. D. Frankel, C. M. Rubin, P. Craw, N. A. Ratchovski, G. Anderson, G. A. Carver, A. J. Crone, T. E. Dawson, H. Fletcher, R. Hansen, E. L. Harp, R. A. Harris, D. P. Hill, S. Hreinsdóttir, R. W. Jibson, L. M. Jones, R. Kayen, D. K. Keefer, C. F. Larsen, S. C. Moran, S. F. Personius, G. Plafker, B. Sherrod, K. Sieh, N. Sitar, and W. K. Wallace,

2003, The 2002 Denali Fault earthquake, Alaska: A large magnitude, slip-partitioned event: *Science*, v. 300, p. 1113-1118.

Elson, 1975, Origin of a clastic dyke at St.Ludger, Quebec: An alternative hypothesis: *Canadian Journal of Earth Science*, v. 12, p. 1048-1053.

Enzel, Y., Kadan, G. and Eyal, Y., 2000, Holocene earthquakes inferred from a fan-delta sequence in the Dead sea Graben: *Quaternary Research*, v. 53, p. 34-48.

Ergun, S., 1952, Fluid Flow Through Packed Column: *Chemical Engineering Progress*, No. 48, pp. 199-254.

Fielding, C. R., and G. A. L. Johnson, 1987, Sedimentary structures associated with extensional fault movement from the Westphalian of NE England, in M. P. Coward, M. F. Dewey, and P. L. Hancock eds., *Continental extensional tectonics: Geological Society Special Publication*, No.28, p. 511-516.

Fisher, Q. J., S. D. Harris, E. McAllister, R. J. Knipe, A. J. Bolton, 2001, Hydrocarbon flow across faults by capillary leakage revisited: *Marine and Petroleum Geology*, v. 18, p. 251-257.

Flekkøy E. G., A. Malthe-Sørenssen and B. Jamtveit, 2002, Modelling hydrofracture: *Journal of Geophysical Research*, v. 107, no. B8, p. 1-11.

Friès, G., and Parize, O., 2003, Anatomy of ancient passive margin slope systems: Aptian gravity-driven deposition on the Vocontian palaeomargin, western Alps, southeastern France: *Sedimentology*, v. 50, p. 1231-1270. doi:10.1111/j.1365-3091.2003.00601.x

Fyfe, W. S. N., N. Price and A. V. Thompson, 1978, *Fluids in the Earth's Crust*: Elsevier Science, Amsterdam, 383 p..

Galli, P., 2000, New empirical relationships between magnitude and distance for liquefaction: *Tectonophysics*, v. 324, p. 169-187.

Gallo, F., and Woods, A. W., 2004, On steady homogeneous sand-water flows in a vertical conduit: *Sedimentology*, v. 51, p. 195-210.

Gay, A., Lopez, M., Cochonat, P., and Sermondadz, G., 2004, Polygonal faults-furrows system related to early stages of compaction – upper Miocene to recent sediments of the Lower Congo Basin: *Basin Research*, v. 16, p. 101-116.

Gibb, F.G.F., and R. Kanaris-Sotiriou, 1988, The geochemistry and origin of the Faroe-Shetland sill complex, in A. C. Morton, and L. M. Parson, eds., *Early Tertiary volcanism and the opening of the northeast Atlantic*: Geological Society [London] Special Publication 39, p. 241-252.

Gilbertson, M. A., and I. Eames, 2001, Segregation patterns in gas-fluidized systems: *Journal of Fluid Mechanics*, v. 433, p. 347-356.

Gill, W. D., and P. H. Kunen, 1957, Sand volcanoes on the slumps in the Carboniferous of County Claire, Ireland: *Quarterly Journal of the Geological Society*, London, v. 113, p. 441-460.

Gomberg, J., Bodin, P., Larson, K., and Dragert, H., 2004, Earthquake nucleation by transient deformations caused by the M=7.9 Denali, Alaska, earthquake: *Nature*, v. 427, p. 621-624.

Goto, Y., and J. McPhie, 1996, A Miocene basanite pepritic dyke at Stanley, northwestern Tasmania, Australia: *Journal of Volcanology and Geothermal Research*, v. 74, p. 111-120.

Gottis, C., 1953, Les filons clastiques "infrarformationnels" du "flysch" numidien Tunisien: *Bulletin de la Societe Geologique de France*, ser. 6, t. 3, p. 775-783.

Goult, N.R., 2001, Mechanics of layer-bound polygonal faulting in fine-grained sediments: *Journal of the Geological Society*, London, v. 159, p. 239-246.

Gras, R., and J. A. Cartwright, 2002, Tornado faults: the seismic expression of the Early Tertiary on PS-data, Chesnut Field UK North Sea: 64th EAGE Conference and Exhibition, Florence (Extended Abstract H020).

Gudmundsson, A., 2001, Fluid overpressure and flow in fault zones: field measurements and models: *Tectonophysics*, v. 336, p. 183-197.

Guhman, A.I., and Pederson, D.T., 1992, Boiling sand springs, Dismal River, Nebraska: Agents for formation of vertical cylindrical structures and geomorphic change: *Geology*, v. 20, p. 8-10.

Hall, A., and Bishop, P., 2002, Scotland's denudation history: An integrated view of erosion and sedimentation at an uplifted passive margin: In Dore, A.G., et al., eds., *Exhumation of the North Atlantic margin: Timing, mechanisms and implications for petroleum exploration*: Geological Society [London] Special Publication 196, p. 13-25.

Hansen, D.M., Cartwright, J.A., and Thomas, D., 2004, 3D seismic analysis of the geometry of igneous sills and sill junction relationships, in Davies, R.J., Cartwright, J.A., Stewart, S.A., Lappin, M., and

Underhill, J.R., eds, 3D seismic technology: application to the exploration of sedimentary basins: Geological Society, London, Memoirs, 29, p. 199-208.

Hansen, J.P.V., Cartwright, J.A., Huuse, M., and Clausen, O.R., 2005, 3D seismic expression of fluid migration and mud remobilization on the Gjallar Ridge, offshore mid-Norway: Basin Research, v. 17, p. 123-139.

Hannum, C., 1980, Sandstone and conglomerate-breccia pipes and dykes of the Kodachrome Basin area, Kane County, Utah: Brigham Young University Geological Studies, v. 27, p. 31-50.

Harland, W.B., Armstrong, R.L., Cox, A.V., Craig, L.E., Smith, A.G., and Smith, D.G., 1990, A geologic time scale, 1989 edition: Cambridge, Cambridge University Press, 263 p.

Harms, J. C., 1965, Sandstone dykes in relation to Laramide faults and stress distribution in the Southern Front Range, Colorado: Geological Society of America Bulletin v. 76, p. 981-1002.

Hawley, J. E., and R. C. Hart, 1934, Cylindrical structures in sandstones: Geological Society of America Bulletin, v. 45, p. 1017-1034.

Hayashi, T., 1968, Clastic dykes in Japan: Japanese Journal of Geology and Geography, v. 37, p. 1-20.

Heller, P.L., Deuker, K., and McMillan, M. E., 2003, Post-Palaeozoic alluvial gravel transport as evidence of continental tilting in the U.S. Cordillera: Geology Society of America Bulletin, v. 115, no. 9, p. 1122-1132.

Henriet, J.P., Batist, M.D., and Verschuren, M., 1991, Early fracturing of Palaeogene clays, southernmost North Sea: Relevance to mechanisms of primary hydrocarbon migration, In Spenser, A.M. (ed), Generation, accumulation and production of Europe's hydrocarbons: Special Publications of the European Association of Petroleum Geologists, no.1 217-227.

Hillier, R.D., and J. W. Cosgrove, 2002, Core and seismic observations of overpressure-related deformations within Eocene sediments of the Outer Moray Firth, UKCS: Petroleum Geoscience, v. 8, p. 141-149.

Hintze, L. F., 1988, Geologic History of Utah: A field guide to Utah's rocks: Brigham Young University, Provo, Utah, 202 p.

Hiscott, R. N., 1979, Clastic sills and dykes associated with deep-water sandstones, Tourelle Formation, Ordovician, Quebec: Journal of Sedimentary Petrology, v. 49, p. 1-10.

Holmes, A.J., Griffith, C.E., and Scotchman, I.C., 1999, The Jurassic petroleum system of the West of Britain Atlantic margin – an integration of tectonics, geochemistry and basin modeling. In Flett, A.J., and Boldy, S.A.R., (eds.), *Petroleum geology of northwest Europe: Proceedings of the 5th conference*: Geological Society, London, p. 41-61

Hovland, M., and Judd, A.G., 1988, *Seabed pockmarks and seepages: impact on geology, biology and the marine environment*: Graham and Trotman, London, United Kingdom.

Huang, Q., 1988, Geometry and tectonic significance of Albian sedimentary dykes in the Sisteron area, SE France: *Journal of Structural Geology*, v. 10, no. 5, p. 453-462.

Hunter, R.E., Gelfenbaum, G., and Rubin, D.M., 1992, Clastic pipes of probable solution collapse origin in Jurassic rocks of the southern San Juan Basin, New Mexico: *U.S. Geological Survey Bulletin*, 1808, Chapter L, L1-L17.

Huntoon, P.W., 2000, Upheaval Dome, Canyonlands Utah: Strain indicators that reveal an impact origin. In: Sprinkle, D.A., Chidsey, T.C., & Anderson, P.B. (eds.), *Geology of Utah's Parks and Monuments*, Utah Geological Association Publication 28, 619-628.

Hurst, A., Cartwright, J., Huuse, M., Jonk, R., Schwab, A., Duranti, D., and Cronin, B., 2003, Significance of large-scale sand injectites as long-term fluid conduits: evidence from seismic data, *Geofluids*, v. 3, p. 263-274.

Huuse, M., Cartwright, J., Gras, R. and Hurst, A., In Press, Km-scale sandstone intrusions in the Eocene of the Outer Moray Firth (UK North Sea): migration paths, reservoirs, and potential drilling hazards: In: Doré, A.G. & Vining, B. (eds) *Petroleum Geology of NW Europe: Proceedings of the 6th Conference*, Geological Society, London, In Press.

Huuse, M., Shoulders, S.J., Netoff, D.I., and Cartwright, J., 2005, Giant sandstone pipes record basin-scale liquefaction of buried dune sands in the Middle Jurassic of SE Utah: *Terra Nova*, v. 17, p. 80-85.

Huuse, M., and Mickelson, M., 2004, Eocene sandstone intrusions in the Tampen Spur area (Norwegian North Sea Quad 34) imaged by 3D seismic data: *Marine and Petroleum Geology*, v. 21, iss. 2, p. 141-155.

Huuse, M. & Cartwright, J. 2004, Sandstone intrusions: Reservoirs and fluid conduits through sealing sequences: *Proceedings of EAGE Conference: Faults and Top Seals: What do we know and where do we go?* Montpellier, France, 8-11 September 2003, P-11, 1-10.

Huuse, M., Duranti, D., Steinsland, N., Guargena, C.G., Prat, P., Holm, K., Cartwright, J.A., and Hurst, A., 2004, Seismic characteristics of large-scale sandstone intrusions in the Palaeogene of the South Viking Graben, UK and Norwegian North Sea. In Davies, R.J., Cartwright, J.A., Stewart, S.A., Lappin, M., and Underhill, J.R., (eds), *Seismic technology: Application to the exploration of sedimentary basins*: Geological Society, London, Memoirs, no. 29, p. 263-277.

Huuse, M., Duranti, D., Guargena, C.G., Prat, P., Holm, K., Steinsland, N., Cronin, B.T., Hurst, A., and Cartwright, J., 2003, Sandstone intrusions: detection and significance for exploration and production: *First Break*, v. 21, p. 15-24.

Huuse, M., Duranti, D., Cartwright, J.A., Hurst, A., and Cronin, B., 2001, Seismic expression of large-scale sand remobilisation and injection in Palaeogene reservoirs of the North Sea Basin and beyond: 63rd EAGE Conference and Exhibition, Amsterdam, Extended Abstracts, L07.

Illiffe, J.E., Robertson, A.G, Ward, G.H.F, Wynn, C., Pead, S.D.M, and Cameron, N, 1999, The importance of fluid pressures and migration to the hydrocarbon prospectivity of the Faroe-Shetland White Zone. In: Flett, A.J., and Boldy, S.A.R., (eds.), *Petroleum geology of northwest Europe: Proceedings of the 5th conference*: Geological Society, London, p. 601-611.

Imlay, R.W., 1980, Jurassic palaeobiogeography of the conterminous United States in its continental setting: U.S Geological Survey Professional Paper 1062.

Jackson, M. P. A., D. D. Schultz-Ela, M. R. Hudec, I. A. Watson and M. L. Porter, 1998, Structure and evolution of Upheaval Dome: A pinched-off salt diapir, *Geological Society of America Bulletin*, v. 110, no. 12, p. 1547-1573.

James, D. M. D., 2003, Discussion on mechanisms and controls on the formation of sand intrusions: *Journal of the Geological Society of London*, v. 160, p. 1-3.

Janke, N. C., 1970, Intrusive sandstone dykes in the Siamo Slate near Negaunee, Michigan: *Discussion: Geological Society of America Bulletin*, v. 81, p. 3179-3180.

Jenkins, O. P., 1930, Sandstone dykes as conduits for oil migration through shales: *AAPG Bulletin*, v. 14, p. 411-421.

Jenssen, A. I., D. Bergslien, M. Rye-Larsen, and R. M. Lindholm, 1993, Origin of complex mound geometry of Palaeocene submarine-fan sandstone reservoirs, Balder Field, Norway, in J. R. Parker ed., *Petroleum geology of NW Europe: proceedings of the 4th Conference*, v. 1, p. 135-143.

Johansson, J., N. E. Braakenburg, D. A. V. Stow, and J. C. Faugeres, 1988, Deep-water massive sands: facies, processes and channel geometry in the Numidian Flysch, Sicily: *Sedimentary Geology*, v. 115, p. 223-265.

Johnson, A. M., and D. D. Pollard, 1973, Mechanics of growth of some laccolithic intrusions in the Henry Mountains, Utah, I: *Tectonophysics*, v. 18, p. 261-309.

Jolly, R. J. H., J. W. Cosgrove, and D. N. Dewhurst, 1998, Thickness and spatial distributions of clastic dykes, northwest Sacramento Valley, California: *Journal of Structural Geology*, v. 20, p. 1663-1672.

Jolly, R. J. H., and L. Lonergan, 2002, Mechanisms and controls on the formation of sand intrusions: *Journal of the Geological Society, London*, v. 159, p. 605-617.

Jones, G. H. S., 1977, Complex craters in alluvium, in D. J. Roddy, R. O. Pepin, and R. D. Merrill, eds., *Impact and explosion cratering*: Pergamon Press, New York, p. 163-183.

Jonk, R., Mazzini, A., Duranti, D., Parnell, J., Cronin, B., and Hurst, A., 2003(a), Fluid escape from reservoirs: implications from cold seeps, fractures and injected sands Part 2. The fluids involved: *Journal of Geochemical Exploration*, v. 78-79, p. 297-300.

Jonk, R., Duranti, D., Parnell, J., Hurst, A., and Fallick, A.E., 2003(b), The structural and diagenetic evolution of injected sandstones: examples from the Kimmeridgian of NE Scotland: *Journal of the Geological Society, London*, v. 164, p. 881-894.

Jowitt, R., Hindle, A., Jones, D., and Rose, p., 1999, Petroleum systems analysis of the Palaeocene play in the West of Shetland area. In: Flett, A.J., and Boldy, S.A.R., (eds.), *Petroleum geology of northwest Europe: Proceedings of the 5th conference*: Geological Society, London, p. 1367-1381.

Judd, J. W., 1873, The secondary rocks of Scotland (Part 1 - Strata of the Eastern Coast): *Quarterly Journal of the Geological Society, London*, v. 29, p. 97-195.

Kalinichev, A. G., 2001, Molecular simulations of liquid and super critical water: Thermodynamics, structure and hydrogen bonding, in R. T. Cygan and K. B. Kubicki, eds., *Molecular modelling theory: Applications in the geosciences: Reviews in Mineralogy and Geochemistry*, v. 42, Mineralogical Society of America, Washington D.C., p. 83-130.

Kanbur, Z., J. N. Louie, S. Chavez-Perez, G. Plank, D. Morey, 2000, Seismic reflection study of Upheaval Dome, Canyonlands National Park, Utah: *Journal of Geophysical Research – Planets* v. 104, E4, p. 9489-9505.

Kano, K., 2002, Middle Miocene volcanoclastic dykes at Kukedo, Shimane Peninsula, SW Japan: fluidisation of volcanoclastic beds by emplacement of syn volcanic andesitic dykes: *Journal of Volcanology and Geothermal Research*, v. 114, p. 81-94.

Kenkman, T., 2003, Dyke formation, cataclastic flow, and rock fluidization during impact cratering: an example from the Upheaval Dome structure, Utah: *Earth and Planetary Science Letters*, v. 214, p. 43-58.

Kenkman, T., and Scherler, D., 2002, New structural constraints on the formation of the Upheaval Dome impact crater: *Lunar and Planetary Science Conference Abstracts*, v. 33, abstract no. 1037.

Kennedy, B., Stix, J., Vallance, J.W., Lavallée, Y., and Longpré, M.A., 2004, Controls on caldera structure: results from analogue sandbox modelling: *Geological Society of America Bulletin*, v. 116, iss. 5/6, p. 515-524.

Knox, R.W.O'B., Holloway, S., and Bailey, H.E., 1997, Stratigraphic nomenclature of the UK northwest margin, 2: Early Palaeogene lithostratigraphy and sequence stratigraphy: *British Geological Survey, Nottingham*.

Knutz, P.C., and Cartwright, J., 2003, Seismic stratigraphy of the West Shetland Drift: Implications for later Neogene palaeocirculation in the Faroe-Shetland gateway: *Palaeoceanography*, v. 18, no. 4, p. 1-11, 1093 doi: 10.1029/2002PA000786.

Kokelaar, B. P., 1982, Fluidization of wet sediments during the emplacement and cooling of various igneous bodies: *Journal of the Geological Society, London*, v. 139, p. 21-33.

Kolymbas, D., 1998, Behaviour of liquefied sand: *Philosophical Transactions of the Royal Society, London, A* 356, p. 2609-2622.

Kowalis, B.J., Christiansen, E.H., Deino, A.L., Zhang, C., and Everett, B.H., 2001, The record of Middle Jurassic volcanism in the Carmel and temple cap Formations of southwestern Utah: *Geological Society of America Bulletin*, v. 113, no. 3, p. 373-387.

Kugler, H.G., 1938, *Nature and Significance of Sedimentary Volcanism: Science of Petroleum*, v. 1, Oxford University Press, p.297-299.

King, D. T., 1998, Wetumpka Melange, a new stratigraphic unit in Alabama: *Gulf Coast Association of Geological Societies Transactions*, v. 48, p. 151-158.

Kriens, B. J., E. M. Shoemaker, and K. E. Herkenhoff, 1999, Geology of Upheaval Dome impact structure, southeast Utah: *Journal of Geophysical Research*, v. 104, no. E8, p. 18867-18887.

Kunii, D., and O. Levenspiel, 1991, *Fluidisation Engineering*, 2nd ed, Butterworth, London.

Larsen, E., and J. Mangerud, 1992, Subglacially formed clastic dykes: *Sveriges Geologiska Undersökning*, v. 81, p. 163-170.

Leva, M., 1959, *Fluidisation*: McGraw-Hill, New York.

Lewis, D. W., 1973, Polyphase limestone dykes in the Omaru Region, New Zealand: *Journal of Sedimentary Petrology*, v. 43, p. 1031-1045.

Li, Y., G. Q. Yang, J. P. Zhang, and L. S. Fan, 2001, Numerical studies of bubble formation dynamics in gas-liquid-solid fluidisation at high pressures: *Powder Technology*, v. 116, p. 246-260.

Lister, J. R., 1990a, Buoyancy-driven fluid fracture: the effects of material toughness and of low-viscosity precursors: *Journal of Fluid Mechanics*, v. 210, p. 263-280.

Lister, J. R., 1990b, Buoyancy driven fluid fracture: similarity solutions for the horizontal and vertical propagation of fluid filled cracks: *Journal of Fluid Mechanics*, v. 217, p. 213-239.

Lister, J. R., 1991, Steady solutions for feeder dykes in a density-stratified lithosphere: *Earth and Planetary Science Letters*, v. 107, p. 233-242.

Liu, L., and Y. Li, 2001, Identification of liquefaction and deformation features using ground penetrating radar in the New Madrid seismic zone, USA: *Journal of Applied Geophysics*, v. 47, p. 199-215.

Lonergan, L., and J. A. Cartwright, 1999, Polygonal faults and their influence on deepwater sandstone reservoir geometries, Alba Field, UK Central North Sea: *AAPG Bulletin*, v. 83, p. 410-432.

Lonergan, L., N. Lee, H. D. Johnson, J. A. Cartwright, and R. J. H. Jolly, 2000, Remobilisation and injection in deepwater depositional systems: Implications for reservoir architecture and prediction: GCSSEPM Foundation 20th Annual Research Conference Deep-water Reservoirs of the World. (3rd to 6th Dec).

Løseth, H., Wensaas, L., Arntsen, B., and Hovland, M., 2003, Gas and fluid injection triggering shallow mud mobilization in the Hordaland Group, North Sea. In Van Rensburgen, P., Hillis, R.R.,

Maltman, A.J., and Morley, C.K. (eds.), *Subsurface Sediment Mobilization*: Geological Society, London, Special Publications 216, p. 139-157.

Loseth, H., Wensaas, Arntsen, B., Hanken, N., Basire, C., and Graue, K., 2001, 1000 m long gas blow-out pipes: 63rd EAGE Conference & Exhibition, Amsterdam, Extended Abstracts, P524.

Lowe, D. R., and R. D. LoPiccolo, 1974, The characteristics and origins of dish and pillar structures: *Journal of Sedimentary Petrology*, v. 44, no. 2, p. 484-501.

Lowe, D. R., 1975, Water escape structures in coarse-grained sediments: *Sedimentology*, v. 22, p. 157-204

MacLeod, M. K., R. A. Hanson, C. R. Bell, and S. McHugo, 1999, The Alba field ocean bottom cable seismic survey: Impact on development: *The Leading edge*, v. 18(November), p. 1306-1312.

Mahaney, W.C., Milner, M.W., Netoff, D.I., Malloch, D., Dohm, J.M., Baker, V.R., Miamoto, H., Hare, T.M., and Komatsu, G., 2004, Ancient wet aeolian environments on Earth: clues to presence of fossil/live microorganisms on Mars: *Icarus*, v. 171, p. 39-53.

Marshak, S., Karlstrom, K., and Timmons, J.M., 2000, Inversion of Proterozoic extensional faults: an explanation for the pattern of Laramide and Ancestral Rockies intracratonic deformation, United States: *Geology*: v. 28, no. 8, p. 735-738.

Martain, A.J., 2000, Flaser and wavy bedding in ephemeral streams: a modern and an ancient example: *Sedimentary Geology*, v. 136, p. 1-5.

Martill, D. M., and J. D. Hudson, 1989, Injection clastic dykes in the Lower Oxford Clay (Jurassic) of central England: relationship to compaction and concretion formation: *Sedimentology*, v. 36, p. 1127-1133.

Martell, A. T., and M. R. Gibling, 1993, Clastic dykes of the Devonian-Carboniferous Horton Bluff Formation, Nova Scotia; storm related structures in shallow lakes: *Sedimentary Geology*, v. 87, p. 103-119.

Massari, F., G. Ghibaud, A. D'Alessandro and E. Davaud, 2001, Water-upwelling pipes and soft-sediment-deformation structures in lower Pleistocene calcarenites (Salento, southern Italy): *Geological Society of America Bulletin*, v. 113, p. 545-560.

Maxwell, J. C., 1962, Origin of slaty and fracture cleavage in the Delaware Water Gap Area, New Jersey and Pennsylvania: *Geological Society of America, Buddington Volume*, p. 281-311.

- Mazzini, A., Jonk, R., Duranti, D., Parnel, J., Cronin, B., and Hurst, A., 2003, Fluidescape from reservoirs: implications from cold seeps, fractures and injected sands Part 1. The fluid flow system: *Journal of Geochemical Exploration*, v. 78-79, p. 293-296.
- McCallum, M.E., 1985, Experimental evidence for fluidisation processes in breccia pipe formation: *Economic Geology*, v. 80, p. 1523-1543.
- McManus J., and S. Bajabaa S, 1998, The importance of air escape processes in the formation of dish-and-pillar and teepee structures within modern and Precambrian fluvial deposits: *Sedimentary Geology*, v. 120, no. 1-4, p. 337-343.
- McMillan, J. M., 1931, Clastic dyke in the Fort Hays Chalk, Kansas: *AAPG Bulletin*, v. 15, p. 842.
- Mendl, G., 2000, *Faulting in brittle rocks – An introduction to the mechanics of tectonic faults*: Springer-Verlag, Berlin, 434 p.
- Melosh, H. J., 1989, *Impact cratering: A geologic process?*: New York, Oxford University Press, 245 p.
- Mitchell, S.M., Beamish, G.W.J., Wood, M.V., Malacek, S.J., Armentrout, J.A., Damuth, J.E., and Olson, H.C., 1993, Palaeogene sequence stratigraphic framework of the Faroe Basin, in Parker, J. (ed.), *Petroleum geology of northwest Europe: Proceedings of the 4th conference*: London, Geological Society, p. 1011–1023.
- Moench, R. H., 1966, Relation of S₂ schistosity to metamorphosed clastic dykes, Rangeley Phillips Area, Maine: *Geological Society of America Bulletin*, v. 77, p. 1449-1462.
- Molyneux, S., J. A. Cartwright, and L. Lonergan, 1999, Conical sandstone injection structures imaged by 3D seismic in the central North Sea, UK: *First Break*, v. 20, p. 383-393.
- Montenat, C., P. Barrier, P. O. d'Estevou, 1991, Some aspects of the recent tectonics in the Strait of Messina, Italy: *Tectonophysics*, v. 194, p. 203-215.
- Morely, C., 2003, Outcrop examples of mudstone intrusions from the Jerudong anticline, Brunei Darussalam and inferences for hydrocarbon reservoirs. In Van Rensburgen, P., Hillis, R.R., Maltman, A.J., and Morley, C.K. (eds.), *Subsurface Sediment Mobilization*: Geological Society, London, Special Publications 216, p. 381-394.

- Mourgues, P., and P. R. Cobbold, 2003, Some tectonic consequences of fluid overpressures and seepage forces as demonstrated by sandbox modelling: *Tectonophysics*, v. 376, p. 75-97.
- Mount, J. F., 1993, Formation of fluidization pipes during liquifaction: examples from the Uratanna Formation (Lower Cambrian), South Australia: *Sedimentology*, v. 40, p. 1027-1037.
- Mudholkar, A. V., and W. Peshwa, 1988, Clastic limestone dykes from the late Proterozoic Bhima Group, South India: *Sedimentary Geology*, v. 57, p. 221-229.
- Muir Wood, R., 1994, Earthquakes, strain cycling and the mobilization of fluids, In Parnell, J., (ed.) *Geofluids: Origin, Migration and Evolution of Fluids and Sedimentary Basins*: Geological Society, London, Special Publication no.78, p. 85-98.
- Murchison, R. I. 1827, On the coal field of Bora in Sutherlandshire and some other stratified deposits in the North of Scotland: *Transaction of the Geological Society of London*, v. 2, p. 293-326.
- Murdoch, L. C., 2002, Mechanical analysis of idealized shallow hydraulic fracture: *Journal of Geotechnical and Geoenvironmental Engineering*, v. 128, no. 6, 488-495.
- Neef, G., 1991, A clastic dyke-sill assemblage in late Miocene strata, Annedale, Northern Wairarapa, New Zealand: *New Zealand Journal of Geology and Geophysics*, v. 34, p. 87-91.
- Nielson, D.R., 1990, Stratigraphy and sedimentology of the middle Jurassic Carmel Formation in the Gunlock area, Washington County, Utah: *Brigham Young University Geology Studies*, v. 36, p. 153-192.
- Netoff, D., 2002, Seismogenically induced fluidization of Jurassic erg sands, south-central Utah: *Sedimentology*, v. 49, p. 65-80.
- Netoff, D., and R. R. Shroba, 2001, Conical sandstone landforms cored with clastic pipes in Glen Canyon National Recreation Area, southeastern Utah: *Geomorphology*, v. 39, p. 99-110.
- Newman, M. St. J., M. L. Reeder, A. H. W. Woodruff, and I. R. Hatton, 1993, The geology of the Gryphon Oil Field, in J. R. Parker ed., *Petroleum geology of NW Europe: proceedings of the 4th Conference*, v. 1, p. 123-133.
- Newsom, J. F., 1903, Clastic Dykes. *Bulletin of the Geological Society of America*, v. 14, p. 227-268.
- Newton, S. K., Flanagan, K. P., 1993, The Alba Field: evolution of the depositional model, in J. R. Parker ed., *Petroleum geology of NW Europe: proceedings of the 4th Conference*, v. 1, p. 161-171.

Nichols, J. N., 1995, The liquefaction and remobilisation of sandy sediments, in A. J. Hartley, and D. J. Prosser, eds., *Characterization of Deep Marine Clastic Systems*, Geological society special publication, No.94, p. 63-76.

Nichols, R. J., R. S. J. Sparks, and C. N. J. Wilson, 1994, Experimental studies of the fluidization of layered sediments and the formation of fluid escape structures: *Sedimentology*: v. 41, p. 233-253.

Nordgård Bolås, H.M., Hermanrud, C., Tiede, G.M.G., 2004, Origin of overpressures in shales: Constraints from basin modelling: *AAPG Bulletin*, v. 88, no. 2, p. 193-211.

Nunn, J. A., and P. Meulbroek, 2002, Kilometer-scale upward migration of hydrocarbons on geopressed sediments by buoyancy-driven propagation of methane filled fractures: *AAPG Bulletin*, v. 86, p. 907-918.

Obermeier, S.F., Pond E.C., Olson, S.M., and Green, R.A., 2002, Palaeoliquefaction studies in continental settings. In: Ettensohn, F.R., Rast, N., and Brett, C.E. (eds.), *Ancient seismites: Geological Society of America Special Paper 359*, p. 13-27.

Obermeier, S. F., 1996, Use of liquefaction-induced features for palaeoseismic analysis - An overview of how seismic liquefaction features can be distinguished from other features and how their regional distribution and properties of source sediment can be used to infer the location and strength of Holocene palaeo-earthquakes: *Engineering Geology*, v. 44, p. 1-76.

Oldham, T and R. Mallet, 1872, Notice of some of the secondary effects of the earthquake of 10th January, 1869, in Cachar: *Proceedings of the Geological Society*

Ookmens, K., 1966, Environmental significance of sand dykes: *Sedimentology*, v. 7, p. 145-148.

Papanastasiou, P. 2000, Hydraulic fracture closure in a pressure-sensitive elastoplastic medium: *International Journal of Fracture*, v. 103, p. 149-161.

Parize, O., 2001, Origin, process and effects of subsurface sediment mobilization on reservoir to regional scale: *Post-meeting field trip in the Vocontian Basin (SE-France)*, 1st ed. Des Association Sedimentologistes Francais, Paris.

Parize, O., B. Beaudoin, and G. Fries, 1999, Deep-water massive sands: facies processes and channel geometry in the Numidian Flysch, Sicily – comment: *Sedimentary Geology*, v. 127, p. 111-118.

Parize, O., 1988; Sills and dykes gréseux sédimentaires: Paléomorphologie, fracturation précoce, injection et compaction: Ecole Des Mines De Paris, Mémoires des sciences de la terre, No.7.

Parker, B.H., 1933, Clastic plugs and dykes of the Cimarron Valley area of Union County, New Mexico: *Journal of Geology*, v. 41, p. 38-51.

Parnell, J., and Kelly, J., 2003, Remobilisation of sand from consolidated sandstones: evidence from mixed bitumen-sand intrusions. In Van Rensburgen, P., Hillis, R.R., Maltman, A.J., and Morley, C.K. (eds.), *Subsurface Sediment Mobilization: Geological Society, London, Special Publications 216*, p. 505-513.

Pavlov, A. P., 1896, On dykes of Oligocene sandstone in the neocomian clays of the district of Alaty in Russia, *Geological Magazine*, v. 3, p. 49-52.

Peterson, F., 1994, Sand dunes, sabkhas, streams and shallow seas: Jurassic palaeogeography in the southern part of the western interior basin. In: Caputo, M.V., Peterson, A., and Franczyk, K.J. (eds.), *Mesozoic Systems of the Rocky Mountain Region USA: Rocky Mountain Section SEPM, Denver*.

Peterson, G. L., 1968, Flow structures in Sandstone Dykes: *Sedimentary Geology*, v. 2, p. 177-190.

Pheonix, D.A., 1958, Sandstone cylinders as possible guides to palaeomovement of ground water. In: Anderson, R. Y., and Harshbarger, J. W. (eds.), *Guidebook of the Black Mesa basin, northeastern Arizona. Ninth field conference: New Mexico Geological Society*.

Phillips, C. A., and G. I. Alsop, 2000, Post-tectonic clastic dykes in the Dalradian of Scotland and Ireland: implications for delayed lithifications for delayed lithification and deformation of sediments: *Geological Journal*, v. 35, p. 99-110.

Pipringos, G. N., & O'Sullivan, R. B., 1978, Principal unconformities in Triassic and Jurassic rocks, Western Interior United States – a preliminary survey: *Geological Society of America Professional paper 1035-A*, A1-A29.

Plint, A. G., 1983, Liquefaction, fluidization and erosional structures associated with bituminous sands of the Bracklesham Formation (Middle Eocene) of Dorset, England: *Sedimentology*, v. 30, p. 525-535.

Pollard, D. D., and A. M. Johnson, 1973, Mechanics of growth of some laccolithic intrusions in the Henry Mountains, Utah II: *Tectonophysics*, v. 18, p. 311-354.

Powell, C. A., 1969, Intrusive sandstone dykes in the Siamo Slate near Negaunee, Michigan: *Geological Society of America Bulletin*, v. 80, p. 2585-2594.

- Powell, C. A., 1970, Intrusive sandstone dykes in the Siamo Slate near Negaunee, Michigan: Reply: *Geological Society of America Bulletin*, v. 81, p. 3181-3184.
- Price, N. J., and J. W. Cosgrove, 1990, *Analysis of geological structures*: Cambridge University Press, Cambridge.
- Rais, S., I. R. Ansari, and D. Raza, 1985, Clastic Dyke and the associated zeolite veins in Talchir Deposits, Sarguja District, Madhya Pradesh: *Current Science*, v. 54, p. 510-511.
- Ramsey, J. G., and M. I. Huber, 1983, *The techniques of modern structural analysis, Volume 1: Strain analysis*: Academic Press, London, 307 p.
- Ransome, F. L., 1900, A peculiar clastic dyke and its associated ore deposits: *Science*, v. 11, p. 548.
- Rao, C. N., 1956, Occurrence of a clastic dyke in the Serampore Colliery, Giridih, Bihar: *Proceedings of the Indian Science Congress*, p. 176.
- Reeve, W. H., 1937, Sandstone dykes in the Dodoma District of Tanganyika: *Geological Magazine*, v. 74, p. 468-475.
- Reimnitz, E., and N. F. Marshall, 1965, Effects of the Alaska Earthquake and Tsunami on Recent Deltaic Sediments: *Journal of Geophysical Research*, v. 70, p. 2363-2376.
- Richardson, J. F., 1971, Incipient fluidisation and particulate systems: In: J. A. Davidson, and D. Harrison (eds), *Fluidization*, Academic Press, London, p. 26-64,
- Riggs, N.R., Ash, S.R., Barth, A.P., Gehrels, G.E., and Wooden, J.L., 2003, Isotopic age of the Black Forest Bed, Petrified Forest Member, Chinle Formation, Arizona: an example of dating a continental sandstone: *Geological Society of America Bulletin*, v. 115, no. 11, p. 1315-1323.
- Rijsdijk, K. F., G. Owen, W. P. Warren, D. McCarroll, and J. J. M. Van Der Meer, 1999, Clastic dykes in over-consolidated tills: evidence for subglacial hydrofracturing at Killiney Bay, eastern Ireland: *Sedimentary Geology*, v. 129, p. 111-126.
- Ritchie, J.D., and Hitchen, K., 1996, Early Palaeogene offshore igneous activity to the northwest of the UK and its relationship to the North Atlantic igneous province. In Knox, R.B.O'B., Corfield, R.M., and Dunay, R.E. (eds.), *Correlation of the Early Palaeogene in Northwest Europe*: Geological Society, London, Special Publications, 101, p. 63-78.

Roberts, S. J., and Nunn, J. A., 1996, Expulsion of abnormally pressured fluids along faults: *Journal of Geophysical Research*, v. 101(B12), p. 28231-28252.

Roche, O., T. H. Druitt, and R. A. F. Cas, 2001, Experimental aqueous fluidization of ignimbrite: *Journal of Volcanology and Geothermal Research*, v. 112, p. 267-280.

Rossetti, D. F., 1999, Soft-sediment deformation structures in late Albian to Cenomanian deposits, Sao Luis Basin, northern Brazil: evidence for palaeoseismicity: *Sedimentology*, v. 46, p. 1065-1081.

Rowe C. A., P. S. Mustard, J. B. Mahoney, and D. C. Katnick, 2002, Oriented clastic dyke swarms as indicators of palaeoslope? - An example from the Upper Cretaceous Nanaimo Group, Canada: *Journal of Sedimentary Research*, v. 72, no. 1, p. 192-200.

Royse, F., 1993, Case of the phantom foredeep: Early Cretaceous in west-central Utah: *Geology*, v. 21, p. 133-136.

Rubin, A. M., 1995, Propagation of magma filled cracks: *Annual Reviews of Earth and Planetary Science*, v. 23, p. 287-336.

Russel, W. L., 1927, The origin of the sandstone dykes of the Black Hills Region: *American Journal of Science*, v. 14, p. 402-408.

Rutten, M. G., and H. J. M. Schonberger, 1957, Syn-sedimentary sandstone dykes in the Aptian of the Serre Chiatieu, Southern France: *Geologie En Mijnbouw*, v. 19, p. 214-220.

Schlee, J. S., 1963, Sandstone pipes of the Laguna area, New Mexico: *Journal of Sedimentary Petrology*, v. 33, p. 112-123.

Schwartz, H., Sample, J., Weberling, K.D., Minisini, D., Moore, J.C., 2003, An ancient linked fluid migration system: cold seep deposits and sandstone intrusions in the Panoche Hills, California: *Geo-Marine Letters*, DOI 10.1007/s00367-003-0142-1, 20 p.

Schweig, E. S., and R. T. Marple, 1991, Bootheal lineament: a possible coseismic fault of the great New Madrid earthquakes: *Geology*, v. 19, p. 1025-1028.

Seed, H. B., and I. M. Idriss, 1971, A simplified procedure for evaluating soil liquefaction potential: *Journal of Soil Mechanics*, v. 97, no. SM9, p. 1249-1274.

Shoemaker, E.M., and Herkenoff, K.E., 1984 Upheaval Dome impact structure: *Lunar and Planetary Science*, v. 15, p. 778-779.

Shoulders, S., and J. A. Cartwright, 2004, A new approach to constraining the depth and timing of large-scale sandstone intrusions: *Geology*, v.32, no.8, p. 661-664.

Shrock, R. R., 1948, *Sequence in Layered Rocks*: McGraw-Hill Book Company, INC.

Sibson, R. H., 2000, Tectonic redistribution from stress transitions: *Journal of Geochemical Exploration*, v. 69-70, p. 471-475.

Simms, M.J., 2003, Uniquely extensive seismite from the latest Triassic of the United Kingdom: evidence for bolide impact?: *Geology*, v. 31, no. 6, p. 557-560.

Skilling, I. P., J. D. L. White, and J. McPhie, 2002, Peprite: a review of magma-sediment mingling: *Journal of Volcanology and Geothermal Research*, v. 114, p. 1-17.

Smart, P.L., R. J. Palmer, F. F. Whitaker, and V. P. Wright, 1987, Neptunian dykes and fissure fills: an overview and account of some modern examples, in N. P. James, and P. W. Choquette, eds., *Palaeokarst*: Springer-Verlag, New York, p. 149-163.

Smith, A. J., and N. Rast, 1958, Sedimentary dykes in the Dalradian of Scotland: *Geological Magazine*, v. 95, p. 234-240.

Smith, K., 2004, The North Sea Silverpit Crater: impact structure or pull-apart basin?: *Journal of the Geological Society, London*, v. 161, p. 593-602.

Smyers, N. B., and G. L. Peterson, 1971, Sandstone dykes and sills in the Moreno Shale, Panoche Hills, California: *Geological Society of America Bulletin*, v. 92, p. 3201-3208.

Song, J. S., C. L. Hyndman, R. K. Jakher, K. Hamilton, and A. Kantzas, 1999, Fundamentals of hydrodynamics and mass transfer in a three-phase fluidised bed system: *Chemical Engineering Science*, v. 54, p. 4967-4973.

Spence, D. A., P. W. Sharp, and D. L. Turcotte, 1987, Buoyancy driven crack propagation: a mechanism for magma migration: *Journal of Fluid Mechanics*, v. 174, p. 135-153.

Stephens, J. V., G. H. Mitchell, and W. Edwards, 1953, *Geology of the country between Bradford and Skipton (Sheet 69)*: 1st ed. Her Majesty's Stationary Office, London.

Stewart, S.A., 1999, Seismic interpretation of circular geological structures: *Petroleum Geoscience*, v. 5, p. 273-285.

Stoker, M.S., Nielsen, T., van Weering, T.C.E., and Kuijpers, A., 2002, Towards an understanding of the Neogene tectonostratigraphic framework of the NE Atlantic margin between Ireland and the Faroe Islands: *Marine Geology*, v. 188, p. 233–248.

Strachan, L. J., 2002, Slump-initiated and controlled syndepositional sandstone remobilisation: an example from the Namurian of County Clare, Ireland: *Sedimentology*, v. 49, p. 25-41.

Strangeways H. F., 1821, Geological sketch of the environs of St.Petersburg: *Transactions of the Geological Society of London*, v. 5, p. 392-458.

Strickland, H. E., 1840, On some remarkable dykes of calcareous grit, at Eathie in Ross-shire: *Transactions of the Geological Society of London*, v.5 p. 599-600.

Stump, B. B., and P. B. Flemings, 2000, Overpressure and fluid flow in dipping structures of the offshore Gulf of Mexico (E.I.330 field): *Journal of Geochemical Exploration*, v. 68-70, p. 23-28.

Sturt, B. A., and H. Furnes, 1976, Spatial and temporal relationships of intrusive limestones from Las Palmas, Canary Islands: *Journal of Sedimentary petrology*, v. 46, p. 555-562.

Sullivan, M., Coombes, T., Imbert, P., and Ahamdach-Demars, C., 1999, Reservoir quality and petrophysical evaluation of Palaeocene sandstones in the West of Shetland area. In: Flett, A.J., and Boldy, S.A.R., (eds.), *Petroleum geology of northwest Europe: Proceedings of the 5th conference: Geological Society, London*, p. 627-633.

Surlyk, F., 1987, Slope and deep shelf gully sandstones, upper Jurassic, east Greenland: *AAPG Bulletin*, v. 71, p. 464-475.

Surlyk, F., and N. Noe-Nygaard, 2001, Sand remobilisation and intrusion in the Upper Jurassic Hareelv Formation of East Greenland: *Bulletin of the Geological Society of Denmark*, v. 48, p. 169-188.

Swarbrick, E. E., 1968, Physical diagenesis: Intrusive sediment and connate water: *Sedimentary Geology*, v. 2, p. 161-175.

Sweeting, M.M., 1972, *Karst landforms: Macmillan Press, London*.

Takahama, N., T. Otsuka, and B. Brahmantyo, 2000, A new phenomenon in ancient liquefaction – the draw-in process, its final stage: *Sedimentary Geology*, v. 135, p. 157-165.

Tanner, P.W.G., 1998, Interstratal dewatering origin for polygonal patterns of sand filled cracks: a case study from later Proterozoic metasediments of Islay, Scotland: *Sedimentology*, v. 45, p. 71-89.

Taylor, B. J., 1982, Sedimentary dykes, pipes and related structures in the Mesozoic sediments of SE Alexander Island: *British Antarctic Survey Bulletin*, v. 51, p. 1-42.

Terry, D.O., J. A. Chamberlain, P. W. Stoffer, P. Messina, and P. A. Jannet, 2001, Marine Cretaceous-Tertiary boundary section in southwaestern South Dakota: *Geology*, v. 29, p. 1055-1058.

Terzaghi, D. W., 1943, *Theoretical soil mechanics*: New York, Wiley.

Thompson, A.E., and Stokes, W.L., 1970, Stratigraphy of the San Rafael Group, southwest and south central Utah: *Utah Geological and Mineralogical Survey Bulletin*, 87, 53p.

Thompson, B. J., R. E. Garrison, R.E and J. C Moore, 1999, Late Cenozoic sandstone intrusion west of Santa Cruz, California: Fluidised flow of water and hydrocarbon saturated sediments. Late Cenozoic fluid seeps and tectonics along the San Gregorio fault zone in the Monterey Bay region, California: *Volume and Guide book, Pacific Section AAPG GB-76*, p. 53-74.

Timbrell, J., 1993, Sandstone architecture of the Balder Formation depositional system, UK Quadrant 9 and adjacent areas, in J. R. Parker ed., *Petroleum geology of NW Europe: proceedings of the 4th Conference*, v. 1, p. 107-121.

Tindall, S.E., and Davis, G.H., 1999, Monocline development by oblique-slip fault-propagation folding: the East Kaibab monocline, Colorado Plateau, Utah: *Journal of Structural Geology*, v. 21, no. 10, p. 1303-1320.

Tinivella, U., F. Accaino, and A. Camerlenghi, 2002, Gas Hydrate and free gas distribution from inversion of seismic data on the South Shetland margin (Antarctica): *Marine Geophysical Researches*, v. 23, no. 2, p. 109-123.

Trifonov, V.G., 2004, Active faults in Eurasia: general remarks: *Tectonics*, v. 380, p. 123-130.

Trude, K.J., 2004, Kinematic indicators for shallow level igneous intrusions from 3D seismic data: evidence of flow direction and feeder location, in Davies, R.J., Cartwright, J.A., Stewart, S.A., Lappin, M., and Underhill, J.R., eds, *3D seismic technology: application to the exploration of sedimentary basins*: Geological Society, London, *Memoirs*, 29, p. 209-217.

Trude, K.J., J. A. Cartwright, R. J. Davies, and J. R. Smallwood, 2003, A new technique for dating igneous sills: *Geology*, v. 31, p.813-816.

- Truswell, J. F., 1972, Sandstone sheets and related intrusions from Coffee Bay, Transkei, South Africa: *Journal of Sedimentary Petrology*, v. 42, p. 578-583.
- Upadhyay, R., 2003, Earthquake-induced soft sediment deformation in the lower Shyok river valley, northern Ladakh, India: *Asian Journal of Earth Sciences*: v. 21, no. 4., p. 413-421.
- Van Der Welien, L.A.M., Van Dam, M.H.H., and Luyben, K.Ch.A.M., 1996, On the relative motion of a particle in a swarm of different particles: *Chemical Engineering Science*, v. 51, no. 6, p. 995-1008.
- Vanneste, K., M. Meghraoui, and T. Camelbeek, 1999, Late Quaternary earth-quake related soft-sediment deformation along the Belgian portion of the Feldbiss Fault, Lower Rhine Graben system: *Tectonophysics*, v. 309, p. 57-79.
- Velde, B., 1996, Compaction trends of clay-rich deep-sea sediments: *Marine Geology*, v. 133, p. 193-201.
- Vitanage, P. W., 1950, Sandstone dykes in the South Platte area, Colorado: *Journal of Geology*, v. 62, p. 493-500.
- Walsh, P., and Zacharz, I.M., 2001, A dissolution pipe palaeokarst of mid-Pleistocene age preserved in Miocene limestones near Staszów, Poland: *Palaeogeography, Palaeoclimatology, Palaeoecology*, v. 174, p. 327-350.
- Walton, M. S., and R. B. O'Sullivan, 1950, The intrusive mechanics of a clastic dyke: *American Journal of Science*, v. 248, p. 1-21.
- Wang, C., Wang, C.H., Manga, M., 2004, Coseismic release of water from mountains: Evidence from the 1999 ($M_w = 7.5$) Chi-Chi, Taiwan, earthquake: *Geology*, v. 32, no.9, p. 769-772.
- Waterson, C. D., 1950, Note on the sandstone injections of Eathie Haven, Cromarty: *Geological Magazine*, v. 87, p. 133-139.
- Wenrich, K.J., Billingsley, G.H., and Van Gosen, B.S., 1992, The potential of breccia pipes in the Mohawk Canyon area, Hualapai Indian Reservation, Arizona: *US Geological Survey Bulletin*, 1683-D, D1-D39.
- White, N., and Lovell, B., 1997, Measuring the pulse of a plume with the sedimentary record: *Nature*, v. 387, p. 888-891.

White, T., Furlong, K., and Arthur, M., 2002, Forebulge migration in the Cretaceous Western Interior basin of the central United States: *Basin Research*, v. 14, p. 43-54.

Williams, D. M., 1976, Clastic dykes from the Precambrian Porsangerfjord Group, North Norway: *Geological Magazine*, v. 113, p. 169-172.

Williams, M. Y., 1927, Sandstone dykes in southeastern Alberta: *Transaction of the Royal Society of Canada*, v. 4, p. 153-171.

Winslow, M. A., 1983, Clastic dyke swarms and the structural evolution of the foreland fold and thrust belt of the southern Andes: *Geological Society of America Bulletin*, v. 94, p. 1073-1080.

Wohletz, K., Water/magma interaction: some theory and experiments on peprite formation: *Journal of Volcanology and Geothermal Research*, v. 114, p. 19-35.

Wolf, L. W., J. Collier, M. Tuttle, and P. Bodin, 1998, Geophysical reconnaissance of earthquake-induced liquefaction features in the New Madrid seismic zone: *Journal of Applied Geophysics*, v. 39, p. 121-129.

Yardley G. S., and Swarbrick, R. E., 2000, Lateral transfer: a source of additional overpressure?: *Marine and Petroleum Geology*, v. 17, no. 4, p. 523-537.

